

South Dakota State University

Open PRAIRIE: Open Public Research Access Institutional Repository and Information Exchange

Electronic Theses and Dissertations

2021

Development of Bio-based Nanocomposites for Biosensor and Indicator Applications in Smart Food Packaging

Abdus Sobhan
South Dakota State University

Follow this and additional works at: <https://openprairie.sdstate.edu/etd>



Part of the [Bioresource and Agricultural Engineering Commons](#), and the [Food Biotechnology Commons](#)

Recommended Citation

Sobhan, Abdus, "Development of Bio-based Nanocomposites for Biosensor and Indicator Applications in Smart Food Packaging" (2021). *Electronic Theses and Dissertations*. 5792.
<https://openprairie.sdstate.edu/etd/5792>

This Dissertation - Open Access is brought to you for free and open access by Open PRAIRIE: Open Public Research Access Institutional Repository and Information Exchange. It has been accepted for inclusion in Electronic Theses and Dissertations by an authorized administrator of Open PRAIRIE: Open Public Research Access Institutional Repository and Information Exchange. For more information, please contact michael.biondo@sdstate.edu.

DEVELOPEMNT OF BIO-BASED NANOCOMPOSITES FOR BIOSENSOR AND IN-
DICATOR APPPLICATIONS IN SMART FOOD PACKAGING

BY

ABDUS SOBHAN

A dissertation submitted in partial fulfillment of the requirements for the

Doctor of Philosophy

Major in Agricultural, Biosystems, & Mechanical Engineering

South Dakota State University

2021

DISSERTATION ACCEPTANCE PAGE

Abdus Sobhan

This dissertation is approved as a creditable and independent investigation by a candidate for the Doctor of Philosophy degree and is acceptable for meeting the dissertation requirements for this degree. Acceptance of this does not imply that the conclusions reached by the candidate are necessarily the conclusions of the major department.

Lin Wei
Advisor

Date

Van Kelley
Department Head

Date

Nicole Lounsbery, PhD
Director, Graduate School

Date

I dedicated to this dissertation to

- My Brother, Md. Mehedi Hasan
- My Mom, Sebatun Nesa
- My dad, Mozammel Haque

ACKNOWLEDGMENTS

I would like to express my deepest gratitude and appreciation to my supervisor Dr. Lin Wei for his constant support, guidance sharing his vast knowledge throughout the project. I would also like to thank Dr. Kasiviswanathan Muthukumarappan for his expert advice, strong support and encouragement throughout my education and research. In addition, I wish to thank my committee members for their guidance and appreciated input: Dr. Ru-anbao Zhou and Dr. Hemachand Tummala. They looked over many chapter drafts and provided invaluable feedback. I truly appreciate and value all of their contribution, research advice and mentorship.

I would like to acknowledge the financial support received from North Central Regional Sun Grant Center at South Dakota State University through a grant provided by USDA NIFA (Grant No. SA1500640); and (2) the Hatch Project (No. 3AR652 and 3AH658) funded by USDA NIFA through South Dakota Agricultural Experimental Station at South Dakota State University. I am thankful to my former colleague Zheson Cen, who taught me the research preliminaries. I would like to thank the people who gave the priceless support during the unexpected challenge and helped me to regain the courage to finish up this dissertation. I am grateful to my all-graduate lab mates: Nadee Kaluwahandi, Robiul Islam Rubel and Emmanuel Arkoh-Mensah for their enormous support throughout research work.

Last but not least, I wish to thank my family members and friends for their continuous support and love throughout my education. I am eternally indebted to my parents Md Mozammel Haque and Sebatun Nesa for their inspirations, encouragement, and prayers

throughout my education. I am thankful to my brother Mehedi Hasan and my sisters Nargis Khatun and Selina Parvin. I owe my deepest appreciation and respect to the almighty God for helping me overcome various obstacles during the research work and giving me the strength to continue on despite of facing several situations.

CONTENTS

ABBREVIATIONS	x
LIST OF TABLES	xii
LIST OF FIGURES	xiii
ABSTRACT	xviii
CHAPTER 1: INTRODUCTION	1
1.1 Research background	1
1.2 Objectives	3
1.3 Literature Review	4
1.3.1 Smart food packaging	4
1.3.2 Market for smart packaging	8
1.3.3 Biosensors for smart food packaging	9
CHAPTER 2: CHARACTERIZATION OF NANOCELLULOSE AND ACTIVATED CARBON NANOCOMPOSITE FILMS' BIOSENSING PROPERTIES FOR SMART FOOD PACKAGING	32
2.1 Introduction	33
2.2 Materials and methods	35
2.2.1 Materials	35
2.2.2 Preparation of NAC films	36
2.2.3 Characterization methods	36
2.2.4 Statistical analysis	42
2.3 Results and discussion	42
2.3.1 Physical properties of film	42
2.3.2 Electrical properties of the NAC film	43
2.3.3 Mechanical properties	47
2.3.4 Thermal stability of films	49
2.3.5 Functional and microstructural properties of film	51
2.4 Conclusions	57
CHAPTER 3: DEVELOPMENT OF AN ACTIVATED CARBON-BASED NANOCOMP SITE FILM WITH ANTIMICROBIAL PROPERTY FOR SMART FOOD PACKAGING	59
3.1 Introduction	60
3.2 Materials and methods	63

3.2.1	Materials	63
3.2.2	Preparation of silver integrated nanocomposite films	63
3.2.3	Transmission electron microscopy analysis (TEM)	65
3.2.4	Fourier transform infrared spectroscopy.....	66
3.2.5	X-ray diffraction	66
3.2.6	Antimicrobial test of silver integrated film.....	66
3.2.7	Thermal analysis of silver integrated film	68
3.2.8	Electrochemical analysis of silver integrated film.....	68
3.3	Statistical analysis	69
3.4	Results and discussion.....	69
3.4.1	Microstructure of AgNPs/AC-CNF film	69
3.4.2	FTIR analysis of AgNPs/AC-CNF film.....	71
3.4.3	XRD analysis of AgNPs/AC-CNF film.....	73
3.4.4	Antimicrobial properties of AgNPs/AC-CNF film.....	75
3.4.5	Thermal analysis of AgNPs/AC-CNF film.....	79
3.4.6	Electrochemical properties of the AgNPs/AC-CNF film	82
3.5	Conclusions	85
CHAPTER 4: SYNTHESIS AND CHARACTERIZATION OF A NOVEL ACTIVATED BIOCHAR-BASED COMPOSITE FOR BIOSENSOR APPLICATION IN SMART FOOD PACKAGING		
4.1	Introduction	88
4.2	Materials and methods	90
4.2.1	Materials	90
4.2.2	Preparation of biochar from corn stover	90
4.2.3	Biochar activation using steam-activation method.....	91
4.2.4	Characterized analysis of activated biochar (ABC).....	93
4.2.5	Characterized analysis of ABC/PLA composite film	96
4.3	Statistical analysis	98
4.4	Results and discussion.....	99
4.4.1	Characterization of activated biochar (ABC)	99
4.4.2	Characterization of ABC/PLA composite	104
4.4.3	ABC/PLA-based biosensor for ammonia (NH ₃) detection	111
4.5	Conclusions	113

CHAPTER 5: SYNTHESIZE OF ELECTRICALLY CONDUCTIVE AND BIODEGRADABLE POLYMER FOR BIOSENSOR BY COMBINATORY USE OF SILVER NANOPARTICLES, ACTIVATED BIOCHAR AND POLYLACTIC ACID

115

5.1	Introduction	116
5.2	Materials and methods	118
5.2.1	Materials	118
5.2.2	Preparation and activation of biochar	119
5.2.3	Biofilm preparation with ABC/PLA polymers	119
5.2.4	Biodegradation of ABC/PLA biofilm	120
5.2.5	Enumeration of microorganism	120
5.2.6	Scanning electron microscopic analysis	121
5.2.7	Development of AgNP/ABC/PLA polymers for biosensor	121
5.3	Statistical analysis	122
5.4	Results and discussion	123
5.4.1	Biodegradability of ABC/PLA biofilm	123
5.4.2	Characterization of AgNP/ABC/PLA polymer	126
5.4.3	Characterization of the fabricated biosensor	130
5.5	Conclusions	136
CHAPTER 6: DEVELOPMENT OF A POLYLACTIC ACID-COATED NANOCCELLULOSE/CHITOSAN-BASED FILM FOR REAL TIME MONITORING OF BEEF SPOILAGE		
6.1	Introduction	138
6.2	Materials and methods	140
6.2.1	Materials	140
6.2.2	Preparation and fabrication of PLA/NCM film	140
6.2.3	Characterization methods	142
6.2.4	Application of PLA/NCM film for monitoring meat spoilage	144
6.3	Statistical analysis	146
6.4	Results and discussion	146
6.4.1	Functional properties of film	146
6.4.2	FTIR spectra	148
6.4.3	pH sensing and optical properties of films	150
6.4.4	Assessment of color specificity of PLA/NCM film	153

6.4.5	Application of PLA/NCM film for beef spoilage trial.....	155
6.5	Conclusions	162
CHAPTER 7: CONCLUSIONS		164
CHAPTER 8: RECOMMENDATIONS FOR FUTURE WORK		166
References.....		168
PUBLICATIONS.....		208

ABBREVIATIONS

NAC	Nanocellulose-based activated carbon
CNF	Cellulose nanofiber
AC	Activated carbon
CV	Cyclic Voltammetry
DPV	Differential Pulse Voltammetry
EIS	Electrochemical Impedance Spectroscopy
LSV	Linear sweep voltammetry
GCE	Glassy Carbon Electrode
TS	Tensile strength
TGA	Thermal gravimetric analysis
DSC	Differential scanning calorimetry
WVP	Water vapor permeability
FTIR	Fourier-Transform Infrared Spectroscopy
SEM	Scanning electron microscopy
AgNPs	Silver nanoparticles
TEM	Transmission electron microscopy analysis
XRD	X-ray diffraction
OD	Optical density
PDA	Potato dextrose agar
I/V	Current/voltage
CMC	Carboxymethyl cellulose
ABC	Activated biochar

PLA Polylactic acid

ACP Accurate control pyrolysis

IR Raman spectroscopy

DMF N, N-dimethylformamide

BET Brunauer-Emmett-Teller

LOD Limit of Detection

NCM Nanocellulose and chitosan doped with methyl red

TVC Total viable count

ΔE Color difference values

CFU Colony form unit

LDR Linear Detection Range

M Molar

mL milliliter

ng nanogram

ppm parts per million

LIST OF TABLES

Table 1.1. Different smart devices for intelligent/smart food packaging with principal, application and drawbacks.....	5
Table 1.2. Biosensor or sensor formats for smart food packaging.....	10
Table 1.3. Typical antimicrobial materials which are used for preparation of bio nanocomposites.....	23
Table 6.1. CIE-Lab color parameters (L^* , a^* and b^*) of the PLA/NCM films after contact with different pH buffer solutions (pH 2-10).....	152

LIST OF FIGURES

Figure 1.1. Basic RFID system for meat packaging	8
Figure 1.2. Common methods for immobilization of biosensing: (A) covalent binding; (B) adsorption; (C) cross-linking; (D) encapsulation; and (E) entrapment.....	13
Figure 1.3. Basic principle of gas sensor for gas (CO ₂) detection after food spoilage.....	14
Figure 1.4. Opportunities of biosensor for smart food packaging development.	15
Figure 1.5. Opportunities for bionanocomposite for smart food packaging development.	21
Figure 1.6. Challenge of biosensor for smart food packaging development.	24
Figure 1.7. Challenge for bionanocomposite for smart food packaging development.....	28
Figure 2.1. Physical properties of 15%, 30% and 50% NAC films. (A) The images of NAC film with its different NAC contents (15%, 30% and 50%); (B) surface morphology of NAC films observed by scanning electron microscopy (SEM) with 300 μm.	43
Figure 2.2. Electrochemical analyses of 15%, 30% and 50% NAC films. (A) Resistance (R _s , KΩ) of NAC films measured by linear sweep voltammogram (LSV); (B) cyclic voltammogram of NAC films; and (C) differential plus voltammogram (DPV) of NAC films; (C) impedance spectra of NAC films.	45
Figure 2.3. Mechanical properties of 15%, 30% and 50% NAC films. (A) Tensile strength (TS) and strain of NAC films; (B) Young modulus of NAC films.	48
Figure 2.4. Thermal analysis of 15%, 30% and 50% NAC films. (A) Typical thermogravimetric (TGA) analysis curves; (B) differential scanning calorimetry (DSC) curves of NAC film.....	50
Figure 2.5. Physiological properties of 15%, 30% and 50% NAC films. (A) Water vapor permeability (WVP) and water solubility of NAC film; (B) water absorption capacity of NAC film depending on time period (2, 4, 6, 8, 10, 12 h); (C) effect of nanocellulose (CNF) on the viscosity of NAC films.	53
Figure 2.6. Infrared spectroscopy (FTIR) spectra of 15%, 30% and 50% NAC films. The films contained different nanocellulose (CNF) and activated carbon (AC) contents.....	55
Figure 2.7. SEM images of NAC film. (A) Nanocellulose (CNF); (B) activated carbon (AC); (C) 15% NAC film; (D) 30% NAC film; (E) 50% NAC film.....	57
Figure 3.1. Schematic diagram for the formation of AgNPs/NAC film using cellulose nanofiber (CNF), activated carbon (AC) and silver nanoparticles (AgNPs) synthesis. ...	65

Figure 3.2. TEM images of: (a-b) CNF bound with AC was identified, (c-d) AgNPs bound with CNF and AC were identified; and (e) EDS elemental mapping images of AgNPs/AC-CNF nanocomposite.....	71
Figure 3.3. Infrared spectroscopy (FTIR) spectra of AgNPs/AC-CNF films (15% to 50% of CNF).....	73
Figure 3.4. X-ray diffraction (XRD) pattern of 70, 140, 250, 350, and 450 ppm of AgNPs/AC-CNF film.....	75
Figure 3.5. Inhibitory effect of AgNPs/AC-CNF film against Gam-positive bacteria <i>S. aureus</i> ATCC 13565 with 108 CFU/mL; Gam-negative bacteria <i>E. coli</i> TOP10 with 108 CFU/mL; and <i>Rhizopus stolonier</i>	78
Figure 3.6. General scheme of inactivation mechanism of microorganism using AgNPs/AC-CNF film disc.....	79
Figure 3.7. Comparative thermal analysis of TGA spectra of AgNPs/AC-CNF film under oxygen (O ₂) and nitrogen (N ₂) condition. (a) TGA curve for different concentration of AgNPs ranged between 70-450 ppm under O ₂ condition; (b) Differential of TGA (DTGA) curve were shown with the similar AgNPs range under O ₂ condition; (c) TGA curve with different concentration of AgNPs from 70 to 450 ppm under N ₂ condition; (d) Differential of TGA (DTGA) curve were shown with the similar AgNPs range under N ₂ condition.	82
Figure 3.8. Electrochemical analyses of AgNPs/AC-CNF films with different AgNPs concentrations (70 to 450 ppm). (a) Cyclic voltammogram of AgNPs/AC-CNF films measured by cyclic voltammetry (CV); (b) differential plus voltammogram (DPV) of AgNPs/AC-CNF films; (c) cyclic voltammogram with different scan rate (2 to 100 mV/s); (d) Resistivity (K Ω . cm) of AgNPs/AC-CNF films measured by linear sweep voltammogram (LSV).....	85
Figure 4.1. Biochar preparation from corn stover using accurate control pyrolysis (ACP) reactor system.	91
Figure 4.2. Biochar activation followed by the steam-activation method.	92
Figure 4.3. Schematic illustration of biosensor fabrication process using drop casting... ..	95
Figure 4.4. A casting process for synthesis of ABC/PLA composite films.....	96
Figure 4.5. Schematic diagram of the experimental set-up for measuring biosensor response to NH ₃	98
Figure 4.6. Characterization of ABCs. (A) Raman spectrums of the ABCs with different temperature range (600°C-1000°C); (B) BET analysis of ABCs; (C) SEM images of ABC/800°C; and (D) Histogram of ABC/800°C. Control sample denotes biochar sample without thermal activation.	101

- Figure 4.7. Electrochemical analysis of ABCs. (A) Current of ABCs; (B) Nyquist current curves obtained by linear sweep voltammetry; (C) Resistance of ABCs; and (D) Plot of peak current (I_p) versus different potential scan rates. Control sample denotes biochar sample without thermal activation. 103
- Figure 4.8. Physical properties of ABC/PLA films. a: Left to right: 85% ABC/PLA film; 70% ABC/PLA film; 50% ABC/PLA film; b: left to right: SEM micrographs of 85% ABC/PLA film; 70% ABC/PLA film; 50% ABC/PLA film. 105
- Figure 4.9. SEM micrographs of ABC/PLA film. (A) 85% ABC/PLA film; (B) 70% ABC/PLA film; (C) 50% ABC/PLA film. 106
- Figure 4.10. Tensile properties of ABC/PLA composite film. (A) Tensile strength and strain; (B) Young's modulus; (C) force vs deformation of 85% to 50% ABC/PLA composite film; and (D) scheme of tensile testing. 107
- Figure 4.11. TGA spectra of ABC/PLA composite film under nitrogen (N_2) condition. (A) TGA curve for different ABC/PLA composite films; (B) Differential of TGA (DTGA) curves of different ABC/PLA composite films. 108
- Figure 4.12. Electrical analysis of 85%-50% ABC/PLA composite. (A) Cyclic voltammogram (CV); (B) differential plus voltammogram (DPV); (C) peak currents of ABC/PLA; (D) current density of ABC/PLA; and (E) cyclic voltammogram with different scan rates (5 to 100 mV/s). 110
- Figure 4.13. A) Resistance response of 85% ABC/PLA-based biosensor to NH_3 concentrations (5 ppm to 230 ppm); (B) Sensitivity of the biosensor to NH_3 gas (80-170 ppm); (C) Comparison of I-V data of 85% ABC/PLA-based biosensor in presence and absence of NH_3 gas (~110 ppm); (D) Stability of the biosensor for fixed NH_3 concentration (50 ppm). 112
- Figure 5.1. Evaluation of biodegradable properties of ABC/PLA biofilm. (A) Weight change of ABC/PLA biofilm over time of 10 weeks buried in filed soil: (B) photographs of ABC/PLA biofilms during biodegradation. Control film refers to the film before biodegradation. 124
- Figure 5.2. Evaluation of biodegradable properties of ABC/PLA biofilm. (A) Isolation of microorganism and fungi grown on the surface of agar media; (B) SEM analysis of recovered ABC/PLA biofilm after biodegradation: (a) SEM observation of control film; (b-c) Mold observation on the biofilm; (d-e) bacteria observation on the biofilm after biodegradation. Control film refers to the film without biodegradation. 125
- Figure 5.3. Electrochemical analyses of AgNPs/ABC/PLA and ABC/PLA polymer. (A) Cyclic voltammogram (CV); (B) differential plus voltammogram (DPV); (C) linear sweep voltammogram (LSV); (D) amperometry voltammogram (AV); and (E) current density of AgNPs/ABC/PLA and ABC/PLA polymer. 128

- Figure 5.4. TGA spectra of ABC/PLA and AgNP/ABC/PLA polymer sample under nitrogen (O_2) condition. (A) TGA curve; (B) Differential of TGA (DTGA) curves of ABC/PLA and AgNP/ABC/PLA polymer sample. 129
- Figure 5.5. Surface area of the activated biochar (ABC) (BET and Langmuir analysis); (B) Sensitivity (%) of the fabricated biosensor developed with AgNP/ABC/PLA polymer for ammonia (NH_3) (5-60 ppm); (C) Sensitivity (%) of the fabricated biosensor developed with ABC/PLA polymer for ammonia (NH_3) (5-60 ppm); (D) Comparison of sensitivity (%) of the fabricated biosensor developed with AgNP/ABC/PLA and ABC/PLA polymer for ammonia (NH_3) (60 ppm)..... 132
- Figure 5.6. Schematic representation of ammonia (NH_3) adsorption with atomic positions and electron transfer in AgNPs/ABC/PLA polymer surface. 134
- Figure 5.7. Evaluation of biosensor properties. (A) Selectivity analysis of the biosensor over the different gas; (B) reliability of the biosensor; and (C) Reusability of the biosensor over 6 times..... 135
- Figure 6.1. Schematic diagram for the formation of PLA/NCM film using cellulose nanofiber (CNF), chitosan, methyl red and polylactic acid (PLA)..... 142
- Figure 6.2. (A) Mechanical properties of NCM and PLA/NCM films; (B) water solubility of NCM and PLA/NCM films; (C) Photodegradation of PLA/NCM film according to CIE-Lab coordinates; (D) Photodegradation of NCM film according to CIE-Lab coordinates exposed to visible light irradiation as a function of time at 21 °C..... 148
- Figure 6.3. Infrared spectroscopy (FTIR) spectra of PLA/NCM films. The films contained nanocellulose (CNF), chitosan and PLA contents. 150
- Figure 6.4. The visible color response of the PLA/NCM film with respect to different pH buffer solutions (pH 2-10). 152
- Figure 6.5. (A) The color change of PLA/NCM film at different simulated conditions; (B) CIEb* color parameters of the PLA/NCM films at different simulated conditions. Control film denotes PLA/NCM film without any sample treatment..... 155
- Figure 6.6. Color variation of PLA/NCM film with respect to beef spoilage at refrigeration condition ($4\pm 0.2^\circ C$). 156
- Figure 6.7. The color change (ΔE) of PLA/NCM film towards the spoiling beef at refrigeration condition ($4 \pm 0.2^\circ C$). 156
- Figure 6.8. (A) Total viable count (TVC) of microorganism in the beef sample in the refrigerant condition; (B) TVC correlated with color change value (ΔE) of PLA/NCM film between 1-10 days; (C) ΔE correlated with TVC in the refrigeration condition. 158
- Figure 6.9. (A) Determination of the pH of beef sample depending on their spoilage between 1 and 10 days; (B) pH of spoiling beef correlated with the color change value (ΔE)

between 1-10 days; (C) pH of spoiling beef sample correlated with the color change value (ΔE) and images of PLA/NCM film after beef spoilage at 1, 5, 6, 8 and 10 days..... 160

Figure 6.10. (A) Determination of evolved ammonium concentration in spoiled beef samples; (B) evolved ammonium concentration correlated with color change value (ΔE) between 1-10 days; (C) evolved ammonium concentration of beef sample correlated with color change value (ΔE) and images of PLA/NCM film after beef spoilage at 1, 5, 6, 8 and 10 days. 162

ABSTRACT

DEVELOPEMNT OF BIO-BASED NANOCOMPOSITES FOR BIOSENSOR AND INDICATOR APPLICATIONS IN SMART FOOD PACKAGING

ABDUS SOBHAN

2021

Smart food packaging based on biosensors has been attracting more and more interest to the industrial community because of the concerns of food quality and safety. A food packaging with biosensor has a scope to enable real-time monitoring of microbial breakdown products of packaged foods. Furthermore, one of the biggest challenges in implementing biosensor for smart packaging materials is the development of bio-sensing active materials that can leverage their electrical, thermal, biodegradable and other functional properties. In this regard, nanocellulose-based activated carbon (NAC) nanocomposite was developed using the activated carbon and nanocellulose gel using the casting method with their different concentrations (15% to 50% of nanocellulose corresponding to 85% to 50% activated carbon). The developed NAC nanocomposites were electrically tested via cyclic voltammetry and results showed that 30% NAC nanocomposite consisted of good electrical properties compared to 30 and 50% of NAC nanocomposite for biosensor developments. Metal nanoparticle enriched natural biopolymer has attained significant attention in the research community, because they can create high specific surface area, adsorption capability, and gas sensing properties into polymer composite or nanocomposites. Different contents of AgNPs with 10-500 ppm were synthesized with 30% NAC nanocomposite and optimized their electrical properties. The results showed that AgNPs/NAC nanocomposite with optimum 450 ppm of AgNPs contained the good electrical properties for biosensor

development. The biosensor developed with optimized AgNPs/NAC nanocomposite resulted in good sensitivity and selectivity to detect microbial breakdown products as a spoilage indicator. Ammonia (NH_3) is one of the microbial breakdown products that released from protein rich food products (such as meat, fish, sea foods etc.) and had a good response in monitoring meat spoilage. The developed biosensor was utilized to monitor NH_3 , and the sensor showed good sensitivity over the range of 5-100 ppm and selectivity to detect the NH_3 .

Biochar is one of the carbon-based materials that belongs a high specific surface area, highly porous structure, good stability, and cost-effectiveness over other carbon items (single or multi carbon nanotubes and graphene). The activated biochar (ABC)-based composite was developed with different ABC and polylactic acid (PLA) levels and the electrical properties of the developed ABC/PLA composite was determined via cyclic and differential voltammograms (CV and DPV). The results showed that 85% ABC/PLA composite has a good electrical property for biosensor development. To improve the gas sensing properties, 85% ABC/PLA composite was further synthesized with 450 ppm of AgNPs (v/v) and casted AgNPs/ABC/PLA nanocomposite. The biosensor was developed with casted AgNPs/ABC/PLA nanocomposite and tested for ammonia over the range of 5-60 ppm. The results revealed that the sensitivity of the developed biosensor increased as the concentrations of NH_3 increased over the range of 5-60 ppm.

An indicator with food packaging has the ability to monitor microbial contaminations in food products. A color indicator film was developed by a film casting method using an ultrasonic suspension of nanocellulose/chitosan blends doped with methyl red synthesis followed by PLA coating (named PLA/NCM film). The color modulation of the

PLA/NCM films was processed via the colorimetric device and revealed considerable color changes (ΔE_s) dependent on the meat spoilage. The PLA/NCM film changed its color upon exposure to different pH buffer solutions (2–10). The total viable microbial counts (TVC) and pH of the beef sample were determined, and the findings showed that the TVC and pH increased simultaneously depending on the state of the beef spoilage.

CHAPTER 1: INTRODUCTION

1.1 Research background

Food contamination has been the highest concern to the consumers since the last few decades [1]. Although the incidences of food contamination can occur throughout the year by various means (i.e., physical, chemical, and biological means), the most fatal contaminations of food are occurred by infectious microorganisms [2]. Many outbreaks of foodborne illness were reported in the USA in 2012-2018, when packaged food items such as tuna, salmon, dairy products, hard-boiled eggs, pork, chicken and ground beef were contaminated by a list of microorganisms: *Escherichia coli* O157:H7; *Listeria*; *Yersinia enterocolitica*, *Clostridium perfringens* and *Salmonella* Typhimurium [3,4]. In other countries like Spain and Korea, a similar incidence of contamination has been observed in packaged foods [5,6]. Although some initial indicators such as color, odor and texture parameters are usually considered for evaluating the quality of foods prior to packaging, but because of outliers, it is difficult to assess the quality of foods after packaging [7]. In such situation, advanced food packaging technology is precisely required which can facilitate a communication between the consumers and packaged foods.

Active food packaging plays a key role in preserving food by increasing and maintaining the shelf life of foods. The main limitation of active food packaging is that it is not able to indicate the quality parameters of packaged foods. These are mostly confined to enhancing the protection and preservation of packaged foods [8,9]. Moreover, modern society seeks to improve the role of active packaging by introducing packaging nanotechnology to track packaged foods [8]. Smart food packaging is another aspect of active packaging that has

evolved due to progress in the nanotechnology and e-commerce [10]. It can sense and inform the condition of the packaged foods with rapidity, and offer communication to the customers either online or offline as to the status of the product [2]. Most smart food packaging materials integrate biosensor and indicator concepts into active packaging materials [7]. Though few numbers of biosensors and indicators i.e., time-freshness indicators, temperature integrators (TTI), microbial spoilage biosensor, pathogen and contamination biosensor for food packaging were invented and promising results have been achieved, the road to the successful application of biosensor and indicators in smart food packaging is still long.

Biopolymer is an organic polymer composed of monomeric units of organic compound, which are covalently bonded to form a biopolymer. It is biodegradable or broken down into the soil by the action of naturally occurring organisms and leaves organic by-products such as CO_2 and H_2O which are safe towards the environment [11]. Biopolymers are mixed with nanosized particles (i.e., carbon nanotubes, nanocellulose, silver, zinc, copper, magnesium and gold nanoparticles) to form bionanocomposites. Bionanocomposites have received considerable attention as an alternative material over the conventional composites (i.e., fibers, carbon fiber source, polyvinyl chloride and so on), because these have a large surface area, improved mechanical, biodegradable, thermal and physical properties and have no highly environmentally concerns over the conventional composites (Rhim, Ng, & Rhim, 2007).

The amount of global annual plastics in food packaging is expected to reach 330 million tons by 2020 [13]. To minimize this amount of conventional plastic materials in the food packaging, bionanocomposites are considered and identified as excellent components with

food packaging materials [14]. Several bionanocomposite packaging films have already been developed for food packaging applications, such as polylysine film [14], starch/layered silicate film [15], nanocellulose film (Sobhan, Muthukumarappan, Cen, & Wei, 2019) and so on. Moreover, combining bionanocomposites and acting them as a biosensor with packaging material is advantageous and could be a new breakthrough for future smart food packaging applications. Despite extensive research at the industrial and academic levels, research in bionanocomposites for food packaging is still in a very early developmental stage. It is necessary to look at the entire life cycle of the packaging, such as raw material extraction and production, balancing cost, health, and environmental considerations. This paper aims to provide an overview of smart food packaging and the challenges and opportunities of biosensors, indicators and bionanocomposite to understand the gaps in ongoing scientific research for smart food packaging. It begins with an introductory outline of existing bionanocomposite and biosensor for food packaging. Then, it analyzes the potential challenge and opportunities of biosensor and bionanocomposite for future smart food packaging industries.

1.2 Objectives

In light of the current knowledge gaps, the goal of this study is to develop the biosensor and indicator for smart food packaging and characterize the different electrical and functional properties of the biosensor and calorimetric properties for indicator, and to employ the biosensor and indicator for smart food packaging in determining food spoilage.

The specific objectives of this proposed study are:

- 1) To prepare the activated carbon based-nanocomposite (NAC) using cellulose nanofiber (CNF) and activated carbon (AC) with various contents of CNF and AC and characterize

the electrochemical, thermal, mechanical, and biodegradable properties of nanocomposite for biosensor development in smart food packaging application (CHAPTER 2).

2) To investigate the effect of silver nanoparticles (AgNPs) with NAC nanocomposite as the gas sensing catalyst and characterize its antimicrobial, electrochemical, and thermal properties for biosensor development in determining food spoilage for smart food packaging (CHAPTER 3).

3) To develop the activated biochar (ABC) from conventional biochar as the semiconductive materials for biosensor development and characterize their electrical and functional properties for biosensor fabrication (CHAPTER 4).

4) To synthesize the ABC with polylactic acid (PLA) and develop ABC/PLA nanocomposite; and characterize their mechanical, electrical, thermal and biodegradable properties (CHAPTER 4).

5) To synthesize AgNPs with ABC/PLA composite as the gas catalysis sensing elements and characterize the electrochemical properties for biosensor development. The developed biosensor was tested to monitor the food spoilage (CHAPTER 5)

6) To develop an effective film indicator using CNF and chitosan followed by methyl red (MR) and characterize the functional and microbial response properties; and to employ the indicator film to monitor for meat spoilage (CHAPTER 6).

1.3 Literature Review

1.3.1 Smart food packaging

Smart food packaging is anything which proposes "something extra" in addition to the food containment and protection. These "extras" can be anything, such as prolonged shelf life to displays for pH, temperature, moisture, and freshness monitoring or to a tracking device

[17]. This packaging innovation not only monitors the freshness of foods and exchanges the information with consumers, but it can also track and trace the products through blockchain technology and improve targeted recalls, though this system for food packaging is still in an early developmental stage. Smart packaging uses different sensors, indicators and smart levels to evaluate storage conditions, food quality and the inside/outside environment of packaging [18]. The commercial smart packaging components which are existed in the market or prevailed under research are shown in Table 1.1 with their trade name, application, advantage and drawbacks.

Table 0.1. Different smart devices for intelligent/smart food packaging with principal, application and drawbacks.

Smart devices	Principle/reagents	Information given	Application	Advantage	Disadvantage	References
Time temperature indicators (TTI)	Mechanical, chemical, enzymatic, microbiological	Storage conditions	Meat preserved under chilled and frozen conditions	Can be combined with packaging, can be measured by electronic devices, can be observed by naked eye	Must be conditioned prior to use, no contact with food, does not provide information about quality of food	[19]
Radio frequency identification tags	Radio waves	Product and manufacturer information	Product tracking, identification, supply chain management, security control	Can be integrated into barcodes, wireless technology, reading multiple products at once, fast and accurate.	The signal can be lost, expensive to commercialization	[20]

Gas indicators	Chemo-sensitive dyes which respond gas	Volatile gas detection	Perishable foods especially fish and meat	Can be inserted into the packaging, can be checked by naked eye, not affected by heat, electromagnetic and stirring. Sensitive, can be observed by naked eye, can be measured by electronic devices.	Does not provide information about gas concentration inside the package, its chemical dye may interfere in food quality.	[21]
Freshness indicators	pH dyes; Dyes reacting with (non-) volatile metabolites	Determining microbial breakdown products	Perishable foods such as meat, fish and poultry	Sensitive, can be observed by naked eye, can be measured by electronic devices.	False negatives results, attached inside the package which may interfere in food qualities.	[20]
Pathogen indicators	Various chemical and immunochemical methods reacting with toxins	Detecting pathogenic bacteria such as <i>E. coli</i> O157	Perishable foods such as fish, meat and dairy foods	Sensitive, can be observed by naked eye, can be measured by electronic devices.	Can produce false and negatives results, chemicals may interfere with foods	[20]
Bar-codes	Symbology	Determining product price, manufacturer information	Product identification, stock reordering and check-out	Identify origin of food product, Ability to track and trace loose food items.	The signal can be lost, expensive to commercialization	[21]
E-nose	Various sensor arrays produce odor profile	Information about contaminants, defects in foods	Monitoring authenticity, quality of foods	Can detect volatile compounds, can be integrated into pattern recognition and decision-making systems.	Expensive for packaging and commercial purpose.	[7]
Biosensors	Electrochemical signal	Binds the targeted pathogens and toxins with biosensor	Monitoring food quality	Can be checked by naked eye, can be measured by electronic devices	Cannot detect low concentrated contamination, may have chemical effect on the food.	[19]

In the market, key components for smart packaging are TTI (Time-Temperature Indicators), Repeat Index, freshness indicator, coloring indicator, barcodes and Radio Frequency Identification (RFID). Among these components, TTIs and RFID are widely known components. TTIs can measure changes in the physical properties of food as a response to temperature and time profile [22]. The restrictions of TTIs devices are on their application, they can be only used in frozen food products [23]. RFID is one of the smart packaging materials which monitor wireless communication between the packaging products throughout tags, readers and computer systems. The benefit of RFID over barcodes is to permit a remote control in where multiple items can be monitored at the same time and they do not need line-of-sight in the device [2]. In a basic RFID system, an RFID tag contains a tiny transponder and antenna that have a unique number or alphanumeric order; a reader performs radio waves to capture data from the RFID tag and transmits the data onto a host computer (which may be more connected to the local network or the internet) for analysis and decision-making through a real-time database server, as is seen in Figure 1. 1. However, the drawbacks of RFID are that they not widely suitable for commercial use with food packaging applications, because their market prices are comparatively high and they cannot be reused, which is not profitable for the food industry. Therefore, there is a great need to do a lot of research on smart food packaging components in order to open market opportunities and to create cheaper and reusable formats of smart food packaging materials.

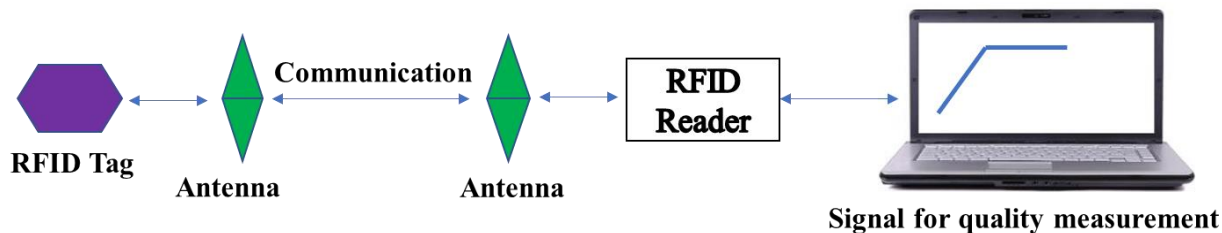


Figure 0.1. Basic RFID system for meat packaging.

1.3.2 Market for smart packaging

According to a survey conducted by the U. S. Department of Agriculture (USDA), in 2015-16 year, adults in U. S consumed more packaged foods compared to 2007–08 year [24]. The average monthly intake of packaged food in the U.S rose from 1.9 times in 2007-08 to 2.4 times in 2015-16, indicating an increase in consumption of 26%. A new report from the industry indicates that the market demand for intelligent food packaging in the U.S is around \$1.5 billion in 2019 [25].

The global market reports employed on smart packaging revealed that the demand for smart packaging was around \$35.33 billion in 2018 [26]. The market growth looks promising, and the overall market value was close to around \$36 billion in 2019. It is predicted that the future of global smart packaging will be grown and is expected to reach around \$44.39 billion by 2024 [23]. Since the food sector accounts for over 51% of the total advanced packaging market and is the key driver affecting the market growth [4], it can be predicted that the global smart food packaging market will be at least \$22.19 billion in 2024. Nowadays, the market demand for smart packaging is mounting over the world and especially it is becoming more popular to the youngest because they require product information

updated. North America is the largest market and holds over 35% of the total share in 2019. The demand for smart packaging is mounting in the US and valued at close to \$3.6 billion in the next few decades [26]. The second-largest packaging market is predicted in Japan which is equivalent to \$2.36 billion. It has been stated that this demand rate will be nearly \$1.69 billion in Australia, \$1.27 million in the UK, and \$1.4 million in Germany in the next decades.

1.3.3 Biosensors for smart food packaging

1.3.3.1 Definition and types

A biosensor is an analytical device which is capable of converting the input signals into the continuous output signal. In the biosensor, it comprises a transducer and receptor. Receptors convert physical or chemical data into an energy form, while a transducer transforms this energy into a useful analytical signal i.e., electrical signal. The biosensor was started in the 1960s by Clark and Lyons [27]. Although, biosensors have been seen to their use in environmental and biomedical areas, however, all of these biosensors are not appropriate in the use of food packaging because of their proper microstructure, sensitivity, specificity, stability and processing cost. Some biosensors have been reported literally and tested for food applications, which are noted as fluorescent and microfluidics sensor, gas detection based sensor, electrochemical-imprinted biosensor, immunosensor, and thermal biosensor [28]. The most common biosensors which are considered for smart food packaging are described below in Table 1.2.

Table 0.2. Biosensor or sensor formats for smart food packaging.

Biosensor type	Biosensor format	Analytes	Detection time	Detection limit	Reference
Microfluidic and fluorescent biosensor	Microfluidic biosensor	<i>Salmonella typhimurium</i>	15 min	10 ⁵ CFU/mL	[29]
	Magnetic based fluorescent biosensor	<i>E. coli</i> O157:H7	2 h	14 CFU/mL	[30]
	Iron coated fluorescence biosensor	<i>Shigella</i> spp	20 min	10 ² CFU/mL	[31]
	Fluorescent Ag+ nanoclusters	Ammonia	60 min	336 nM	[32]
Electrochemical based biosensor	Poly(dimethylsiloxane) coated microfluidic sensor	H ₂ O ₂	30 mi	5 nM	[33]
	Potentiometric aptasensor	<i>Salmonella typhimurium</i>	10 min	10 ¹ CFU/mL	[34]
	SWCNT-based biosensor	<i>Y. enterocolitica</i>	30 min	10 ⁵ CFU/mL	[35]
	CNT based electronic transistor	<i>Salmonella Infantis</i>	1 h	10 ² CFU/mL	[36]
	Amperometric biosensor	L-malic acid	2 min	2.9×10 ⁻⁵ g/L	[37]
Gas biosensor	Xanthanin biosensor	Xanthanin	-	0.1 μM	[38]
	Poly (3-hexyl thiophene) organic field-effect transistor	NH ₃	6 min	100 ppm	[39]
	FET-type sensor	SO ₂	3 min	10 ppm	[40]
	Microcantilever sensor	H ₂ S	2 h	1 ppm	[41]
	Pd coated SnO ₂ nanofiber	H ₂	40 s	0.25 ppm	[42]
	Carbon co-doped acetone sensor	Acetone	100 s	10 ppm	[43]

1.3.3.2 Fluorescent and microfluidics biosensors

The fluorescent-based biosensor consists of a fluorescent or phosphorescent dye which is immobilized with a solid polymer matrix. Dye-polymer coatings are integrated into the thin film and create the biosensor device [44]. The presence of molecular oxygen released in the packaging headspace is influenced into the sensitive coatings of the fluorescent sensor by simple diffusion method and quenches luminescence in a dynamic approach. The concentration of oxygen is then measured using a predetermined calibration curve depending on the degree of alteration in luminescence parameters [45]. This process using a fluorescence-based oxygen sensor is reversible and does not consume either dye or oxygen in the photochemical reactions involved, as well as does not generate byproducts. In addition, a fluorescence-based biosensor can produce a variety of colors in contact with food pathogens. Besides, this biosensor can also work as an electronic tongue or noses which reduce the detection time for pathogens from days to hours. The other biosensor format based on the microfluidic device has been reported for pathogen detection efficiently in real time and with high sensitivity. Silicon-based microfluidic systems are popular as the so-called laboratory-on-a-chip sensor device. The great advantage of microfluidic sensors is their miniature structure in the system and can detect tiny compounds in volumes with time. Although these sensor devices are widely used in some specific areas including medical, biological and chemical analysis, there is no available report for food packaging research and can be a scope for developing smart food packaging.

1.3.3.3 Electrochemical based biosensors

The electrochemical-based biosensor is one of the promising concepts for monitoring food quality based on its function. There are two kinds of electrochemical biosensor depending

on biological recognition mechanism: 1) biocatalytic sensor devices, and 2) affinity-based biosensor [46]. The biocatalytic biosensor consists of redox enzymes, whole cells, or tissue slices as recognition materials which enable to detect target biomolecules. Whereas, in affinity-based sensors, recognition elements are considered as antibodies, antibody fragments, or aptamers. Biocatalytic biosensor devices belong to a range of benefits, i.e., simplistic form and easy to use, small in size, inexpensive, and typically do not require additional equipment, which make it easy to adapt with packaging materials [47]. In addition, these biosensors are highly selective and specific to the target substrate and do not require any pretreatment and separation steps [48]. Although, the identification of selective enzyme is challenging, however, most of these analytes for the biosensors can be recruited from the metabolites of enzymatic reactions. In addition, biocatalytic-based biosensor using whole cells or tissue slices which does not require extensive purification processes and have better activity than isolated enzymes. There are some disadvantages of these biocatalytic sensor devices, including the loss in selectivity and specificity due to the presence of other contaminating enzymes, and slow response time [46]. The advantages of the electrochemical biosensor are that (1) these have a minimum limit of detection, (2) the technique used in the sensor is relatively simple, and (3) these have lower background signal. Some common electrochemical biosensors are reported in the literature for foods, in where single-walled carbon nanotube (SWCNT) based-biosensor was used to detect microorganisms in foods [49], diamine oxidase (DAO)-based biosensor was used to determine the amines in atmospheric packaged foods [50], DNA-based biosensor was used for the potential carcinogen detection in food sample [51] and so on.

Various immobilization methods for ensuring efficient selectivity and specificity of the electrochemical biosensor have been reported in the studies [52]. The common immobilization methods are that 1) covalent binding; 2) surface adsorption; 3) conjugating to nanoparticles; 4) encapsulation; 5) enzyme entrapment method using polymer or gel [53] (Figure 1. 2). The immobilization technique can successfully enhance biosensor stability. The lifetime of biocatalytic sensors is bound to 2-8 weeks, as the enzyme or other recognition components of the biosensor gradually loses its activity [46]. Normally, this lifetime of 2-8 weeks is too short for packaging applications and it needs sufficient time to track the freshness of food products.

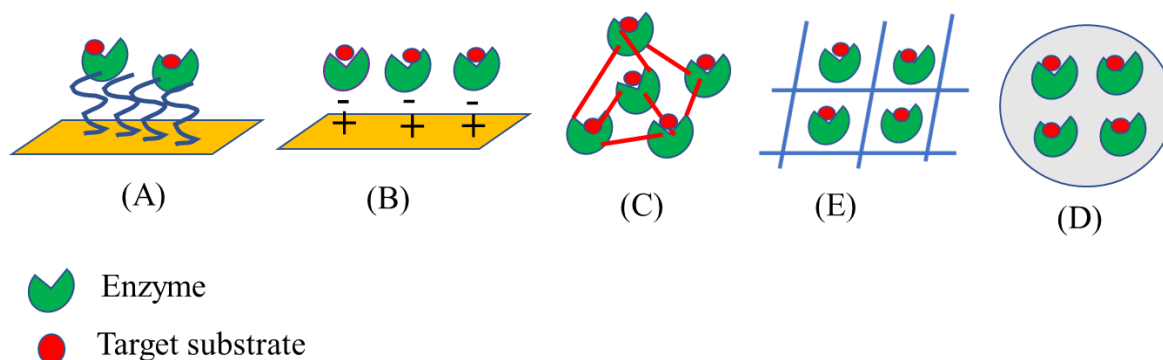


Figure 0.2. Common methods for immobilization of biosensing: (A) covalent binding; (B) adsorption; (C) cross-linking; (D) encapsulation; and (E) entrapment.

1.3.3.4 Gas sensors

The gas sensor is useful for gas leakage detection in the packaging to determine food quality [54]. It can monitor the presence of spoilage gas i.e., basic nitrogen compounds, oxygen or carbon dioxide which are released during food spoilage [22]. In addition, it could be a rapid and sensitive alternative tool for assessing the rancidity in meat products and are used

to detect carbamate pesticides in fruits and vegetables. It has three parts: the sensing electrode which works as a working electrode, counter electrode, and reference electrode. The counter electrode is separated by a thin layer electrode and a reference electrode is used to maintain the constant potential at the working electrode. Firstly, gas diffuses through the hydrophobic barrier and comes to contact with the working electrode. The working electrode has a gas sensing element that responds to the target gas and produces an electrochemical signal. Carbon dioxide sensors are one of gas sensor which is used to determine the level of CO_2 gas using the sensing electrode. The concept of a gas sensor has been shown in Figure 1. 3 to detect CO_2 materials inside the food packages. Gas sensors are superior over conventional sensing methods because these can be employed in the hazardous area, specific to the target gas molecules, and are not influenced by the electromagnetic interferences [8].

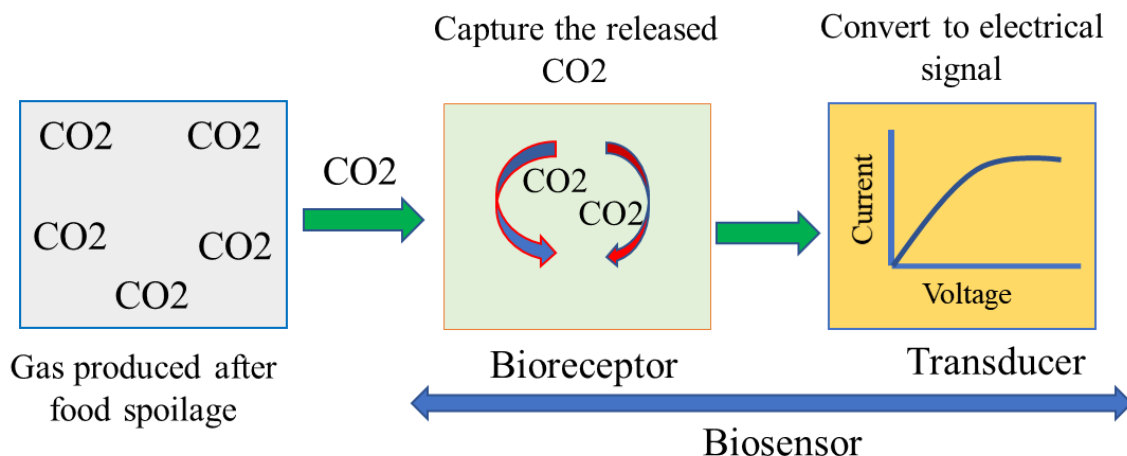


Figure 0.3. Basic principle of gas sensor for gas (CO_2) detection after food spoilage.

1.3.3.5 Opportunities of biosensors for smart food packaging

Biosensors have been used in many fields such as food industry, medical science, environmental field, engineering, and marine field. They can provide better stability and sensitivity than traditional methods. The application of biosensors can create many opportunities for developing smart food packaging in food packaging-related areas. Among these, the potential opportunities for biosensors to develop smart food packaging are shown in Figure 1. 4.

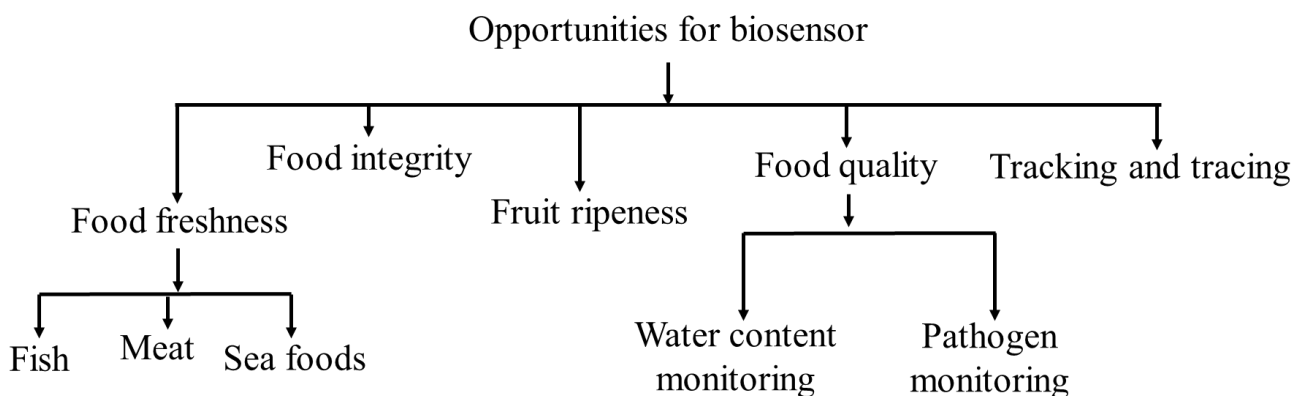


Figure 0.4. Opportunities of biosensor for smart food packaging development.

1.3.3.5.1 Biosensor for food freshness

Food freshness refers to fresh foods that have not yet been spoiled and preserved. In the case of vegetables and fruits, this term considers fresh foods that have recently been harvested and treated; in the case of meat, the freshness of food means they have recently been slaughtered and butchered; in the case of fish, food freshness refers to recently caught or chopped and kept cold. Biosensor is considered to assess food freshness and opted to monitor target metabolites produced during food spoilage. In the previous studies, different biosensors have been used for determining freshness of products, for example, a calorimetric

based biosensor was developed to monitor fish and meat products throughout the detection of basic nitrogen compounds, ammonium gas (NH_3) and nitrogen oxide (NO_2) formed during the amination of aldehydes and ketones in the course of microbial metabolism [55]; glucose biosensor which is modified with L-cysteine and nano-gold solution was developed to monitor the beef freshness throughout the inspecting glucose levels during the meat spoilage [45], though the commercial applications from these biosensors for food packaging have not been either tried. These biosensors, including calorimetric-based and glucose biosensor, can be considered and integrated with food packaging materials to develop smart food packaging, thus they can measure meat, fish and sea food's freshness by monitoring basic nitrogen compounds and glucose levels as a freshness indicator. Xanthanin is one of the major indicators produced during adenine nucleotide degradation in animal tissues [54]. In addition, xanthanin biosensor that is immobilized with xanthine was developed for evaluating xanthanin levels in meat [38,56]. In this case, the xanthanin biosensor can be considered for meat and fish packaging to perform the detection of xanthanin during protein degradation in meat or fish, thus they can confirm the food freshness in packaged products such as ham, luncheon meat, red sausage, etc.

1.3.3.5.2 Biosensor for meat and fish integrity

Food integrity includes food safety, food quality, and food authenticity. Food safety applies to all those risks, chronic or acute, which can affect the consumer's health. Food quality includes all other characteristics that influence the market value of a product. Authenticity of food means the food was not adulterated. In the enclosed areas, fish and meat are spoiled by microorganisms and the pH of these products is altered rapidly [22,57]. The pH indicating sensor is used to detect the pH of spoiled foods as an indicator and to determine the

fish and meat integrity for human consumption. This pH indicating biosensor can be an opportunity in combination with fish and meat packaging to measure food integrity by measuring pH levels of packaged meat, fish and poultry products. The fundamental features of pH indicating sensor are that they consist of dyes and change the dye color in the response of the acidic or basic environment. This sensor system is fast and sensitive, and the response of this sensor is correlated with the pH of spoiled foods [2], thus it can be useful for smart food packaging development to enable the real-time monitoring of meat and fish quality. The concept of pH indicating sensor can be further developed by integrating calorimetric dye method to produce a colorimetric mixed-dye-based food spoilage indicating sensor. The expansion of this concept is a potential possible area for future biosensor development to monitor the other types of packaged foods i.e., poultry and poultry products, desserts, easily prepared foods, seafood products, bakery products, and fresh-cut fruits and vegetables [57]. Although the concept of pH indicating sensor is many in the literature [57,58], the development of pH-based biosensor or indicator for smart food packaging can be a new potential area for future food packaging research because it could be rapid, sensitive, specific, and reusable. Various noses and tongues as the sensors have been created and these sensors have been used to detect food adulterants [59], though their commercial use has not yet been performed. These sensors can be considered for developing smart packaging materials in future to determine the authenticity of foods.

1.3.3.5.3 Biosensor for assessing fruit ripeness

When the unripe fruits are sold in the markets, they are easily bruised and become inappropriate for human consumption. When ripe fruits are sold in the market, it is difficult to determine their ripeness level. After packing the foods for ready to eat, it becomes more

difficult to determine the fruit ripeness because of the packaging materials that cause the obstacle in determining the fruit ripeness. To evaluate fruit maturity, some biosensors have already been developed in research such as a bioelectronic tongue biosensor for simultaneous detection of sugar and phenolic compounds in grapes [60]; an imprinted polymer biosensor for detecting α -pinene, γ -terpinene and terpinolene as maturity integrator in mango [61] and amperometric biosensor for detecting L-malic acid occurred naturally in fruits and used to determine fruit ripeness [37]. These biosensors can be used with packaging materials to develop smart food packaging materials and can obtain an opportunity to determine the maturity index of packaged fruits and vegetables such as apples, grapes, bananas, tomatoes, and mango. In addition, ripeSense™ was developed using sensor labels which can interact with the aromas originated from ripe fruits [2]. In this sensor, when fruits ripen well, it changes the color from red to orange and finally forms yellow color. By observing this sensor color change, retailers and consumers can make choices for their preferred ripe fruits. Thus, they can reduce fruit damage.

1.3.3.5.4 Biosensor for food pathogens and contaminant detection

The biosensor based on color change property is reported to detect the chromogenic substrates of enzyme which is produced by food spoiling microbes [62]. The optical biosensor is one kind of color-based sensor that is based on acoustic transduction and it can show color changes in contact with microbes. It is reported also for detecting microbial contaminants i.e., *Salmonella typhimurium*, *Staphylococcal enterotoxin A* and *B*, *Salmonella* group B, D and E, *E. coli* and *E. coli* 0157:H7 [2]. This optical biosensor may obtain an opportunity to be used in food packaging to detect those mentioned food pathogens. Nanospheres silica immobilized with a fluorescent dye has been described in the literature [63]

and this biosensor may be suitable for meat and dairy food packaging, because it can detect the contaminated microbes i.e., *E. coli* 0157:H7 with showing the color change when meat and fish are spoiled. In addition, a DNA-based biosensor was developed which can detect food spoilage pathogens i.e., *L. monocytogenes* [64] and a single-walled carbon nanotube-based biosensor was developed to detect food pathogens, *Yersinia enterocolitica* [49]. These electrochemical-based biosensors can be used in food packaging and obtain an opportunity to monitor the spoilage condition of packaged foods. Conducting polymer-based sensors have been reported for detecting the food spoilage gas, which is released during microbial metabolism [65]. These conductive polymers are formed by inserting conducting nanoparticles into a polymer matrix, where resistance change corresponds with the amount of gas released. These conducting-based biosensors can be used with packaging polymer to develop smart food packaging sensors.

1.3.3.5.5 Biosensor for tracking and tracing of food package

Blockchain is a distributed digital ledger which can offer transparency beyond the label. In blockchain technology, QR codes are used as an optical label that contains information about the item. Therefore, it can monitor the origin of products and the location where the product was cultivated and can easily be communicated to the consumer. In the past study, QR code-based sensors have been tried to track the aquatic products into the cold chain and have found their traceability [66]. This blockchain technology has not been tried yet for smart food packaging and can be a potential area for future smart food packaging to determine product traceability, though it has some limitations, i.e., costly process, higher energy consumption, and complexity. Since most people are now being associated with the internet over the world, the tracking and monitoring of purchased food products using

sensors and transmitting sensor signals via internet are not difficult for them. Therefore, blockchain technology using QR-based sensors can open the door for a business to manufacture smart food packaging materials for packaging companies. Thus, they can associate with customer needs and increase their satisfaction and loyalty. The optical-based biosensors are used to track the recombinant proteins in process media and downstream in bioprocess [67,68]. These optical type sensors can have the opportunity to be used to trace and track food supply chain inefficiencies in the food packaging industry and can reduce product costs, ensure significant product performance, and ultimately increase profit margins [69]. Global positioning system (GPS) sensors, which is used to track transport systems and monitoring clouds [70]. This system can be manipulated into the food packaging system to monitor the traceability of food packaging when they are transported to another location or in storage. GPS sensors are monitored by a satellite-based navigation system with a network of 24 satellites that provide position, velocity, and timing information. Although this concept of GPS application for food packaging is new, it can be useful for large-scale food packaging in the future.

1.3.3.6 Opportunities of bionanocomposites for smart food packaging

Bionanocomposites can have enormous opportunities for developing smart food packaging due to their physical, barrier, antimicrobial, mechanical and biodegradable properties. The most common opportunities obtained from bionanocomposites have been shown in Figure 1. 5. In the past study, various bionanocomposites such as alkyd/epoxy/graphene oxide (GO), polyester/organically modified clay and graphite platelet/epoxy were narrated [71], and these bionanocomposites exhibited the desired mechanical, thermal and bio-synthetic properties. Based on these properties, these bionanocomposites can be used in smart food

packaging which can enhance the mechanical, thermal and barrier properties of smart food packaging.

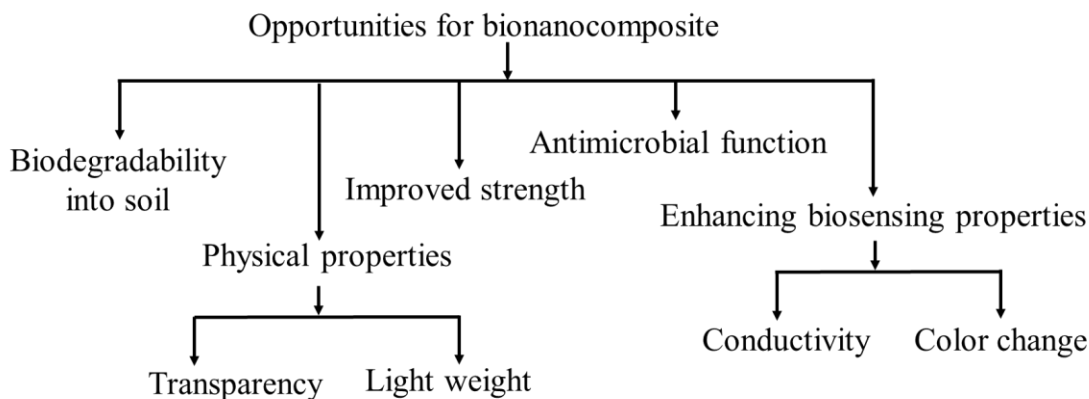


Figure 0.5. Opportunities for bionanocomposite for smart food packaging development.

Generally, most of the traditional packaging is made up of non-degradable composites which can cause environmental pollution because traditional packaging systems can impede the oxygen flow rate to the soil, and thus they decrease the fertility of the land [72,73]. To mitigate these difficulties, different agar-based bio-nanocomposites were prepared by combining different nanofillers, for example, copper nanoparticles and reducing agents (sodium hydroxide and ascorbic acid) [74]. The advantage of these bionanocomposites is that they can absorb ultraviolet light and bear good biodegradable properties. Thus, these bionanocomposites may have an opportunity to be used in smart food packaging as these bionanocomposites do not have health concerns, are readily biodegradable in the soil and environmentally friendly [73]. The current biodegradable materials without having bionanocomposite bear poor barrier, mechanical and functional properties. Therefore, the appliance of bionanocomposites into the commercial packaging materials can be a scope for improving their biodegradable, mechanical, thermal and barrier properties, and thus

they can help to manage the world's waste problem. In addition, bionanocomposites provide many advantages due to their high transparency, lightweight, and moisture resistance [75,76]. Therefore, it may gain the opportunity to be used in smart food packaging to prepare transparent and light weight food packaging materials.

Antimicrobial properties of bionanocomposite retard the growth of microbes in food products [77]. Due to having high contact surface area and enhanced surface reactivity properties, they can be the potential to inactivate the pathogenic microorganisms compared to other micro- or macro-scale counterparts, thus increasing the shelf life of the food products [78,79]. Antimicrobial agents which are effectively used to prepare the bionanocomposites have been illustrated in Table 1. 3. There are mainly two types of antimicrobial agent, which are organic and inorganic. The organic antimicrobial agents are generally less stable compared to inorganic antimicrobial agents, especially at high temperature and pressure conditions. Organic ones are therefore not appropriate for formulating active or smart food packaging films and pose a major obstacle. Consequently, recent research has been focused on inorganic antimicrobial agents such as metals and metal oxides. The most commonly used antimicrobial materials are metallic nanoparticles which are referred to as silver, copper, gold, and platinum and their oxides (TiO₂, ZnO, MgO). As can be observed in Table 1. 3, there are different antimicrobial agents that can be used for packaging to increase food security and the shelf life of foods. Direct addition of these antimicrobial agents with foods can lead to the leaching into food products and cause unintended reactions with food components such as lipids or proteins. Hence, antimicrobial-enhanced packaging films can prove to be more effective. This will help to achieve a regulated and sustained migration of the antimicrobial compound into the foods, enabling microbial inhibition as well as

residual activity reduction during the transportation, processing and storage of the food product. Furthermore, bionanocomposites are not greatly leached into the packaged foods, and toxic effects of bionanocomposite are not highly reported in studies [80,81]. In addition, antimicrobial bionanocomposites can monitor packaged foods such as microbial contamination or expiration dates and take specific measures to record and inform information about the quality or safety of packaged foods.

Table 0.3. Typical antimicrobial materials which are used for preparation of bio nanocomposites.

Classification	Antimicrobial agents	Example	Reference
Organic	Clay	Montmorillonite (MMT)	[11]
		Cloisite Na+	
	Nanoclay	Cloisite 30B	
		Cloisite 20A	
		Cloisite 10A	
	quaternary ammonium modified MMT	[80]	
	Ag-zeolite		
	Natural biopolymer	Chitosan	[82]
		Cellulose	
	Enzyme	Peroxidase, lysozyme	[83]
	Synthetic antimicrobial agents	Quaternary ammonium salts,	[82]
		EDTA	
		Propionic acid	
		Benzoic acid	
		Sorbic acid	
Inorganic	Metal	Silver	[83]
		Copper	
		Gold	

	Platinum	
Metal oxide	Zinc oxide (ZnO)	[84]
	Titanium oxide (TiO ₂)	
	Magnesium oxide (MgO)	
	Silver oxide (Ag ₂ O)	

1.3.3.7 Challenge for biosensor for smart food packaging

There are different kinds of challenges imposed for biosensor in developing smart food packaging. The most common challenges for biosensor in developing smart food packaging can be as follows (Figure 1. 6).

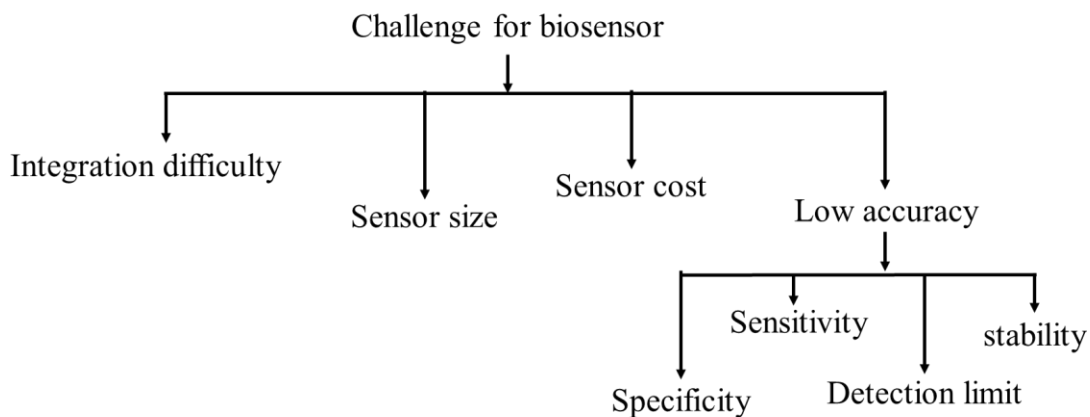


Figure 0.6. Challenge of biosensor for smart food packaging development.

1.3.3.7.1 Challenges of biosensor's size and integration into smart food packaging

Biosensor structure and size depend on what type of detection is associated with the research work. For food packaging, a tiny structure of the biosensor is desired. However, the integration of tiny biosensors into the food package is challenging because of its sensitivity and specificity. Nanosensor like tiny chips is invisible to the human eye and can be

embedded in a food packaging or in containers to allow the monitoring of food quality. But the challenge of nanosensors is that they have limited energy, which is applicable for limited field measurement [85,86]; therefore, the development of wireless nanosensor networks (WNSNs) is essential for smart food packaging industry. However, WNSN is still in its early stages of research and development for application in smart food packaging.

Various nanobiosensors are used to detect food pathogens, pollutants and toxins. Among them, fluorescence-based nano-biosensors [31], microfluidic-based nano-biosensors [87] and SPR nanobiosensors are notable [88]. Although these nanobiosensors are label-free and perfect for quantitative identification, their use for smart food packaging has some challenges, as it requires integral sensor size, high sensitivity and low processing costs. The imprinted polymeric sensor can detect the food pathogens throughout their color change. Though this invention is excellent, it is not fit perfectly with the food packaging materials as it demands expensive polymer material [23] and the integration of imprinted biosensors with packaging has not yet been performed. In addition, they are time-consuming, employ expensive instrumentation, and require qualified panels of evaluation [89]. Because of these limitations, there is a challenge to improve the size and integration method of a biosensor for developing smart food packaging. In addition, the production cost of the biosensor is one of the challenging factors for its commercialization.

1.3.3.7.2 Properties' improvement challenges for biosensor into smart food packaging

Biosensors are widely used technology to detect food pathogens, harmful chemicals, and toxins in the medical and agricultural areas. However, there are some challenges in using biosensors in food packaging, including detection limit, detection time, specificity and stability. These biosensors used need to be improved prior to a successful application of

biosensors in smart food packaging. The detection limit is the minimum amount of the biological entity that can be detected. The detection limit lower than the threshold limit for biosensor is desired because the threshold limit of a pathogen could make a person sick. The threshold limit for infectious food pathogens is varied between $10-10^2$ CFU/ mL (Wang et al., 2020). However, the limits of detection for biosensor are within 10^2-10^6 CFU/mL [91]. Because of this, it is necessary to reduce the detection limit of biosensors, which is a challenging step. In a similar manner, the detection time is the minimum time to detect the biological entities using a biosensor with its sensitivity and specificity. The lower detection time is preferred for biosensor measurements over the conventional methods. The specificity of biosensor describes that the biosensor can differentiate the target entities from non-targeted materials in a sample. As non-harmful bacterial cells, fibers, and proteins interfere with biosensor detection, the high specificity of the biosensor is preferred to reduce the non-specific binding with the biosensor. The stability of biosensor is an important factor, especially when it is considered for food packaging (i.e., meat packaging) because biosensor with high stability is required for industrial benefit. Gas sensor can show stability as 50 days at 20 °C and at least 14 days at 4 °C, but they decrease its stability within 7 days by losing color and sensitivity to CO₂ at room temperature. For smart food packaging, a biosensor is needed to be used for a longer period. But it is still challenging to extend the stability of biosensors for a longer period for smart food packaging, requiring many considerations for the properties of the biosensor.

1.3.3.7.3 Challenges for screen printed sensor into smart food packaging

Thin-film electronics are integrated with printed sensor systems to develop screen-printed biosensors and useful in order to monitor the temperature of perishable foods [92]. They

can detect the presence of oxygen and carbon-dioxide gas levels and can be used for smart food packaging, but their use for food packaging can have some challenges. For example, the sensing materials of a screen-printed biosensor, which are known to be thin-film coatings, have low gas diffusion barriers and are not consistent with the sensing response when the oxygen concentrations are altered [93]. In addition, the reusable thin-film electronics have not come yet which may pose a challenge to the food industry for cost reduction [94]. Although the attention to smart food packaging is increasing globally in recent times, the proper design of a screen-printed electrode for smart food packaging needs to be made from an industrial point of view. Recently, smart labeling and stickers (i.e., food sentinel system barcode, Ageless-eye oxygen indicator, and food fresh labeling) are used in a minor case to communicate with the customer about food safety information. However, these labeling and stickers have some limitations for food packaging applications, for example, the sensitivity and stability of these labeling are very limited (1-7 days) and the results are unstable with the time period. But overcoming these difficulties from labeling and stickers is challenging because it requires many considerations such as the nature of sensing materials, coating process and labeling cost. Also, they require visual and disposal instructions to provide to the consumer to judge the product's integrity. But this is an extra burden and challenging for a food packaging company to teach the consumer about how to safely consume the food product and how to dispose of it after expiration. In addition, the design and manufacturing of screen-printed electrodes for smart packaging technology are one of the challenging steps from the perspective of an industrial view.

1.3.3.8 Challenges of bionanocomposite for smart food packaging

Bionanocomposite consists of nanomaterial components with its polymer matrix and can be beneficial for food packaging applications. Although the potential beneficial effects of bionanocomposites for food packaging have been well described in studies [13], the negative impacts and challenges for bionanocomposites are largely unknown. The challenges for bionanocomposite can be many and the potential challenge for developing smart food packaging are shown in Figure 1. 7.

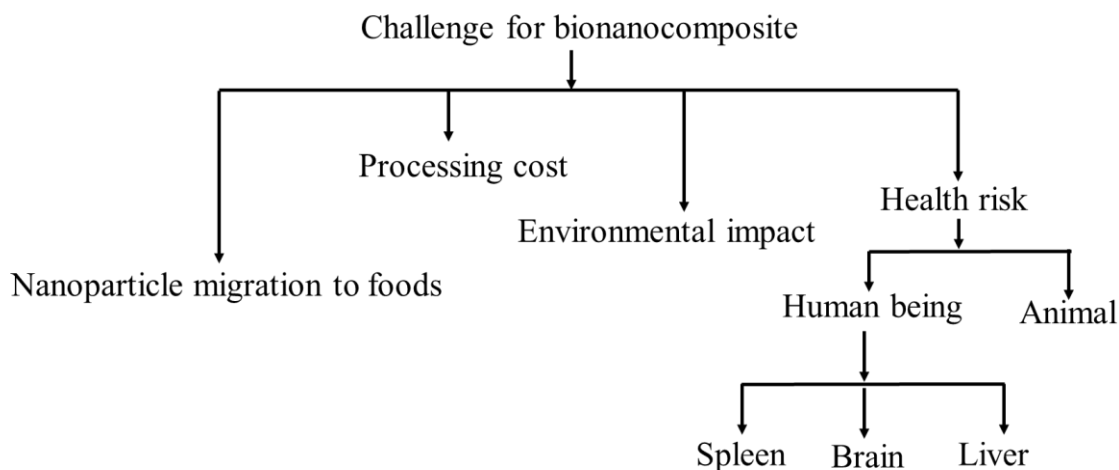


Figure 0.7. Challenge for bionanocomposite for smart food packaging development.

Bionanocomposites are made from a combination of different nano-particles and biopolymers [95]. It has been reported that these nanoparticles may be released from the bionanocomposites and consequently transferred to the foods [96,97]. The migrations of these nanoparticles to foods may be beyond the cellular barriers and can cause oxidative damage to foods. Many people are concerned about the ingestion of these nanoparticles from foods to the human body, but little is known about what happens when nanomaterials enter the

body. Although the release of these nanoparticles i.e., clay from potato starch films, Ag⁺ ions from polypropylene nanosilver composites and zinc from chitosan nanocomposites have been reported in previous studies [95,98], this transition is negligible and below the limit of quantification. The harsh effect of these migrated nanoparticles depends on the physical and chemical properties of the nanoparticles, such as their size, and on the physiological state of the organs of the entry [97]. But there is a particular concern in considering that nanoparticles can migrate into the liver, spleen, brain, and fetus from gas intestinal track, though it is little known about the long-term behavior of nanoparticles. Therefore, it is a major challenge to prevent the migration of nanomaterials from bionanocomposite materials to food mass when considering smart food packaging.

In addition, widespread migration of nanomaterials from food packaging to environments such as soil and water may bring a negative consequence for nature. Due to the large surface area of the nanoparticles, they can react with heavy metals in the soil and water when released [97], therefore they can impose a threat to plant and animal life. Furthermore, if the nanomaterials are not degraded effectively into the soil, they can be accumulated on the soil substrates and damage the fertility of the land [97]. Though the naturally derived nanomaterials like antimicrobial agents are environmentally safe and can represent a lower perceived risk to the food consumer by reducing the risk of food spoilage, the extraction of antimicrobial agents (i.e., sorbates and sorbic anhydride) from the natural source is difficult due to unavailable natural resources. In addition, the processing cost of the bionanocomposites is relatively high compared to the conventional composites.

1.3.3.9 Opportunities and challenges of combined biosensor and bionanocomposite

Biosensor and bionanocomposite are used differently in terms of role and function. Integrating biosensors and bionanocomposites into packaging materials can be a breakthrough in smart food packaging. Their combination with packaging materials can be done in two ways, 1) integration of biosensor and bionanocomposite distinctively with packaging materials; 2) integration of bionanocomposite and their use as a biosensor in packaging materials. The role of the biosensor in the package is to sense the food integrity, while the role of bionanocomposite is to act as the antimicrobial, gas barrier, thermal and mechanical property's enhancer. The use of these combinations in packaging materials can lead to some limitations and has some challenges. First, it requires a simplified method for efficient integration with the packaging system. Because, the sensitivity, specificity, and stability of biosensor are three critical factors, which desires to be stable when they will be used with packaging materials. The sensitivity of sensor material can be influenced based on the packaging type nanomaterials.

To act bionanocomposite as biosensing materials is another challenge due to its functional properties. Different conductive biopolymers, such as polyacetylene, polyphenylene vinylene, polythiophene, and polyphenylene sulfide, are used with different pH fluorescent dye materials (congo red, methyl red, bromophenol blue and so on) to offer biosensing response. Though they show biosensing properties during molecule detection, they do not presume mechanical and thermal properties. This limitation of this sensing packaging film can be removed by adding reinforcement materials, thus the combined functionality of biosensor and bionanocomposite material can be achieved.

Metal nanoparticles are very suitable for chemical sensing, they provide a highly porous surface, and can absorb the analyte molecules like spoilage gas compounds (ammonium,

carbon-di-oxide, etc.). To develop biosensing bionanocomposites, various nano-metals, metal oxides and carbon based nanomaterials have been used such as activated carbon-based bionanocomposites, graphene/chitosan bionanocomposite [99], and zinc oxide-based nanocomposites [100]. Although the invention of biosensing bionanocomposites is excellent, there are some challenging aspects to be considered for smart food packaging. For example, the cost of these biosensing bionanocomposites is relatively high and they have low sensing sensitivity which is not profitable for food packaging applications. Moreover, the research of biosensing bionanocomposite is in its developmental stage and no effective application of it for smart food packaging has emerged yet. A lot of factors need to be taken into consideration, i.e., integration, balancing cost, health, and environmental issues. In this case, multidisciplinary research is required to overcome barriers in the global market and serve the benefit for commercial products.

CHAPTER 2: CHARACTERIZATION OF NANOCELLULOSE AND ACTIVATED CARBON NANOCOMPOSITE FILMS' BIOSENSING PROPERTIES FOR SMART FOOD PACKAGING

(Published in Carbohydrate Polymers, doi.org/10.1016/j.carbpol.2019.115189)

ABSTRACT

The goal of this research is to develop a functional nanocellulose and activated carbon (NAC) film and characterize its biosensing properties for smart packaging applications. The NAC film was prepared from activated carbon powder and nanocellulose gel using the casting method. The nanocellulose contents in the films were varied from 15% to 50% (w/w). Physicochemical properties of the produced films were measured, such as electrical conductivity, water absorption capacity, solubility in water and mechanical properties. The electrical conductivity of the NAC film decreased when nanocellulose content increased. The tensile strength (TS), strain and Young's modulus of films increased significantly from 0.03 to 4.78 MPa, 0.13 to 1.94% and 97.64 to 247.3 MPa, respectively, when the nanocellulose contents increased. Thermal stability was also determined using *thermal gravimetric analysis* (TGA) and differential scanning calorimetry (DSC). The results showed that thermal decomposition was stable in a temperature range of 350 – 400 °C.

Keywords: Activated carbon, Nanocellulose, Nanocomposite, Biosensor, Smart packaging.

1.4 Introduction

Food scientists have become interested in electrochemical biosensor research because its potential for determining the quality of food more easily than conventional methods [49]. Although many studies have been reported on the concept of biosensing for smart food packaging [22,81], biosensor-based packaging for food integrity and quality is not yet common. Indirect indigenization of biosensors in food packages is not suitable due to their poor selectivity, sensitivity and accuracy [101]. In addition, the structure of tiny biosensors for packaging is difficult due to their low signal properties [89]. To overcome these limitations, direct electron transfer is preferred over package components, which ensures low cost, fast response and high sensitivity [102]. In direct electrochemistry, the most commonly used ingredients are carbon [103], gold [104], silver [105] and metal oxides [106]. They are used to promote improved electron transfer rates. Among these electro-promoters, carbon is a suitable and widely used material for electrocatalysis and electroanalysis [107]. It has different forms, including graphene, carbon nanotube (single or multi-walled) and activated carbon [108].

Activated carbon (AC) was chosen for this study because it has recently attracted widespread attention because of its desirable physico- and electro-chemical properties, such as uniform porosity, large surface area, low toxicity, good electrical conductivity, and surface functionality [109,110]. It has a mesoporous structure, which can absorb the gas or liquid molecules quickly because of its well-ordered pore structure, narrow pore size distribution and high specific surface area [111]. In addition, the adsorption properties of AC have been studied for their use in biosensors [112]. These unique properties of AC make an ideal support for the preparation of electrode materials in multiple applications, such as super-capacitors, batteries [109], catalysis and bioanalysis [113]. In the present study,

nanocellulose was loaded with the AC in order to achieve a carbon film format that can work as conductive materials.

Cellulosic nanofibers (CNF) (4-25 nm diameter) have gained attention as reinforcement materials [114]. They have unique and attractive features, including biodegradability, low expense, good chemical stability, low density and high aspect ratio [115,116]. The alignment and orientation of CNF with polymer matrixes reforms ordered structures, making them good candidates for the design of sensing and biosensing film [117]. Unfortunately, CNF materials are dielectric; however, the electrical conductivity of CNF can be improved by adding carbon materials like AC for uses in biosensing devices [101].

Incorporation of CNF into the nanocomposite membrane is reported to exhibit electrical, mechanical and barrier properties, hence it garners significant scientific attention [118]. The surface charge of CNF is controlled by different chemical treatments, such as partial carboxymethylation and phosphorylation [118]. Nanocellulose modified with carbon materials (a single walled-carbon nanotube) is also reported as an efficient catalyst for electrochemical oxidation, which leads to remarkable electrochemical characteristics [119]. In this study, a NAC film that combines the advantages of nanocomposites prepared with AC and CNF was fabricated to form mechanical, thermal and electrochemical sensing film for smart food packaging. It is expected to afford excellent adsorptive capacity, catalytic and conductive properties and offer potential use in smart food packaging. Although different kinds of the film have been made for the food packaging such as pectin and nano-cellulose film [120], starch film reinforced by laver [121], chitosan film [122]; gelatin film [123], poly-lactic acid film [124] and so on, all of these films have poor mechanical characteristics and even they are not suitable for the use of electrical conductivity. Furthermore, although

some films produced by conductive polymers, such as polypyrrole and polyaniline polymer, are reported in the literature for smart packaging [19,125], these films exhibit poor mechanical and thermal properties, consume the high cost of raw materials and its electrical current sensitivity fluctuates over the time [126]. Depending on these features, the NAC film has been considered as an alternative to being potential for smart packaging, although the NAC film is still under developing. To the best of our knowledge, there is no similar research or NAC film used for smart food packaging was reported. The current study focuses on the NAC film preparation by combining AC and CNF and an analysis of their effects within various mechanical, physical and thermal conditions. The main goal of this research is to integrate the biosensor concept into smart food packaging. Therefore, the objectives of this study are to 1) prepare NAC films with various CNF and AC contents; and 2) observe the electrochemical, thermal and mechanical properties of CNF and AC film.

1.5 Materials and methods

1.5.1 Materials

The activated carbon (Norit® GAC 1240 Plus) was procured from Cabot Corporation (Georgia, USA). The purity of AC was greater than 98%. The aqueous gel of CNF (5–20 nm, crystalline index: >87%, purity of 3%) was purchased from the Process Development Center at University of Maine (Orono, ME, USA). A 10% (v/v) phosphate buffer saline (PBS, 0.1 M, pH 7.4, 0.8% NaCl) was procured from Thermo Fisher Scientific and prepared by mixing with purified water. Potassium hexacyanoferrate $[\text{K}_2\text{Fe}(\text{CN})_6]^{-3}$ was purchased Sigma Aldrich (St. Louis, MO, USA). The potassium chloride (KCl, purity \geq 99.0%) used for our solution was bought from Sigma Aldrich (St. Louis, MO, USA). Throughout the experiments, triple distilled water was used.

1.5.2 Preparation of NAC films

To synthesize NAC films, the first step is to prepare CNF suspensions. 2.5 g of CNF aqueous gel was put into 30 mL of deionized water and then gently stirred at about 50°C for 30 min to create a CNF suspension. Subsequently, based on calculation, different amounts of AC powder were individually added to the prepared CNF suspensions to get NAC mixtures with AC contents of 85%, 70% and 50% of dry weight, corresponding to CNF contents of 15%, 30% and 50% of dry weight. After that, the solution of NAC mixture was homogenized for 15 min to get a new NAC suspension using a hand-held homogenizer (PRO scientific, USA). After homogenization, 30 mL of each NAC suspension was poured into a petri dish for casting a NAC film. As different NAC suspensions were poured into petri dishes, they were dried to form NAC films in an oven at 60 °C for 12 h. The dried films were peeled from the petri dishes and then conditioned in a container at 50-60% relative humidity (RH) and room temperature for 2 days prior to any analysis or characterization. All different types of NAC films were prepared in triplicate for characterization. The final dried films were named according to the CNF contents and are termed 15%, 30% and 50% NAC films in this study. Thickness of the film was measured throughout a hand-held micrometer (Esslinger, MN, USA).

1.5.3 Characterization methods

1.5.3.1 Electrochemical properties

The NAC films were characterized electrically using linear sweep voltammetry (LSV), cyclic voltammetry (CV), differential pulse voltammetry (DPV) and electrochemical spectroscopy (EIS). For LSV measurement, a two-electrode system was set up, where one of the multiple-input electrodes was considered as a working electrode and a common ground

was used the counter electrode. The reference electrode and counter electrode from the instrument were linked to each other. To measure the resistances of NAC film, a 2-pair distance with 6 mm gaps was chosen as the base sensing platform [47]. A change in resistance was confirmed throughout the electrical responses inspected in NAC film. In this study, LSV measurements were done with a potentiostat device for each repetition (DY2013, Digi-Ivy, Inc., Austin, USA). The slope of the current/voltage curve obtained from 0.0 to 0.1 V for each measurement was calculated using linear regression analysis. Afterward, the resistance (R_s) was calculated from the inverse of current/voltage value. In this case, the experimental data from LSV are described as means and the standard deviations were calculated depending on the number of repeated tests.

CV and DPV measurements were performed to characterize the stepwise modification of the electrode surface. For these tests, a gold working electrode (2 mm diameter), platinum wire as a counter electrode and Ag/AgCl (3.0 mol L⁻¹ KCl) as a reference electrode, which were immersed in PBS buffer (pH 7.4) containing 2.5 mmol L⁻¹ [Fe (CN)₆]³⁻ and 0.1 mol L⁻¹ KCl during the test. 15%, 30% and 50% NAC were sequentially dropped onto the working electrode and the signals of CV and DPV were collected. The scan rate for CV and DPV was 100 mVs⁻¹, while the potential ranged from +0.6 to -0.2 V. EIS technique was performed to compare the impedance properties of NAC films. The frequency range for EIS fluctuated between 0.1 and 10⁶ Hz at an amplitude of 0.01 V using EC-lab software (Bio-Logic Science Instruments). All the experiments were completed at room temperature (20 ± 2 °C).

1.5.3.2 Thermal stability

Thermal properties of the NAC films were analyzed using a differential scanning calorimeter (DSC) (DSC-Q2000, TA Instruments, USA) and thermogravimetric analyzer (TGA) (Q5000 SA, TA Instruments, USA). Sample preparation for TGA and DSC was performed by following the procedure described previously with one minor modification [127]. 3 mg of each 15%, 30%, and 50% NAC film sample were directly placed into a hermetically sealed pan using a Tzero hermetic lid. Afterwards, the specimens were heated under a nitrogen atmosphere in the range of 20–400 °C with a heating rate of 10 °C.min⁻¹ and a gas flow rate of 20 mL.min⁻¹. The reference was an empty aluminum pan.

1.5.3.3 Mechanical properties

The mechanical properties of NAC films were evaluated according with ASTM D882 [77]. Prior to the test, the film strips were cut uniformly to 50 mm long and 20 mm wide. Afterwards, the strips were conditioned in a desiccator for 24 h at 25 °C at 50% relative humidity. A texture analyzer (Texture Technologies Corp., Scarsdale, NY, USA), equipped with Texture Exponent 32 software, was used to measure tensile force and deformation. The initial grip spacing, and crosshead speed were set at 100 mm and 0.5 mm/s, respectively. Tensile strength, strain and Young's modulus of the films were calculated from the force and deformation data recorded by the software. Three replications of the NAC film were evaluated for each measurement. Tensile strength (TS), strain and Young's modulus were calculated using the following equation:

$$TS = \frac{\text{Maximum applied force}}{\text{Film thickness} \times \text{Film width}} \quad (1)$$

$$\text{Strain} = \frac{\text{Elongation}}{\text{Original length of film}} \quad (2)$$

$$\text{Young's modulus} = \frac{\text{TS}}{\text{Strain}} \quad (3)$$

1.5.3.4 Solubility in water

Solubility of the NAC film in water is defined as the dispersing rate of the film particles per weight of the film into the water. It was determined by following the studies previously described with minor modification [114]. To determine the water solubility of the films, they were cut into rectangular pieces ($40 \times 30 \text{ mm} \approx 200 \text{ mg}$) and stored in a desiccator with desiccant (P_2O_5) to keep $\text{RH} \leq 10\%$ for 2 days. The initial weight of each film strip was recorded and then placed into beakers with 100 mL deionized water ($18 \text{ M}\Omega$). Afterwards, films were agitated with a constant stirring rate (300 rpm) for 1 hour at room temperature. After stirring, the remaining pieces of the film were filtered through filter paper (Whatman no.1) and then dried in an oven at $70 \text{ }^\circ\text{C}$ until they attained a constant weight. The weights of film samples were measured in triplicate for each test. Water solubility was calculated with following equation described previously [77].

$$\text{Solubility (\%)} = \frac{(\text{Initial dried weight of film} - \text{Final dried weight of film})}{\text{Initial dried weight of film}} \times 100 \quad (4)$$

1.5.3.5 Water absorption capacity

The water absorption capacity of NAC film is defined as the rate of maximum water absorbed by the film to achieve the desired consistency. The water absorption capacity of NAC film was determined by following the procedure previously described [77]. Briefly, NAC films ($40 \times 30 \text{ mm} \approx 200 \text{ mg}$) were firstly dried in $60 \text{ }^\circ\text{C}$ for 2 h and then weighed. Afterward, the dried NAC film strips were added to 150 mL of distilled water and permitted to stand for 2 h for swelling. Finally, the swollen films were weighted after draining and this procedure was performed in triplicate for each film measurement. The amount of water

retained by the NAC films per dried weight sample was calculated using the following equation.

$$\text{Water absorption capacity (\%)} = \frac{(\text{Final weight after water absorption} - \text{Initial weight})}{\text{Initial weight}} \times 100 \quad (5)$$

1.5.3.6 Water vapor permeability

Water vapor permeability (WVP) is considered as a property of NAC film that permits the passage of water vapor through the microspore of NAC film. The WVP of NAC film was determined gravimetrically using a dry cup method described in the previous study with slight modification [120]. Briefly, the test cup was filled with distilled water (15 mL) and then tightly covered with NAC film strips (diameter: 22 mm). Afterwards, each cup sample with film was initially weighed and then placed into the desiccator with $\leq 10\%$ RH for 1 days. Subsequently, each cup was weighed again to evaluate the water vapor permeability of NAC film. The WVP of the film was calculated as the ratio of weight loss of water per unit square area of the film sample with the following equation.

$$\text{WVP} = \frac{\text{Initial weight of cup sample} - \text{Final weight of cup sample}}{\text{Area of film used}} \quad (6)$$

1.5.3.7 Viscosity measurements

The viscosity of the NAC film suspension was determined by following the procedure previously described with minor modification [121]. To determine the viscosity of the film suspension, rheometer (ATS Rheosystems, Bordentown, NJ, USA) was used and fixed it at room temperature (20 ± 0.1 °C). The temperature of the tested samples was monitored by platinum resistance thermometer sensors (accuracy of ± 0.1 °C) and controlled by a Peltier system. The NAC suspension of 15 mL volume was poured into a rheometer cup

and then the viscometer spindle was dipped into the cup solution for 2 min to obtain thermal equilibrium conditions between spindle and the NAC suspension. Then, the rheometer spindle was operated at 30 rpm with continued shearing. Tests for each film suspension were performed in triplicate.

1.5.3.8 Fourier transform infrared spectroscopy

A Tensor 37 spectrophotometer was used to inspect the interactions between nanocellulose and activated carbon through the fourier transform infrared spectroscopy (FTIR) spectra. The sample holder of FTIR for the solid films was aligned at 45° to the incident beam and parallel to the ground. The range of FTIR spectra was performed with 500 to 4000 cm^{-1} and collected with 64 scans with regulation of 4.0 cm^{-1} by the omnic spectroscopy software [128].

1.5.3.9 Scanning electron microscopy

The microstructures of nanocellulose modified with activated carbon were visualized under scanning electron microscopy (SEM) (Hitachi-S-3400, filament-based SEM, MO, USA). For SEM observation, samples of the film were first cut ($2\text{ mm} \times 2\text{ mm}$) and then dried at $60\text{ }^\circ\text{C}$ for 24 h. To evaluate the internal structure, films were then immersed into liquid nitrogen and fixed into the support. Then, the film was coated with Au using a sputter-coater (DC-150, sputtering system, 10 nm of Au) prior to SEM observation. The surfaces of the Au-coated film sample were examined under an electric voltage of 10 kV at a working distance of 10 mm with a $1500 \times$ magnification.

1.5.4 Statistical analysis

The measurements of each test of the film sample were replicated three times and the data were reported as an average \pm standard deviation. Analysis of data were performed by a one-way analysis of variance and the differences between the means were compared using the Duncan multiple range test with a defined significance level of $p < 0.05$.

1.6 Results and discussion

1.6.1 Physical properties of film

The NAC films and their surface morphology with varying CNF (wt. %) and AC (wt. %) contents have been shown in Figure 2. 1. The films were physically and visually inspected and shown to be flexible, free standing and not transparent. The thickness and weight of each film were measured and found not significantly different from each other with increasing CNF and decreasing AC contents. The average thickness and weight (diameter: 71 mm) of films were recorded as 0.37 mm and ca. 500 mg, respectively. The produced films exhibited black color in their final appearance. But, depending on the CNF contents, an increase in the milky and opaque characteristics appeared in the film surface. These films were generally easy to handle and homogeneous with no flaws (Figure 2. 1A). The surface morphology of films observed under SEM indicated that 50% NAC imparted a relatively compact and hard surface compared to the 15% and 30% NAC films (Figure 2. 1B). Therefore, 50% NAC film formed the strongest adhesion on the interface between AC and CNF.

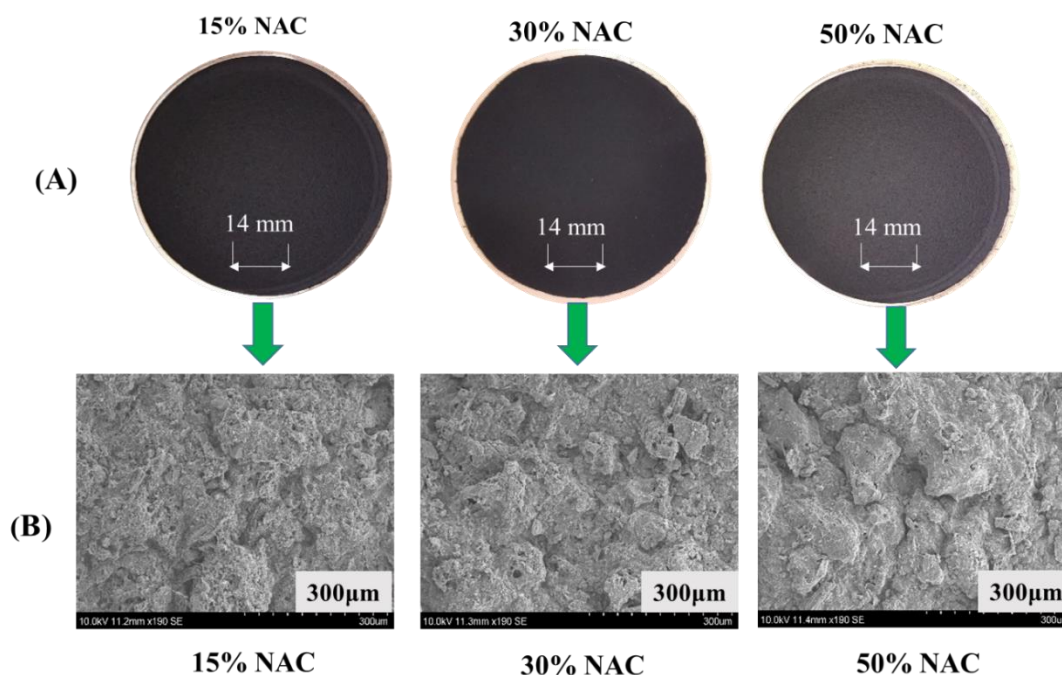


Figure 0.1. Physical properties of 15%, 30% and 50% NAC films. (A) The images of NAC film with its different NAC contents (15%, 30% and 50%); (B) surface morphology of NAC films observed by scanning electron microscopy (SEM) with 300 μm.

1.6.2 Electrical properties of the NAC film

The initial investigation was focused on determining the electrical properties of NAC film synthesized with varying CNF and AC contents. NAC films have AC materials that are the semiconducting ingredients; thereby they can obtain electrical conductivity. During the film formation, the hydrophilic side walls of the AC are irreversibly adsorbed onto the hydrophobic ends of CNF via π - π stacking interaction with noncovalent bonding [129]. Thus, the effects of CNF as a recombining agent synthesized with AC obtains resistance response during electrical analysis. Figure 2. 2A demonstrates that binding of CNF with

AC decreased the current flow and increased the resistance (R_s) of the NAC film. As can be observed, resistance values significantly increased from 1.5 k Ω to 12.5 k Ω , when the CNF contents to the film increased from 15% to 50%. It is estimated that CNF molecules significantly increased resistance response to the film. This increase in resistances, i.e. a decrease in current, is reported by acquiring the negative charge received from non-conductive materials [77]. Interestingly, film synthesized with >50% CNF, which means <50 AC, have not produced resistance (R_s), which confirms that NAC film blended with $\leq 50\%$ CNF is suitable for producing sensor properties. Therefore, NAC films blended with ≤ 50 CNF and ≥ 50 AC can have potential for developing biosensing film for smart food packaging.

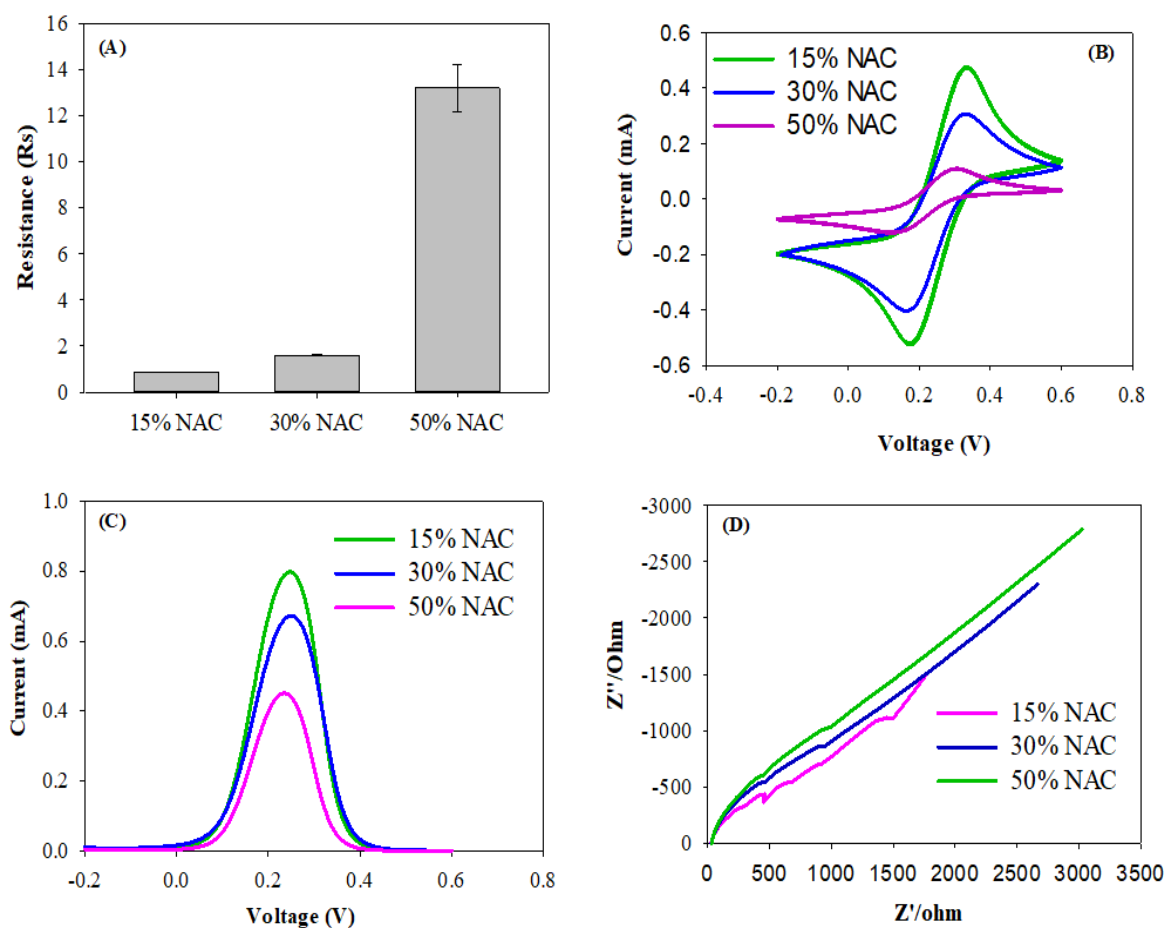


Figure 0.2. Electrochemical analyses of 15%, 30% and 50% NAC films. (A) Resistance (R_s , $K\Omega$) of NAC films measured by linear sweep voltammogram (LSV); (B) cyclic voltammogram of NAC films; and (C) differential plus voltammogram (DPV) of NAC films; (D) impedance spectra of NAC films.

Figure 2. 2B shows, when the Au electrode was assembled with the 15% NAC film suspension, a significant peak current was achieved. This rise of peak current demonstrated that the suspension of 15% NAC film merged with the Au electrode employed a large surface area and enabled to efficient electron transfer in the $[\text{Fe}(\text{CN})_6]^{3-}$ solution. After assembling the electrode with 30% NAC, the peak current decreased. When the sensing

electrode surface assembled with 50% NAC, the peak current was further reduced. This current reduction indicated that the binding of CNF with the AC molecules hindered the diffusion of the redox species to the electrode surface, and thus resulted in a decrease in voltammetry current behavior. A similar current reduction was observed when non-conductive reagents (1-pyrenebutanoic acid succinimidyl ester and carboxymethyl cellulose) were immobilized on single or multi-walled carbon nanotubes (SWCNTs or MWCNTs) connected Au electrode surface [49,130].

As can be seen in Figure 2. 2C, the 15% NAC amended electrode showed the highest peak current compared to the 30% and 50% NAC film. After increasing CNF, ranged from 30% to 50%, and decreasing AC, from 70% to 50%, the signal of peak current was further reduced. Peak current decreased with CNF content. This can be explained by the fact that decreasing AC and increasing non-conductive CNF in the film improved steric inhibition between the reducible groups; therefore, they reduced current response and hybridized the Au electrode surface.

The electrochemical impedance spectroscopy (EIS) was identified using 15%, 30% and 50% NAC film deposited on the Au sensor electrode. Figure 2. 2D shows that the impedance of 50% NAC film was significantly higher compared to the impedance of 15% and 30% NAC. A similar phenomenon was reported previously whereby the addition of 1-pyrenebutanoic acid succinimidyl ester to the carbon nanotube connected electrode surface caused a significant rise of impedance [47]. Several factors could play a role in reducing the peak current and increasing the impedance. For example, one possibility is that the CNF is the nanocrystal reinforcement components and AC is the hydrophobic mesoporous components [111,114]. After ultrasonic suspension, CNF was bonded with AC to form a dense

network held together by strong inter-CNF-AC bonds, which resulted in an increase of the steric hindrance and inhibited the electrical current flow. Furthermore, increased negative charges, which was produced from the redox reaction, prevented the negatively charged $[\text{Fe}(\text{CN})_6]^{3-}$ anions in the redox solution, and resulted in an increase in the EIS impedance [131].

1.6.3 Mechanical properties

As can be observed in Figure 2. 3, when the CNF (wt. %) increased in the film, mechanical properties, such as tensile strength (TS), strain and Young's modulus, increased simultaneously. The similar results were found in the previous study, when biopolymer-based films combined with nanoparticles increased the TS, strain and Young's modulus [77]. This increase of TS to packaging materials can be the vital criteria for food packaging applications [120]; the high TS of NAC film is desired and can permit the film to resist the normal stress encountered during food shipping, handling and transportation. One possible reason of increasing TS, strain and Young's modulus is related to interfacial interaction between AC and CNF because the nanosized CNF particles, of an optimal length of 5–20 nanometers, are hydrophilic materials which are perfectly twisted with hydrophobic particle AC and produced the rigid pathways in the NAC film matrix.

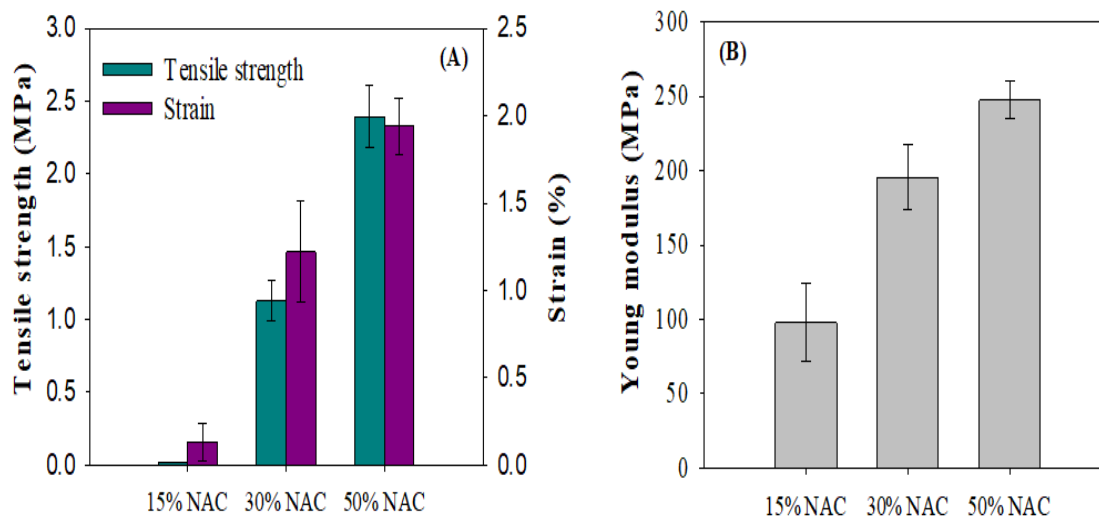


Figure 0.3. Mechanical properties of 15%, 30% and 50% NAC films. (A) Tensile strength (TS) and strain of NAC films; (B) Young modulus of NAC films.

The films with CNF allow more rigidity and strength during the application of tensile force, thus they resulted in a decrease in the plasticizer properties. When the 15% NAC film was employed, TS was negligible and gave under lower strain during tensile force. This illustrates that films with higher TS are more preferred and convenient for food packaging applications [132]. In a previous study [114], nanoclay based polymer film produced an increased TS and Young's modulus. According to Wu et al., nanoclay particles used as a filling agent to the film increased TS and wear performance of the starch film [129]. As 50% NAC films have significantly higher TS ($p < 0.05$) to bear the maximum applied load than the 15% and 30% NAC film, the 50% NAC film can be considered more suitable for food packaging applications.

1.6.4 Thermal stability of films

The thermal degradation properties of NAC films depending on the CNF and AC were determined using TGA (Figure 2. 4A). The degradation stages have been divided into three main regions, which occurred consecutively. In stage-I, temperature ranged between 100 to 270 °C, where physically weak and chemically strong bound water molecules were evaporated from the film sample. The second stage is the transition region, occurring between 270 and 390 °C, when NAC film composites structurally degraded, and the weight losses occurred at about 60 %. As can be observed, 50% NAC film was significantly degraded at this stage compared to other film contents. Therefore, it can be concluded that 15% NAC film was more rapidly crystallized than 30% and 50% NAC film sample because it has a low amount of nanocellulose than 30% and 50% NAC film. Moreover, the sample of 50% NAC film was significantly thermally affected compared to the 15% and 30% NAC film at this stage due to enhancing the thermal degradation of the large amount of nano-cellulose. The third stage was seen between 390 and 590° C. In this stage, mass loss occurred due to the oxidation of residual organic matter. The NAC film with higher CNF contents produced higher degradation, which shows that higher AC blended into the film can be thermally stable.

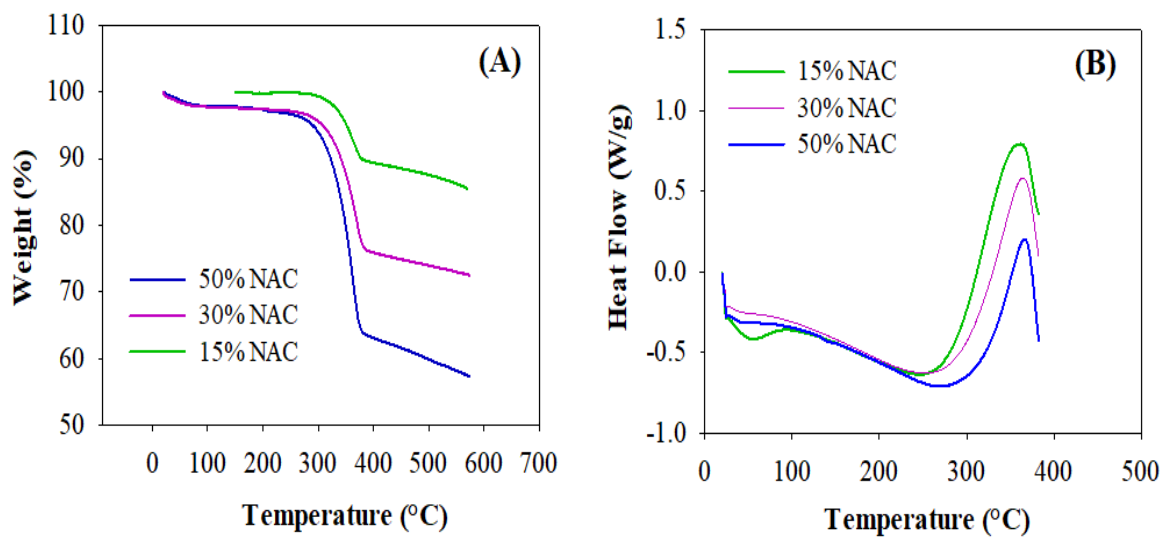


Figure 0.4. Thermal analysis of 15%, 30% and 50% NAC films. (A) Typical thermogravimetric (TGA) analysis curves; (B) differential scanning calorimetry (DSC) curves of NAC film.

The thermal attributes of NAC film determined by differential scanning calorimetry (DSC) are shown in Figure 2. 4B. In general, the NAC sample absorbed heat and then is subjected to release of the bound water molecules until crystallization. The lowest crystallized temperature for this film appeared at ca. 280 °C. After that, NAC films began to decompose and release exothermic heat flow. The peak temperature related to melting points for NAC samples was ca. 390 °C. The heat flow rate was also considered in this study. The heat flow rate of 15% NAC film was significantly higher than those of the 30% and 50 % NAC films. These results indicated that higher thermal energy was released to dissociate the interactions in the film matrix. Furthermore, 50% NAC films demonstrated lower heat flow, which may be related to the mechanism of CNF-AC interaction. This can be explained that 50% NAC films absorbed significantly higher heat and released less heat flow

during the sample degradation. It is reported that low heat flow is associated with strengthening the interactions in starch films treated with nanoclay [127]. Since 15% NAC has a relatively higher percentage of AC (85%) and lower percentage of CNF (15%), it leads to significantly higher heat flow because of the enhancing of exothermic behaviors of AC in the NAC film. Therefore, it can be concluded that the thermal properties of NAC films can be affected by the method of film preparation.

1.6.5 Functional and microstructural properties of film

1.6.5.1 Water solubility and absorption capacity

The NAC films' water solubility was tested to define the comparative applications of NAC films for smart food packaging. In general, AC is highly sensitive to water molecules compared to CNF. Therefore, an increase in CNF quantity (i.e., a decrease in AC) into the film reduced water solubility performance (Figure 2. 5A). This is because the incorporation of CNF to the film suppresses the water diffusion rate. By incorporating the crosslinking structures or incorporation of nanoparticles to the biopolymer-based film, the water solubility rate was reduced in a similar manner [77]. According to the Voon et al., when the nanoclay, used as a reinforcing agent, was incorporated into the starch film, the water solubility of the film decreased [132], which was consistent with the solubility results obtained from our test.

Water vapor permeability was also tested to verify the barrier functions of NAC film. For food packaging, a film with high vapor barrier properties is desired because it can reduce moisture transfer rates between the outside packaging environment and inside packaged food. As can be shown in Figure 2. 5A, 15% NAC film showed significantly higher water vapor permeability compared to 50% NAC film. As 50% NAC film is more efficient in

preventing water vapor permeability than 15% and 30% NAC film, it may be preferred for food packaging application. Increasing the CNF content of the NAC film has a greatly reduced water vapor permeability (WVP). This is because CNF can fill up the microspore structures distributed over the films, thus decreasing WVP. Free water vapor molecules do not interact as strongly as with nanocomposite films alone [120]. Chitosan-based films with added zinc oxide nanoparticles further reduced WVP significantly [107].

Our work further determined the water absorption capacity of the NAC film; results are illustrated in Figure 2. 5B. As observed, the water absorption capacity of 15% NAC film was significantly higher compared to the 30% and 50% films. Conversely, water absorbance increased for all films between 2 and 4 h, then decreased from 4 to 8 h for 15% and 50% NAC film. A plateau of water absorbance capacity was observed between 2 and 14 h for 30% NAC film. Introducing an increased quantity of CNF (15% to 50%) and decreasing AC (85% to 50%) reduced the water absorption capacity. This decrease in water absorption capacity could be attributed to the hydrophobic interactions between CNF and AC in the film structure. As AC has a large surface area and porous structure, so 15% NAC film has higher absorption capacity in its microspore structure. This result was consistent with result of starch-based film [133,134]; when the quantity of nanoclay grew in the film, water absorbance capacity decreased significantly.

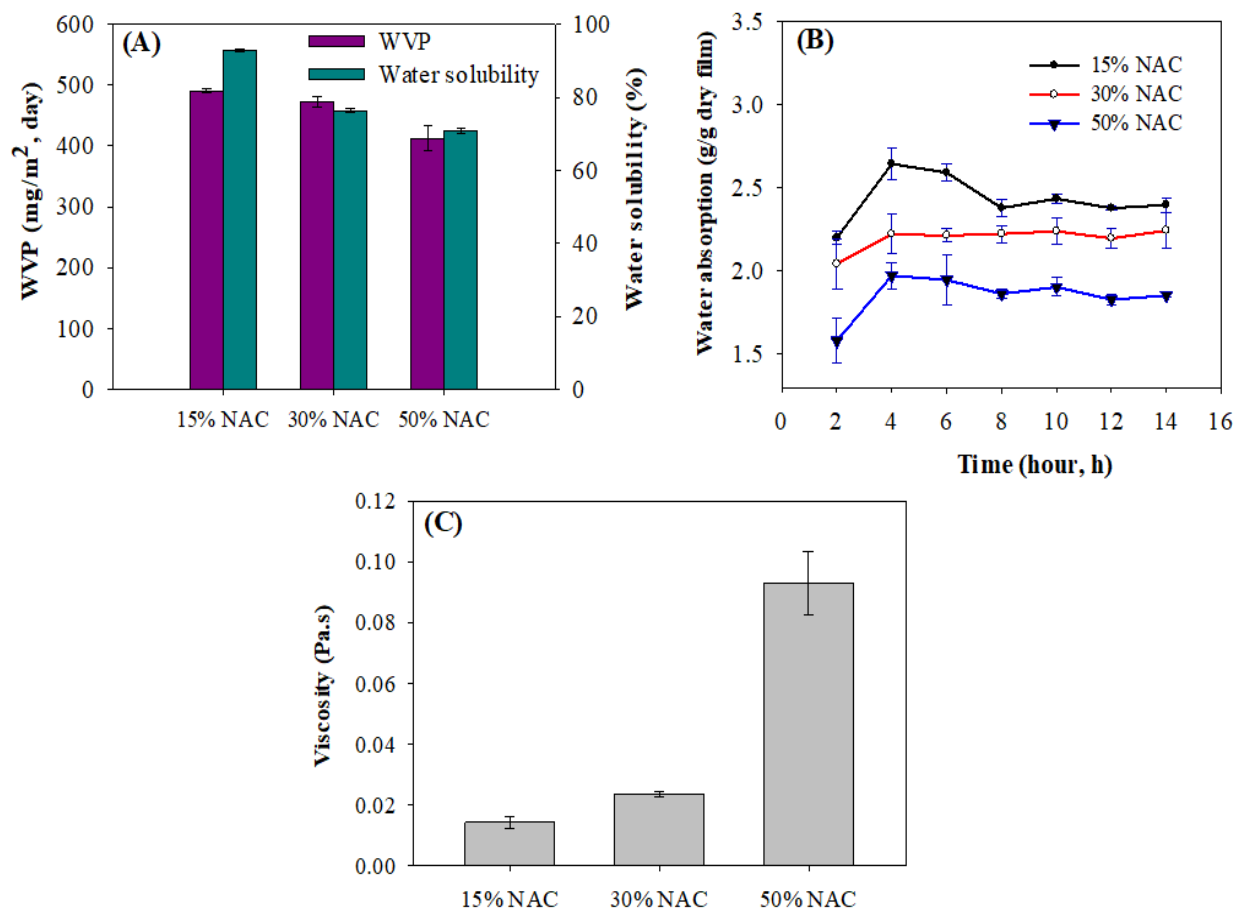


Figure 0.5. Physiological properties of 15%, 30% and 50% NAC films. (A) Water vapor permeability (WVP) and water solubility of NAC film; (B) water absorption capacity of NAC film depending on time period (2, 4, 6, 8, 10, 12 h); (C) effect of nanocellulose (CNF) on the viscosity of NAC films.

Viscosity is one of the main factors that affects the processability of the casting film [121]. In order to determine the effect of CNF and AC to produce NAC film, viscosity was measured using a Hybrid Rheometer. As seen in Figure 2. 5C, viscosity of the 50% NAC film suspension was significantly higher than 15% and 30% film suspensions. At the 15% NAC

suspension, the viscosity was not affected significantly. This result was consistent with the viscosity result obtained from starch film suspension, where the quantity of laver content in the starch film increased, the viscosity of film suspension increased [121].

1.6.5.2 Infrared spectroscopy analysis (FTIR)

In order to ensure proper interactions between CNF and AC, FTIR spectrum was performed through UV-vis characterization and their wave spectra is presented in Figure 2. 6. All of the NAC films showed no significant difference in the FTIR band. The characterized peaks were displayed to 690 cm^{-1} , 1085 cm^{-1} , 1600 cm^{-1} , 2349 cm^{-1} , 2900 cm^{-1} and 3450 cm^{-1} , which correlated to C=C bending (alkene), the stretching vibration of carboxy groups (C-O), aromatic carbon-carbon double bonds (C=C), carbon-dioxide bonds (O=C=O), hydrocarbon bonds (H-C) and alcohol bond (O-H, strong intermolecular bond), respectively. As observed in the Figure 2. 6, the peak intensity associated with the NAC film decreased with increasing CNF and the intensities were dependent on the relative compositions of the NAC films. This result implied that peak intensities were influenced with the CNF concentrations and they were successfully incorporated with AC in the NAC film. Similar phenomenon was observed when peak intensities decreased as nanocellulose concentrations increased to the polyaniline-based film [126].

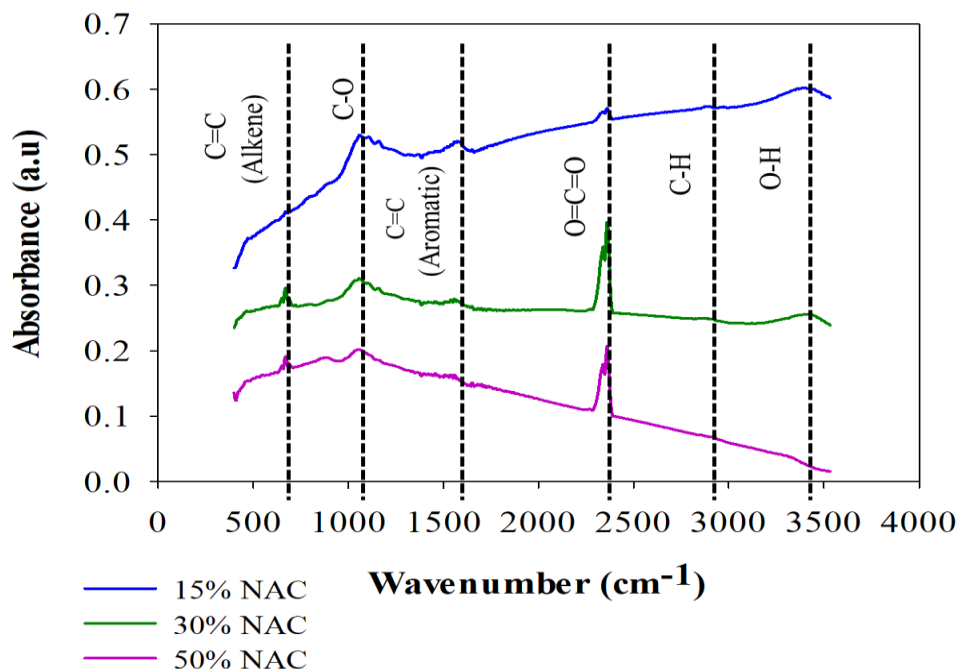


Figure 0.6. Infrared spectroscopy (FTIR) spectra of 15%, 30% and 50% NAC films. The films contained different nanocellulose (CNF) and activated carbon (AC) contents.

1.6.5.3 SEM analysis of activated carbon

Scanning electron microscopy (SEM) is considered as an important technique for evaluating the microstructure, as well as the size distribution, of native and AC modified CNF particles. The SEM micrographs showed balanced dispersion and random direction in the NAC film. The intricate and homogenized structure indicated that two constituent elements (CNF and AC) improve the mechanical properties of NAC film. As shown in Figure 2. 7A, CNF formed thin fibers at the nanometer scale throughout the film and produced a compact network. The internal microscopic structures of AC with an open edge have been shown in Figure 2. 7B. As observed in Figure 2. 7C, 15% NAC film indicated an appropriate distribution of CNF nanoparticles with AC particles, which implied a suitable homogenizing

method in this work. Figure 2. 7D showed an internal microstructure of 30% NAC film and displayed the cross-linking structure of CNF with AC materials. Figure 2. 7E, belonging to the 50% NAC film, illustrates abundant amounts of CNF throughout the film microstructure. White spots were observed in all the film structures and attributed to natural impurities inside the film matrixes. It is also notable that CNF particles were well dispersed and in a more appropriate manner with AC to form the NAC film (Figure 7E). These SEM analysis images revealed that high quantity of CNF reformed the complex film networks and interconnected structures. This result supports the decrease in water vapor permeability rates and the intricate structure suggests that the tensile properties of NAC film should increase. Dehnad et al. also explained similar microstructures of chitosan-nanocellulose biocomposites, where nanocellulose bound with chitosan particle were distributed throughout the film [135].

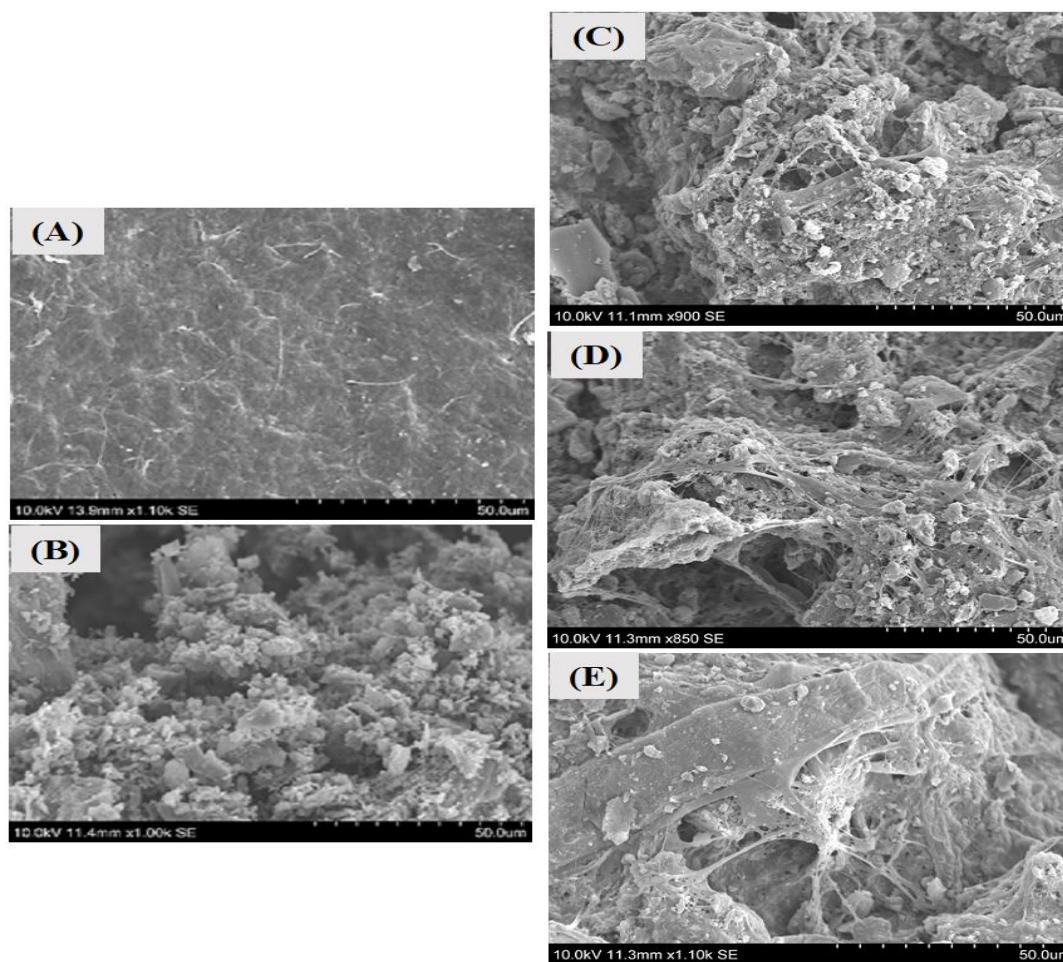


Figure 0.7. SEM images of NAC film. (A) Nanocellulose (CNF); (B) activated carbon (AC); (C) 15% NAC film; (D) 30% NAC film; (E) 50% NAC film.

1.7 Conclusions

A NAC film prepared with CNF and AC was developed first time for smart food packaging applications. The study verified that the CNF contents significantly affected the physico-chemical properties of NAC films. The films with higher CNF can form a compact and intricate NAC film structure. The electrical conductivity of NAC films decreased as CNF increased in the film. The increasing CNF significantly decreased the water vapor permeability and water absorption capacity but increased tensile properties of the NAC films,

i.e., tensile strength (TS), strain and Young's modulus. The thermal properties of all films are thermally stable until 270 °C. The SEM images showed that the microstructural binding of CNF with AC in film structure resulted in the proper dispersion of CNF in the film. Although 50% NAC films compared to the 15% and 30% NAC films were mechanically appropriate for the rough use, they have poor electrical properties for the biosensing function which is not suitable for the smart food packaging. In addition, 30% NAC film which exhibits the good mechanical strength than 15% NAC film and has considerable electrical properties for preparing the biosensing films. Therefore, they can be considered for the food packaging. Though details of CNF and AC interaction should be investigated in future study, the properties of the NAC films show very promising potential of use in smart food packaging

CHAPTER 3: DEVELOPMENT OF AN ACTIVATED CARBON-BASED NANO-
COMP SITE FILM WITH ANTIMICROBIAL PROPERTY FOR SMART FOOD
PACKAGING

(Published in Materials Today Communications, doi: [org/10.1016/j.mtcomm.2020.101124](https://doi.org/10.1016/j.mtcomm.2020.101124))

ABSTRACT

This work is to develop silver integrated nanocomposite film based on activated carbon (AC) and cellulose nanofiber (CNF) and characterize its functional properties for smart food packaging. The nanocomposite film was produced using a casting method, which used the ultrasonic suspension of CNF impregnated with AC and silver nanoparticles (AgNPs), named activated carbon-based silver-cellulose film (AgNPs/AC-CNF). The antimicrobial properties of the film were tested against food pathogens, *Staphylococcus aureus* and *Escherichia coli*. It was found that AgNPs concentrations in the range of 140-450 ppm inhibited the growth of *S. aureus* and *E. coli* on the agar plates. The conductivity of AgNPs/AC-CNF film was also examined for its cyclic voltammetry (CV), differential plus voltammetry (DPV) and linear sweep voltammetry (LSV) using a potentiostat. The results obtained by CV and DPV showed that peak current increased from 0.2 to 1.1 μA and 0.78 to 1.16 μA , respectively. The electrical resistivity of the film decreased from 6.8 to 1.9 $\text{k}\Omega\cdot\text{cm}$ as AgNPs increased over the range of 70 to 450 ppm. Transmission electron microscopy (TEM) analysis of the film showed that AgNPs were dispersed evenly within the film and well-connected with the pores of CNF and AC

particles. This AgNPs/AC-CNF film showed promise to be an effective antimicrobial conductive film for smart food packaging applications.

Keywords: Antimicrobial film; Silver nanoparticle; Nanocomposite; Nanocellulose; Activated carbon; Smart packaging

1.8 Introduction

Smart food packaging is becoming increasingly popular among customers [58]. This is because it can offer communication to consumers as to the status of the product [2]. Due to consumer preference for safe and high-quality food, the market for smart food packaging is growing and expected to reach about \$62.54 billion by 2023 [23]. Though a variety of packaging materials have already been developed based on renewable natural biopolymers, such as polysaccharides, proteins and lipids, all of these materials have some limitations, such as they incorporate costly raw ingredients [136], impair processing difficulties [26], have poor mechanical and thermal properties [137] or carry negligible electrical conductivity [123]. All these factors show a great need for the development of new packaging materials to address all of these issues in order to provide safer and natural food packaging materials.

Metal nanoparticle enriched natural biopolymer has attained significant attention in the research community. They can provide unique properties to polymer materials such as the high ratio of a surface atom to the inner surface atoms, quantum size effect, high specific surface area, and high interpenetrating capacity into the other materials [138,139]. They can also be used for numerous applications, such as photonic and electric sensors, catalysts, artificial tissue, and filters [140]. Among metallic nanoparticles, the most commonly used

components are identified as Au, Zn, Cu, Ag, Fe, Sn and Ti [141]. From those listed, silver nanoparticle (AgNP) is a well-established antimicrobial metal nanoparticle. They can combat several microorganisms, such as bacterium, viruses, and protozoans, in clinical and public health hygiene [142]. They exhibit remarkable catalytic activity, surface-enhanced Raman scattering activity, high electrical and thermal properties [143]. In previous study, AgNPs enriched biofilms were made and proved to be effective at inhibiting microorganisms [123].

Silver ions (Ag^+), which can dissociate from the AgNPs, have been reported to be non-toxic ingredients to human cells, though they can still have antimicrobial effects at lower concentrations [144,145]. According to the report of the Food and Drug Administration (FDA), AgNPs are the safe metal nanoparticle; therefore they have been permitted to be used in all of the food-contact polymer materials in the USA market [145]. The European Union issued a new regulation, EU n. 10/2011 commission 14 January 2011, for food packaging materials where they permitted silver compounds to be applied with the packaging materials [145]. Instead, they considered the banning of some other metallic particles, such as lead (Pb), mercury (Hg), and titanium (Ti) nanoparticles, with the packaging materials. In the preceding studies, the migration of AgNPs from starch-based film and low-density polyethylene film has been described [146,147]. However, the migration of such NPs to foods was negligible and below the limit of quantification [148]. Overviewing all of these characterized features of AgNPs, NPs were chosen to synthesize with nanocellulose and activated carbon to promote good antibacterial, high electrical, and thermally characterized nanocomposite film for smart packaging.

For the past few decades, carbon materials have gained tremendous attention to develop biosensor, electrical double-layer capacitors and supercapacitors, and energy storage devices (i.e., battery) [47,49,149,150]. The most common carbon material items are referred to as activated carbons, graphene, carbon nanotubes (single or multi-walled), carbon aerogels, and carbon fiber [151–153]. Activated carbon (AC) was chosen in this study because it has uniform physico- and electro- chemical properties when compared to the other mentioned carbon materials. They have low toxicity, excellent absorption capacity due to large microporosity (pore dimension <2 nm), large surface area (1000– 2500 m²/g) [154], high electron transfer capability, and surface functionality with host polymer [152].

Cellulose nanofiber (CNF), which has 4-25 nm diameter and 4-45 nm length, has been reported as one of the reinforcement materials for film preparation [135,155]. The attractive features of CNF have been reported in the studies such as flexibility, biocompatibility, low cost, high aspect ratio, low density, and good chemical stability [115,116]. In addition, the physical proper combination between AC, CNF and Ag nanoparticles can lead to an enhanced sensing capability and improve the electrical and antimicrobial features [136,156,157]. To the best of our knowledge, this is the first report to produce the synthetic antimicrobial, electrical, and thermally stable polymer nanocomposite where AgNPs were in-situ synthesized and their presence enabled the fast electron transportation channels to achieve its conductivity. CNF was mixed as binder to AC and AgNP was also synthesized with them to develop the activated carbon-based silver-cellulose film. The aim of this study was to develop antimicrobial conductive polymer nanocomposite for smart food packaging. The objectives of this study are to 1) characterize the AgNPs/AC-CNF film with

various AgNPs contents; and 2) observe the antimicrobial, electrochemical, and thermal properties of AgNPs/AC-CNF film.

1.9 Materials and methods

1.9.1 Materials

The activated carbon powder with greater than 98% of purity was purchased from Cabot Corporation (Norit® GAC 1240 Plus, Georgia, USA). The aqueous gel of CNF with purity of 3% solid, diameter: 5–20 nm and crystalline index: >87%, was procured from the Process Development Center at University of Maine (Orono, ME, USA). Silver nanoparticles (AgNPs), particle size of Ag: 2 nm, were procured from US Research Nanomaterials Inc. (Houston, USA). Phosphate buffered saline (PBS) was purchased from Thermo Fisher Scientific and the solution of PBS [10% (v/v), 0.1 M, pH 7.4, 0.8% NaCl] was prepared by mixing with purified water. The potassium hexacyanoferrate [$\text{K}_2\text{Fe}(\text{CN})_6$]⁻³ powder and potassium chloride (KCl, purity $\geq 99.0\%$) used for preparing the redox solution was purchased from Sigma Aldrich (St. Louis, MO, USA). Throughout the experiments, triple distilled water was used.

1.9.2 Preparation of silver integrated nanocomposite films

Silver integrated nanocomposite film was prepared using a casting method. To prepare the nanocomposite film, a few steps were followed. First, a 30 mL of AgNPs suspension was prepared with deionized water and concentrations were maintained at 70, 140, 250, 350 and 450 ppm. Secondly, 2.5 g of CNF gel were then added individually at each concentration of AgNPs mixed solutions (70-450 ppm). The obtained solution was gently agitated with 300 rpm at 50 °C to thoroughly mix CNF with AgNPs. After that, 1.4 g of AC power

were individually added to each solution to get AgNPs/AC-CNF mixture, where AC consists of 70% of the dry weight resulting in CNF consisting of 30% of dry weight. Following this, the mixture of AgNPs/AC-CNF was homogenized for 15 min using a handheld homogenizer (4000 rpm). The new homogenized mixture prepared was poured into the Petri-dish (diameter 13 cm) and dried in the oven at 60 °C for 16 h to create the AgNPs/AC-CNF dried film containing with different AgNPs amounts. The dried AgNPs/AC-CNF film was peeled from the Petri-dish and conditioned in a desiccator with 50-56% RH for 2 days prior to the analysis or characterization. The final dried films were named as 70, 140, 250, 350, 450 ppm of AgNPs/AC-CNF film according to their AgNPs concentration. The film without AgNPs was also prepared and used as a control throughout the test. The thickness of the film was measured using a handheld micrometer and the average thickness of the film was 0.37 mm. The synthesis process of AgNPs/AC-CNF nanocomposite film was summarized and shown in Figure 3.1.

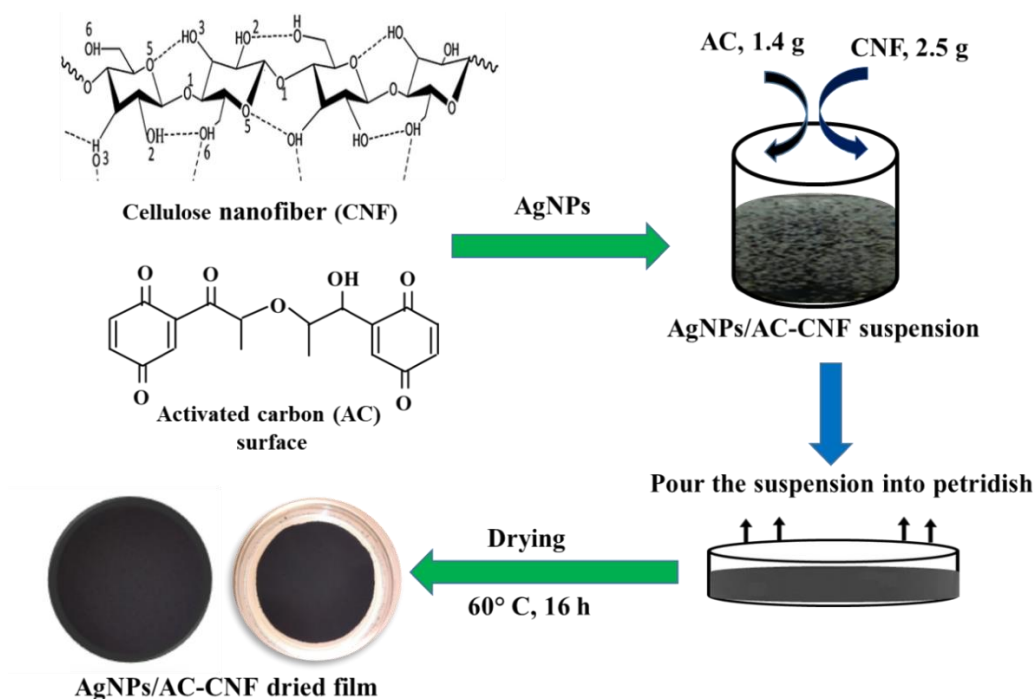


Figure 0.1. Schematic diagram for the formation of AgNPs/NAC film using cellulose nanofiber (CNF), activated carbon (AC) and silver nanoparticles (AgNPs) synthesis.

1.9.3 Transmission electron microscopy analysis (TEM)

The microscopic structure of the AgNPs/AC-CNF films was analyzed using a TEM (JEOL 2100F) under an acceleration voltage of 200 kV and element mapping on a Philips Tecnai G2 microscope in the microscopy lab at South Dakota State University (SDSU). The sample preparation of AgNPs/AC-CNF film for TEM was performed by depositing a drop of the AgNPs/AC-CNF film dispersion onto formvar-coated copper grids (400 mesh). The excess liquid upon the formvar-coated copper grids was absorbed with filter paper and the remaining residuals of the film were negatively stained with 2% uranyl acetate before the observation under TEM. The grid was dried at room temperature for 30 min and was imaged under TEM.

1.9.4 Fourier transform infrared spectroscopy

To identify the possible functional groups of AgNPs/AC-CNF film and analyze the interactions between CNF and AC, fourier transform infrared spectroscopy (FTIR) analysis was performed using a Tensor 37 spectrophotometer. AgNPs/AC-CNF film with different AC and CNF contents were considered in the presence of AgNPs compounding (250 ppm). The sample holder portion of the FTIR was aligned to the incident beam with 45° and maintained parallel with the ground. The FTIR spectra range was varied between 500 and 4000 cm⁻¹ and collected with 64 scans with the regulation of 4.0 cm⁻¹ by the omnic spectroscopy software [128].

1.9.5 X-ray diffraction

The crystalline phase and surface composition of AgNPs/AC-CNF film was analyzed using a X-ray diffractometer (XRD). The spectrum was recorded by Cu-K α radiation with $\lambda = 1.5418 \text{ \AA}$, scanned in the 2θ range of 20–80° with a step interval of 0.0167 [158].

1.9.6 Antimicrobial test of silver integrated film

A food pathogen, *Staphylococcus aureus* ATCC 13565, was selected to test the antimicrobial properties of the AgNPs/AC-CNF film. This pathogen was collected from the Food Safety lab, SDSU, Brookings, SD 57007. The strain of *S. aureus* was stored as a spore suspension into 20% (v/v) glycerol at -20 °C. Prior to the use of *S. aureus*, the frozen bacterial strain was thawed and washed with distilled water to remove all glycerol. The washed strain of *S. aureus* was cultured overnight in nutrient broth media. Afterward the growing culture of *S. aureus* was washed three times with deionized water and centrifuged at 12,000 \times g to collect *S. aureus* cells. The collected *S. aureus* cells were suspended into the

phosphate buffer saline (PBS, pH7.4, 0.1M) and maintained the concentration of 10^8 CFU/mL through the optical density (OD_{600}) measurement and colony counting.

In order to determine the antimicrobial properties of AgNPs/AC-CNF film, the agar disc diffusion method was followed [159]. Agar Mueller-Hinton (Merck) plates were considered for growing *S. aureus*, and 100 μ L of washed *S. aureus* (10^8 CFU/mL) was evenly spread onto the agar plates. In all cases, AgNPs/AC-CNF film was cut into small discs with 2 cm diameter. The film discs with different concentrations of AgNPs were individually placed in different plates that direct contact with the agar plates of *S. aureus*. Afterward, the spreading plates were incubated at 37 °C for 24 h for growth of *S. aureus*. The inhibition zone diameter at each plate around the film disc was measured using a hand-held micrometer (Esslinger, MN, USA) and imaged the inhibition zone using a digital camera.

A major Gram-negative bacterial strain, *E. coli* TOP10 (Thermo Fisher Scientific), was similarly tested through the disc diffusion method to inspect the antimicrobial activity of AgNPs/AC-CNF film. For this test, a stock solution of *E. coli*, which was collected from the biology and microbiology laboratory at SDSU, was thawed. The *E. coli* cells were suspended into the Miller broth media (Carolina, NY, USA) for overnight growing at 37° C with 200 rpm. The overnight grown broth culture of *E. coli* was washed three times using deionized water and centrifuged at 12,000 \times g and maintained its concentration of 10^8 CFU/mL throughout OD_{600} measurement. 100 μ L of 10^8 CFU/mL of *E. coli* cells was spread onto the Miller agar plates. Then the film discs (ϕ 2 cm diameter) were placed at the center of plates and incubated at 37 °C for 24 h. The inhibition zone diameter around the disc was measured and the zone was scanned using the digital camera.

Rhizopus stolonifera, a common bread mold, was used to analyze the antifungal property of AgNPs/AC-CNF film. Potato dextrose agar (PDA) plates were prepared to grow *Rhizopus stolonifera*. To perform the disc diffusion method, the film disc (ϕ 2 cm diameter) was placed at the center of the PDA plates. Afterward, an agar disc of 10-days-old PDA culture of *Rhizopus stolonifera*, which obtained from microbiology lab at SDSU, was placed upon the periphery of the PDA agar plates. The plates were then incubated at 27 °C for 9 days and the zone of inhibition diameter was recorded.

1.9.7 Thermal analysis of silver integrated film

Thermal analysis of AgNPs/AC-CNF film was performed throughout the thermogravimetric analyzer (TGA) (Q5000 SA, TA Instruments, USA). 3 mg of AgNPs/ AC-CNF film sample was taken into a hermetically sealed pan using a Tzero hermetic lid. The sample specimens were put into TGA under nitrogen and oxygen gas environment in the temperature range of 20 to 550 °C.

1.9.8 Electrochemical analysis of silver integrated film

AgNPs/AC-CNF film was electrically characterized using cyclic voltammetry (CV), differential plus voltammetry (DPV) and linear sweep voltammetry (LSV). For CV and DPV tests, a redox solution was used which was prepared from PBS buffer (pH 7.4, 0.1M) containing 2.5 mmol L⁻¹ [Fe (CN)₆]³⁻ and 0.1 mol L⁻¹ KCl. The three electrode systems were considered: a gold electrode as a working sensing surface with 2 mm diameter, a platinum wire as counter electrode and Ag/AgCl containing 3.0 mol L⁻¹ KCl as the reference electrode. Afterward, AgNPs/ AC-CNF film suspension with different AgNPs contents (70-450 ppm) were sequentially applied onto the working electrode and dried at 60 °C for ~10 min. After drying, the sensing surface of the working electrode was immersed into the

redox solution. Following this, the signals of CV and DPV were collected when the scan rate was maintained at 100 mVs^{-1} and the potential ranged from +600 mV to -200 mV.

In order to measure the current/voltage (I/V) value using LSV, two electrode systems were considered: a working electrode was connected to the one point of the multiple inputs of the potentiostat. The reference and counter electrode were connected to the ground point of multiple inputs of the potentiostat. In case of I/V measurement, a 2-pair distance of 13 mm gap upon the AgNPs/ AC-CNF film was chosen. One end of the 2-pair distance was connected to the working electrode, whereas another end was connected to the reference and counter electrode, and then the electrical response of I/V was measured using LSV. The slope of I/V curve, which was obtained between 0.0 and 100 mV, was estimated using linear regression analysis. Afterward, the resistance was calculated from the inversion of I/V. Three replications were carried out for each AgNPs/NAC film. The mean and standard deviation of replications was used to describe the experimental data obtained from LSV.

1.10 Statistical analysis

The statistical analysis of the data was performed by one-way analysis of variance (ANOVA) and significant analysis of the data was carried out by Duncan's multiple range test with considering a defined significance level of $p < 0.05$.

1.11 Results and discussion

1.11.1 Microstructure of AgNPs/AC-CNF film

The surface morphological features of AgNPs/AC-CNF film obtained from TEM with different scan magnifications were presented in Figure 3.2. As seen in Figure 3.2a-b, CNF elements bound with AC particles were identified. AC particles have a mesoporous

structure and are a hydrophobic substance [155], therefore the hydrophobic AC particles (50-60 nm in length) wrapped the hydrophilic CNF particles during the film formation and produced the overlapping regions over the film sheet. Large portions of CNF with longer edge were inspected, and black dotted AC particles densely clustered CNF edges under TEM (Figure 3.2a-b). In previous studies, similar micrographs of CNF (length 10-100 nm) were reported under TEM, while CNF combined with different types of hydrophobic elements (i.e. carbon aerogels) was inspected [158,160]. In Figure 3.2c-d, AgNPs (Ag. 2 nm) anchored with CNF and AC were seen under the high resolution TEM. The particles of AgNPs were aggregated with each other and anchored with AC and CNF. This agglomeration tendency of AgNPs was assumed to be due to their having high surface energy, which resulted from the reduced domains [161]. This phenomenon is considered by the fact that the agglomerated AgNPs particles remained from the inner side of the film toward the air-side surface of the film. Referring to the previous work by Ontong et al. [162], the synthesized colloidal AgNPs had a zeta potential of -18.76 ± 1.21 mV, indicating that the surface of AgNPs are negatively charged and can be stable in the aqueous solution. The EDX analyses were shown in Figure 3.2e and indicated that the film sample consisted of three elements: carbon, silver and oxygen which were distributed throughout the film, confirming that the blue dots were composed of AgNPs, red dots were activated carbon (AC) and green dots were oxygen (O). It has been assumed that these AgNPs particles with dozens to hundreds of nanometers were connected with each other to produce a strong and conductive pathway for electrochemical analysis.

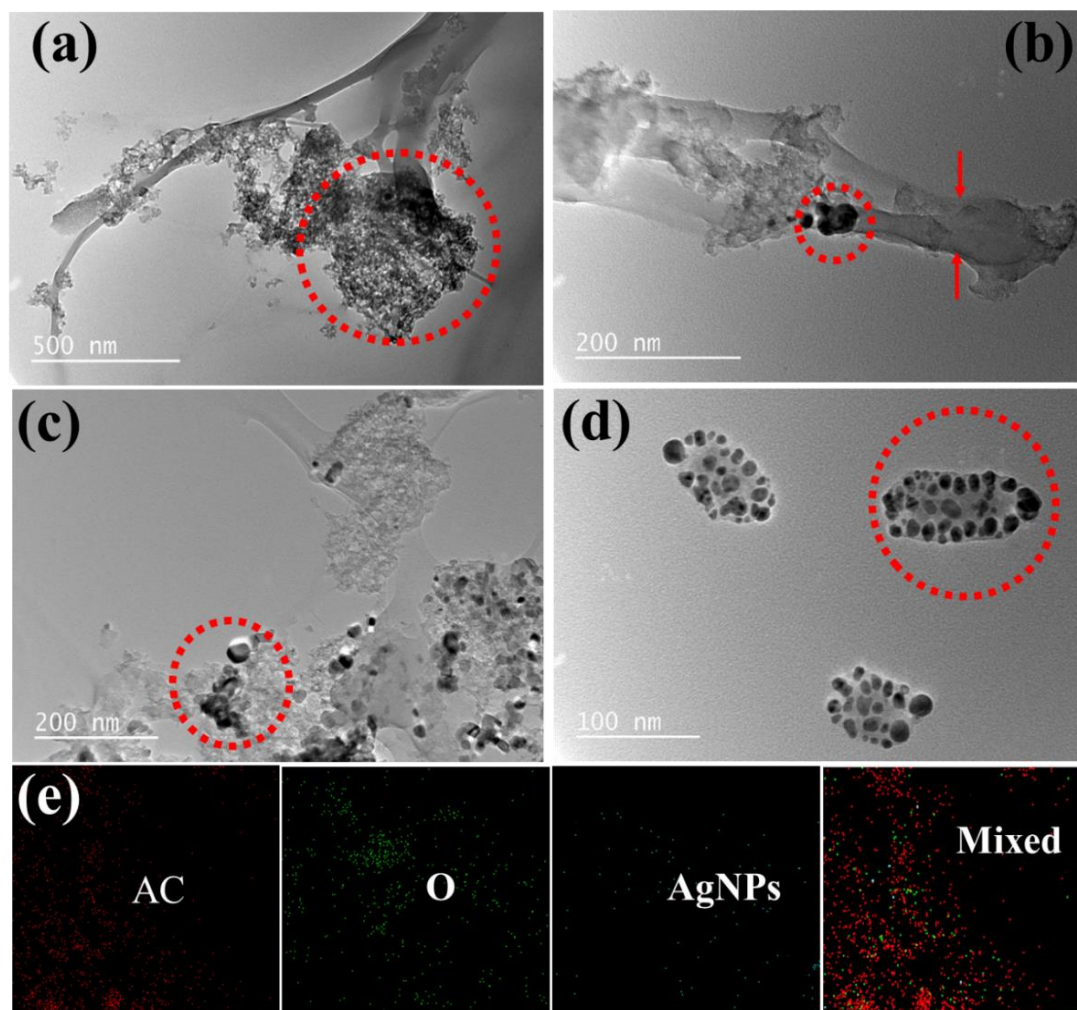


Figure 0.2. TEM images of: (a-b) CNF bound with AC was identified, (c-d) AgNPs bound with CNF and AC were identified; and (e) EDS elemental mapping images of AgNPs/AC-CNF nanocomposite.

1.11.2 FTIR analysis of AgNPs/AC-CNF film

The FTIR analysis of the AgNPs/AC-CNF film was performed to know the vibrational band characteristics of the film and compare molecular interactions between the functional groups of the film. The results of the band spectrum showed that no significant band difference between the 15%, 30% and 50% of AgNP/AC-CNF film was formed, and the peak

bands were displayed at similar points, which described that all of the films constituted of AC and CNF components (Figure 3.3). The characterized peak bands of all of these films were demonstrated to 690 cm^{-1} , 1050 cm^{-1} , 1600 cm^{-1} , 2400 cm^{-1} and 3400 cm^{-1} , which correlated to the stretching vibration of C = C bending (alkene), amine groups (C-N), aromatic carbon-carbon double bonds (C=C), carbon-dioxide bonds (O = C=O) and alcohol bond (O-H, strong intermolecular bond), respectively. These peak bands confirmed that strong carbon-carbon double bonds (aromatic and alkene bond) were formed during the film casting. It is noticeable that the intensity of these bands decreased with increasing CNF to the film from 15% to 50%. This result might be the clue to explain the behaviors of AgNPs/AC-CNF film, which can be strengthened with CNF for smart packaging application. As can be seen in Figure 3, FTIR was not sufficient to identify the AgNPs peaks to the film in this study, and it requires more high technology to inspect the presence of AgNPs coupled with AC and CNF in the film.

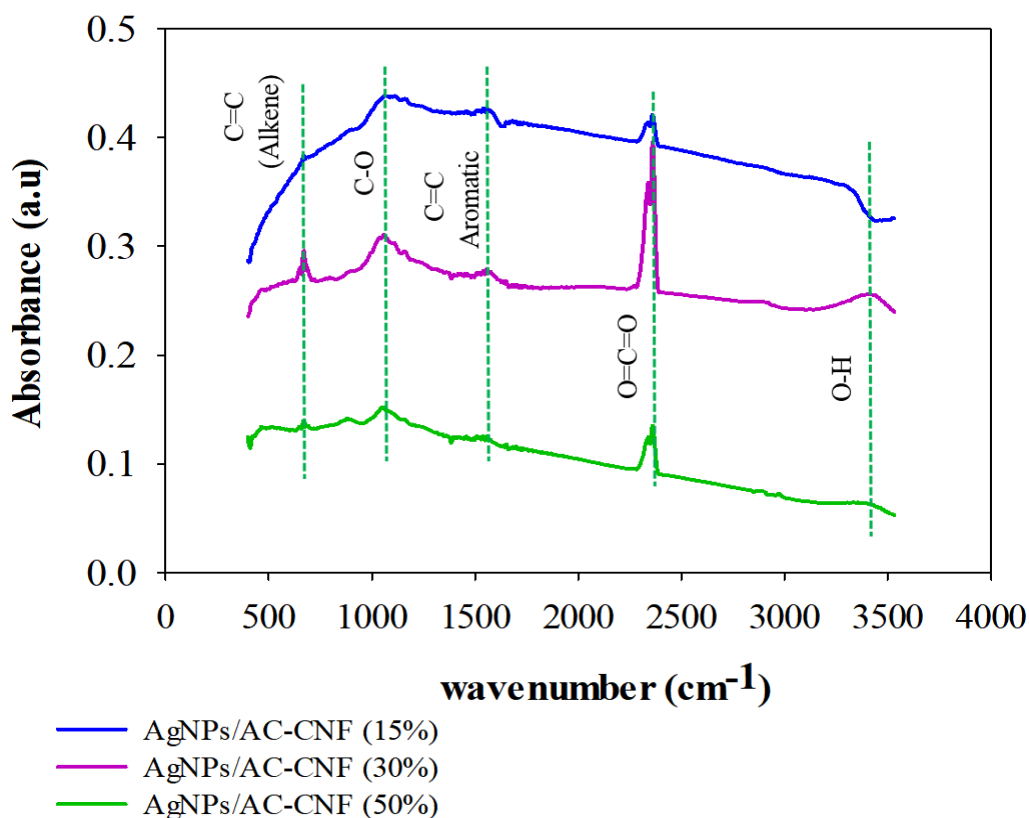


Figure 0.3. Infrared spectroscopy (FTIR) spectra of AgNPs/AC-CNF films (15% to 50% of CNF).

1.11.3 XRD analysis of AgNPs/AC-CNF film

The AgNPs/AC-CNF film integrated with different concentrations of AgNPs ranged from 70 to 450 ppm were analyzed using the XRD pattern. The result of the diffraction peaks of AgNPs/AC-CNF film was presented in Figure 3.4, where there were no obvious differences in the peaks between the concentrations of AgNPs in the films. As can be seen in Figure 3.4, the diffraction peaks for AgNPs/AC-CNF film appeared at $2\theta=44.4$, 64.5 and 77.3 , which were indexed corresponded to Bragg's reflections of the (200), (220), and (311) planes of face-centered cubic (fcc) nanocrystals, respectively. The results obtained from XRD confirmed that AgNPs into the film has a face-centered cubic (FCC) structure.

A similar phenomenon of the AgNPs integrated polyaniline (PANI) film was found in the previous studies [163]. The higher intensity and narrow width of diffraction peaks demonstrated that a higher degree of crystallinity of AgNPs with CNF and AC was formed. Interestingly, there was no clear peak indexed obtained for the control film and 70 ppm of AgNPs/AC-CNF film. This absence of diffraction peaks can be explained by the fact that a combination of the small quantity of AgNPs synthesized with CNF and AC was not enough to be identified using XRD. It can be also assumed that both ionic- and physical-crosslinking of polymeric mixtures influenced the stabilization of AgNPs in the polymeric nanocomposites.

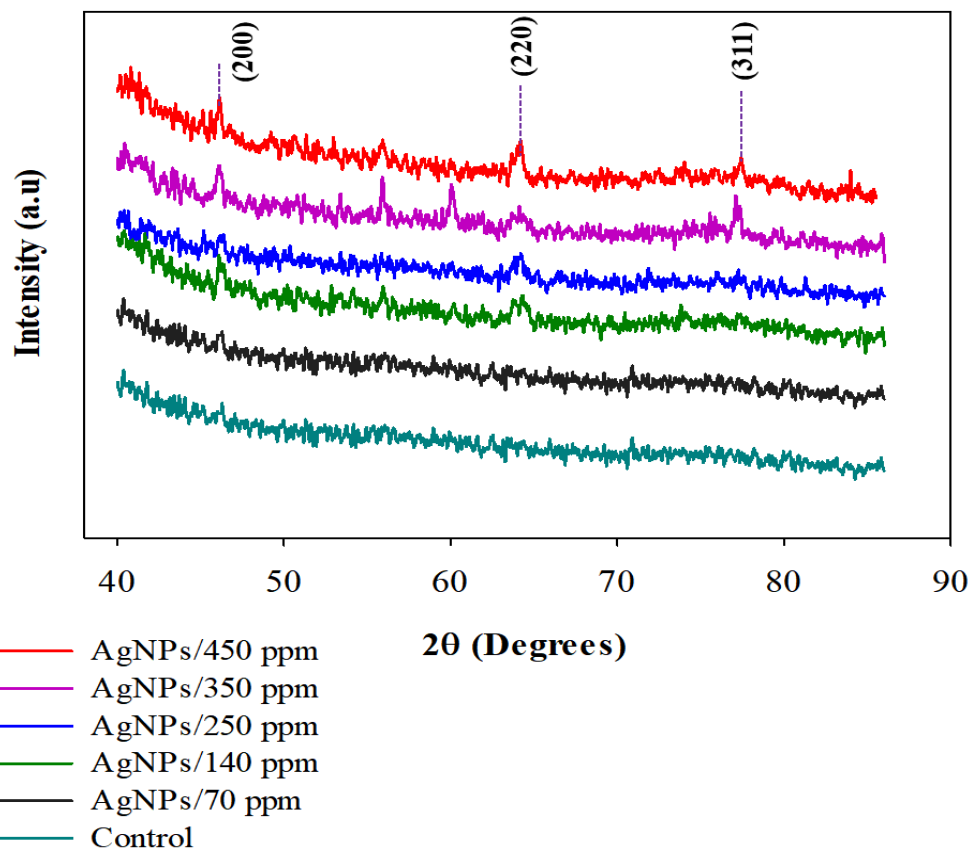


Figure 0.4. X-ray diffraction (XRD) pattern of 70, 140, 250, 350, and 450 ppm of AgNPs/AC-CNF film.

1.11.4 Antimicrobial properties of AgNPs/AC-CNF film

The antimicrobial properties of AgNPs/AC-CNF film with different AgNPs concentrations, ranged from 140 ppm to 450 ppm AgNPs, were evaluated against Gram-positive bacteria *S. aureus* and Gram-negative bacteria *E. coli* by the agar disc diffusion method. The results revealed that antimicrobial inhibition zone was created around the film disc (Figure 3.5). The neat bio-composite as a control film, without compounding any amount of AgNPs, did not produce inhibitory activity of *S. aureus* and *E. coli* on agar plates. The size of inhibition zone on plates continuously increased as concentrations of AgNPs

increased from 140 ppm to 450 ppm, which demonstrated a significant antimicrobial effect of AgNPs/AC-CNF film against on *S. aureus* and *E. coli* microbes. It is assumed that Ag⁺ ions were initially dissociated from AgNPs/CNF-AC film disc on agar medium; and those released Ag⁺ ions inactivated the growing microbes, *E. coli* and *S. aureus*. In the previous studies, a similar dissociation phenomenon has been reported, where Ag⁺ ions were primarily dissociated from carboxymethyl cellulose (CMC) and furcellaran-gelatin film and later the released Ag⁺ ions inhibited the microbes, *S. aureus* and *E. coli*, on the agar plates [123,164]. The largest inhibition zone was created with ~5.8 mm for *S. aureus* and ~6.1 mm for *E. coli* for 450 ppm of AgNPs/NAC film. This confirmed that highly concentrated silver integrated film has a potential antimicrobial effect to inhibit the microorganism for growing on the agar plate. According to the standard antibacterial test SNV 195920–1992, a film material can be considered to have potential antimicrobial activity, if its inhibition zone measurement exceeds 1 mm [148]. As the control film has no effect on antimicrobial activity, it can be confirmed that CNF and AC do not contain any antimicrobial function against inhibiting the microbes. This antimicrobial action inspected for AgNPs/AC-CNF films might be exerted throughout the different mechanisms [165]. Firstly, AgNPs generates the reactive Ag⁺ ions throughout the oxygen/oxidative stress which inhibit the growth of microbial population on the agar plates [166]. Other possible reasons are the size of AgNPs (Ag. 2 nm), smaller nano-size AgNPs can diffuse throughout the bacterial membrane and inactivate their growing activity. Bacteria have an outer membrane containing a lipopolysaccharide or peptidoglycan layer, so positive charge of silver ions binds to the negatively charged bacterial cell and inactivate the growing function throughout the encapsulation process [162]. The schematic diagram of the antimicrobial process using

AgNPs/AC-CNF film has been shown in Figure 3.6. This was the first study that analyzed the antimicrobial activity of AgNPs/AC-CNF film incorporated with Ag⁺ ions.

Antifungal test using AgNPs/AC-CNF film was verified against fungi *Rhizopus stolonifer*. As seen in Figure 3.5, no inhibition zone effect was inspected around the Ag integrated film disc. This result confirms that AgNPs are not sufficient to eliminate *Rhizopus stolonifer*. The fungi cell wall composed of chitin, which is one of the rigid protein with confining filamentous and hyphae structure when compared to fungi cell wall [166]; therefore their responses to AgNPs have been seen different. It is suspected that Ag⁺ ions diffused from AgNPs/AC-CNF film disc could not penetrate the *Rhizopus* cell wall membrane because of their filamentous and branching hyphae. Thus they imposed significant inhibition on the reactivity of Ag⁺ ions [167]. In addition, no concentration-effect was inspected by the AgNPs/AC-CNF film to suppress the growing of *Rhizopus stolonifer*. It can be concluded that AgNPs/AC-CNF film containing 140 to 450 ppm of AgNPs was not sufficient enough in preventing *Rhizopus stolonifer* in this study, and further studies on the AgNPs/AC-CNF film are needed to evaluate the antifungal properties.

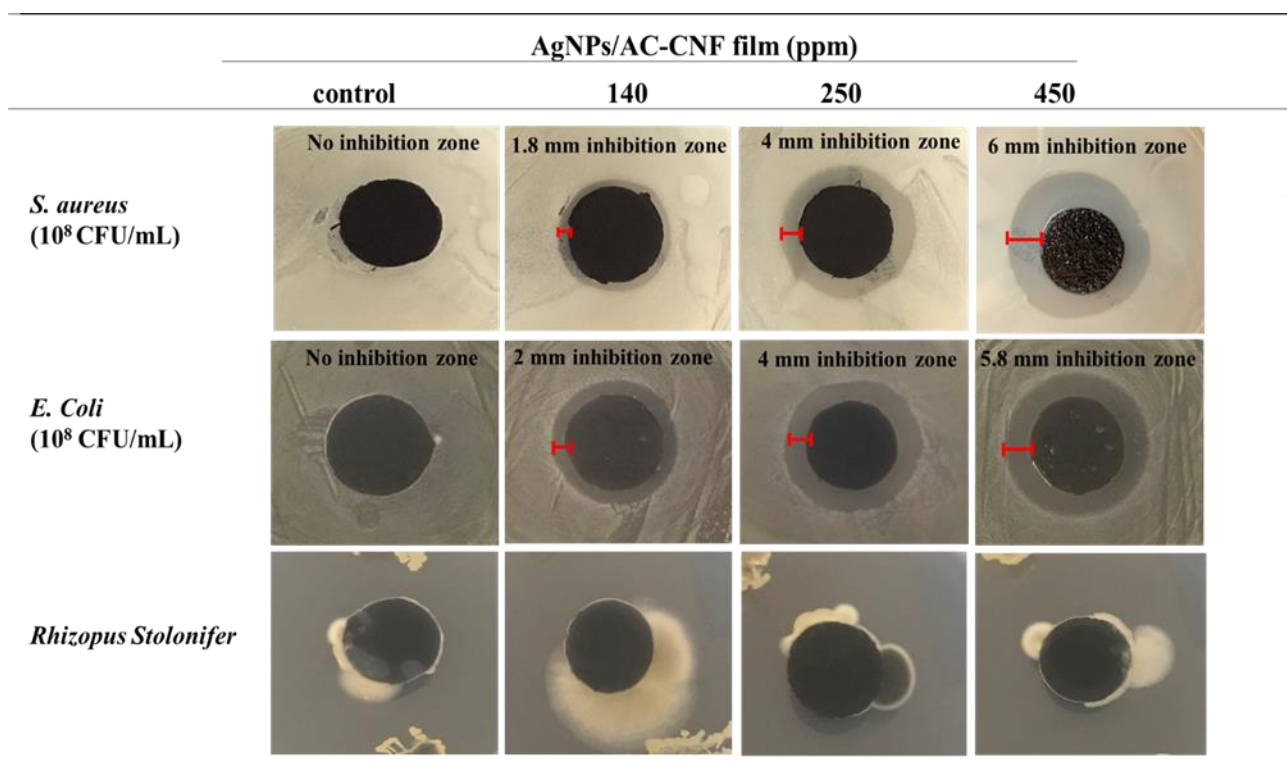


Figure 0.5. Inhibitory effect of AgNPs/AC-CNF film against Gam-positive bacteria *S. aureus* ATCC 13565 with 10^8 CFU/mL; Gam-negative bacteria *E. coli* TOP10 with 10^8 CFU/mL; and *Rhizopus stolonifer*.

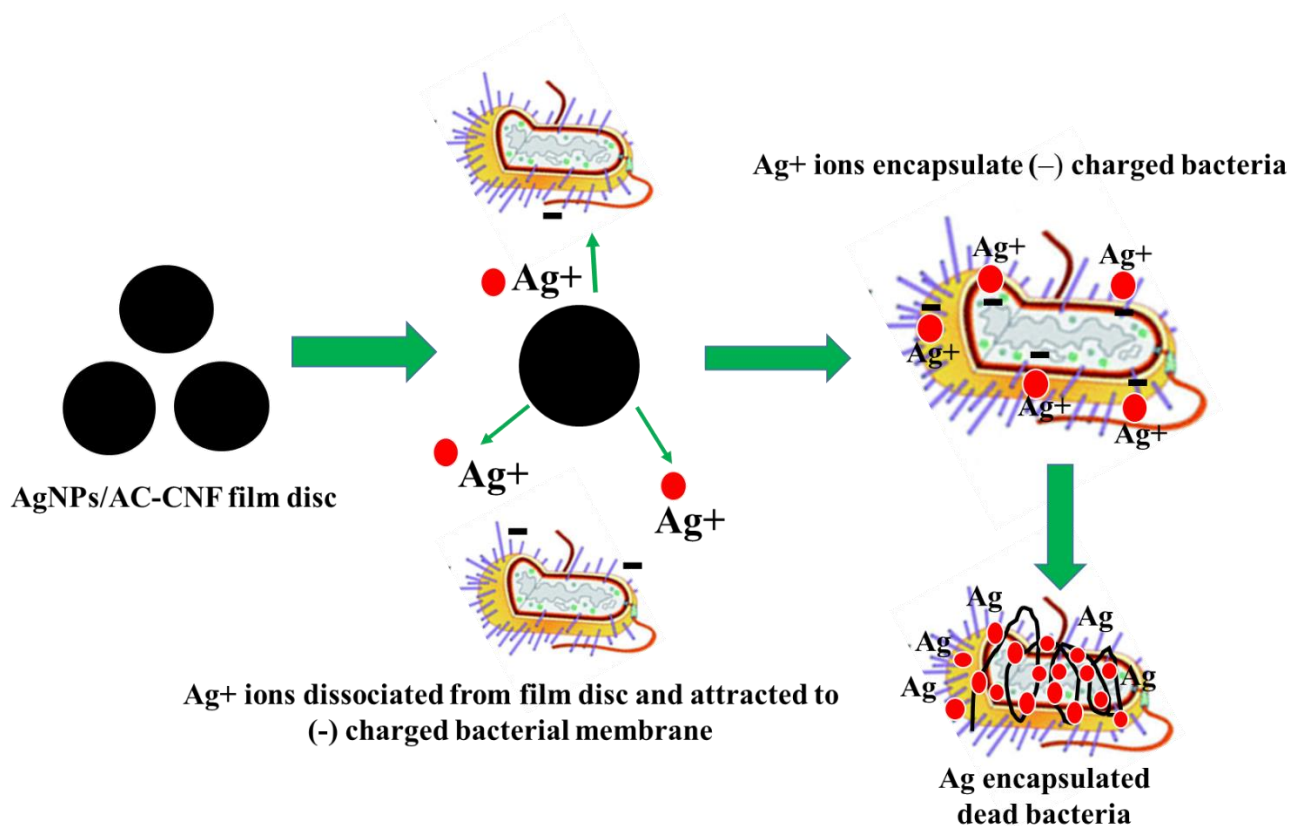


Figure 0.6. General scheme of inactivation mechanism of microorganism using AgNPs/AC-CNF film disc.

1.11.5 Thermal analysis of AgNPs/AC-CNF film

To characterize the thermal stability of AgNPs/AC-CNF films with different AgNPs contents, TGA and DTG thermograms under the nitrogen (N₂) and oxygen gas (O₂) conditions were obtained in the temperature range of 20–550 °C, as shown in Figure 3.7. In Figure 3.7a-b under the O₂ gas condition, the thermal decomposition stage of the film was separated into the three main regions, which occurred consecutively. First, the initial weight loss occurred at 50-270 °C for all AgNPs/AC-CNF integrated film. In this stage, it is suspected that physically weak and unbound water molecules were evaporated due to the water

dehydration from the film. Second, significant weight loss occurred between 290-430 °C. In this stage, control (without AgNPs compounding) and 70 ppm of AgNPs/AC-CNF film were significantly degraded between 290 and 310 °C and their weight loss continued to 85% and 90% subsequently (3.7a-b). Although, in this stage, the film with more than 70 ppm AgNPs, which mean 140 to 450 ppm of AgNPs/AC-CNF film, degraded from ~ 250 °C to 450 °C and showed thermally more stable (weight loss less than 82%). In the meantime, 450 ppm of AgNPs/AC-CNF film was less thermally degraded and had a thermal stability compared to the other films, confirming weight loss of 60%. The third stage for all of these films occurred at 310-510 °C. In this stage, oxidation or carbonization of residual organic matter was produced and the carbonized residuals with AgNPs remained in the aluminum pan.

Under nitrogen condition (Figure 3.7c-d), the AgNPs/AC-CNF films did not exhibit exactly the same weight loss behavior as the O₂ condition. Briefly, the primary weight loss was obtained from ~50 °C to ~300 °C. In this phase, it is related to unbound and physically weak water removal from the sample. The second weight-loss originated from 300 to 350 °C occurred due to the thermal decomposition of AgNPs/AC-CNF film, which is associated with cellulose chain cracking. The overall thermal decomposition behavior for 350 ppm and 450 ppm of AgNPs/AC-CNF film was alike, but their weight loss behavior was slightly different, related to ~25% and ~20% respectively. The thermal stability of AgNPs/AC-CNF film increased as AgNPs contents increased in such nanocomposite film, as shown in Figure 3.7c-d. A similar phenomenon of thermal stability was inspected in the previous work, where weight loss of polyacrylamide composite film reduced potentially as metal nanoparticles integrated to the film increased continuously [137]. The enhanced

thermal decomposition temperatures for the films were assumed to be specific intermolecular interactions between AgNPs, AC and CNF matters, resulting in a decrease in thermal decomposition with increasing AgNPs contents [39]. This enhanced thermal stability of the film confirmed that AgNPs have served as the heat barrier components with activated carbon and nanocellulose during the thermal decomposition; and their interactions in this system had therefore governed by short range attractive force or van der Waals force [163,168]. The third weight loss is attributed to carbonization of cellulose or remaining residual organic matter after thermal decomposition. In this phase, cellulose particles were suspected to be carbonized with its other residuals (i.e., carbon and AgNPs) into the aluminum pan.

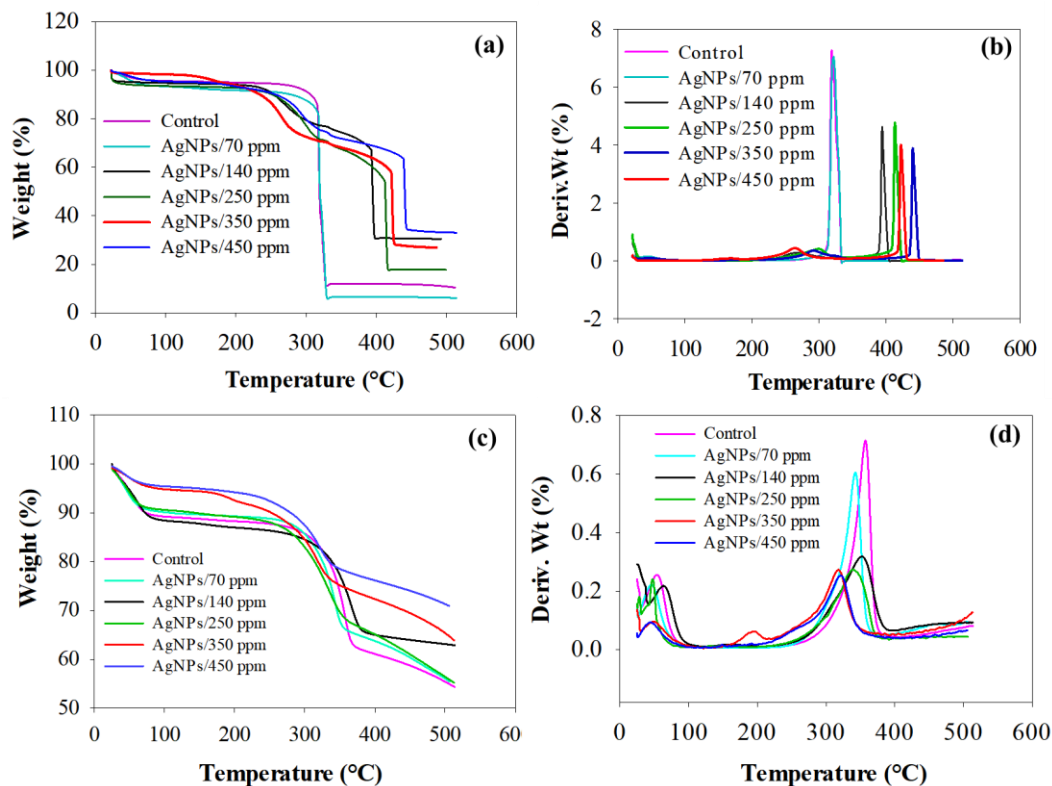


Figure 0.7. Comparative thermal analysis of TGA spectra of AgNPs/AC-CNF film under oxygen (O₂) and nitrogen (N₂) condition. (a) TGA curve for different concentration of AgNPs ranged between 70-450 ppm under O₂ condition; (b) Differential of TGA (DTGA) curve were shown with the similar AgNPs range under O₂ condition; (c) TGA curve with different concentration of AgNPs from 70 to 450 ppm under N₂ condition; (d) Differential of TGA (DTGA) curve were shown with the similar AgNPs range under N₂ condition.

1.11.6 Electrochemical properties of the AgNPs/AC-CNF film

AgNPs/AC-CNF film sample, presumably AgNPs ranged from 70 to 450 ppm, were electrically characterized throughout the stepwise modification of the working electrode via CV, and DPV. As observed in Figure 3.8a, the peak currents obtained from CV increased from 0.2 to 1.1 μA as AgNPs contents in the film increased from 70 to 450 ppm. This rise

of peak current demonstrated that the film sample with increasing AgNPs occupied a large surface area on the electrode and enabled efficient electron transfer in the $[\text{Fe}(\text{CN})_6]^{3-}$ solution.

Similarly, AgNPs/AC-CNF film sample with increasing AgNPs contents revealed the increasing DPV peak current, as observed in Figure 3.8b. This current increase indicated that a large amount of AgNPs with AC-CNF molecules facilitated the diffusion of the redox species to the electrode surface, and therefore resulted in an increase of voltammetry current. In previous study, a similar phenomenon of an increase of current was observed, while the working electrode was modified with increasing amounts of metal nanoparticle enriched nanocomposites [169]. This can be explained by the fact that increasing AgNPs within the film reduced steric inhibition between the reducible groups; therefore, they improved current response and hybridized the working electrode surface.

To verify the merits of AgNPs/AC-CNF synthesized electrode with one particular amount of AgNPs (250 ppm), CV with different scan rates between 5 and 100 mV/s were measured. As observed in Figure 3.8c, the peak current increased with increasing the scan rate from 2 to 100 mV/s, which indicated that the peak current has a good linear relationship with increasing scan rate. The rising peak current due to increasing scan rate confirmed that the rates of electronic and ionic transport are rapid enough at present scan rates. However, CV curves keep their original shapes with increasing scan rates, indicating good ionic and electronic conduction of AgNPs/AC-CNF film and confirmed that the electrode process is a surface controlled process [156].

The resistivity of AgNPs/AC-CNF film was characterized using LSV. As observed in Figure 8d, resistivity decreased as AgNPs contents increased from 70 to 450 ppm, which

confirm that AgNPs contents due to its high electrical conductivity reduced bio-sensing resistance of the film. The change in resistivity occurred significantly at higher AgNPs contents than the lower contents of AgNPs, though CNF and AC contents into the AgNP/AC-CNF film remained consistent. This resultant resistivity values fluctuated from 6.8 to 1.9 k Ω .cm as AgNPs concentrations decreased from 450 to 70 ppm. This is because the film with higher contents of AgNPs consisted of a large amount of Ag⁺ ions which significantly carried the current at the same voltage. Another reason for decreasing the resistivity of AgNPs/AC-CNF film might be introduced because of the synergetic effect that occurred between AC particles and AgNPs [170]. This decrease in resistivity, i.e. an increase in voltammetry current, can be due to the negative charge received from the AgNPs [49]. Meanwhile, AgNPs bundled with AC-CNF were thought to serve more electron transfer channels, which played a pivotal role in decreasing resistivity with increasing AgNPs contents, resulted in better conductivity of the film which one of new factors of this AgNPs/AC-CNF film in this study.

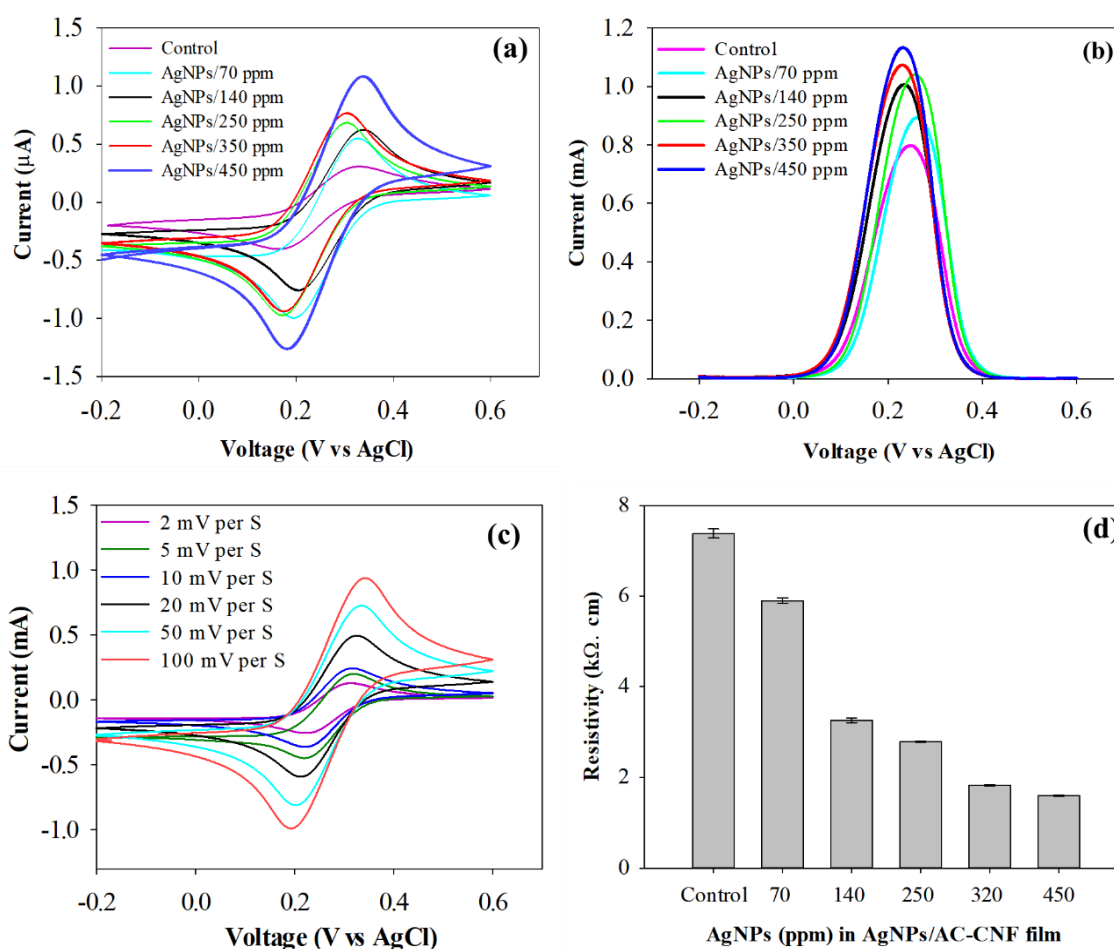


Figure 0.8. Electrochemical analyses of AgNPs/AC-CNF films with different AgNPs concentrations (70 to 450 ppm). (a) Cyclic voltammogram of AgNPs/AC-CNF films measured by cyclic voltammetry (CV); (b) differential pulse voltammogram (DPV) of AgNPs/AC-CNF films; (c) cyclic voltammogram with different scan rate (2 to 100 mV/s); (d) Resistivity (KΩ. cm) of AgNPs/AC-CNF films measured by linear sweep voltammogram (LSV).

1.12 Conclusions

An antimicrobial conductive and thermal stable film based on AC, CNF, and AgNPs were developed throughout the new efficient film casting methodology. This polymer nanocomposite film which combines antimicrobial conductive properties encountered the

processability difficulties because of having recombining CNF constituents. The AgNPs/AC-CNF film obtained efficient antimicrobial and electrical pathways due to having AgNPs and AC particles coupled to the film matrix. The microstructure of AgNPs/AC-CNF film obtained from TEM showed the aggregated AgNPs coupled with the compact bundle of CNF and AC materials. The results of the conductivity of the film showed that the electron transfer throughout the film was achieved and increased as the AgNPs integration to the film increased over the range. This study reveals a new way to produce antimicrobial conductive polymeric nanocomposite based on CNF, AC and AgNPs, which can play potential applications in both electronic devices, sensors, and antimicrobial membranes to offer the smart food packaging film.

CHAPTER 4: SYNTHESIS AND CHARACTERIZATION OF A NOVEL ACTIVATED BIOCHAR-BASED COMPOSITE FOR BIOSENSOR APPLICATION IN SMART FOOD PACKAGING

(Published in International Journal of Polymer Analysis and Characterization, doi.org/10.1080/1023666X.2021.1921497)

ABSTRACT

The aim of this study is to develop an activated biochar-based composite for biosensor applications in smart food packaging. Biochar was made from corn stover and activated using the steam-activation method. The activated biochar (ABC) was synthesized with polylactic acid (PLA) by a solvent casting method. While ABC ranged from 85% to 50%, PLA content varied from 15% to 50% (w/w) in the composite. The electrical conductivity of the developed ABC/PLA composite was measured through differential plus voltammetry (DPV) and cyclic voltammetry (CV) using a potentiostat. It was found that the current increased from 0.3 to 2.31 mA for CV and 0.16 to 1.02 mA for DPV when ABC contents changed from 50% to 85%. The tensile strength (TS) and Young 's modulus of the ABC/PLA composite film increased from 0.81 to 3.04 MPa and 56.31 to 102.69 MPa respectively when PLA contents increased from 15% to 50%. The biosensor was fabricated with 85% ABC/PLA-based composite using a drop-casting method. The resistance of the fabricated biosensor increased as the concentration of NH_3 increased over the range of 80 to 170 ppm. The results indicated that ABC/PLA composite could be a very promising material in economic feasibility and sustainability for future commercialization.

Keywords: Activated biochar; composite; Polylactic acid; Biosensor; Smart packaging

1.13 Introduction

Over the last few decades, food scientists have been increasingly interested in developing a variety of food safety measures to serve the qualitative foods [171]. Particular interest in this regard is the development of an on-package sensor for smart food packaging, which could be a rapid, concise, reliable, cost-effective and non-destructive tool for assessing the real-time freshness of foods [172,173]. Smart food packaging is an upgraded packaging nanotechnology that enables a communication between consumers and packaged foods about the condition of the packaged product [26]. Some smart packaging components have been made, for example pH sensitive nanocomposite [174], polyamide composite film [175] and time-temperature-based indicator (TTI) [21] and Al-doped ZnO composite film [176], but most of these components contain expensive raw sensing ingredients [16] and impair processing difficulties [123].

The market of petroleum-based polymers such as polystyrene, polypropylene, polyvinyl chloride, etc., has expanded in the twentieth century due to construction, automation and packaging industries [177]. However, the petroleum-based polymers have some drawbacks, such as they are non-biodegradable; affect the environment after their burning; and impede land fertility in contact with soil [178]. Therefore, we need to reduce our reliance on petroleum-based polymers to mitigate the environmental crisis. There is a growing interest in research into environmentally friendly and biodegradable polymers, which have become a popular topic worldwide [179]. Of the biodegradable polymers, polylactic acid (PLA) is the most widely used eco-friendly polymer and occupies an important position in the market due to its biomedical, tissue engineering, food service wares and packaging film application [145,180]. Despite having suitable packaging related properties, PLA has some drawbacks also, such as brittleness [181], poor processability, poor heat resistance

[182,183] and low toughness [184]. To mitigate these problems, PLA can be mixed with different carbon components i.e., multi-walled carbon nanotube, graphene, activated carbon and biochar that comes with some benefits as they improve the mechanical, thermal and electrical properties [185,186]. Among the carbon items, biochar from corn stover is an inexpensive and renewable source materials. In this study, PLA has been considered for using with biochar for biosensor construction as a cost effective and rapid sensor tool for smart food packaging.

Biochar is one of the richly carbonaceous items which is derived from anaerobic thermal decomposition of biomass feedstocks such as agricultural crops, wood, leaves, woodchips, and waste [187,188]. For years, it has been using as pollutant adsorbent [189]. Biochar has some advantages over other carbon items (single or multi carbon nanotubes, activated carbon and graphene), such as it bears high specific surface area; has a highly porous structure, good stability, and cost-effectiveness [190–192]. The conventional biochar is normally in millimeter-scale and not electrically conductive; therefore, it shows the difficulty in constructing biosensors [193]. Rather, with its activation, the biochar with size reduced to nano or micro-scale can create electrical conductivity and formulate the biosensor and biosensing composite. In addition, after activation, biochar can obtain a greater surface area and more adsorption sites for target analytes, and promote rapid electron transfer during sensing and biosensing [192].

In this study, PLA has been imparted with activated biochar to produce the conductive composite and this composite was used to develop biosensor for smart food packaging. To the best of our knowledge, this is the first study on activated biochar from corn stover and PLA blends for the biosensor development for smart food packaging and no research has

been performed yet on its use for determining food freshness. Therefore, the goal of this work is to develop biosensor using activated biochar from corn stover and PLA blends for smart food packaging. The objectives of this study are to 1) activate biochar from corn stover and characterize their properties for biosensor development; 2) develop activated biochar-based composite and characterize its physical, electrical, and thermal properties.

1.14 Materials and methods

1.14.1 Materials

Poly(lactic acid) (PLA) employed in this research work was procured from Sigma Aldrich (St. Louis, MO, USA). The density, melting point and glass transition temperature of PLA were 1.24 g/cm³, 160°C and 57.8°C, respectively. The potassium chloride (KCl) with purity with 99.0%) and potassium ferrocyanide (C₆FeK₄N₆) were procured from Sigma Aldrich (St. Louis, MO, USA) and used for biosensor characterization. Phosphate buffered saline (PBS) was purchased from Thermo Fisher Scientific and made by combining with purified water at 10% (v/v).

1.14.2 Preparation of biochar from corn stover

Biochar was derived from corn stover, locally accumulated from corn fields at Brookings, SD 57007, using the accurate control pyrolysis (ACP) method developed by Dr. Lin Wei at the South Dakota State University (SDSU) [194]. The corn stover was weighed first and transferred into the hopper of ACP reactor. Second, the corn stover inside the hopper was fed via a feeder and transferred in the reaction chamber of the ACP reactor, where corn stover was pyrolyzed to a vapor phase containing organic compounds and water vapor. The heat conduction within the reaction chamber was occurred and made the pyrolysis process easier and speedier. After pyrolysis, the hard biochar was produced and moved from the

reaction chamber to a char bin chamber where the solid biochar particles were isolated from the vapor streams. Afterwards, the vapor streams were exited and condensed into liquid bio-oil in a condenser. The biochar particles were collected from char bin and used for activation using steam-activation method (Figure 4.1).

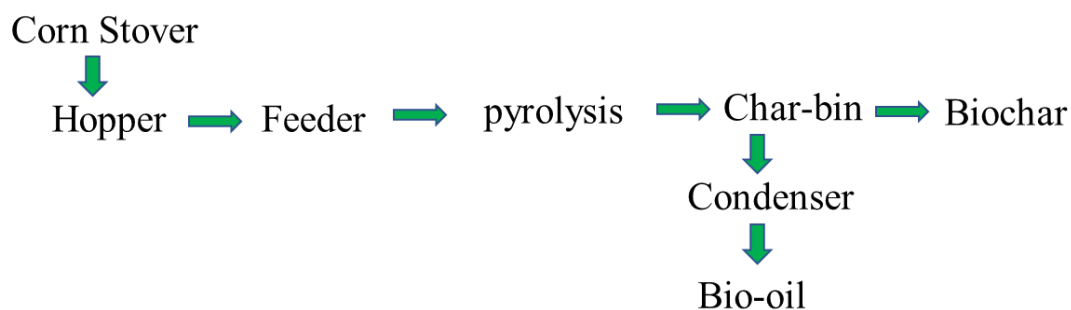


Figure 0.1. Biochar preparation from corn stover using accurate control pyrolysis (ACP) reactor system.

1.14.3 Biochar activation using steam-activation method

To activate the biochar sample, a steam-activation system was designed and fabricated for the activation process. The configuration of this system is shown as Figure 4.2, which consists of: 1) high-temperature steam chamber; 2) N₂ gas flow chamber; 3) tubular reactor and 4) gas outlet line. First, the biochar particles obtained from corn stover were finely milled using the omni mixer homogenizer (Waterbury, Ct., USA). Thereafter, the fine biochar particles were suspended in distilled water and centrifuged at 5000 rpm for 5 min. Following this, the supernatants containing biochar were collected and dried in an oven at 100°C overnight. Second, 2 grams of dried biochar sample was taken into a tubular reactor (3). Then the tubular reactor was placed into the reactor chamber. Thereafter, N₂ gas with 200 cm/min from the gas chamber (1) and steam with 2 mL/min via steam chamber (2)

were continuously flowed to the tubular reactor during the activation process. Biochar activation was monitored at different temperatures, from 600 to 1000°C of the tubular reactor, for 1 h. It is noted that this transmitted steam to tubular reactor allowed the activation of the biochar particles and the flowed N₂ gas evacuated the steam from the tubular reactor through the outlet line. After that, tubular reactor with activated biochar was taken out from reaction chamber and the activated biochar (ABC) was collected for further analysis.

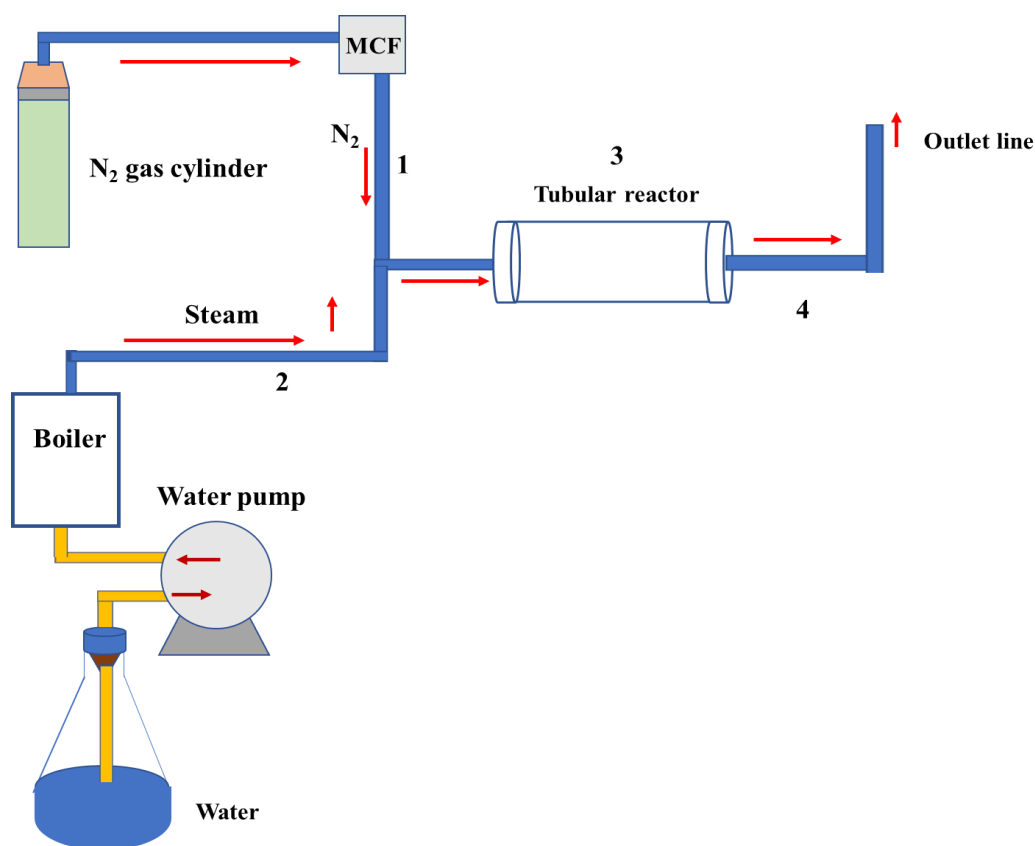


Figure 0.2. Biochar activation followed by the steam-activation method.

1.14.4 Characterized analysis of activated biochar (ABC)

1.14.4.1 Raman spectroscopy analysis

Raman spectroscopy is one of the spectroscopic techniques used to determine chemical and structural properties of sample molecules. To identify the structural characteristics of ABC, ABCs generated at different temperatures were analyzed using Raman spectroscopy (LabRAM HR, HORIBA Scientific). A linearly polarized laser light with a wavelength of $\lambda = 532$ nm was considered by a diffraction-limiting spot size ($0.61 \lambda/NA$). The wavenumber range was taken between 1000 and 2000 cm^{-1} for IR spectrums.

1.14.4.2 Brunauer-Emmett-Teller (BET) analysis

The surface area and pore size distributed in the activated biochar sample were evaluated using a Surface Area and Porosity Analyzer (Micromeritics ASAP 2020, USA) which was automated with the nitrogen gas sorption system. For this test, the activated biochar samples were degassed under vacuum at 110°C overnight to remove residual moisture prior to nitrogen gas adsorption. The adsorption curves of nitrogen gas obtained for each biochar sample was used to compute the specific BET surface area, and the pore grades.

1.14.4.3 Scanning electron microscopic analysis

Microstructural analysis of ABCs has been observed by scanning electron microscopy (SEM) (Hitachi-S-3400, filament-based SEM, MO, US). For ABCs, the ABCs samples were first smeared on the SEM observation template with 2 mm×2 mm. Afterwards, the surfaces of ABC were observed at a working distance of 10 mm with a magnification of 1500× under 10 kV electrical voltage.

1.14.4.4 Development of biosensor for ABCs characterization

The biosensor consisted of Au-electrodes upon alumina substrate and was used as the primary sensing platform. To construct the biosensor platform, Au-electrodes were threaded over the alumina substrate using electron-beam evaporator (Case Western Reserve University, Ohio, USA). Afterwards, the Au-electrodes were dried using N₂ and kept into vacuum chamber after electrical testing. The electrical conductivity of the Au-deposited platform was also tested to ensure that the Au-electrodes were able to work effectively. The biosensor fabrication was performed according to a drop casting method [35,150,195] (Figure 4.3). First, ABC samples activated at 600-1000°C were individually sonicated for 1 h at the concentration of 1 mg/mL in DMF (N, N-dimethylformamide). Afterwards, an aliquot of 15 µL of sonicated ABC suspensions was dropped onto the biosensor surface for alignment. The aligned biosensor was annealed at 80°C for 10 min in a dryer to bond the ABC residuals to the electrode surface. Following this step, the annealed electrode was rinsed with deionized water to elute the unbound ABCs from the biosensor surface. After following this step, linear sweep voltammetry (LSV) measurements were performed from 0.0 to 0.1 V for each measurement to estimate electrical conductivity of ABCs.

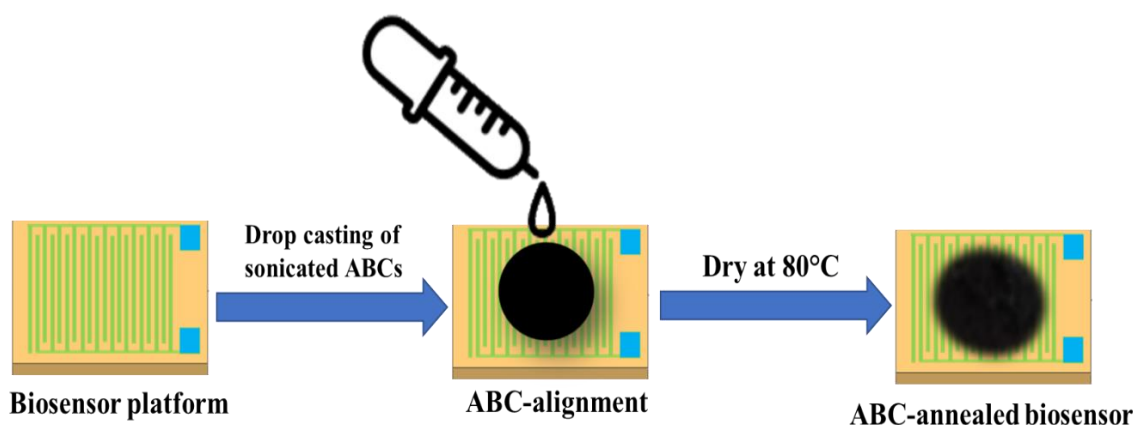


Figure 0.3. Schematic illustration of biosensor fabrication process using drop casting.

1.14.4.5 Preparation of ABC/PLA composite film

Composite film is a type of film which is a flat, thin and dry form of composite. A schematic diagram of the fabrication of ABC/PLA composite film has been shown in Figure 4. 4. This composite film was synthesized using a solvent casting method. First, different ABC/PLA labels (w/w) were prepared, which were 85% (85% ABC with 15% PLA), 70% (70% ABC with 30% PLA) and 50% (50% ABC with 50% PLA). Next, ABC/PLA mixtures were homogenized for 15 min with a handheld homogenizer (PRO scientific, USA). After homogenization, the homogenized mixture was poured into the stainless-steel petri-dish and dried at room temperature ($\sim 20^{\circ}\text{C}$) for at least 1 day. The dried films were peeled from the stainless-steel petri-dish and then conditioned with 50–60% relative humidity (RH). ABC/PLA films were prepared in triplicate for film characterization. The thickness of the film was measured using a handheld micrometer (Esslinger, MN, USA).

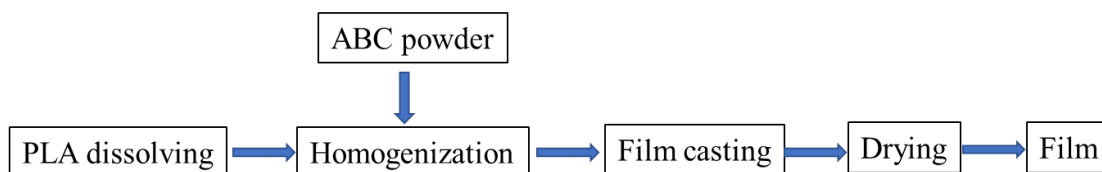


Figure 0.4. A casting process for synthesis of ABC/PLA composite films.

1.14.5 Characterized analysis of ABC/PLA composite film

1.14.5.1 Mechanical analysis

Mechanical analysis is a technique which is used to measure the tensile properties of composite film. ABC/PLA composite film was mechanically analyzed by following the method developed previously [16]. A texture analyzer fitted with Texture Exponent 32 software (Texture Technologies Corp., Scarsdale, NY, USA) was used to compute tensile force and deformation. Before the test, the film strips had been cut consistently to 50 mm long and 20 mm wide. The crosshead speed was set to 60 mm/min. Tensile strength (TS), strain, and Young's modulus were determined based on the strength and deformation data recorded by the following equation.

$$TS = \frac{\text{Maximum applied force}}{\text{Film thickness} \times \text{Film width}} \quad (1)$$

$$\text{Strain} = \frac{\text{Elongation}}{\text{Original length of film}} \quad (2)$$

$$\text{Young's modulus} = \frac{TS}{\text{Strain}} \quad (3)$$

1.14.5.2 Thermogravimetric analysis

Thermal analysis of ABC/PLA composite film were performed by thermogravimetric analyzer (TGA) (Q5000 SA, TA Instruments, USA). For this test, 3 mg of each ABC/PLA

film was placed directly in a hermetically sealed pan. Afterwards, the specimens were subsequently heated in a 20–400 °C range under a nitrogen atmosphere with a heating rate of 10 °C.min⁻¹ and a gas flow rate of 20 mL.min⁻¹.

1.14.5.3 Electrical analysis of ABC/PLA composite

Cyclic voltammetry (CV) and differential plus voltammetry (DPV) were used for characterizing ABC/PLA composites prepared by film casting process. For this test, a redox solution, containing 2.5 mmol L⁻¹ [Fe (CN)₆]³⁻ and 0.1 mol L⁻¹ KCl prepared in PBS buffer (pH 7.4, 0.1 M), was used. Three electrodes were considered as a working electrode of 2 mm diameter, Ag/AgCl of 3.0 mol⁻¹ KCl as the reference electrode and a platinum wire as a counter electrode. ABC/PLA film suspension was added sequentially to the sensing surface of working electrode and was dried overnight at room temperature. After that, the fabricated working electrode with reference and counter electrode was dipped in redox solution. After the scans, the CV and DPV signals were obtained while the scan rate of 100 mV⁻¹ was sustained and the voltage was between +600 mV and -200 mV.

1.14.5.4 ABC/PLA-based biosensor development for ammonia (NH₃) detection

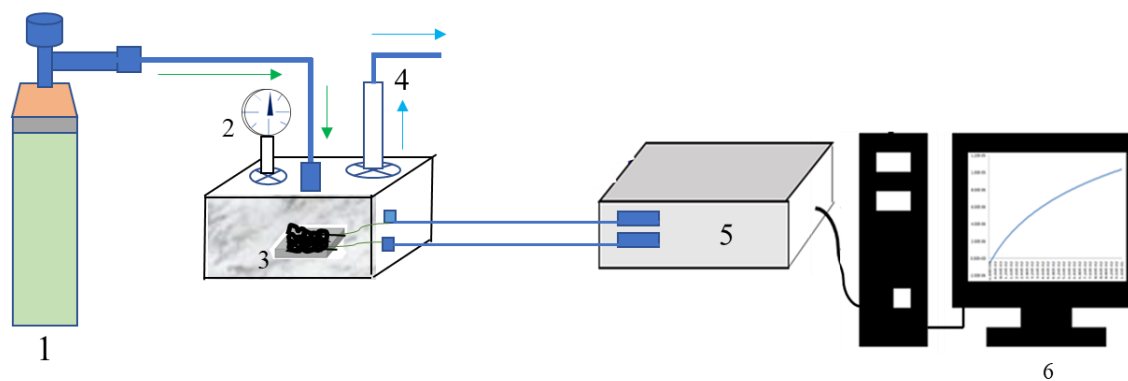
Figure 4. 5 shows a schematic diagram of the experimental setup for measuring the biosensor's response with regard to standard NH₃ gas balanced with nitrogen (N₂). This system was formed using hammond gas chamber (188 mm × 120 mm × 50 mm) including electrical connections lined with the 85% ABC/PLA-based biosensor and NH₃ gas tank. The desired concentrations of NH₃ flowed into hammond gas chamber were maintained by computer-based gas control system.

In this study, linear sweep voltammetry (LSV) analysis was performed at each step using a potentiostat (DY2013, Digi-Ivy, Inc., Austin, USA). The slope of the current/voltage

(I/V) between 0.0 V and 0.12 V was estimated using linear regression analysis. The sensitivity of the biosensor towards the exposure of NH_3 was calculated as:

$$\text{Sensitivity} = (R_1 - R_0) / R_1$$

where, R_0 = the resistance of the biosensor without gas (base resistance) and R_1 = the resistance of the biosensor when exposed to gas.



- | | | |
|--|------------------|-------------|
| ① NH_3 balanced with N_2 | ② Pressure gauge | ③ Biosensor |
| ④ Gas outlet line | ⑤ Potentiostat | ⑥ Computer |

Figure 0.5. Schematic diagram of the experimental set-up for measuring biosensor response to NH_3 .

1.15 Statistical analysis

The statistical data analysis was carried out by one-way analysis of variance (ANOVA) and significant analysis of the data was performed by Tukey test with considering a defined significance level of $p < 0.05$.

1.16 Results and discussion

1.16.1 Characterization of activated biochar (ABC)

1.16.1.1 Physical properties of ABC sample

Raman spectroscopy is a useful technique that is used to characterize and understand the materials properties, including molecular and chemical structure, crystallinity, phase and molecular interaction [188]. In order to generate highly conductive biochar, biochar was thermally activated for developing biosensor for smart food packaging application. After activation with different temperature, the biochar was further characterized using Raman spectroscopy to illustrate the physical features. The Raman spectrums of ABC for different temperature have been displayed in Figure 4. 6. In this Figure4.6A, two highly peak bands were inspected corresponding to G band at 1590 cm^{-1} and D band at 1380 cm^{-1} . The D band correlates to the vibration of defective carbon or sp^3 carbon atoms in the disordered graphite structure, while G band conforms to the in-plane vibration of sp^2 carbon atoms in the two dimensional hexagonal lattice of graphene [196,197]. The intensity ratio of D to G (I_D/I_G) was found to 0.81, 0.61, 0.94, 0.89 and 0.87 for $600\text{ }^\circ\text{C}$, $700\text{ }^\circ\text{C}$, $800\text{ }^\circ\text{C}$, $900\text{ }^\circ\text{C}$ and $1000\text{ }^\circ\text{C}$ respectively. It is clearly seen that the intensity ratio of I_D/I_G for ABC/ $800\text{ }^\circ\text{C}$ was higher as 0.94 compared to the other intensity ratio (I_D/I_G) for other activation temperatures, indicating more vacancy defects were produced in ABC at $800\text{ }^\circ\text{C}$ [188]. Thus, it can be said that temperature has an effect for biochar activation.

The surface area and pore volume upon the biochar are the crucial factors when biochar is considered for biosensor construction for gas absorption and as the potential filler for polymeric composite preparation [198]. The extensive surface area and internal pore structure of biochar can contribute to high absorption capability and serve a good mechanical

interlocking between filler and matrix [199]. BET surface area and pore volume of biochar activated at different temperature has been displayed in Figure4. 6B. As seen in Figure4. 6B, BET surface area along with the pore volume of biochar at 800°C was significantly higher, as 825.89 m²/g and 0.21 cm³/g respectively, compared to the other biochar sample activated at 600°C, 700°C 900°C and 1000°C. This increased surface area and pore volume might be occurred because of the removal of carbon mass and volatile matters from biochar surface during activation process [200]. Greater surface area is desirable because it aids in absorbing gas and molecules to a greater extent. However, biochar activated at 600°C, 700°C, 900°C and 1000°C showed lower BET surface area. It might be volatile matters were not effectively removed from biochar surface and not effectively activated at those temperature. In addition, no surface area was detected for control biochar sample due to a negative isotherm due to its releasing N₂ gas.

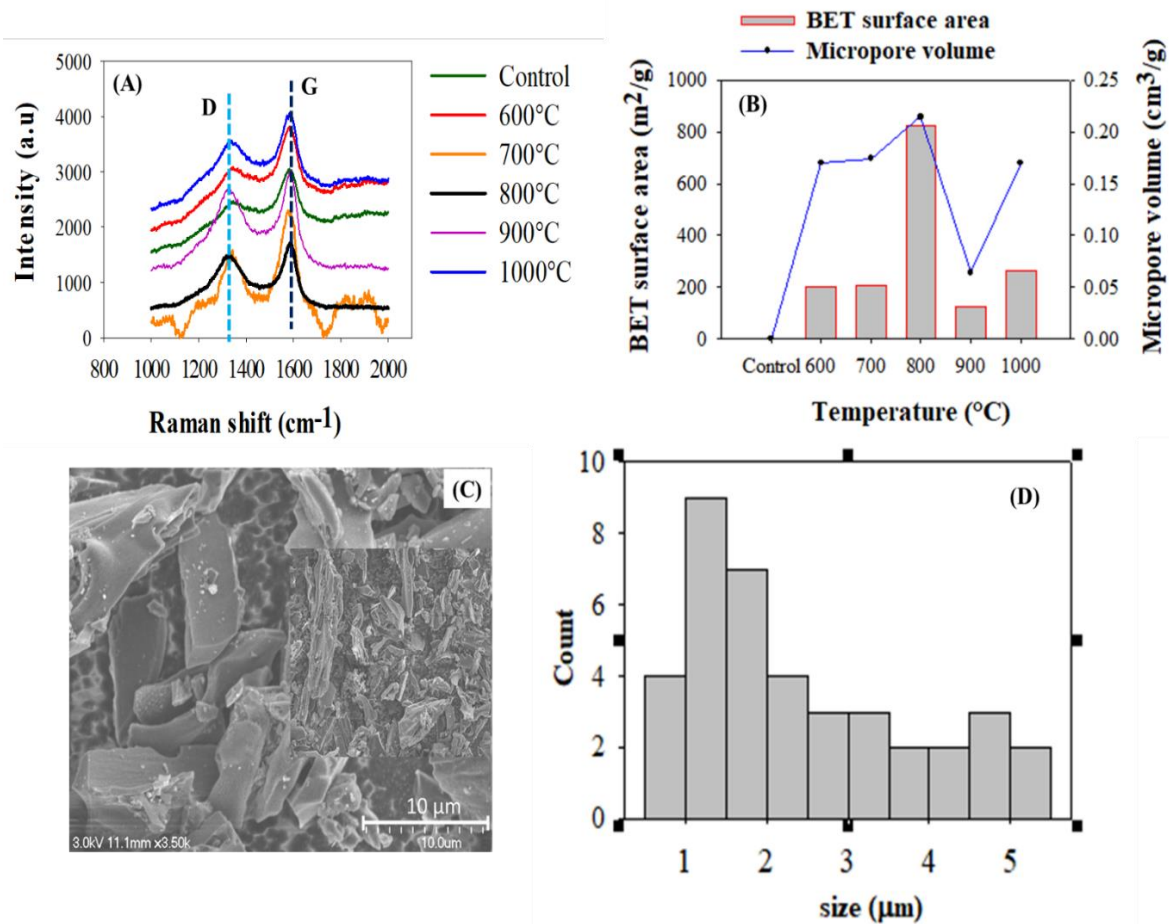


Figure 0.6. Characterization of ABCs. (A) Raman spectrums of the ABCs with different temperature range (600°C-1000°C); (B) BET analysis of ABCs; (C) SEM images of ABC/800°C; and (D) Histogram of ABC/800°C. Control sample denotes biochar sample without thermal activation.

In the SEM analysis, it is seen in Figure 4. 6C, the ABC/800°C had irregular and heterogeneous shape. The size distribution of the ABC/800°C was determined using Java-based image processing program (ImageJ developer, USA). The mean size distribution of ABC/800°C was illustrated in Figure 4. 6D. Approximately 41.01% of ABC/800°C is 1-2

μm , 17.94% is 2-3 μm , and 25.62% is 3-4 μm , the average particle size is 3 μm , indicating that micro-size ABC particles were successfully produced.

1.16.1.2 Electrical analysis of ABC sample

To investigate the electrical conductivity of the ABCs, biosensor was developed with ABC/600°C, ABC/700°C, ABC/800°C, ABC/900°C and ABC/1000°C and characterized their electrical properties. As can be seen in Figure 4. 7A, the current obtained at ABC/800°C was much higher than those of other biosensors made with ABC/700°C, ABC/900°C and ABC/1000°C. No current was detected for the biosensor prepared by ABC/600°C sample. This indicates that the biochar was slightly activated at 700°C, 900°C and 1000°C but not electrically properly activated at 600°C. In Figure 4. 7B, Nyquist current curves obtained by linear sweep voltammetry (LSV) were presented and found that current at ABC/800°C was significantly higher compared to current at ABC/700°C and ABC/900°C, which confirmed that ABC/800°C sample is consisted of highly conductive ABCs particles. Since the biosensor made with ABC/600°C did not show electrical conductivity, which ensured that ABC activation was not perfect at less than 700°C, though the electrical conductivity at 700°C, 900°C and 1000°C was much lesser. As can be seen in Figure 4. 7C, the resistance of the biosensor made with ABC/800°C was much lower compared to the biosensor made with ABC/700°C, ABC/900°C and ABC/1000°C, which means that the larger electron transfer property at ABC/800°C was achieved. These conductivity results of ABCs confirmed that the physical and chemical properties of ABCs were changed under temperature treatment during activation [188]. To further characterize ABC/800°C sample, linearity plot of peak current (I_p) vs. different potential scan rates (mV/s) was constructed throughout the CV cycle and found that there is a good co-relation

between I_p and scan rates (Figure 4. 7D). In previous studies, the non-conductive carbon of cellulose and lignin was converted to conductive graphene, while SP^3 carbons were transformed into SP^2 carbon [193]. Due to its high electrical conductivity, ABC/800°C sample was considered for the preparation of biosensing composites in this study.

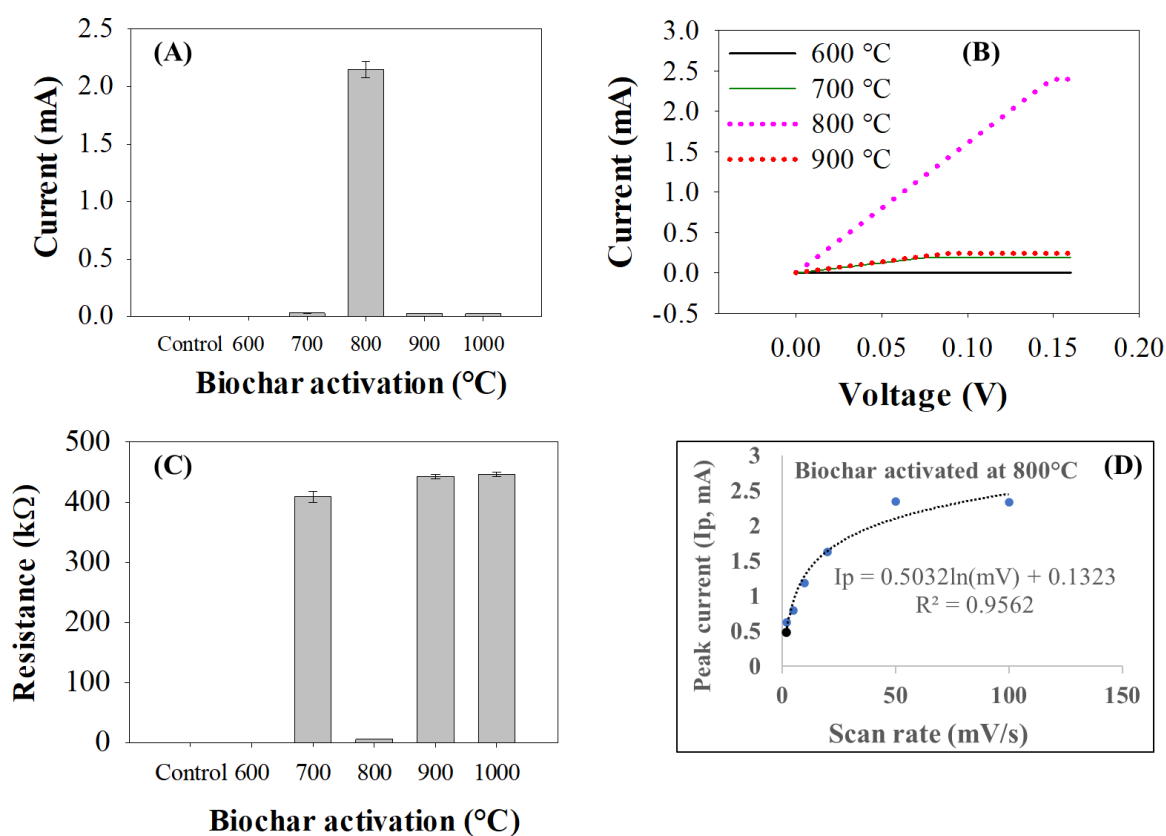


Figure 0.7. Electrochemical analysis of ABCs. (A) Current of ABCs; (B) Nyquist current curves obtained by linear sweep voltammetry; (C) Resistance of ABCs; and (D) Plot of peak current (I_p) versus different potential scan rates. Control sample denotes biochar sample without thermal activation.

1.16.2 Characterization of ABC/PLA composite

1.16.2.1 Physical properties of ABC/PLA composite film

ABC/PLA composite films containing 85-50% of ABC/800°C (w/w) corresponding to 15-50% PLA (w/w) were shown in Fig 4. 8a. The surface morphological features of the films were evaluated using SEM to observe surface layers of the PLA/ABC film, as seen in Figure 4. 8b. The composite film was not transparent and had a black color in its final appearance because it contained biochar particles. The average weight of each film was measured as ~500 mg and the thickness varied between 0.35-0.37 mm. These films were homogeneous and easy to use by hand. SEM micrographs of the film showed that increasing the PLA content to the film formed a relatively dense and hard surface to the final appearance compared to the decreasing PLA contents to the film (Figure 4. 8b). Therefore, 50% ABC/PLA film showed the greatest adhesion at the interface between ABC and PLA compared to 85% ABC/PLA film. It was seen in SEM (Figure4. 8b) that the 85% ABC/PLA film had a large number of micropores on their film appearance, which could be a clue for absorbing gas or molecules inside the micro-pore volumes.

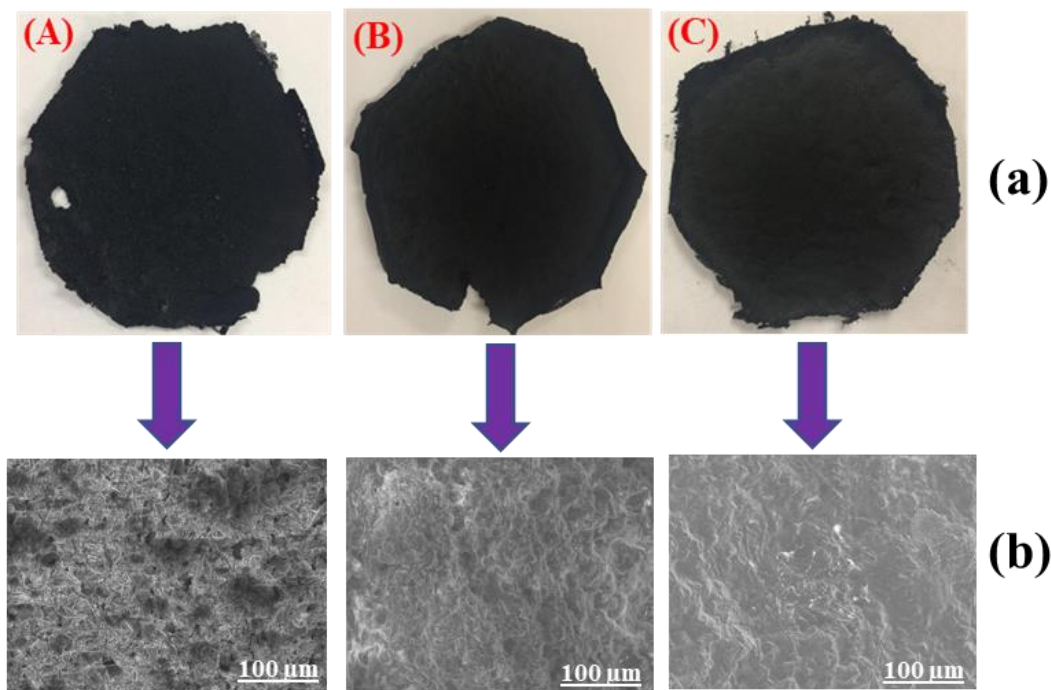


Figure 0.8. Physical properties of ABC/PLA films. a: Left to right: 85% ABC/PLA film; 70% ABC/PLA film; 50% ABC/PLA film; b: left to right: SEM micrographs of 85% ABC/PLA film; 70% ABC/PLA film; 50% ABC/PLA film.

To investigate the deeper microstructure of ABC/PLA composite film, SEM analysis with 10 μm scale bars was performed. The size distribution of native ABC and PLA particles in the film were seen in the SEM micrographs. The random orientations of ABC combined with lesser PLA contents were seen in 85% ABC/PLA film (Figure 4. 9A). The compact binding of ABC with increasing PLA was formed in 70% ABC/PLA film (Figure 4. 9B). The abundant amounts of PLA were inspected in 50% ABC/PLA film and ABCs were not clearly observed in 50% ABC/PLA film (Figure 4. 9C). This is because a compact and strongest bond was formed between ABC and PLA in 50% ABC/PLA film. This intricate

structure of 50% ABC/PLA film indicates that the constituent elements of PLA and ABC may improve the mechanical properties of ABC/PLA film.

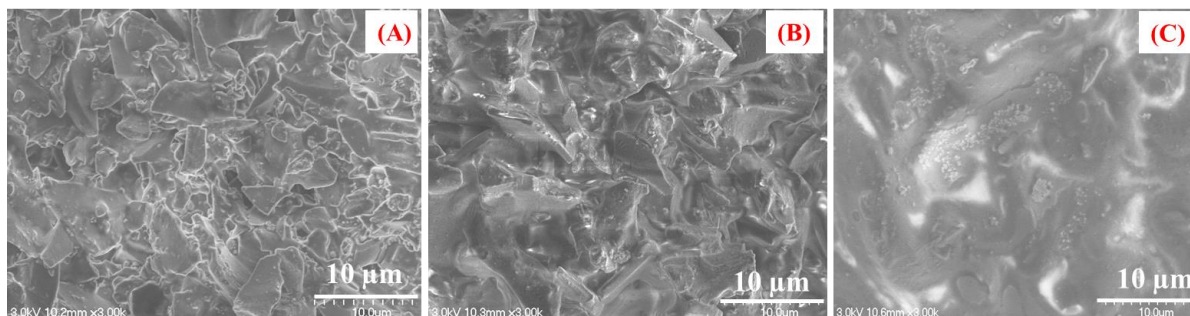


Figure 0.9. SEM micrographs of ABC/PLA film. (A) 85% ABC/PLA film; (B) 70% ABC/PLA film; (C) 50% ABC/PLA film.

1.16.2.2 Mechanical properties of ABC/PLA composite

Mechanical properties of ABC/PLA composite film were determined to examine the tensile properties of the film with respect to applied force. As can be seen in Figure 4. 10, when the ABC contents in the ABC/PLA film decreased from 85% to 50% and PLA contents alternatively increased in the ABC/PLA film from 15% to 50%, the tensile properties, including tensile strength (TS), Young's modulus and strain increased at the same time. This increase of tensile properties with increasing PLA and decreasing ABC is one of the reasons for rising the tensile properties of ABC/PLA film. This increasing PLA contents to the film may allow the film to withstand the normal stress faced during the shipment, handling and transportation of foods [120]. The other possible reason of increasing tensile properties of the film is related to interfacial interaction of increasing PLA with decreasing ABC, because PLA as the plasticizer agent which may strictly bind ABCs in the ABC/PLA film [201]. Therefore, it permits the higher tensile force during the film deformation; and

resulted in an increase in tensile strength. Compared to the films, 50% ABC/PLA film has higher tensile properties ($p < 0.05$).

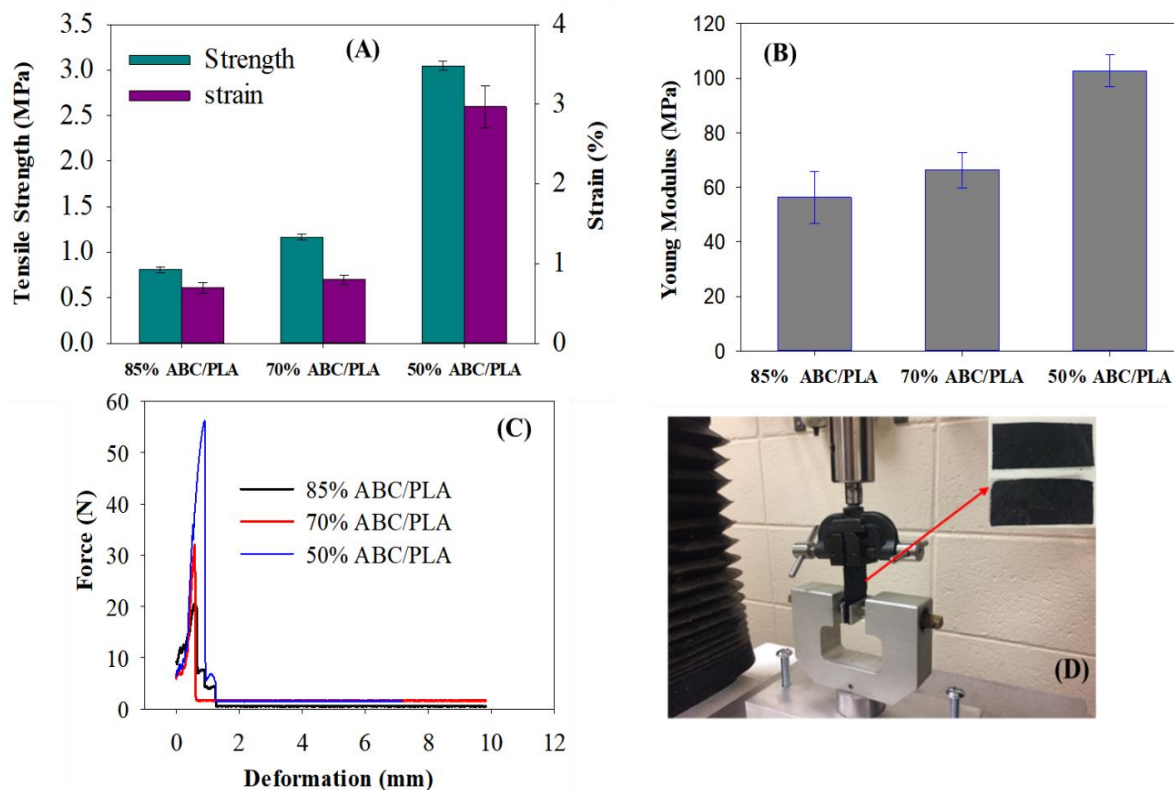


Figure 0.10. Tensile properties of ABC/PLA composite film. (A) Tensile strength and strain; (B) Young's modulus; (C) force vs deformation of 85% to 50% ABC/PLA composite film; and (D) scheme of tensile testing.

1.16.2.3 Thermal properties of ABC/PLA film

TGA analysis was performed to understand the thermal behavior of ABC/PLA composite film in the temperature range of 20–500°C under nitrogen gas (N_2) conditions, as shown in Figure 4. 11. The thermal decomposition stage of the ABC/PLA composite film is divided into three main consecutive regions, and these three regions occur continuously. First, the initial weight loss of ABC/PLA composites occurred at 20-200°C. At this phase,

it is thought that the physically unbound water molecules from ABC/PLA composite were evaporated. Secondly, between 290-430°C, the weight of the ABC/PLA composite is significantly reduced. At this phase, the 50% ABC/PLA-based composite was significantly degraded between 200 and 400°C compared to the 70% and 85% ABC/PLA-based composite film. At the same time, compared with the content of other composites, 85% ABC/PLA composite has less thermally degraded because of containing less amount of PLA. The third stage of all these composites occurred at 400-450°C. At this stage, the residual organic matter was oxidized or carbonized, and the carbonized residue remains in the aluminum pan. Similar thermal stability phenomena has been examined in previous work, in which the weight loss of silver integrated composite film decreased as the metal nanoparticles into the film increased [202].

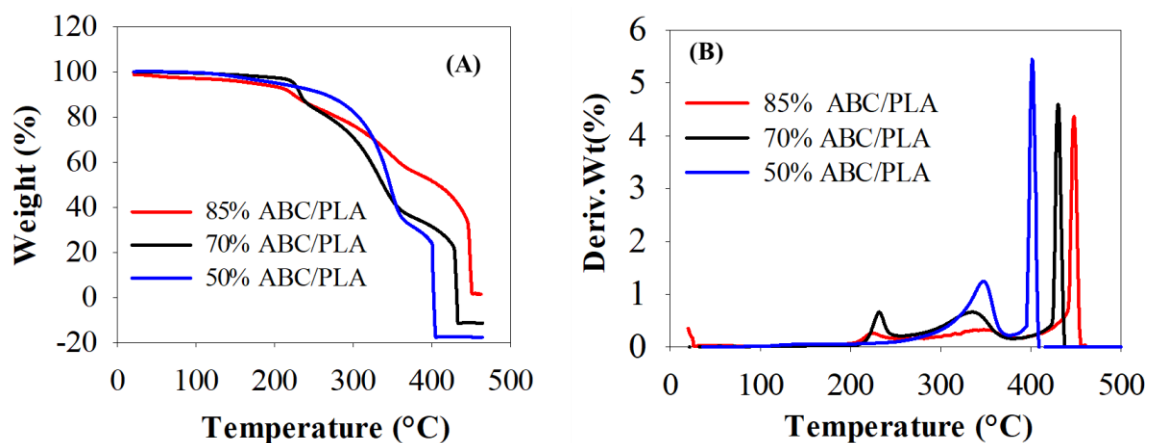


Figure 0.11. TGA spectra of ABC/PLA composite film under nitrogen (N₂) condition. (A) TGA curve for different ABC/PLA composite films; (B) Differential of TGA (DTGA) curves of different ABC/PLA composite films.

1.16.2.4 Electrical properties of ABC/PLA composite

Biosensor developed with 85 to 50% of ABC/PLA-based composite was characterized electrically using cyclic (CV) and differential plus (DPV) voltammetry analysis. According to the Figure 4. 12A, while ABC contents in the ABC/PLA composite rose from 50% to 85%, the CV current increased from 0.32 mA to 2.3 mA. This increase of peak current implied that the composite with increasing ABC and decreasing PLA employed a greater surface of the gold working electrode and effectively transferred electrons in the $[\text{Fe}(\text{CN})_6]^{3-}$ solution. In the similar manner, as shown in Figure 4. 12B, peak current obtained by DPV increased as ABC concentrations into the ABC/PLA composite increased from 50% to 85%. This increase in DPV current demonstrated that a large amount of ABC promotes the dispersion of redox ions to the gold working electrode surface, thus leading to a rise in voltammetry current. In previous studies, a similar increase of current was noticed, while the working electrode was fabricated with activated carbon-based composites from lower to higher concentration [47,149,195]. The peak current of CV and DPV was presented in Figure 4. 12C. It is seen that peak current increased as the ABC in the PLA/ABC composite increased. Current density for different ABC/PLA composite film has been displayed in Figure 4. 12D. 85% ABC/PLA-based composite showed higher current density with higher performance compared to 70% and 50% ABC/PLA-based composite. To validate the advantages of the PLA/ABC composite, CV current was characterized with different scan rates from 5 to 100 mV/s. The peak current rose as the scan rate increased from 2 to 100 mV/s, which revealed that the peak current of CV has a good linear relationship with the increase in scan rate. Though 50% ABC/PLA composite has high tensile properties, but it possessed low thermal stability and poor electrical conductivity. Besides, 70% ABC/PLA composite has poor electrical conductivity and low thermal stability. Because

of this, 85% ABC/PLA composite containing higher electrical conductivity is suitable for biosensor development for smart food packaging.

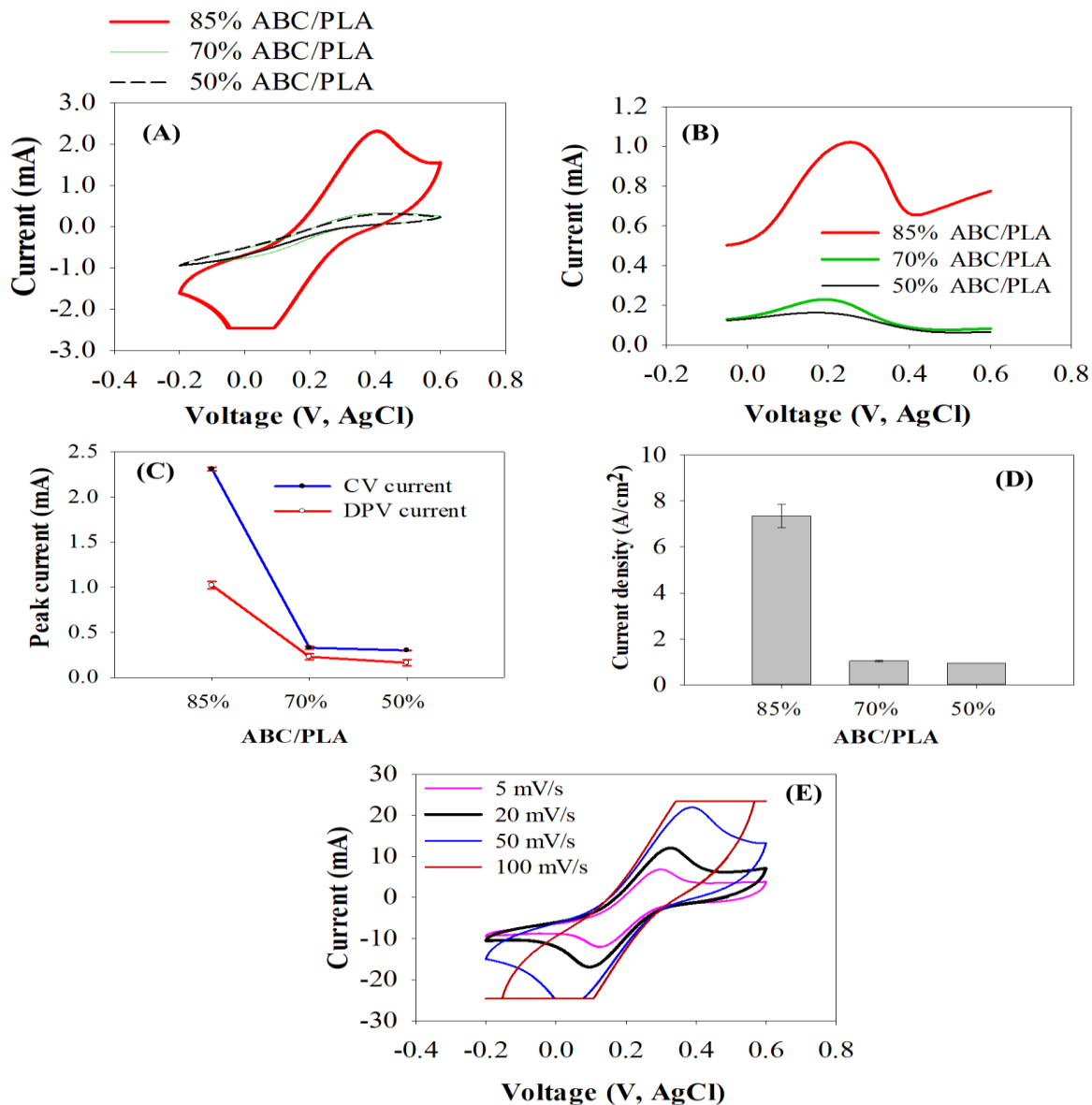


Figure 0.12. Electrical analysis of 85%-50% ABC/PLA composite. (A) Cyclic voltammogram (CV); (B) differential plus voltammogram (DPV); (C) peak currents of ABC/PLA;

(D) current density of ABC/PLA; and (E) cyclic voltammogram with different scan rates (5 to 100 mV/s).

1.16.3 ABC/PLA-based biosensor for ammonia (NH₃) detection

The biosensor fabricated with 85% ABC/PLA-based composite was examined with regard to different standard NH₃ concentrations to understand how the developed biosensor is related to the adsorption mechanism. Ammonia (NH₃) is one of the popular components of volatile gas that is emitted with other volatile materials, including esters, ketones, alcohol and aldehydes during beef spoilage [203–205] and wanted to check in this test how the 85% ABC/PLA biosensor behaves with the standard NH₃ specimens. The resistance (R) values of the 85% PLA/ABC-based biosensor when responding to the selected concentration of NH₃ have been presented in the Figure 4. 13A. It is seen that when the concentrations of NH₃ increased the R values of the biosensor also rose. This is a typical characteristic of carbon-based biosensor (single or multi-walled carbon) which reacts to increasing concentration of the NH₃ [206]. The reason of increasing resistance might be related to the hole depletion of the sensing material; thus, it influences the conductivity of the biosensor. In addition, activated biochar has a large surface area (~825 m²/g) which might be enabled the biosensor to absorb NH₃ gas in its micro-pore surfaces. However, the R values were not significant at a concentration of 0-80 ppm (p>0.05). The significant linear range of R was seen between 80 and 170 ppm, and then no significant variation in the R values were inspected. The lack of linear increase in R values higher than 170 ppm concentration might be attributed to the fact that biosensor was fully saturated with the NH₃ gas concentration. The regression coefficient (R²) value of the 85% ABC/PLA-based biosensor from the

linear regression line was calculated to be 0.9378. The optimum concentration range of NH_3 for the 85% ABC/PLA-based biosensor was between 80-170 ppm; therefore, the limit of detection (LOD) of the 85% ABC/PLA-based biosensor was determined to be 80 ppm.

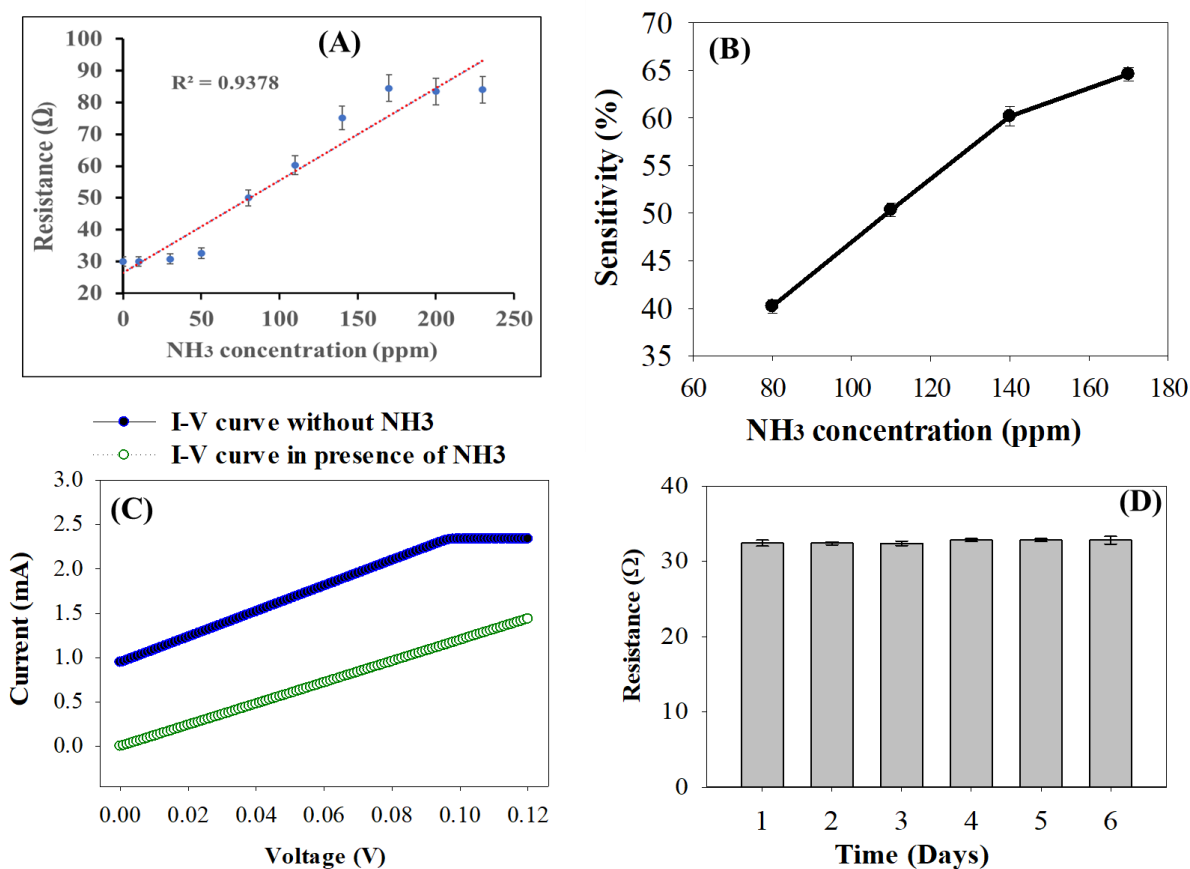


Figure 0.13. A) Resistance response of 85% ABC/PLA-based biosensor to NH_3 concentrations (5 ppm to 230 ppm); (B) Sensitivity of the biosensor to NH_3 gas (80-170 ppm); (C) Comparison of I-V data of 85% ABC/PLA-based biosensor in presence and absence of NH_3 gas (~110 ppm); (D) Stability of the biosensor for fixed NH_3 concentration (50 ppm).

The sensitivity of 85% ABC/PLA-based biosensor was determined at different concentrations of NH_3 gas from 80 to 170 ppm (~20°C) and displayed in Figure 4. 13B. The

dependence of sensitivity on the NH_3 in this range was linear. Nyquist curves for determining NH_3 -sensing using 85% ABC/PLA-based biosensor have been shown in Figure 4. 13C. The data shows the current-voltage (I-V) relationship in presence and absence of NH_3 gas. As can be seen in I-V curve, biosensor exposed to NH_3 revealed lower current compared to unexposed biosensor. Stability of the biosensor was also tested to a fixed NH_3 concentration (~50 ppm) over the 6 days. It is seen that resistance of the biosensor did not reveal the significant fluctuation over the 6 days period, which implies that biosensor possessed good stability (Figure 4. 13D).

1.17 Conclusions

In this study, biochar was activated at different temperatures and activated biochar (ABC) with higher conductivity was generated at 800°C . ABC/ 800°C served extensive surface area of $825.89 \text{ m}^2/\text{g}$ and micropore volume of $0.21 \text{ cm}^3/\text{g}$ for high-efficiency adsorption of the target analytes. The produced ABCs were efficient in producing ABC/PLA composite throughout film casting process. The ABC/PLA film microstructure obtained from SEM confirmed that 85% ABC/PLA film possessed multiple micropores on its surface and were aligned with PLA in the film formation. Compared to 70% and 85% ABC/PLA films, 50% ABC/PLA films are mechanically appropriate for rough use, but they have weak biosensing electrical properties that are not suitable for smart food packaging. The biosensor fabricated with 85% ABC/PLA-based composite resulted in higher electrical conductivity and revealed a sensitivity of ~40% at 80 ppm of NH_3 as a LOD. This study disclosed that 85% ABC/PLA-based composite have a potential role to be used for biosensor applications for smart food packaging.

CHAPTER 5: SYNTHESIZE OF ELECTRICALLY CONDUCTIVE AND BIODEGRADABLE POLYMER FOR BIOSENSOR BY COMBINATORY USE OF SILVER NANOPARTICLES, ACTIVATED BIOCHAR AND POLYLACTIC ACID

ABSTRACT

The aim of this study is to develop the electrically conductive and biodegradable polymer for biosensors and characterize its biodegradable, electrical, and thermal properties. A solvent casting method was adopted to synthesize activated biochar (ABC) with polylactic acid (PLA) to develop the biodegradable ABC/PLA polymer. The developed biodegradable polymer was utilized to prepare a biofilm via a film casting technique. The developed biofilm was studied via biodegradation and results showed that weight loss of ABC/PLA biofilm effectively occurred over 10 weeks of biodegradation from ~9% to ~48.7%. An in-situ oxidative synthesis method was adopted to combine silver nanoparticles (AgNPs) with ABC/PLA polymer carbon paste to produce conductive and biodegradable polymer (AgNP/ABC/PLA). The obtained AgNP/ABC/PLA polymer was electrically characterized for biosensor development via differential plus voltammetry (DPV), linear sweep voltammetry (LSV), cyclic voltammetry (CV), and amperometric voltammetry (AV). It was found that the peak current increased from 0.4 to 1.3 mA for CV; 0.6 to 0.9 mA for DPV, when AgNP contents were combined with a polymer. The biosensor was developed with AgNP/ABC/PLA polymer and found that the fabricated biosensor enhanced its sensing performance to detect ammonia (NH₃) over the range of 5-60 ppm. The results indicated that the biosensor fabrication with AgNPs/ABC/PLA polymer could be very promising and potential to detect ammonia in food and environment application.

Keywords: Activated biochar; composite; Polylactic acid; Biosensor; Smart packaging

1.18 Introduction

The development of highly sensitive, cost-effective, eco-friendly, and biodegradable polymer for biosensors has become one of the most recent research hotspots because of rising concerns regarding food and environmental safety [207]. Food safety has attracted great attention worldwide with outbreaks of foodborne illness in recent years. Therefore, in order to effectively monitor the freshness of foods, the development of eco-friendly, fast, concise and economical polymer for biosensors is in demand [172]. Intelligent food packaging is a newly type of packaging nanotechnology that consists of biosensor or indicator concepts. It aids the customers to communicate with the packaged foods offline and online [26]. Although several biosensors for intelligent food packaging are being researched such as pH-sensitive biosensor using anthocyanin [208], Time-temperature indicators (TTIs) [19], Radio frequency identification tags [43], E-nose sensor [7], the drawback of these components are that their sensing materials are not biodegradable or environmentally friendly; contain expensive raw ingredients, and are still in the developmental stage.

To address these issues, there is a badly need for the development of an eco-friendly and biodegradable polymer for making biosensors to evaluate food safety. In addition, to minimize the packaging waste for the environment, there is a rising global concern in seeking environmentally friendly and biodegradable polymers for food packaging [179]. Polylactic acid (PLA) is one of the biodegradable and environment-friendly polymers [185]. It has a wide range of applications in biomedicine, tissue engineering, food service wares, and packaging films [145,180]. In the previous studies, PLA has been synthesized with single-

or multi-walled carbon nanotube and graphene to develop the bio-nanocomposite that comes with some benefits as they can presume good, mechanical and thermal properties [185,186]. However, single or multi-walled carbon nanotube and graphene are expensive carbon ingredients and not beneficial for biosensor development in food packaging applications. Therefore, there is a need to seek for alternative materials, that are inexpensive, of good electrical conductivity, and high adsorption capacity, to construct the biosensor.

Biochar is one of the richly carbonaceous items which is derived from the anaerobically thermal decomposition of biomass materials [199]. It has a wide variety of advantages over other carbon materials (single and multi-carbon nanotubes, and graphene) such as it is cost-effective; bears high specific surface area; has a highly porous structure and more adsorption sites for target analytes [190–192]. The conventional biochar is normally in millimeter-scale and not electrically conductive; therefore, it is difficult to develop a biosensor using conventional biochar items [188]. Instead, with its activation, the biochar with their reduced size (nano or micro-scale) obtains electrical conductivity and can formulate biosensor.

Ammonia is one of the volatile bioamine compounds that can be excreted from a variety of natural sources such as animal, human, and plant sources [209]. Ammonia excretion has been reported from the wastage of protein-based agricultural and livestock products [207]. After protein deamination, the peptide nucleotide catabolites and amino acids of protein are degraded, and thereby ammonia along with other different volatile basic amines are evolved [210]. Therefore, there is a scope to monitor ammonia as an indicator in protein-rich food products and environment using a biosensor. A wide variety of the biosensor has already been developed using different metals (Au, Zn, Cu, Fe, Sn, and Ti) and their oxides

(SnO₂, TiO₂, MoO₃, V₂O₅, In₂O₃, and so on) to detect ammonia [211,212]. These sensors, on the other hand, perform well at high operating temperatures, usually in the 200–500 °C range, resulting in high power consumption [213]. In addition, these biosensors are not well suited for the intelligent food packaging to monitor ammonia as an indicator, because their biosensing materials are not biodegradable and contain costly raw ingredients which are not beneficial for intelligent food packaging.

According to the Food and Drug Administration (FDA), silver nanoparticles (AgNP) are a safe metal nanoparticle that have been authorized for use in all food contact polymers on the US market [202]. In the previous study, AgNPs have been used with single or multi-walled carbon nanotubes as a dopant metal to detect ammonia at room temperature [209]. In this study, activated biochar has been considered to be used with PLA and AgNPs for a polymer biosensor construction as a low-cost, biodegradable and rapid sensing component for intelligent food packaging. The overall aim of this research was to develop biodegradable and conductive polymer for biosensors and characterize their functional properties. The specific objectives are to 1) develop and characterize biodegradable and electrical properties of AgNPs/ABC/PLA polymers; 2) characterize the conductive properties of AgNPs/ABC/PLA polymer; and 3) employ the developed biosensor to detect ammonia gas.

1.19 Materials and methods

1.19.1 Materials

Poly(lactic acid) (PLA) was provided by from SOC3D Company (MI, USA) and a solution of PLA was prepared by dissolving PLA into chloroform (w/w). Silver nanoparticles (AgNPs, Size: 2 nm) were bought from US Research Nanomaterials Inc. (Houston, USA). The potassium chloride (KCl, purity 99.0%) and potassium ferrocyanide (C₆FeK₄N₆) were

procured from Sigma Aldrich (St. Louis, MO, USA). Acetic acid with purity of 99% and chloroform (CHCl_3) was procured from Sigma Aldrich (St. Louis, MO, USA). PBS solution was ordered from Thermo Fisher Scientific and combined with a highly pure water that had been adjusted to a concentration of 10% (v/v). Triple-distilled water was utilized throughout the entire experiments.

1.19.2 Preparation and activation of biochar

Biochar was made from field corn stover by following the pyrolysis method described previously [194]. The biochar produced was activated by a steam-activation system by following the method described previously [214]. First, the biochar obtained from corn stover were finely milled using the omni mixer homogenizer (Waterbury, Ct., USA). Thereafter, the fine ground biochar was suspended in distilled water and centrifuged at 8000 rpm for 5 min. Following this, the biochar-containing supernatants were collected and dried in an oven at 80°C overnight. Second, dried biochar sample was taken into the reactor and were continuously activated at 800°C using steam for 1 h. After that, activated biochar was taken out from reactor and collected for further analysis.

1.19.3 Biofilm preparation with ABC/PLA polymers

To prepare the biofilm, a solvent casting method was adopted and followed a few steps sequentially. First, ABC powder and PLA (5:1) were manually mixed into 20 g of chloroform solvent. Afterward, the ABC/PLA mixture was slightly stirred overnight, and the completely dissolved ABC/PLA mixture was homogenized for 15 min with a handheld homogenizer (PRO scientific, USA). Following homogenization, the homogenized mixture was poured in a glass petri dish, allowed to dry at room temperature (21 °C) for at least one day. Then, the dried biofilms were peeled from the glass petri-dish and then

conditioned with 50–60% relative humidity (RH). The thickness of the film was measured using a handheld micrometer (Esslinger, MN, USA).

1.19.4 Biodegradation of ABC/PLA biofilm

To investigate the biodegradation of ABC/PLA biofilm, a rectangular glass container (25 cm × 12 cm) was filled with field soil. Afterward, the pre-weighed biofilm (2.54 cm × 2.54 cm) was buried vertically at 2 cm below the soil's surface. Afterwards, the glass bottle was sealed with lids containing 1 cm diameter of air holes to allow for gaseous exchange and incubated at room temperature (21 °C) for 3 months. In every week, the soil glass container was weighed to determine water loss by evaporation and constantly maintained the weight loss of soil by replacing it with sterile water using a fine spray. To determine the biodegradation of the buried film, the ABC/PLA biofilm disc was taken out from the soil and loosely bound soil with the biofilm was removed with a soft brush and properly clean the biofilm surface. Afterward, the biofilms were dried to reduce excess water absorbed by the biofilm and the weight of the biofilm was remeasured. The average weight loss was determined by the following equation:

$$\text{Weight loss \%} = \frac{(M_i - M_f)}{M_i} \times 100 \quad (1)$$

Where, M_i is the initial dried weight of the ABC/PLA biofilm disc; M_f is the dried weight of biofilm disc after burial.

1.19.5 Enumeration of microorganism

To count the microorganisms bound to the biofilm surface, the buried ABC/PLA biofilm was taken out from the soil sample and loosely bound soil with the biofilm was removed with a soft brush [215]. Thereafter, the biofilms were placed into the peptone water, and

the surface of the biofilm was scrapped three times with a sterile razor blade to elute the microorganisms into peptone water. The buffer suspension collected from the biofilm surface was serially diluted and plated onto plate count agar and Potato Dextrose Agar (PDA) plates supplemented with chloramphenicol (25 g mL^{-1}). Afterwar, the plated agar media were incubated at the same temperatures at which the biofilm discs were originally buried.

1.19.6 Scanning electron microscopic analysis

The microstructure of ABC/PLA biofilm was examined by scanning electron microscopy (SEM) after biodegradation (Hitachi-S-3400, filament-based SEM, MO, US). For SEM analysis, the test samples were scanned at a working distance of 10 mm with a magnification of $1500\times$ under 10 kV electrical voltage.

1.19.7 Development of AgNP/ABC/PLA polymers for biosensor

Activated biochar was initially acid-treated with acetic acid under reflux conditions to improve their surface reactivity, dispersion ability and eliminate the non-carbonaceous compounds [212]. Briefly, 1 g of activated biochar was treated with acetic acid (3 M) in a round bottom flask equipped with a condenser. The obtained mixture was first ultra-sonicated followed by stirring for 30 min. Then the sonicated mixture was further refluxed at $120 \text{ }^\circ\text{C}$ for 8 h. The resulting mixture was diluted with the addition of water and washed until neutral pH was reached. Afterwar, the obtained sample was dried overnight in an oven at $60 \text{ }^\circ\text{C}$. Afterward, acid-treated activated biochar (ABC) was mixed with PLA into a chloroform solvent and then gently agitated for at least 10 h. Afterward, Silver nanoparticles (AgNP) at a concentration of 450 ppm (v/v) were added to the ABC/PLA mixture. Then, the obtained mixture, the mixture of AgNPs/ABC/PLA, was gently agitated with 300 rpm at $50 \text{ }^\circ\text{C}$ for at least 2 h and further sonicated for 2 h using an ultrasonicator. Afterward, the

sonicated polymer paste was dropped onto 2 mm diameter of the working electrode for fabrication and then dried the fabricated electrode overnight at room temperature.[49] Subsequently, the fabricated working electrode was followed by dipping the electrode into redox solution [2.5 mmol L⁻¹ [Fe (CN)₆]³⁻ and 0.1 mol L⁻¹ KCl in PBS buffer (pH 7.4, 0.1 M)] for characterization.

In order to fabricate the biosensor, an interdigital micro-array biosensor platform was considered. Then, a 2 μL aliquot of the AgNP/ABC/PAL sonicated polymer paste was aligned on the micro-array biosensor surface. The aligned biosensor was annealed in a dryer at 80 °C for 10 min to bind the AgNP/ABC/PLA polymer to the surface. After completing this step, the annealed biosensor was rinsed with deionized water to elute the unbound residuals. After following this step, the fabricated biosensor was dried at room temperature and the conductivity of the fabricated biosensor was tested using a multimeter to confirm that the fabricated biosensor was able to work efficiently. Afterward, the fabricated biosensor was equipped into an air-tight biosensing test chamber with electrical feedthroughs. Then, a test gas of NH₃ blanced with nitrogen was introduced into the test chamber and detected by monitoring and recording the change of current passing through the fabricated biosensor using a potentiostat (DY2013, Digi-Ivy, Inc., Austin, USA). The sensitivity of the biosensor towards the exposure of NH₃ was calculated as:

$$\text{Sensitivity (\%)} = (R_1 - R_0) / R_1 \times 100 \quad (2)$$

where R_0 = the resistance of the biosensor without gas (base resistance) and R_1 = the resistance of the biosensor when exposed to the gas.

1.20 Statistical analysis

The statistical data analysis was carried out by one-way analysis of variance (ANOVA) and

significant analysis of the data was performed by Tukey test with considering a defined significance level of $p < 0.05$.

1.21 Results and discussion

1.21.1 Biodegradability of ABC/PLA biofilm

Biodegradation of the ABC/PLA biofilm was performed with field soil to analyze the weight loss of the biofilm after the biodegradation over 10 weeks. Figure 5.1 shows the weight loss of ABC/PLA biofilm after each period of the biodegradation. As can be seen that after 2 weeks, ABC/PLA biofilm showed a lower percentage of weight loss (~10%); however, from 2 to 4 weeks of biodegradation, the ABC/PLA biofilms showed an increasing percentage of weight loss (~25%). Between 4-7 weeks, the weight loss of the biofilm increased to ~40% and continued till 10 weeks with ~49 % of weight loss. The percentage of weight loss of the ABC/PLA biofilms at these periods (10 weeks) was about five times compared to 2 weeks of biodegradation.

Weight loss of ABC/PLA biofilm might be happened due to many reasons. One possible reason for weight loss of the biofilm is the microbial growth upon the buried ABC/PLA biofilm surface, which might be degraded the biofilm compositions, resulted in weight loss of ABC/PLA biofilm [216]. Surface roughness of the biofilm components is another possible reason for biodegradation [217]. It has been reported that higher surface roughness of the biofilm can increase the biodegradation of the buried film by providing more sites for bacterial colony settling and proliferation. In addition, hydrophobicity is one key factor determining microbial attachment to the polymer surface. Since ABC materials are hydrophobic materials, during the biofilm buried, ABC/PLA biofilm might have promoted bacterial adhesion on the biofilm surface and accelerated the biodegradation rate. It is seen in

Figure 5. 1B that after 4 weeks, the surface of the ABC/PLA biofilm has cracked down and produced more binding sites upon the film surface, these sites might bind the soil microorganisms upon the film.

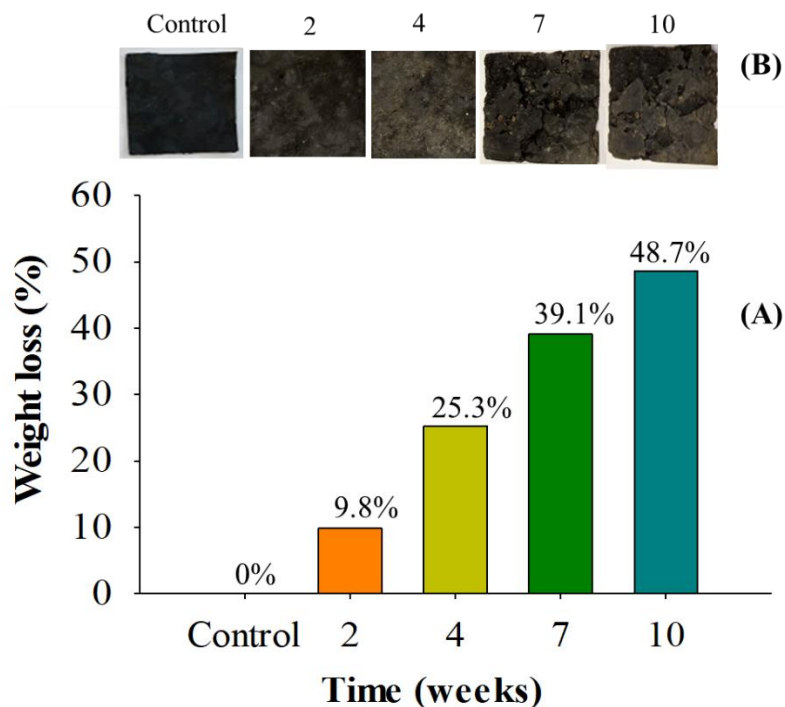


Figure 0.1. Evaluation of biodegradable properties of ABC/PLA biofilm. (A) Weight change of ABC/PLA biofilm over time of 10 weeks buried in filed soil: (B) photographs of ABC/PLA biofilms during biodegradation. Control film refers to the film before biodegradation.

In soil, the major microbial community is bacteria, fungi and protozoa, but bacteria are present in greater numbers [218]. Since bacteria can thrive in both aerobic and anaerobic conditions, they have a better chance of colonization than molds, which are mainly aerobic microorganisms. As seen in Figure 5. 2A, the bacterial and fungal populations in the soil were isolated and grown on the agar media. These grown microorganisms were suspected

to cause biodegradation of ABC/PLA composite film. As can be seen in SEM images (Figure 5. 2B), the microorganisms were attached to the PLA/ABC biofilm surface and microbial attachment upon the biofilm was spread throughout the biofilm.

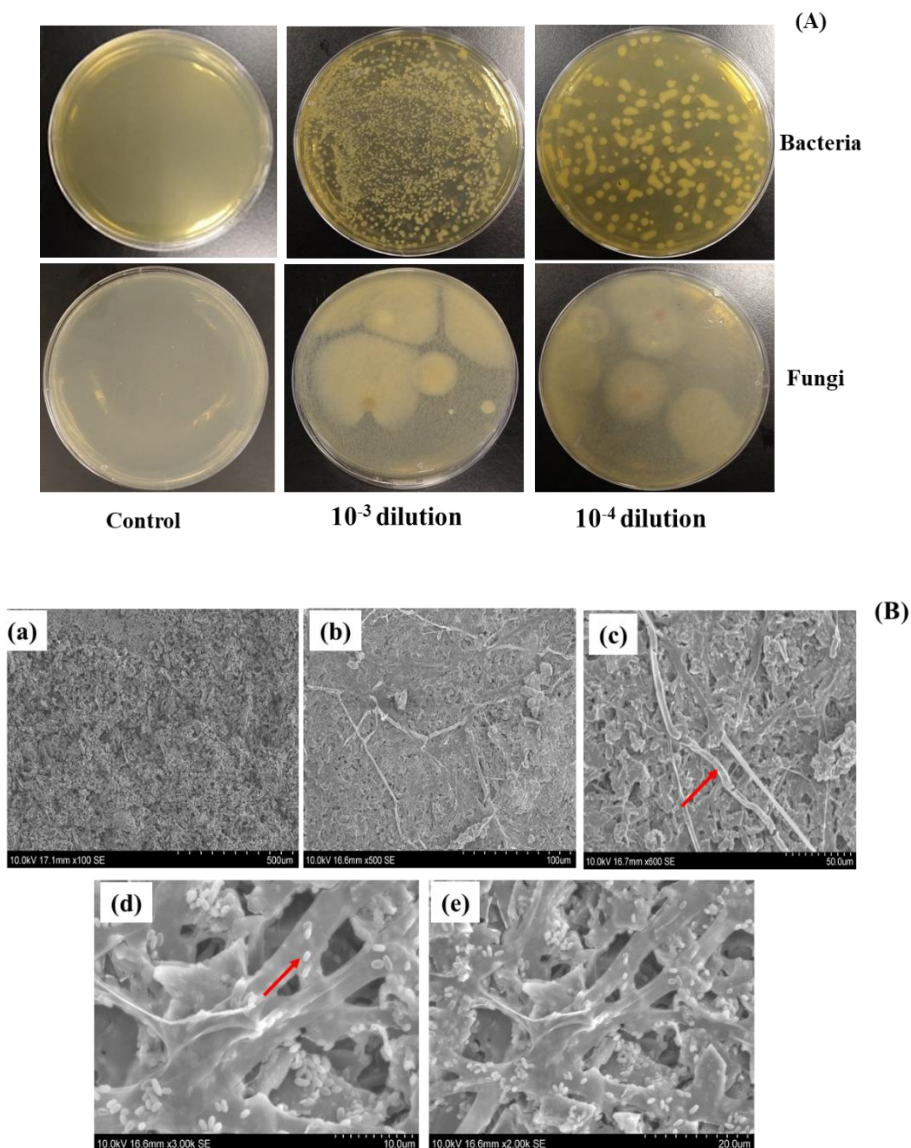


Figure 0.2. Evaluation of biodegradable properties of ABC/PLA biofilm. (A) Isolation of microorganism and fungi grown on the surface of agar media; (B) SEM analysis of recovered ABC/PLA biofilm after biodegradation: (a) SEM observation of control film; (b-c)

Mold observation on the biofilm; (d-e) bacteria observation on the biofilm after biodegradation. Control film refers to the film without biodegradation.

It was assumed that these bound microorganisms to the PLA/ABC biofilm surface were attributed to the reason of biodegradation by utilizing the hydrocarbons of ABC/PLA film as a carbon source. In contrast, the control biofilm, that was unburied at room temperature, was clear and had not bound the microorganisms/fungal growth. It is reported that a variety of microorganisms use the hydrocarbon as nutrients, particularly when starved and lacking essential nutrients [215], thus they played a crucial role for biodegradation.

1.21.2 Characterization of AgNP/ABC/PLA polymer

1.21.2.1 Electrical analysis

The electrical properties of AgNP/ABC/PLA and ABC/PLA polymers were evaluated through the stepwise modification of the working electrode via DPV, CV, LSV and AV. The peak currents determined by CV and DPV increased after AgNP deposition compared to the peak current for the electrode without AgNPs deposition to polymer (Figure 5. 3A and B). The increasing peak current confirmed that AgNP integrated polymer occupied a wide surface area on the electrode and allowing effective electron transfer in the $[\text{Fe}(\text{CN})_6]^{3-}$ solution and facilitated the redox species to be diffused to the electrode surface, and therefore resulting in a rise in voltammetry current. A similar increase in current was found in a previous study, while the working electrode was fabricated with increasing quantities of metal nanoparticle enriched nanocomposites [202]. In the case of AgNP integrated polymer, the current obtained by LSV and AV increased (Figure 5. 3C and D). This increase in voltammetry current might be occurred due to the negative charge obtained from the

AgNPs. Meanwhile, it was thought that AgNPs/ABC/PLA polymer served more electron transfer channels, which played a pivotal role in increasing current. The current density on the fabricated electrode has been displayed in Figure 5. 3E. It is seen that the electrode fabricated with AgNP/ABC/PLA polymer showed higher current density with higher performance. This increasing current density can be explained by the fact that AgNPs in the polymer decreased steric inhibition between the reducible groups; therefore, they improved the current response of the working electrode surface. Considering the electrical properties and other factors, it can be concluded that AgNP integrated polymer is suitable for biosensor development.

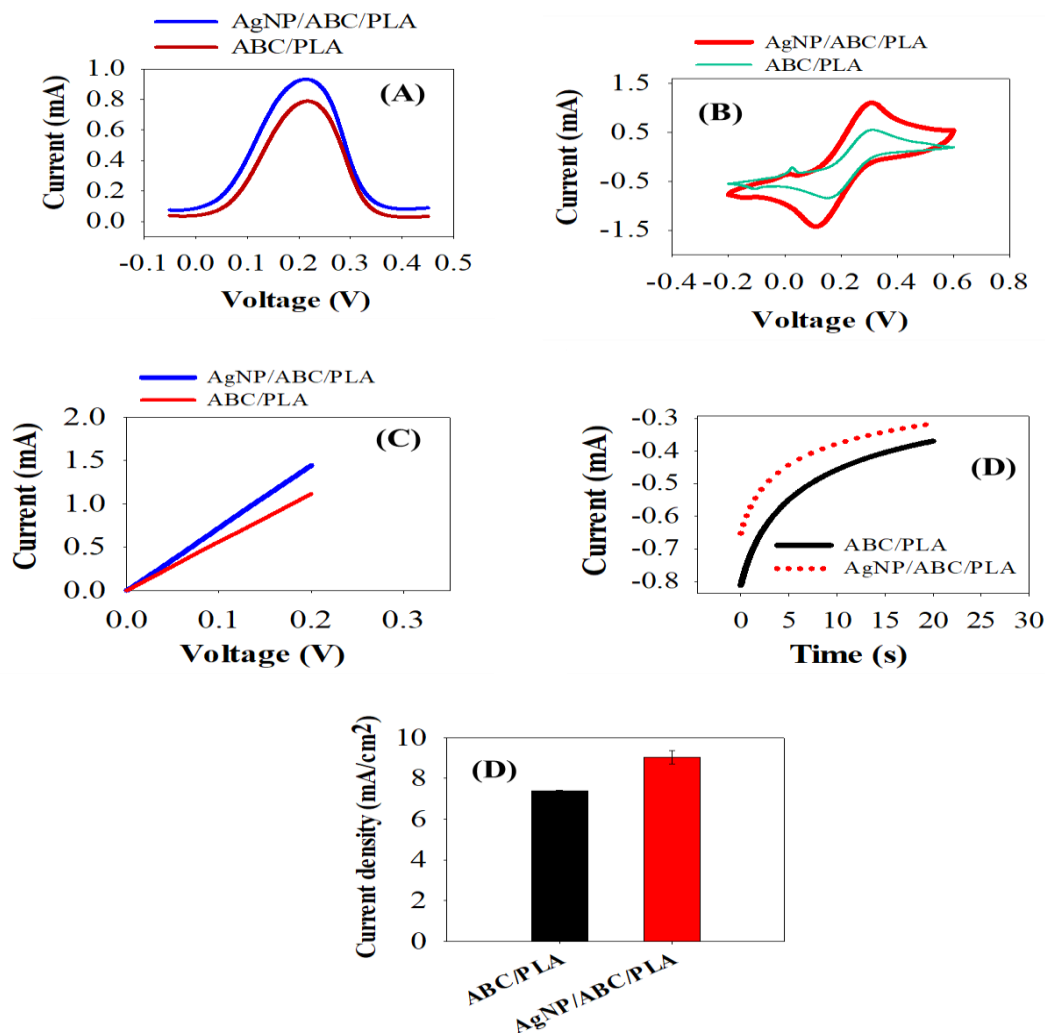


Figure 0.3. Electrochemical analyses of AgNPs/ABC/PLA and ABC/PLA polymer. (A) Cyclic voltammogram (CV); (B) differential pulse voltammogram (DPV); (C) linear sweep voltammogram (LSV); (D) amperometry voltammogram (AV); and (E) current density of AgNPs/ABC/PLA and ABC/PLA polymer.

1.21.2.2 Thermal stability analysis

TGA analysis was performed to compare the thermal stability of AgNPs/ABC/PLA and ABC/PLA polymer in 20–500°C under oxygen gas (O₂) conditions. As shown in Figure 5.

4, the initial weight loss was continued between 20-200°C. It is thought that the physically unbound water molecules from the polymer sample were evaporated. Secondly, between 290-430°C, the weight of the ABC/PLA polymer sample is significantly reduced. At this phase, the ABC/PLA polymer was significantly degraded between 200 and 400°C compared to the AgNP/ABC/PLA polymer sample, while AgNP/ABC/PLA polymer sample has less thermally degraded because of containing AgNPs. The third stage of all these composites occurred at 400-450°C. At this stage, the residual organic matter was oxidized or carbonized, and the carbonized residue remains in the aluminum pan. Similar thermal stability phenomena have been examined in previous work, in which the weight loss of silver integrated composite film decreased as the metal nanoparticles into the film increased [202].

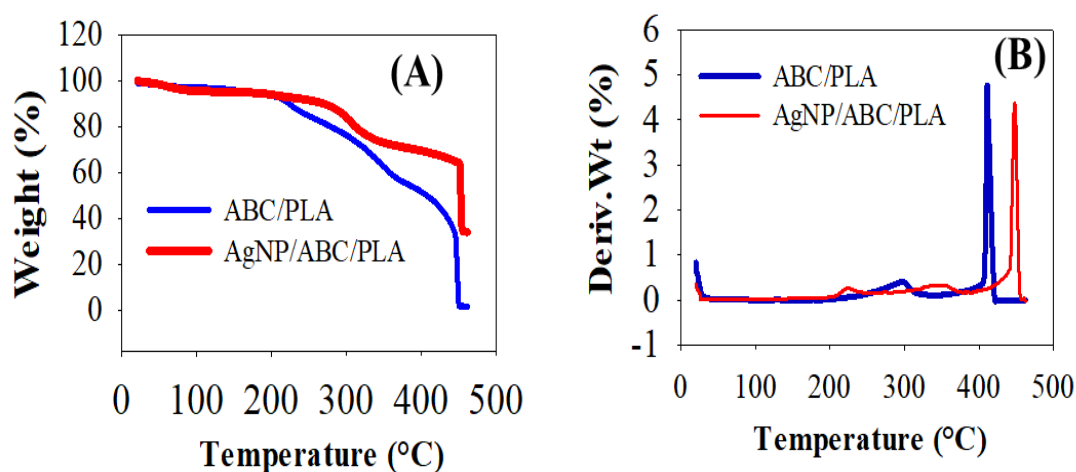


Figure 0.4. TGA spectra of ABC/PLA and AgNP/ABC/PLA polymer sample under nitrogen (O_2) condition. (A) TGA curve; (B) Differential of TGA (DTGA) curves of ABC/PLA and AgNP/ABC/PLA polymer sample.

1.21.3 Characterization of the fabricated biosensor

1.21.3.1 Sensitivity analysis

The surface area and pore volume upon the biochar are the crucial factors for biological molecule and gas absorption as a potential filler for polymeric composite preparation [198]. The extensive surface area and internal pore structure of biochar can contribute to the high absorption capability and serve good mechanical and thermal properties between filler and matrix.[199] As seen in Figure 5. 5A, BET and Langmuir surface area of ABC was significantly higher, as 825.89 m²/g and 0.21 cm³/g respectively. In the previous studies, it has been shown that the BET surface of carbon nanotube and graphene was referred to 458.8 and 582 m²g⁻¹, respectively [219,220]. Compared to carbon nanotube and graphene, ABC has a larger surface area and micropore volume that serve as a good candidate for gas absorption. Though, the physical absorption of gas molecules by the biochar is higher compared to SWCNTs and graphene. However, the carbon items can poorly absorb the lower concentrations of gas molecule and weakly react particularly with gas molecules, and thereby it gives the low sensitivity because of a little charge transfer from gas to carbon items [187,221].

The ammonia sensing performance of the fabricated biosensor, before and after AgNPs deposition, was tested and the biosensor's sensitivity response has been shown in Figure 5. 5. When the biosensor was exposed to a selected and lower concentrations of ammonia, the sensitivity of the fabricated biosensor increased from ~5 to 25%, as the gas concentration increased from 5 to 60 ppm. And the results of the biosensor when responding to the lower selected concentration of NH₃ have been presented in Figure 5. 5B. A similar phenomenon was seen for the AgNP/MWCNT-based biosensor, while biosensor response increased with rising ammonia concentrations [222]. The reason for increasing sensitivity

might be related to the AgNPs of the polymer composite significantly reacted to the increasing concentrations of ammonia and led to the hole depletion of the sensing material; thus, it influences the conductivity of the biosensor.

However, the sensitivity of the biosensor without AgNP deposition, on the other hand, was ranged from 0.2 to 1.0 percent at the same concentration (Figure 5. 5C). This phenomenon is attributed to the fact that AgNPs played an important role in improving ammonia sensitivity, which is why AgNP-synthesized carbon paste exhibited higher sensitivity to ammonia than the sensor fabricated without AgNPs deposition. In addition, although activated biochar (ABC) has a large surface area ($\sim 825 \text{ m}^2/\text{g}$), the biosensor developed without AgNPs deposition might be weekly absorbed lower quantities of ammonia gas in its micro-pore surfaces. The comparison of the sensitivity of the fabricated biosensor before and after AgNPs deposition was displayed in Figure 5. 5D. It shows that the biosensor fabricated with AgNP/ABC/PLA polymer shows higher sensitivity.

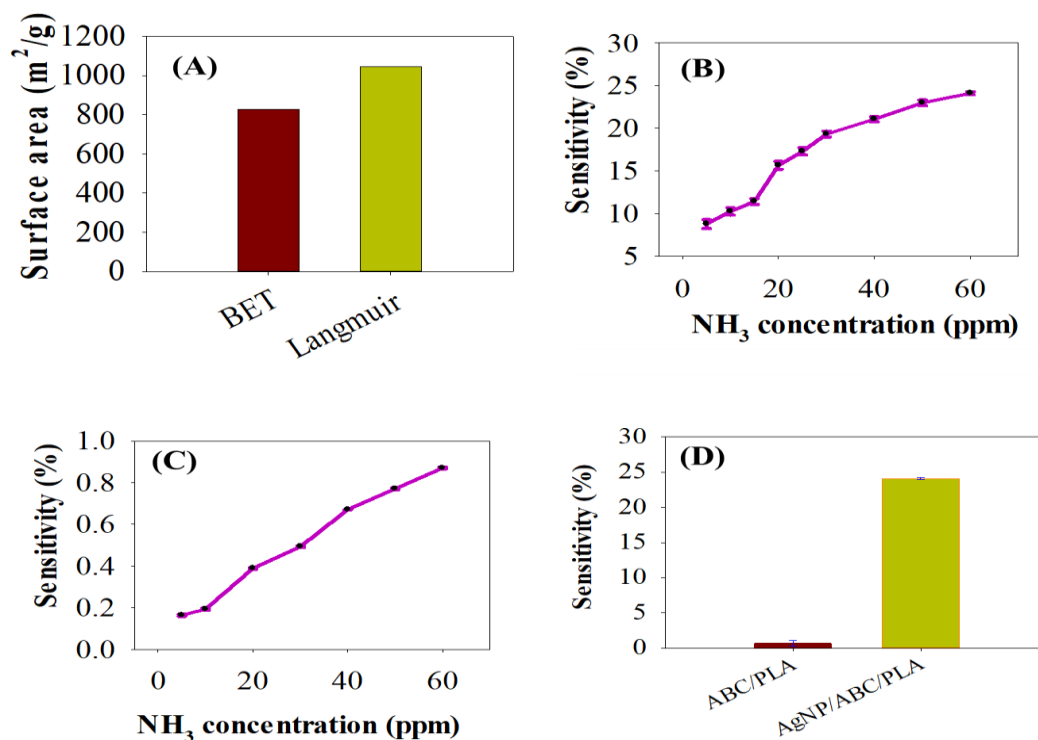


Figure 0.5. Surface area of the activated biochar (ABC) (BET and Langmuir analysis); (B) Sensitivity (%) of the fabricated biosensor developed with AgNP/ABC/PLA polymer for ammonia (NH₃) (5-60 ppm); (C) Sensitivity (%) of the fabricated biosensor developed with ABC/PLA polymer for ammonia (NH₃) (5-60 ppm); (D) Comparison of sensitivity (%) of the fabricated biosensor developed with AgNP/ABC/PLA and ABC/PLA polymer for ammonia (NH₃) (60 ppm).

1.21.3.2 Ammonia sensing mechanisms

Biochar has some functional groups (e.g., carboxyl and hydroxyl groups) at their surface and they play a key role in providing metal-binding sites.[223] In the previous studies, aluminum (Al), copper (Cu), and lead (Pb) binding onto biochar surface have been reported due to complexation of metals with the carboxyl groups at their surface [223,224]. In

AgNPs/ABC/PLA polymer, we assumed that these carboxyl groups were bound with AgNPs. The schematic representation of ammonia (NH_3) adsorption with atomic positions and electron transfer in AgNPs/ABC/PLA polymer surface has been shown in Figure 5. 6. When the electric interaction occurs between AgNPs and carboxyl groups, oxygen attracts valence electrons of silver at atmospheric pressure and room-temperature because the electronegativity of silver (Ag) is higher than that of silver in the carboxyl groups [209]. The positive Ag ions create the hole depletion regions at the surface of AgNP/ABC/PLA and generate effective ammonia adsorption sites. Furthermore, the ammonia molecule contains a lone-pair electron that serves as an electron donor. When they come into contact with Ag, they provide electrons and easily react with them [209]. In addition, the electron affinity level of Ag is ranged between 2.0-2.5 eV, and ammonia can easily share electrons to the oxidized Ag on the biosensor surface [209]. In addition, the biochar surface has numerous micropores that allow ammonia molecules to be absorbed on the biochar surface. After ammonia adsorption on the surface of the AgNP/ABC/PLA surface, the energy balance in the adsorption area will change. Since activated biochar (ABC) is a p-type semiconductor, the transfer of charge from Ag to ABC will cause holes to be depleted, resulted in increased electrical resistance.

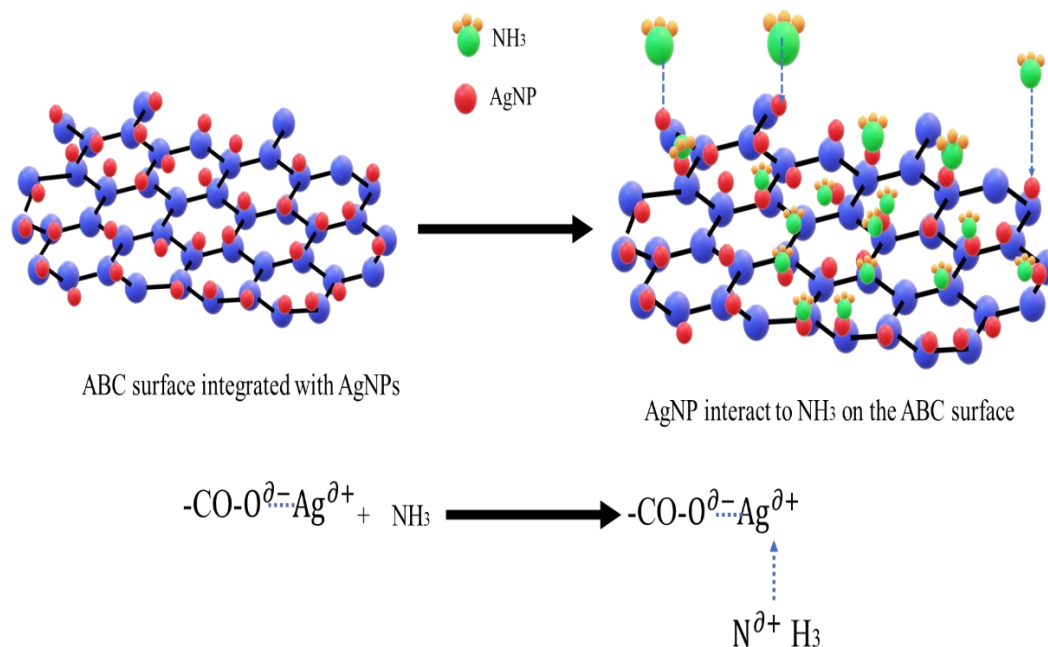


Figure 0.6. Schematic representation of ammonia (NH₃) adsorption with atomic positions and electron transfer in AgNPs/ABC/PLA polymer surface.

1.21.3.3 Selectivity, reliability and reusability properties

Selectivity is an important property of the biosensor. To determine the selectivity of a AgNP/ABC/PLA-based biosensor, the developed biosensor was tested on several other gases, including hydrogen (H₂), oxygen (O₂) and nitrogen (N₂). The sensing performances have been displayed in Figure 5. 7A. As can be seen, the AgNP/ABC/PLA-based sensor has excellent selectivity to ammonia among all other components. The sensor exhibited a lower electrical response to the other gases including H₂, O₂ and N₂. The negligible resistance of the biosensor was inspected for O₂. This means that O₂ is an oxidizing gas and an electron acceptor. During the sensing response, a charge transfer from sensor to O₂ has been occurred. Reliability of the biosensor was also tested over 50 days in the air. It is seen that the resistance of the biosensor did not reveal the significant fluctuation over the 50

days period, which implies that the biosensor possessed good reliability (Figure 5. 7B). Repeatability of the sensor was studied over 6 times. After each time sensor test, the biosensor response was verified. The results exhibited that the resistance of the biosensor was almost identical until 3-time use. Afterward, the sensor response has fluctuated for a slight upward drift in the current. The reason for the slight drift may be the same sensor surface was not retained after reuse after 3 times.

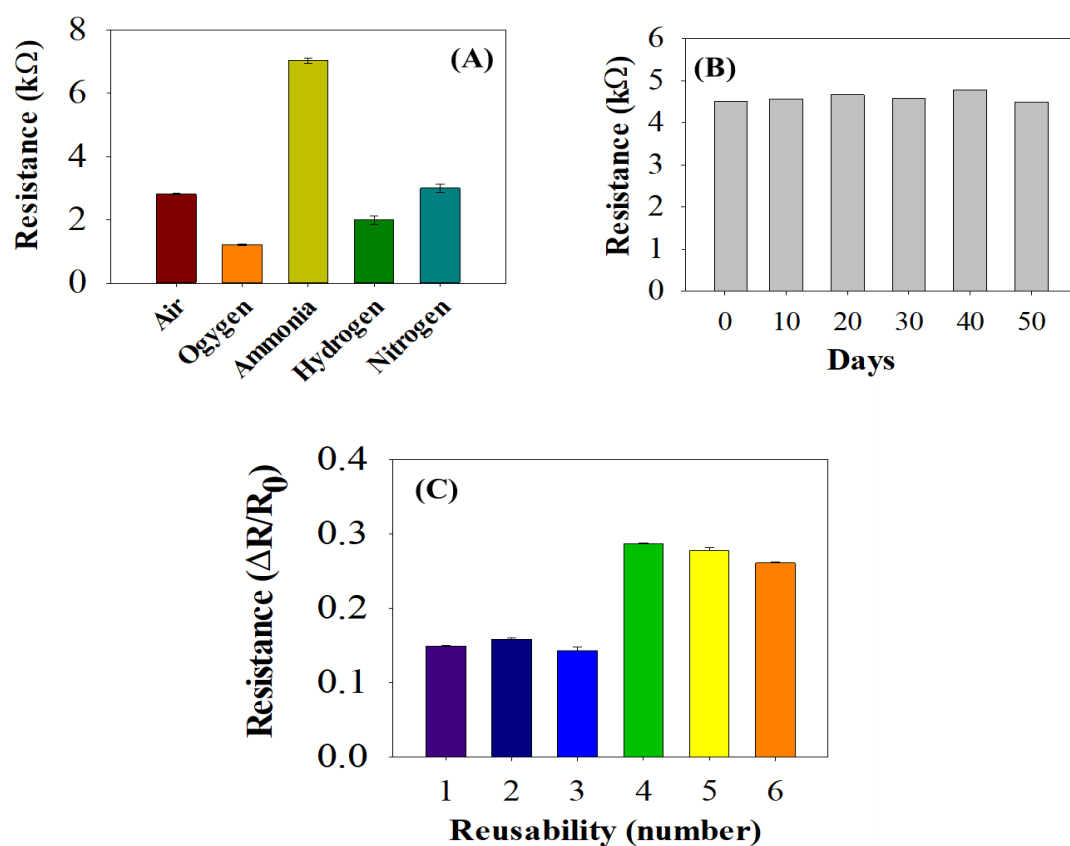


Figure 0.7. Evaluation of biosensor properties. (A) Selectivity analysis of the biosensor over the different gas; (B) reliability of the biosensor; and (C) Reusability of the biosensor over 6 times.

1.22 Conclusions

ABC/PLA biofilm was developed, and biodegradability properties of the biofilm were verified. The results confirmed that ABC/PLA biofilm was effectively biodegraded under the field soil. The SEM microstructure of the biofilm confirmed that bacteria and fungi were effectively attached on the biofilm surface during biodegradation. The thermal stable properties of AgNP/ABC/PLA polymer were greater than those of non-Ag integrated polymer. The electrode fabricated with AgNP/ABC/PLA polymer had a higher current compared to the electrode fabricated with non-Ag-integrated polymer. The biosensor sensitivity improved noticeably as the NH_3 concentrations increased from 5 to 60 ppm. Furthermore, the results suggested that the biosensor developed with AgNPs/ABC/PLA polymer could be very promising in detecting the lower concentration of NH_3 .

CHAPTER 6: DEVELOPMENT OF A POLYLACTIC ACID-COATED NANOCELLULOSE/CHITOSAN-BASED FILM FOR REAL TIME MONITORING OF BEEF SPOILAGE

(Published in Analytical Methods, doi.10.1039/D1AY00365H)

ABSTRACT

Food safety is one of the biggest challenges in global markets. There is a critical need to develop a simple, affordable, and environmentally friendly color indicator that can fast and conveniently monitor and indicate the quality of packaged food products at home, supermarkets, shops, etc. This study aimed to develop a nanocellulose/chitosan-based film coated with polylactic acid (PLA) to monitor beef spoilage in real-time. This film was fabricated by casting suspension of nanocellulose/chitosan mixture doped with methyl red, followed by a coating of PLA on the film surface, named PLA/NCM film. The film displayed a visible color change in response to different pH buffer solutions (2–10). The PLA/NCM film was applied to monitor the spoilage of beef at a refrigeration condition (4 °C) and showed an apparent color change after 5 days as a threshold for the beef spoilage. The color modulation of the PLA/NCM films was processed for each time via the colorimetric device and revealed substantial color difference values (ΔE) after 5 days of beef spoilage. The total viable microbial counts (TVC) and pH of the beef sample were determined, and the findings showed that the TVC and pH increased simultaneously during the beef spoilage. Although further research is necessary, the PLA/NCM film has the potential to be a color indicator for applications in both smart food packaging and real-time monitoring spoilage of beef and other meat products.

Keywords. Smart packaging; Indicator; Film; Polylactic acid; Food Spoilage

1.23 Introduction

Smart packaging is a packaging system which can monitor the condition of the packaged foods or food environments and improve the quality of food during transportation and storage [20]. The most common techniques used to monitor the condition of foods are time-temperature indicators, radio frequency identification, thermochromic ink, gas chromatography and electronic chemical nose [2]. These methods monitor the volatile and biogenic amines produced as metabolites related to food spoilage. The most common metabolites produced after meat and fish spoilage are ionized or deionized ammonia, histamine, tyramine, cadaverine and putrescine [173,225,226]. However, these methods have some drawbacks. For example, they require a higher level of expertise, are time-consuming and expensive, and have low precision [47,49,150,195,227]. In addition, these packaging materials are not recyclable and are poorly biodegradable, led to unnecessary waste disposal and environmental contamination issues [228]. There is therefore a need for a fast, convenient, low-cost, and eye-catching method to assess the quality of packaged food products at home, supermarkets, shops, etc.

Chitosan is one of the copolymers that comprises of β -(1-4)-2-amino-d-glucose and β -(1-4)-2-acetamido-d-glucose units [229]. The polysaccharide backbones in chitosan have excellent physicochemical properties that make them ideal for use in food packaging, biomedical applications, and the chemical industry. Recently, chitosan has received an approval from the U.S. Food and Drug Administration (FDA) and regulatory agencies for their usage as the biomaterials in a variety of commercial food products [230]. In the previous studies, the use of chitosan has been reported with brown rice starch, Chinese root

extract, alizarin, etc. for developing packaging film [229,231,232]. We have considered chitosan in our study because it owns excellent film formability, high transparency, biodegradability, and high mechanical property [229].

The most popular organic polymer in nature is cellulose, which has attractive features such as biocompatibility, low cost, low density, and good mechanical properties [233]. Cellulose nanofibers (CNF) with a width of 50 nm have been identified as a reinforcing material for packaging film formation [16]. The ideal characteristics of CNF are transparency, inexpensive, low density, flexibility and good chemical stability [202]. In addition, CNF acts as an excellent additive modifier to improve the film's performance and has eco-friendly, and naturally degradable properties [233]. The physical combination of CNF and chitosan, along with methyl red (MR) as an acid-base indicator, can offer a potential pH-sensing nanocomposite for film preparation.

The first generation of biodegradable polyester is poly-lactic acid (PLA) and has been commonly used in the form of pure or blended polymer as food packaging film [234,235]. The reason for using PLA in this study is its biodegradable and biocompatibility properties which eliminates health challenges in food packaging, and its benefits due to its abundance, cleanliness, and reasonable cost. Furthermore, the coating of PLA as a thin layer enhances the mechanical strength of the film and considerably rises porosity upon the film, resulting in a higher surface area, which helps the sensing element to be entrapped onto the film surface [234,236]. Although different film indicators for food spoilage have been developed, such as pH indicator film [237], anthocyanin film [238], azo-anthraquinone film [174], and dye-based indicator film [239], all of these films have lower mechanical strength, poor color stability, and difficulty to determine onset-detection associated with

the spoilage threshold. To overcome these limitations, PLA/NCM film as an on-packaged indicator has been considered as a new alternative approach via eye-catching detection of meat spoilage. To the best of our knowledge, no studies have been reported so far on this functionalized dyestuff with nanocellulose/chitosan, so we decided to use this film to monitor meat spoilage. The main aim of this work is to develop PLA/NCM film as an on-packaged indicator for real-time monitoring of meat spoilage. The objectives of this work are to 1) develop PLA/NCM film and characterize the functional and microbial response properties, and 2) to employ the indicator film to monitor for meat spoilage.

1.24 Materials and methods

1.24.1 Materials

CNF's aqueous-based gel with 3 percent solid purity and 87 percent crystalline index was obtained from the University of Maine Process Development Center (Orono, ME, USA). Chitosan with a deacetylation degree of 75 % and Methyl red (MR) were acquired from Sigma-Aldrich (St. Louis, MO, USA). The stock solution of MR was made by dissolving MR into 70% (v/v) of ethanol solution to yield a concentration of 1 mg/mL. Polylactic acid (PLA) employed in this research was procured SOC3D Company (MI, USA) and the solution of PLA was prepared by dissolving PLA in chloroform (w/w). The density, melting point and glass transition temperature of PLA were 1.24 g/cm³, 160°C and 57.8°C, respectively.

1.24.2 Preparation and fabrication of PLA/NCM film

The PLA/NCM film's solution was prepared as described below. Initially, 30 mL of MR suspension was prepared with 70% of ethanol, and concentrations of MR in ethanol were maintained at 1mg/mL. Second, 4.5 g of CNF gel was taken with MR solution and then

slightly agitated for 20 min to produce an MR dopped CNF suspension. Then, 0.5 g of chitosan was added to the MR dopped CNF suspension and then homogenized with a handheld homogenizer (4000 rpm) for 15 min. The prepared homogenized mixture of MR, CNF and chitosan was then transferred into a petri-dish (diameter 13 cm) and dried two days at room temperature (21 °C) to get a dried MR dopped nanocellulose/chitosan film, which is renamed as NCM film. Afterward, the dried NCM film was dipped into 2% PLA (wt.%) solution and coated the film for 5 min to generate PLA/NCM film. Afterward, PLA/NCM film was dried for 8 h at room temperature (21 °C). Then, the PLA/NCM film was washed with deionized water (D.I) to eliminate unbound color residues within the film surface. Thereafter, PLA/NCM film was again dried for 8 h at room temperature and kept in a desiccator at 50–60% relative humidity (RH) for 2 days. A hand-held micrometer was used to measure film thickness (Esslinger, MN, USA). The synthesis process of PLA/NCM film was summarized and shown in Figure 6. 1.

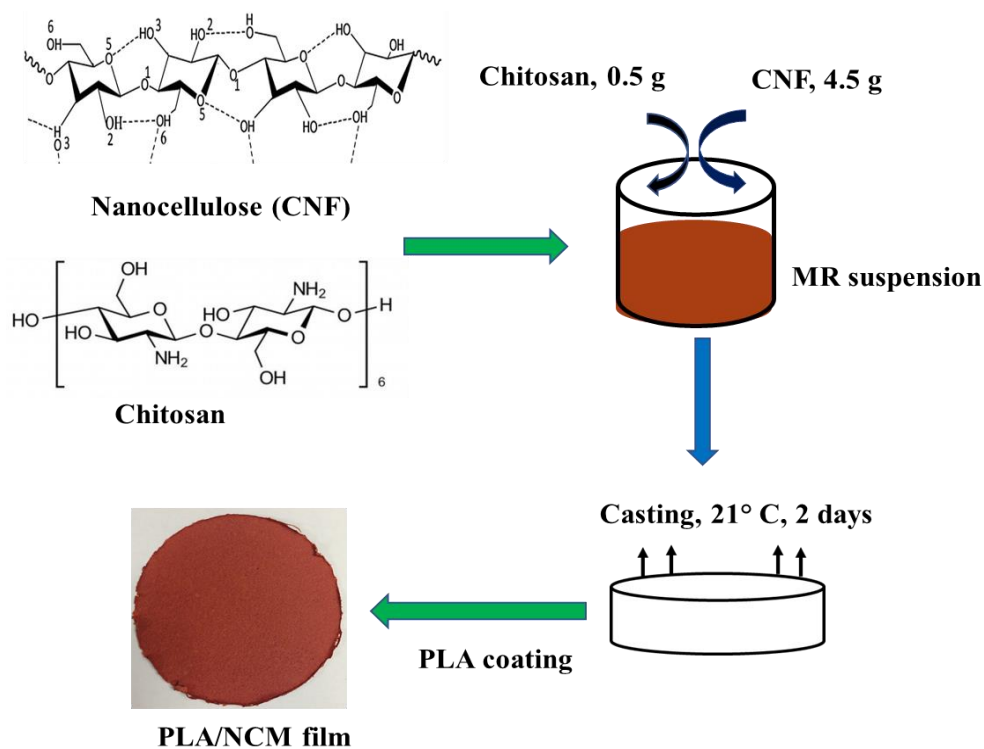


Figure 0.1. Schematic diagram for the formation of PLA/NCM film using cellulose nano-fiber (CNF), chitosan, methyl red and polylactic acid (PLA).

1.24.3 Characterization methods

1.24.3.1 Mechanical analysis

PLA/NCM film (50 mm long and 20 mm wide) was mechanically analyzed by following the method developed previously [16]. A texture analyzer fitted with Texture Exponent 32 software (Texture Technologies Corp., Scarsdale, NY, USA) was used to compute tensile force and deformation. The crosshead speed was set to 60 mm/min. Tensile strength (TS) and strain were determined based on the strength and deformation data recorded by the following equation.

$$TS = \frac{\text{Maximum applied force}}{\text{Film thickness} \times \text{Film width}} \quad (1)$$

$$\text{Strain} = \frac{\text{Elongation}}{\text{Original length of film}} \quad (2)$$

1.24.3.2 Photodegradation analysis

Photodegradation of the PLA/NCM film (2 cm x 2 cm) was evaluated by following the method described previously [240,241]. For this analysis, the film samples were placed at 38 cm distance from the aperture of visible light irradiation (40 W, halogen lamp, white color) at room temperature (21 °C) and atmospheric pressure. The color change of the film was measured using a hand-held color reader (Precise color reader, WR-10QC, China) on the daily basis.

1.24.3.3 Fourier transform infrared spectroscopy (FTIR)

FTIR analysis of the PLA/NCM film was conducted by following the Tensor 37 spectrophotometer to analyze the functional groups of the film components. The sample holder of the FTIR device was directed at 90° to the incident beam and parallel to the ground. The FTIR spectra were recorded at room temperature in the range of 500 to 4000 cm⁻¹ and collected with 20 scans at 4.0 cm⁻¹ resolution using the omnic spectroscopy software.

1.24.3.4 Color analysis of PLA/NCM film

Color analysis of PLA/NCM film was performed according to the previously described method [226]. First, a square piece of the PLA/NCM film (2 cm x 2 cm) was subjected to the various pH buffers (2-10). Afterward, the color change values (L*, a* and b*) of each PLA/NCM film were assessed via the hand-held color reader (Precise color reader, WR-10QC, China). A CIE-Lab color scale was applied to determine the degree of lightness

(L*), redness (+a*) or greenness (-a*), and yellowness (+b*) or blueness (-b*) of the films. The color evaluation was carried out in three different points of the film. The total color difference (ΔE) value was determined by the following formula.

$$\Delta E = [(L^*_{\text{film}} - L^*_{\text{standard}})^2 + (a^*_{\text{film}} - a^*_{\text{standard}})^2 + (b^*_{\text{film}} - b^*_{\text{standard}})^2]^{0.5} \quad (3)$$

1.24.4 Application of PLA/NCM film for monitoring meat spoilage

1.24.4.1 Beef spoilage analysis using PLA/NCM film

Meat freshness refers to fresh meat that has not yet been spoiled or contaminated. Freshly sliced beef sample with a pH of 5.1 to 5.4 was obtained from Walmart Super Market, Brookings, SD and the sample was delivered to the lab within 30 min. The average post-mortem time of this meat when bought was around 2 h. Then, 10 g of beef sample was taken into petri-dish and a thin strip of PLA/NCM film was placed inside of that petri-dishes in direct contact with beef in the petri-dish atmosphere. Afterward, the petri-dish was tightly packed with parafilm to eliminate air dispatch. Then, it was stored at refrigeration temperature (4 ± 0.2 °C) in order to assess the performance of the film for monitoring the beef spoilage. The temperature of the refrigerator was monitored using a thermometer during the storage period.

1.24.4.2 Microbial analysis of beef sample

The total viable count (TVC) of microorganisms in the beef samples was counted by following the previously described method with a minor modification [9]. To perform this analysis, approximately 10 g of beef samples were weighed and placed in sterilized Ziplock freezer bags [237]. Thereafter, 90 mL of peptone water solution was added and homogenized in a stomacher under the aseptic conditions for the 60 s at room temperature (Seward

stomacher 400). The homogenized samples were then kept in the refrigerant condition (4 ± 0.2 °C) and allowed to deteriorate. During the beef spoilage trial, serial dilutions of the sample were prepared. Afterward, 0.1 mL of the appropriate dilutions were spread on the plate count agar (TSA; Merck, Darmstadt, Germany) and incubated the plates overnight at 25 °C. After overnight incubation, agar plates were counted, and the results were correlated with the PLA/NCM film's response. Colonies were counted and reported as log colony forming units (CFU) per gram.

1.24.4.3 pH and ammonia ions analysis in beef sample

The pH values of the beef sample were measured using a pH electrode (Mettler Toledo GmbH/Switzerland). To measure the pH values, nearly 10 g of beef samples was added in the 90 mL of DI water and then homogenized in a stomacher under the aseptic conditions for the 60 s at room temperature. The homogenized samples were then kept in the refrigeration condition (4 ± 0.2 °C). Afterward, the glass electrode of pH meter was dipped in the homogenate beef sample and then periodically recorded the pH values in relation to time and temperature. In a similar manner, to determine the ammonium concentrations in the beef sample, an ammonium electrode was used (Oakton, Cole-Parmer, Vernon Hills, IL, USA). The ammonium electrode response was measured by dipping the electrode in a homogenized beef sample. The electrode response values obtained were interpolated in the calibration curve that was constructed between 50 and 300 mg/L of standard ammonium solution (Standard ammonium chloride, Oakton, USA). The concentrations of the ammonium ion into the beef sample after their spoilage were calculated using the linear part of the calibration curve [$R^2= 0.9628$]. Each analysis was repeated three times.

1.25 Statistical analysis

A fully randomized design was used to conduct all experiments. The statistical data analysis was carried out by one-way analysis of variance (ANOVA) using the sigma plot software (Version 14.0, Sigma plot., Chicago, IL, USA). The significant analysis of the data was performed by Tukey test with considering a defined significance level of $p < 0.05$.

1.26 Results and discussion

1.26.1 Functional properties of film

Mechanical properties of NCM and PLA/NCM film were determined to examine the tensile properties of the film with respect to applied force. As can be seen in Figure 6. 2A, PLA/NCM film showed higher tensile properties (i.e., tensile strength and strain) compared to the NCM film at the same time. This increase of tensile properties may allow the film to withstand the normal stress faced during the shipment, handling and transportation of foods [120]. The other possible reason for the increasing tensile properties of the film is related to interfacial interaction of PLA with NCM, because PLA is the plasticizer agent which may strictly bind film components during the film coating [201]. Therefore, it permits the higher tensile force during the film deformation; and resulted in an increase in tensile strength. Compared to the films, PLA/NCM film can be considered more suitable for food packaging applications.

The water solubility of the film was analyzed to define the comparative applications of NCM and PLA/NCM films for smart_food packaging. The water solubility of the NCM film was higher than that of the PLA/NCM film (Figure 6. 2B). In comparison to PLA, chitosan and nanocellulose are highly susceptible to water molecules. Therefore, when the PLA was applied to the NCM film surface for coating, it reduced its water solubility performance. This is because the coating of PLA to the film can suppress the water diffusion

rate. A similar phenomenon was observed in the previous study, where the water solubility of the film was decreased after PLA coating to the film,[236] which was consistent with the solubility results obtained from our test. The photodegradation of the PLA/NCM film was carried out to characterize the color degradation properties of the film during light exposure at room temperatures. As can be seen in Figure 6. 2C, the color parameters (L^* , a^* and b^*) for the PLA/NCM film did not potentially fluctuate during the exposition to light within 5 days. Whereas, after 3 days, the color parameters for NCM films fluctuated, and the color of NCM film degraded (Figure 6. 2D). This phenomenon suggested that PLA coating upon the film surface has an effect to reduce the photodegradation.

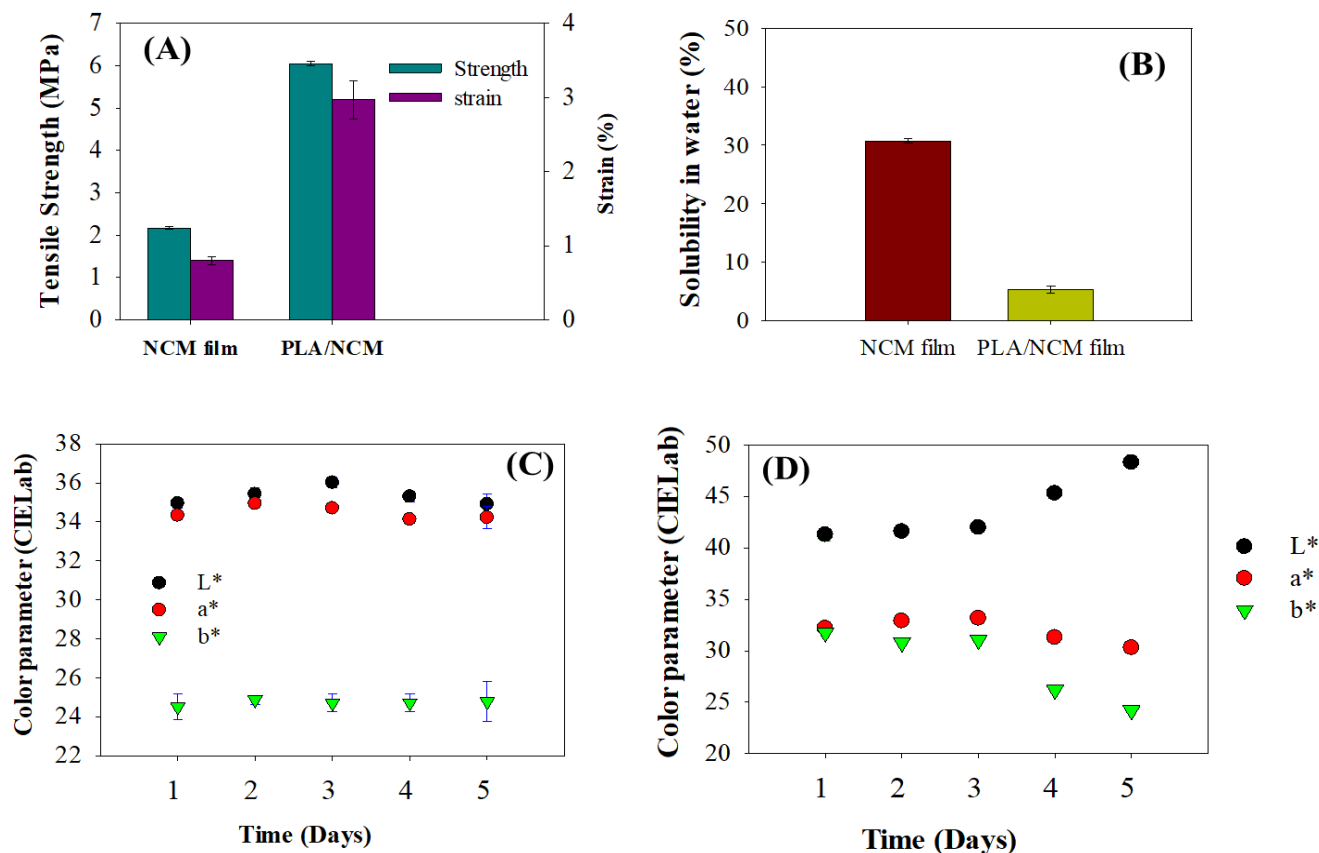


Figure 0.2. (A) Mechanical properties of NCM and PLA/NCM films; (B) water solubility of NCM and PLA/NCM films; (C) Photodegradation of PLA/NCM film according to CIE-Lab coordinates; (D) Photodegradation of NCM film according to CIE-Lab coordinates exposed to visible light irradiation as a function of time at 21 °C.

1.26.2 FTIR spectra

FTIR spectra of PLA/NCM film and film individual compositions such as PLA, nanocellulose and chitosan is presented in Figure 6.3. As can be seen, PLA gives the peak at 1083 cm^{-1} , representing vibrational stretching of C-O (primary alcohol); 1731 cm^{-1} , representing stretching vibration of C=O (aldehyde); and 2956 cm^{-1} , representing C-H stretching vibration absorption (alkane). Nanocellulose gives a peak at 1011 cm^{-1} , representing C-

F stretching (fluoro compounds); 2884 cm^{-1} , representing C-H stretching vibration absorption (alkane); and 3316 cm^{-1} , representing N-H stretching (aliphatic primary amine). Chitosan gives a peak at 1047 cm^{-1} , representing carbon-nitrogen (C-N, amine) stretching; 1623 cm^{-1} , representing C=C stretching vibration (conjugated alkene); 2920 cm^{-1} , representing carbon-hydrogen bonds (C-H, aliphatic). The characterized peaks of PLA/NCM film were displayed to 1047 cm^{-1} , 1731 cm^{-1} , and 2920 cm^{-1} , which is associated with the vibration absorption of carbon-nitrogen (C-N, amine), carbon oxygen double bonds (C=O, aromatic), and aliphatic carbon-hydrogen bonds (C-H), respectively. These observed peaks of PLA/NCM film indicated that strong interfacial adhesions were performed between C=O groups of PLA, N-H aliphatic functional groups of nanocellulose, and C-N functional groups of chitosan. A similar phenomenon has been previously observed in PLA coating polyphenol/chitosan film, in where the PLA copolymer contained carboxyl (C=O) groups in the polyphenol/chitosan films [242].

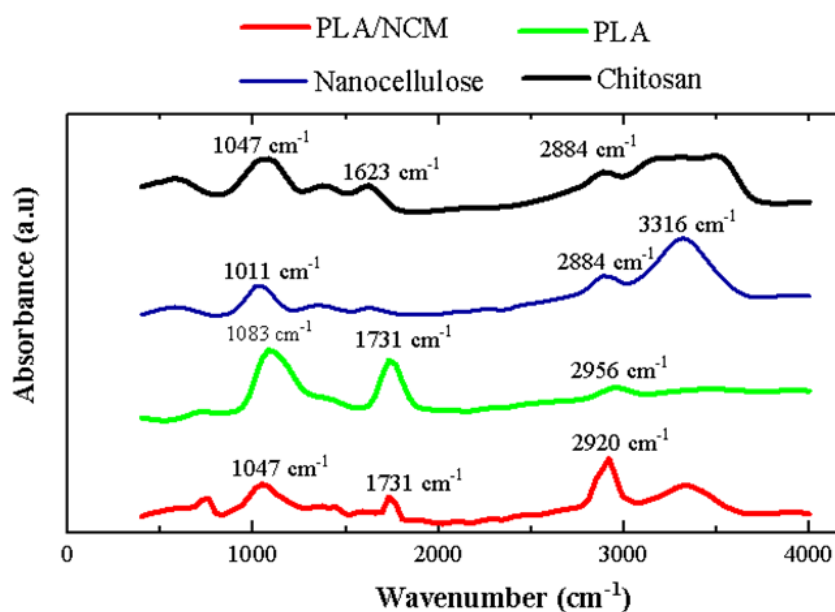


Figure 0.3. Infrared spectroscopy (FTIR) spectra of PLA/NCM films. The films contained nanocellulose (CNF), chitosan and PLA contents.

1.26.3 pH sensing and optical properties of films

The color change properties of PLA/NCM film were evaluated depending upon the various pH buffer solutions (pH 2-10). As can be observed in Figure 6. 4, PLA/NCM film shows different color change properties, which are deep red color when in contact with pH 2-5.5, orange color when reacted to pH 6, and yellow color at pH 6.5-10. These color variations of PLA/NCM films are associated with the structural alteration of methyl red throughout the hydrazone-diazo tautomeric conversion when exposed to different pH levels [243]. When the pH is between 2-5.5, the PLA/NCM film appears dark red color because of the presence of quinone forms in the acidic condition (HMR⁺, dark red) [243]. When the pH values increased between 6.5-10, the color of the film changed from dark red to yellow. This is because the structural alteration of methyl red (pK_a 5.1) occurred throughout the benzenoid formation in alkaline conditions (MR⁻, yellow) [243]. The results of the colorimetric change were assessed using the CIELab scale (Table 6. 1), which were consistent with those observed visually in Figure 6. 4. As can be seen that the lightness of the films (L*) was slightly affected with pH alterations. It shows that when the pH has varied from pH 5.5 to pH 10, PLA/NCM film tended to be the brightest (higher L* values). However, when the pH values varied from pH 2 to pH 5.5 or pH 6.5 to pH 10, no significant changes in the L* values were observed. The evaluation of a* values was not greatly affected with the pH variation. Nonetheless, b* values showed a trend color variation and tended to yellow at higher pH values (Table 6. 1). Briefly, PLA/NCM film showed lower b* values at

pH 2-5 (dark red color), and then showed increasing values of b^* in pH 6-10, confirming that the visible and eye detected color has been formed. It is seen that the ΔE values increased as pH values in contact with film increased from pH 2 to 10. The higher ΔE values for PLA/NCM films after contact with pH buffer solutions (pH 6-10) indicated that the new color formation occurred that was identified by the human eye. According to these results, PLA/NCM film could be useful as a pH-indicator film with the future food packaging industry because it is very sensitive in a wide pH range. In addition, the current food industry is expanding worldwide, they need to use an eye-catching film with good mechanical properties to avoid false positive and negative results when determining the degree of freshness [237]. The produced PLA/NCM film could be potential for usage with food packaging materials for food industrial applications such meat industry due to its pH sensitive and colorful nature.

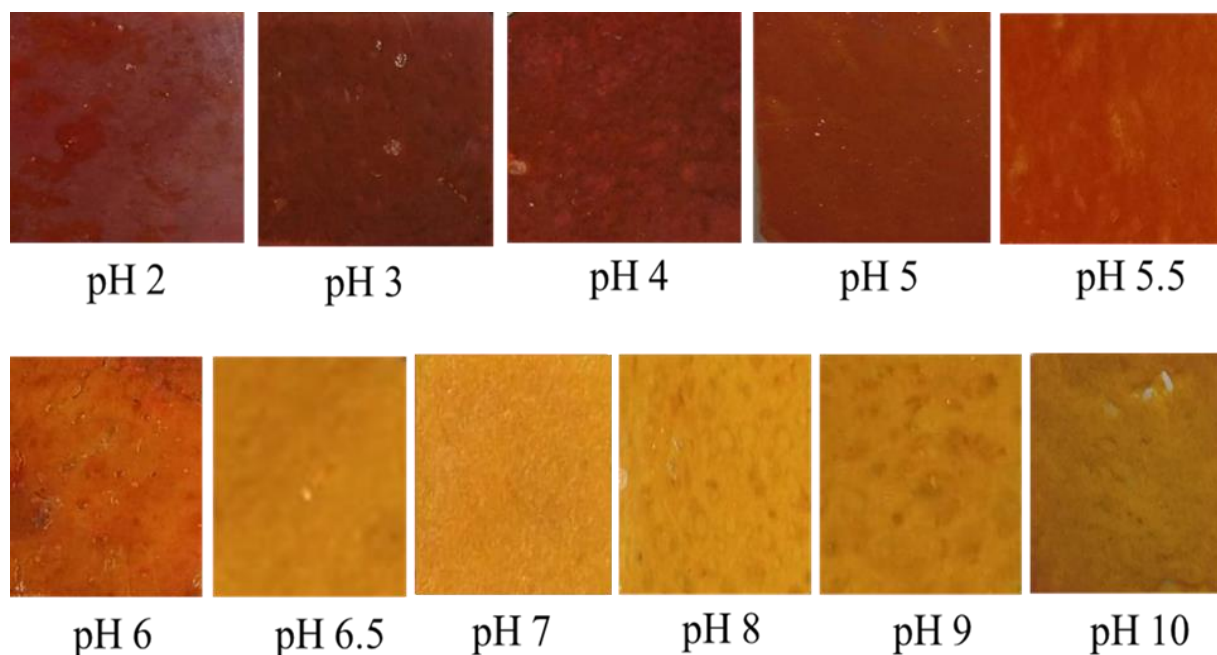


Figure 0.4. The visible color response of the PLA/NCM film with respect to different pH buffer solutions (pH 2-10).

Table 0.1. CIE-Lab color parameters (L^* , a^* and b^*) of the PLA/NCM films after contact with different pH buffer solutions (pH 2-10).

PLA/NCM Calorimetric indicator film				
	L^*	a^*	b^*	ΔE
pH 2	33.56 ± 0.54	16.88 ± 0.14	5.79 ± 0.34	
pH 3	32.43 ± 0.35	13.64 ± 0.13	6.48 ± 0.51	3.87 ± 0.76
pH 4	31.62 ± 0.24	14.52 ± 0.19	7.39 ± 0.19	3.56 ± 0.96
pH 5	31.03 ± 0.03	13.22 ± 0.02	7.65 ± 0.13	4.93 ± 0.53
pH 5.5	31.83 ± 0.40	14.16 ± 0.06	6.46 ± 0.21	3.34 ± 0.56

pH 6	37.98±0.15	22.56±0.41	19.14±0.49	15.17±0.70
pH 6.5	43.36±0.44	18.84±0.08	36.43±0.29	32.25±0.51
pH 7	43.33±0.24	18.27±0.27	33.07±0.31	29.02±0.64
pH 8	43.53±0.02	18.13±0.02	33.61±0.36	29.59±0.93
pH 9	43.04±0.49	16.29±0.06	33.80±0.29	29.62±0.67
pH 10	42.61±0.25	21.69±0.28	34.71±0.58	30.22 ±0.53

N.B: The ΔE values of films were calculated using Eq. (1) and considered the standard color parameters of films using pH 2 as a standard.

1.26.4 Assessment of color specificity of PLA/NCM film

The key components of foods are known as polysaccharides, lipids, amino acids and vitamins, and they act as precursors for assessing the quality of foods [174]. During the food spoiling, these components are broken down and thereby they produce various organic and inorganic volatile compounds. For example, during the beef, fish and seafood spoilage, various types of biogenic amines are released such as ionized or unionized ammonia (NH_3), histamine, tyramine, and ethylamine compounds [226]. During the fruit spoilage, various types of small molecular volatile compounds are evolved such as different kinds of aldehydes, ketone, carbon dioxide, acetic acid, and a small amount of HCl [174]. To evaluate the color specificity of the PLA/NCM film, the PLA/NCM film was applied with different commercial basic biogenic amines and organic or inorganic compounds such as ammonia (NH_3), histamine, tyramine, acetic acid and hydrochloric acid (HCl) to observe the film's color change. The apparent color change of the PLA/NCM film in contact with different commercial basic biogenic amines and organic or inorganic compounds has been shown in Figure 6. 5A. The PLA/NCM film was brown in color under HCl and acetic acid

conditions. However, the PLA/NCM film showed yellow color when the PLA/NCM film was applied in the biogenic amine compounds such as ammonia, tyramine, and histamine. All these color changes of the film were detected by the naked eye. There is no dramatic difference in color change among histamine, tyramine and ammonia. This indicates that the PLA/NCM film prepared in this study has a selective color change property from red to yellow to the biogenic amine compounds which are normally produced in the alkaline condition. This result also demonstrated that the PLA/NCM film could be a suitable candidate as the indicator label for detecting beef, fish and seafood spoilage, because these protein-rich food products produce biogenic amine compounds during their spoilage. The color index of the film was quantitatively analyzed by color parameters (CIEb*). It showed that PLA/NCM film showed significant yellow color (+*b) to histamine, tyramine and ammonium condition (Figure 6. 5B). The higher *b means more obvious yellow color in the films were produced. On the other hand, PLA/NCM film showed lower *b values in response to HCl and acetic acid and thus it can have a great potential for detection of food spoilage.

(A)

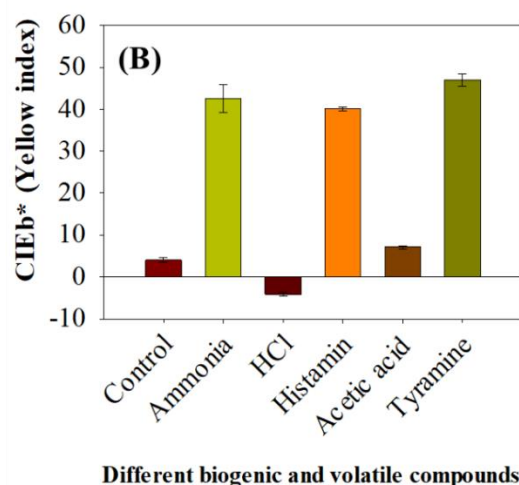
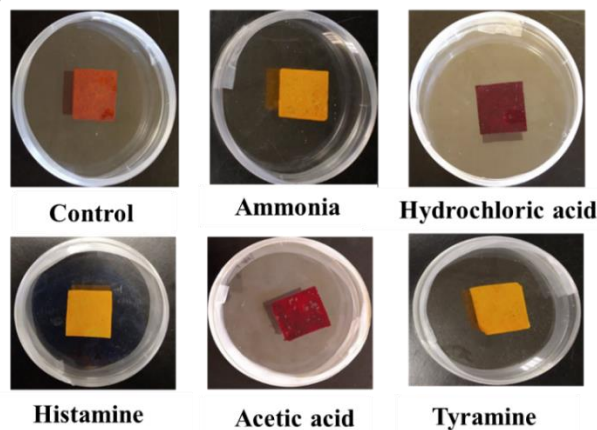


Figure 0.5. (A) The color change of PLA/NCM film at different simulated conditions; (B) CIEb* color parameters of the PLA/NCM films at different simulated conditions. Control film denotes PLA/NCM film without any sample treatment.

1.26.5 Application of PLA/NCM film for beef spoilage trial

1.26.5.1 Assessment of beef spoilage using PLA/NCM film

The PLA/NCM film was placed in contact with beef samples, allowing the film to respond to the spoiled beef with a very distinct color change from red to yellow under the refrigeration condition (4 ± 0.2 °C). These color changes of the film were monitored periodically until no further color change observed during the beef spoilage (Figure 6. 6). In the fresh state of the beef, PLA/NCM film showed red color between 1-3 days and then turned slightly to orange-yellow between 3-5 days. Thereafter, the color of the PLA/NCM film changed significantly to yellow between 6-10 days. Furthermore, no color change was inspected between 6-10 days. The color changes of the PLA/NCM film were distinguished by the naked eye in every state of beef spoilage. Based on the color change properties, it can be assumed that within 1–3 days, the quality of beef might be fresh, and its quality gradually decreased after 3 days at refrigerant condition. To further assess the color change properties of the PLA/NCM film, the ΔE value, which is the color difference value of the PLA/NCM film, was counted (Figure 6. 7). As can be seen, between 1-5 days, ΔE values slightly increased and then rapidly increased after 5 days and continued to 10 days. No drastic color change was observed between 6-10 days. The color change of the film was significant when the ΔE value was greater than 7.36 ± 0.23 after 5 days, belonging to a different color space.

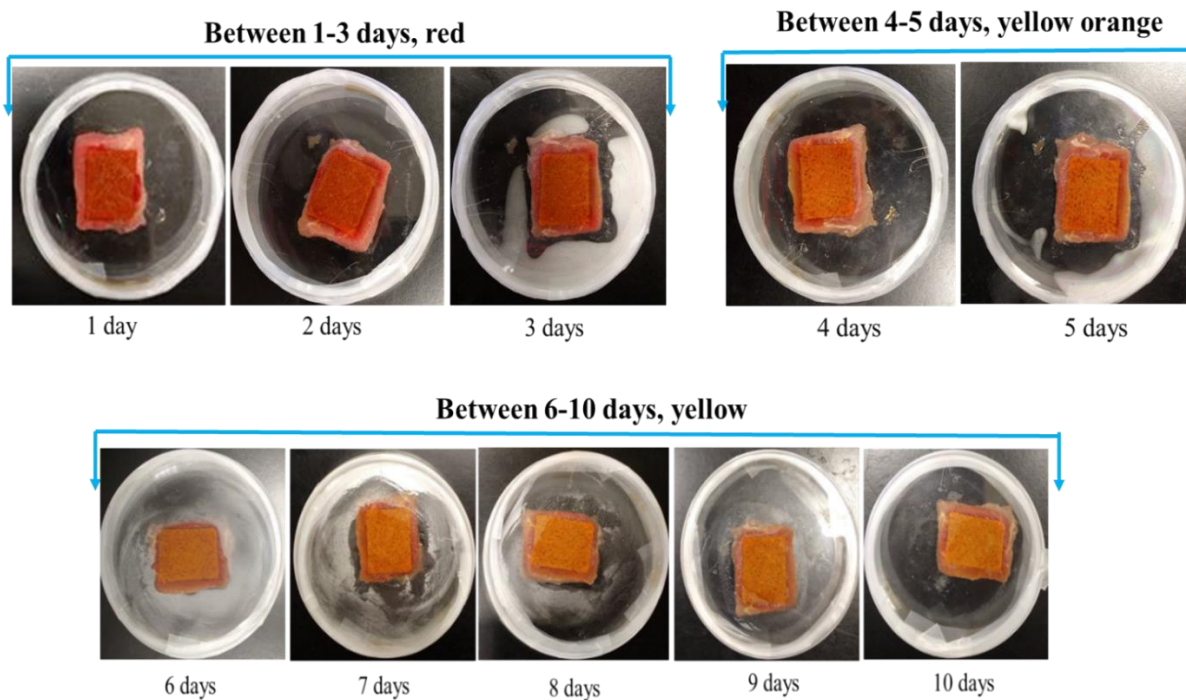


Figure 0.6. Color variation of PLA/NCM film with respect to beef spoilage at refrigerant condition ($4 \pm 0.2^\circ\text{C}$).

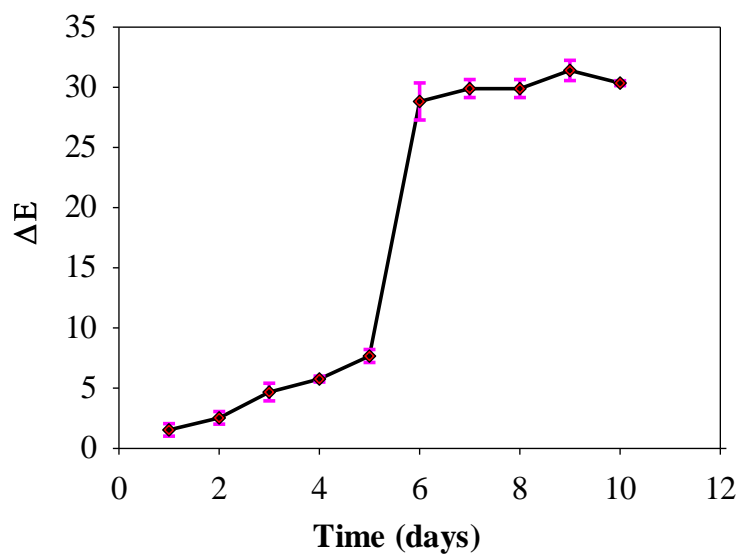


Figure 0.7. The color change (ΔE) of PLA/NCM film towards the spoiling beef at refrigeration condition ($4 \pm 0.2^\circ\text{C}$).

1.26.5.2 Assessment of microbial degradation of beef using PLA/NCM film

As can be seen in Figure 6. 7A, the initial TVC count in beef was 1.95 log (CFU/g) and gradually reached at 8.67 log (CFU/g) by 10 days. According to international trade, when the TVC count exceeds the normal level of TVC [6 logs (CFU/g)], meat is considered to be a poor quality product and unfit for consumption [244]. It has been noted that the TVC count exceeded 6 log (CFU/g) after 5 days at 4 °C. After 5 days, the TVC count in beef was 6.9 log CFU/g, which was unsafe for consumption and exceeded the minimum level of beef acceptability. It has been noted that the TVC count exceeded 6 log (CFU/g) after 5 days at 4 °C. After 5 days later, TVC count in beef was 6.9 log CFU/g, which were unsafe for consumption and exceeded the minimum level of beef acceptability.

The ΔE of PLA/NCM film was correlated with the TVC count and it was found that TVC values were consistent with ΔE of the PLA/NCM film (Figure 6. 7B and C). When ΔE value is 9.2 ± 0.96 at 5 days, the cut-off value for TVC [Log (CFU/g)] was 4.8 ± 0.96 . After this point, ΔE values suddenly rose and exceeded the threshold level of the TVC [6 log CFU/g]. Which is why this point can be used as an onset of detection for PLA/NCM film as the threshold of spoilage at refrigerant condition, and this value was termed as the onset of detection or cut-off value for PLA/NCM film. This result was in good agreement with the findings of Taherkhani et al., who reported a beef at chiller condition can last for 5 days for consumption [238]. From this perspective, 5 days at refrigerant condition has been considered as the threshold for beef consumption. Thus, it can be proven that the PLA/NCM film can be used to indicate the presence of high microbial populations in packaged beef by the color change that can be seen using the naked eye for visual detection.

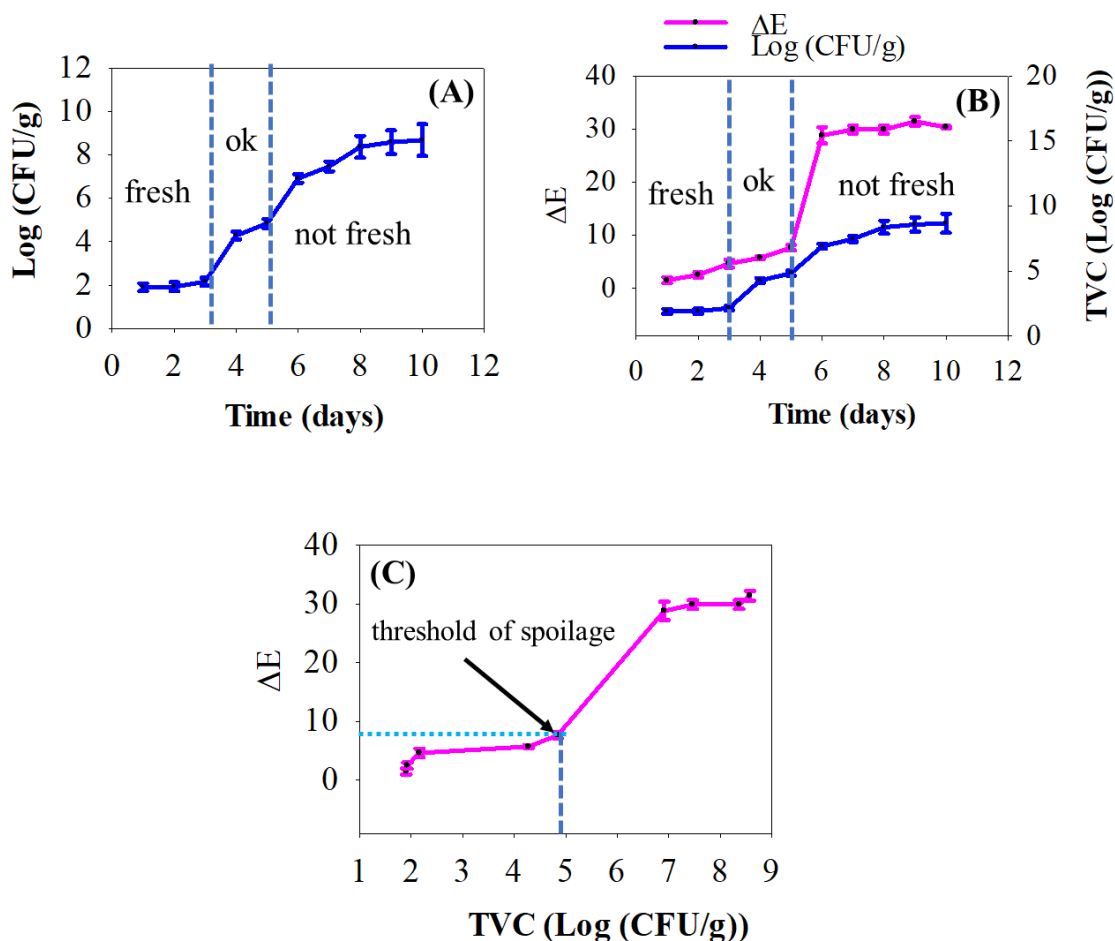


Figure 0.8. (A) Total viable count (TVC) of microorganism in the beef sample in the refrigerant condition; (B) TVC correlated with color change value (ΔE) of PLA/NCM film between 1-10 days; (C) ΔE correlated with TVC in the refrigerant condition.

1.26.5.3 Assessment of pH in spoiling beef with color response of PLA/NCM film

The pH value of beef sample was evaluated with regard to ΔE of the PLA/NCM film, and the results were shown in Figure 6. 8. As can be observed in Figure 6. 8A, the pH values increased depending on the condition of spoiled beef. At a fresh stage, the pH of the beef was 5.58 and increased to pH 5.93 until 5 days, while ΔE of the PLA/NCM film increased and reached at 9.2 as the threshold of consumption at 5 days. It is noted that the increase

of pH was consistent with the increase of ΔE of the film (Figure 6. 8B and C). Therefore, the pH of beef was considered to be one of the parameters to indicate the beef spoiled or deteriorated. In general, the cell densities of fresh beef are higher at normal pH levels (< 6). However, when pH increases and exceeds normal pH levels (> 6), the cell densities of the meat decreases and gets spoiled or deteriorated [173]. Previous studies have shown a similar phenomenon, while the pH of beef increased with the increase of beef spoilage [237]. While the meat products decompose, the basic alkaline amine compounds are produced, thereby they raise the pH of the spoiling beef sample.

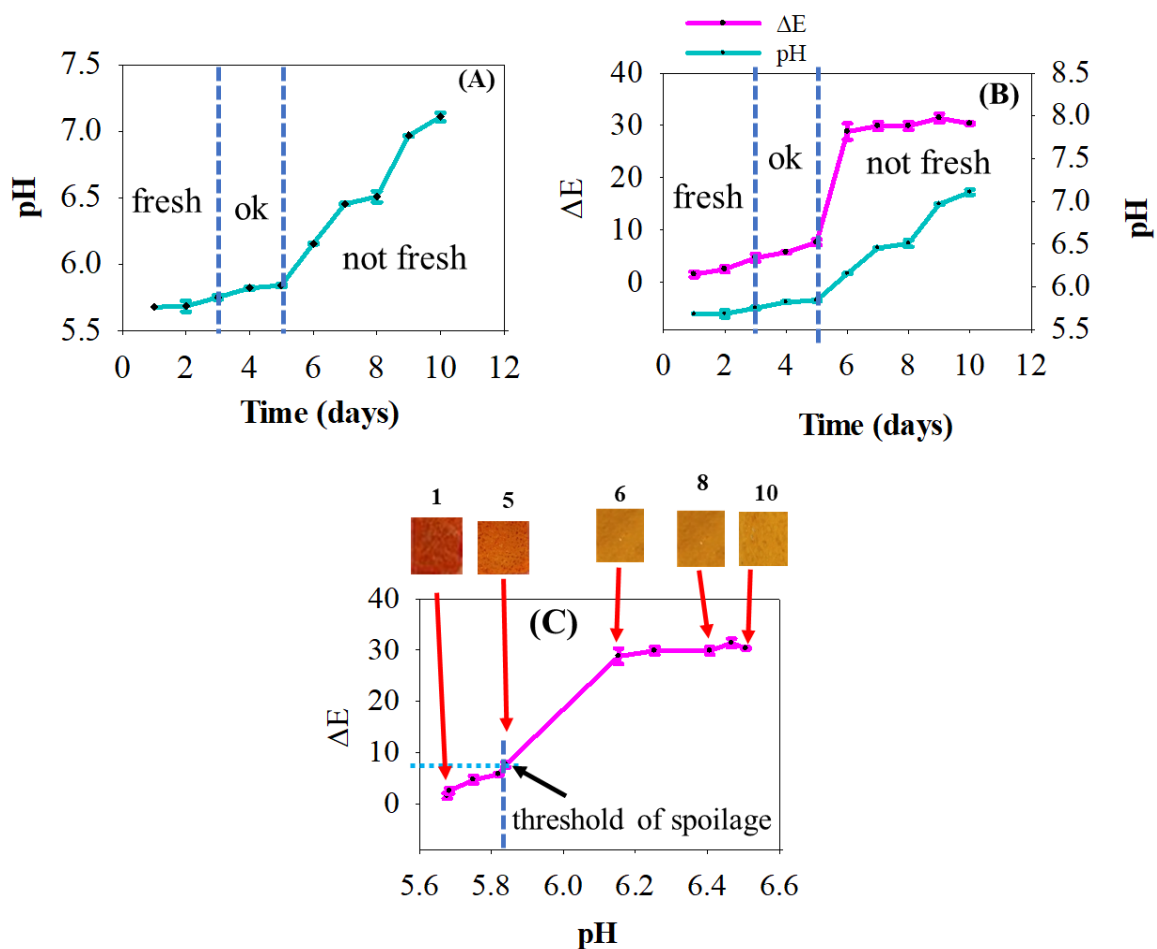


Figure 0.9. (A) Determination of the pH of beef sample depending on their spoilage between 1 and 10 days; (B) pH of spoiling beef correlated with the color change value (ΔE) between 1-10 days; (C) pH of spoiling beef sample correlated with the color change value (ΔE) and images of PLA/NCM film after beef spoilage at 1, 5, 6, 8 and 10 days.

1.26.5.4 Assessment of ammonium concentrations in spoiling beef

Meat and meat products are a good source of protein with high biological value (26-30% of protein in beef meat, w/w) [210]. After protein deamination, the peptide nucleotide catabolites and amino acids of beef tissue are degraded because of microbial deterioration, and thereby ammonia along with other different volatile basic amines are evolved [237].

The most common volatile basic amines after beef deamination are termed as ionized or deionized ammonia, methylamine, histamine, putrescine, tyramine, and cadaverine [245,246].

The ammonia electrode was used to reliably monitor the increased levels of evolved volatile basic ammonia ions released and correlated it with the film color change (ΔE). Within 1-5 days, no significant ammonium ion concentration was detected in the beef sample (Figure 6. 9A and B). After 5 days, the ammonium ion concentrations greatly increased and varied from 41 to 111 mg/L between 6 and 10 days. According to European Food Safety Authority, a level of ammonium concentration between 0.5 mg/L and 5 mg/L in water can pose a risk to human health [247]. Which is why beef was considered as an unsafe product for consumption after 5 days and exceeded the minimum level of beef acceptability. In general, in these refrigerant conditions, deamination of protein in beef tissue slowly occurs, during which volatile basic amines are slowly formed [248]. Therefore, the ammonium concentrations in beef slowly rose during the period of beef monitoring at refrigerant conditions.

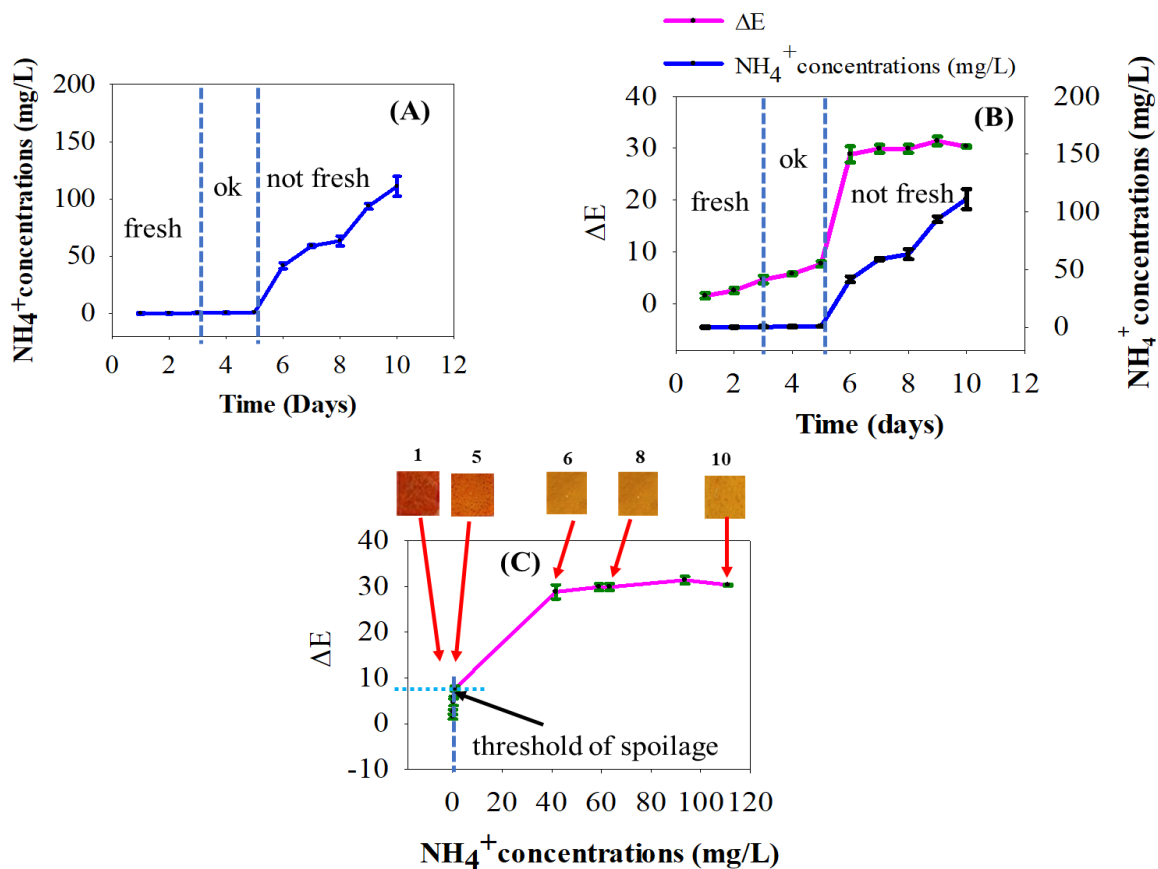


Figure 0.10. (A) Determination of evolved ammonium concentration in spoiled beef samples; (B) evolved ammonium concentration correlated with color change value (ΔE) between 1-10 days; (C) evolved ammonium concentration of beef sample correlated with color change value (ΔE) and images of PLA/NCM film after beef spoilage at 1, 5, 6, 8 and 10 days.

1.27 Conclusions

The PLA/NCM film was created by film casting methodology by adding methyl red (MR) to the nanocellulose/chitosan blend for the real-time monitoring of beef spoilage. This indicator film exhibited distinct color change properties depending on the different pH buffer solutions in the range of 2-10. The FTIR spectra of the PLA/NCM film confirmed the

successful coating of PLA on the film. The PLA/NCM film revealed the distinct color change in contact with biogenic amines and the significant color change properties were achieved. The ΔE of PLA/NCM film showed a good relationship with the TVC and confirmed the safe level of TVC in the beef was achieved at 5 days. The pH and ammonium concentration increased depending on the beef spoiling level and a relationship between film color change (ΔE) and pH in spoiled beef was established. This study provided a promising indicator for monitoring the spoilage of high protein foods such as meat and seafood to inform consumers in real-time of product quality and safety.

CHAPTER 7: CONCLUSIONS

In this research, bio-based nanocomposite materials for smart food packaging were developed using biopolymers such as cellulose nanofiber (CNF), polylactic acid (PLA), and semiconducting materials such as activated biochar and activated carbon for biosensor, and CNF and chitosan followed by methyl red for indicators. The physical and functional properties of bio-based nanocomposite, such as mechanical, thermal, electrical, crystalline, and microstructural properties were evaluated. In addition, the calorimetric properties of indicator film were studied. The specific findings from this dissertation are as follows:

1. Activated carbon had a great influence on electrical properties i.e., current increased, while resistance decreased, due to the increasing activated carbon concentrations to the film. Whereas nanocellulose (CNF) had a significant influence on the mechanical and thermal properties of the bio-based nanocomposite materials. 30% NAC films showed good mechanical strength and considerable electrical properties for the biosensor development compared to 15% and 50% NAC film.

2. AgNPs as the gas sensing dopants were synthesized with 30% NAC nanocomposite. TEM confirmed the aggregated AgNPs coupled with the compact bundle of CNF and AC materials. AgNPs/NAC nanocomposite showed antimicrobial activity to *S. aureus*, resulting in an inhibition zone on the agar media. The electrical conductivity of the AgNPs/NAC nanocomposite increased depending on the AgNPs concentration over the range of 25-450 ppm and the optimum current was obtained at 450 ppm of AgNPs.

3. Biochar was properly activated at 800°C and the activated biochar (ABC/800°C) showed an extensive surface area of 825.89 m²/g and micropore volume of 0.21 cm³/g. The ABCs

synthesized with polylactic acid (PLA) yielded ABC/PLA composite throughout the film casting process and SEM for the ABC/PLA composite confirmed that ABCs were effectively bound with PLA throughout the composite. 85% ABC/PLA composite exhibited good thermal and electrical properties compared to 70% and 50% ABC/PLA composite for biosensor development.

4. AgNPs were synthesized with 85% ABC/PLA nanocomposite as the gas sensing dopants and exhibited a good electrical conductivity for the biosensors. The biosensor fabricated with AgNP/ABC/PLA nanocomposite revealed a sensitivity of ~40% at 80 ppm of NH₃ as a limit of detection (LOD). Resistance of the biosensor (ΔR) was greatly influenced when AgNP/ABC/PLA-based biosensor reacted to NH₃ concentrations.

5. The PLA/NCM film indicator was developed by adding methyl red (MR) to the nanocellulose/chitosan blend for the real-time monitoring of beef spoilage. This indicator film exhibited distinct color change properties depending on the different pH buffer in the range of 2-10. The ΔE of PLA/NCM film showed a good relationship with the TVC and confirmed the safe level of TVC in the beef was achieved at 5 days at refrigeration conditions.

CHAPTER 8: RECOMMENDATIONS FOR FUTURE WORK

We discovered several important findings from this timely research work. At the same time, it also showed some new ideas of interest for future research and development, which are summarized as follows:

1. Proper surface modification of AgNPs/NAC or AgNP/ABC/PLA-based polymer biosensor is required for substantial gas absorption. Different unique surfactants (reagents of surface modification) for biosensors would be sought to verify the sensing efficiency.
2. Polymer nanocomposites with low degradation temperatures may have reduced mechanical and electrical properties. Therefore, conductive nanocomposite with higher thermal and mechanical stabilities will be developed in the future in order to preserve the fundamental properties of nanocomposites for biosensors.
3. Various integration techniques for integrating metal particles (Ag, Au, Cu, Zn, and Co) with polymer nanocomposite will be sought to verify the future biosensor efficiency.
4. The optimization of each technique will be carried out in order to determine the ideal nanocomposite processing parameters. It is also believed that the combination of any two or all three of these techniques will improve the properties of nanocomposites to new levels and make them suitable for practical biosensor applications.
5. Environmentally friendly nanocomposite processing techniques are the central point of this research project. Therefore, we will try to use less harmful and volatile chemicals when developing nanocomposite for biosensor or indicators and reduce energy consumption by controlling processing temperature. Simpler processing

techniques can be introduced instead of the complicated physical and chemical methods typically used in nanocomposites processing, without compromising the properties and functionalities of nanocomposites.

6. Since tiny biosensor specimens are favored for smart food packaging in order to assess product integrity over time, we will attempt to manufacture tiny biosensor specimens in the future and check the tiny biosensor's sensitivity properties for packaging content.
7. Since the possible risks of biosensors to human health remain uncertain, the particle sizes of materials used in biosensor development are important considerations, and the use of materials for biosensors and smart packaging materials should be proven healthful.

References

- [1] C. Nerín, M. Aznar, D. Carrizo, Food contamination during food process, *Trends Food Sci. Technol.* 48 (2016) 63–68. doi:10.1016/j.tifs.2015.12.004.
- [2] B. Kuswandi, Y. Wicaksono, Jayus, A. Abdullah, L.Y. Heng, M. Ahmad, Smart packaging: Sensors for monitoring of food quality and safety, *Sens. Instrum. Food Qual. Saf.* 5 (2011) 137–146. doi:10.1007/s11694-011-9120-x.
- [3] C. Faille, C. Cunault, T. Dubois, T. Bénézech, Hygienic design of food processing lines to mitigate the risk of bacterial food contamination with respect to environmental concerns, *Innov. Food Sci. Emerg. Technol.* 46 (2018) 65–73. doi:10.1016/j.ifset.2017.10.002.
- [4] P. Madhusudan, N. Chellukuri, N. Shivakumar, Smart packaging of food for the 21st century - A review with futuristic trends, their feasibility and economics, *Mater. Today Proc.* 5 (2018) 21018–21022. doi:10.1016/j.matpr.2018.6.494.
- [5] C.M.A.P. Franz, H.M.W. den Besten, C. Böhnlein, M. Gareis, M.H. Zwietering, V. Fusco, Reprint of: Microbial food safety in the 21st century: Emerging challenges and foodborne pathogenic bacteria, *Trends Food Sci. Technol.* 84 (2019) 34–37. doi:10.1016/j.tifs.2019.01.009.
- [6] G. Astill, T. Minor, S. Thornsbery, Changes in U.S. produce grower food safety practices from 1999 to 2016, *Food Control.* 104 (2019) 326–332. doi:10.1016/j.foodcont.2019.05.007.
- [7] M. Ghaani, C.A. Cozzolino, G. Castelli, S. Farris, An overview of the intelligent packaging technologies in the food sector, *Trends Food Sci. Technol.* 51 (2016) 1–

11. doi:10.1016/j.tifs.2016.02.008.
- [8] S.Y. Lee, S.J. Lee, D.S. Choi, S.J. Hur, Current topics in active and intelligent food packaging for preservation of fresh foods, *J. Sci. Food Agric.* 95 (2015) 2799–2810. doi:10.1002/jsfa.7218.
- [9] H. Chen, M. Zhang, B. Bhandari, C. Yang, Development of a novel colorimetric food package label for monitoring lean pork freshness, *LWT - Food Sci. Technol.* 99 (2019) 43–49. doi:S0023643818307801.
- [10] T. V. Duncan, Applications of nanotechnology in food packaging and food safety: Barrier materials, antimicrobials and sensors, *J. Colloid Interface Sci.* 363 (2011) 1–24. doi:10.1016/j.jcis.2011.07.017.
- [11] S.H. Othman, Bio-nanocomposite materials for food packaging applications : types of biopolymer and nano-sized filler, *Agric. Agric. Sci. Procedia.* 2 (2014) 296–303. doi:10.1016/j.aaspro.2014.11.042.
- [12] J. Rhim, P.K.W. Ng, J. Rhim, Natural biopolymer-based nanocomposite films for packaging applications, *Crit. Rev. Food Sci. Nutr.* 47 (2007) 411–433. doi:10.1080/10408390600846366.
- [13] A.M. Youssef, S.M. El-Sayed, Bionanocomposites materials for food packaging applications: Concepts and future outlook, *Carbohydr. Polym.* 193 (2018) 19–27. doi:10.1016/j.carbpol.2018.03.088.
- [14] C. Wu, J. Sun, Y. Lu, T. Wu, J. Pang, Y. Hu, In situ self-assembly chitosan/ ϵ -polylysine bionanocomposite film with enhanced antimicrobial properties for food

- packaging, *Int. J. Biol. Macromol.* 132 (2019) 385–392.
doi:10.1016/j.ijbiomac.2019.03.133.
- [15] V.H. Campos-Requena, B.L. Rivas, M.A. Pérez, K.A. Garrido-Miranda, E.D. Pereira, Release of essential oil constituent from thermoplastic starch/layered silicate bionanocomposite film as a potential active packaging material, *Eur. Polym. J.* 109 (2018) 64–71. doi:10.1016/j.eurpolymj.2018.08.055.
- [16] A. Sobhan, K. Muthukumarappan, Z. Cen, L. Wei, Characterization of nanocellulose and activated carbon nanocomposite films' biosensing properties for smart packaging, *Carbohydr. Polym.* 225 (2019) 115189.
doi:10.1016/j.carbpol.2019.115189.
- [17] K.L. Yam, P.T. Takhistov, J. Miltz, Intelligent packaging: concepts and applications, *J. Food Sci.* 70 (2005) 1–10.
- [18] A. Mousavi, M. Sarhadi, A. Lenk, S. Fawcett, Tracking and traceability in the meat processing industry : a solution, *Br. Food J.* 104 (2002) 7–19.
doi:10.1108/00070700210418703.
- [19] E. Mohebi, L. Marquez, Intelligent packaging in meat industry : an overview of existing solutions, *J. Food Sci. Technol.* 52 (2015) 3947–3964.
doi:10.1007/s13197-014-1588-z.
- [20] Z. Fang, Y. Zhao, R.D. Warner, S.K. Johnson, Active and intelligent packaging in meat industry, *Trends Food Sci. Technol.* 61 (2017) 60–71.
doi:10.1016/j.tifs.2017.01.002.

- [21] J.M. Soon, L. Manning, Developing anti-counterfeiting measures: The role of smart packaging, *Food Res. Int.* 123 (2019) 135–143.
doi:10.1016/j.foodres.2019.04.049.
- [22] A. Pacquit, K. Tong, H. Mclaughlin, J. Frisby, B. Quilty, D. Diamond, Development of a volatile amine sensor for the monitoring of fish spoilage, *Talanta*. 69 (2006) 515–520. doi:10.1016/j.talanta.2005.10.046.
- [23] C.E. Realini, B. Marcos, Active and intelligent packaging systems for a modern society, *MESC*. 98 (2014) 404–419. doi:10.1016/j.meatsci.2014.06.031.
- [24] Ag and Food Statistics Selected Charts, United States Dep. Agric. (2017) 28.
- [25] I. Packaging, *Active & Intelligent Packaging 2019*, Free. Gr. Inc. (2019).
- [26] D. Schaefer, W. M. Cheung, Smart packaging: opportunities and challenges, *Procedia CIRP*. 72 (2018) 1022–1027. doi:10.1016/j.procir.2018.03.240.
- [27] P. Mehrotra, Biosensors and their applications - A review, *J. Oral Biol. Craniofacial Res.* 6 (2016) 153–159. doi:10.1016/j.jobcr.2015.12.002.
- [28] Y.W. Park, S.M. Kim, J.Y. Lee, W. Jang, Application of biosensors in smart packaging, *Mol. Cell. Toxicol.* 11 (2015) 277–285. doi:10.1007/s13273-015-0027-1.
- [29] S. Wang, L. Zheng, G. Cai, N. Liu, M. Liao, Y. Li, X. Zhang, J. Lin, A microfluidic biosensor for online and sensitive detection of *Salmonella typhimurium* using fluorescence labeling and smartphone video processing, *Biosens. Bioelectron.* 140 (2019) 111333. doi:10.1016/j.bios.2019.111333.

- [30] L. Xue, L. Zheng, H. Zhang, X. Jin, J. Lin, An ultrasensitive fluorescent biosensor using high gradient magnetic separation and quantum dots for fast detection of foodborne pathogenic bacteria, *Sensors Actuators, B Chem.* 265 (2018) 318–325. doi:10.1016/j.snb.2018.03.014.
- [31] N. Elahi, M. Kamali, M.H. Baghersad, B. Amini, A fluorescence Nano-biosensors immobilization on Iron (MNPs) and gold (AuNPs) nanoparticles for detection of *Shigella* spp, *Mater. Sci. Eng. C.* 105 (2019) 110113. doi:10.1016/j.msec.2019.110113.
- [32] J.X. Dong, Z.F. Gao, Y. Zhang, B.L. Li, N.B. Li, H.Q. Luo, A selective and sensitive optical sensor for dissolved ammonia detection via agglomeration of fluorescent Ag nanoclusters and temperature gradient headspace single drop microextraction, *Biosens. Bioelectron.* 91 (2017) 155–161. doi:10.1016/j.bios.2016.11.062.
- [33] B. V. Chikkaveeraiah, H. Liu, V. Mani, F. Papadimitrakopoulos, J.F. Rusling, A microfluidic electrochemical device for high sensitivity biosensing: Detection of nanomolar hydrogen peroxide, *Electrochem. Commun.* 11 (2009) 819–822. doi:10.1016/j.elecom.2009.02.002.
- [34] R. Hasan, T. Pulingam, J. Nelson, A. Nadyra, S. Jyan, T. Wei, F. Ibrahim, B. Fen, K. Lin, Carbon nanotube-based aptasensor for sensitive electrochemical detection of whole-cell *Salmonella*, *Anal. Biochem.* 554 (2018) 34–43. doi:10.1016/j.ab.2018.06.001.
- [35] A. Sobhan, J. Lee, M.K. Park, J.H. Oh, Rapid detection of *Yersinia enterocolitica*

- using a single-walled carbon nanotube-based biosensor for Kimchi product, *Lwt.* 108 (2019) 48–54. doi:10.1016/j.lwt.2019.03.037.
- [36] R.A. Villamizar, A. Maroto, F.X. Rius, I. Inza, M.J. Figueras, Fast detection of *Salmonella Infantis* with carbon nanotube field effect transistors, *Biosens. Bioelectron.* 24 (2008) 279–283. doi:10.1016/j.bios.2008.03.046.
- [37] E. Vargas, M.A. Ruiz, F.J. Ferrero, S. Campuzano, V. Ruiz-Valdepeñas Montiel, A.J. Reviejo, J.M. Pingarrón, Automatic bionalyzer using an integrated amperometric biosensor for the determination of L-malic acid in wines, *Talanta.* 158 (2016) 6–13. doi:10.1016/j.talanta.2016.05.050.
- [38] R. Devi, S. Yadav, R. Nehra, S. Yadav, C.S. Pundir, Electrochemical biosensor based on gold coated iron nanoparticles / chitosan composite bound xanthine oxidase for detection of xanthine in fish meat, *J. Food Eng.* 115 (2013) 207–214. doi:10.1016/j.jfoodeng.2012.10.014.
- [39] V.R. Rajeev, A.K. Paulose, K.N.N. Unni, Ammonia gas detection using field-effect transistor based on a solution-processable organic semiconductor, *Vacuum.* 158 (2018) 271–277. doi:10.1016/j.vacuum.2018.10.016.
- [40] G. Jung, Y. Jeong, Y. Hong, M. Wu, S. Hong, W. Shin, J. Park, D. Jang, J.H. Lee, SO₂ gas sensing characteristics of FET- and resistor-type gas sensors having WO₃ as sensing material, *Solid. State. Electron.* 165 (2020) 107747. doi:10.1016/j.sse.2019.107747.
- [41] L. Tang, P. Xu, M. Li, H. Yu, X. Li, H₂S gas sensor based on integrated resonant dual-microcantilevers with high sensitivity and identification capability, *Chinese*

- Chem. Lett. (2020) 2–5. doi:10.1016/j.ccllet.2020.01.018.
- [42] F. Wang, K. Hu, H. Liu, Q. Zhao, K. Wang, Y. Zhang, Low temperature and fast response hydrogen gas sensor with Pd coated SnO₂ nanofiber rods, *Int. J. Hydrogen Energy*. (2020). doi:10.1016/j.ijhydene.2019.12.152.
- [43] J.Y. Shen, M. Di Wang, Y.F. Wang, J.Y. Hu, Y. Zhu, Y.X. Zhang, Z.J. Li, H.C. Yao, Iron and carbon codoped WO₃ with hierarchical walnut-like microstructure for highly sensitive and selective acetone sensor, *Sensors Actuators, B Chem.* 256 (2018) 27–37. doi:10.1016/j.snb.2017.10.073.
- [44] X. Wang, O.S. Wolfbeis, *Fiber-optic chemical sensors and biosensors* (2008–2012), *Anal. Chem.* 85 (2013) 487–508. doi:10.1021/ac303159b.
- [45] M. Smiddy, N. Papkovskaia, D.B. Papkovsky, J.P. Kerry, Use of oxygen sensors for the non-destructive measurement of the oxygen content in modified atmosphere and vacuum packs of cooked chicken patties ; impact of oxygen content on lipid oxidation, *Food Res. Int.* 35 (2002) 577–584.
- [46] N.J. Ronkainen, H. Brian, W.R. Heineman, *Electrochemical biosensors*, *Chem. Soc. Rev.* 39 (2015) 1747–1763. doi:10.1039/b714449k.
- [47] A. Sobhan, J.-H. Oh, M.-K. Park, S.W. Kim, C. Park, J. Lee, Assessment of peanut allergen Ara h1 in processed foods using a SWCNTs-based nanobiosensor, *Biosci. Biotechnol. Biochem.* 8451 (2018) 1–9. doi:10.1080/09168451.2018.1453295.
- [48] W. Putzbach, N.J. Ronkainen, Immobilization techniques in the fabrication of nanomaterial-based electrochemical biosensors: a review, *Sensors.* 13 (2013)

4811–4840. doi:10.3390/s130404811.

- [49] A. Sobhan, J. Lee, M.-K. Park, J.-H. Oh, Rapid detection of *Yersinia enterocolitica* using a single-walled carbon nanotube-based biosensor for Kimchi product, Elsevier Ltd, 2019. doi:10.1016/j.lwt.2019.03.037.
- [50] M. Di Fusco, R. Federico, A. Boffi, A. MacOne, G. Favero, F. Mazzei, Characterization and application of a diamine oxidase from *Lathyrus sativus* as component of an electrochemical biosensor for the determination of biogenic amines in wine and beer, *Anal. Bioanal. Chem.* 401 (2011) 707–716. doi:10.1007/s00216-011-5131-z.
- [51] N.D.M. Sani, L.Y. Heng, R.S.P.M. Marugan, N.F. Rajab, Electrochemical DNA biosensor for potential carcinogen detection in food sample, *Food Chem.* 269 (2018) 503–510. doi:10.1016/j.foodchem.2018.07.035.
- [52] R. Bandyopadhyaya, E. Nativ-roth, O. Regev, R. Yerushalmi-rozen, Stabilization of individual carbon nanotubes in aqueous solutions, *Nano Lett.* 2 (2002) 25–28. doi:10.1021/nl010065f.
- [53] M.M. Rodríguez-delgado, G.S. Alemán-nava, J.M. Rodríguez-delgado, G. Dieck-assad, S.O. Martínez-chapa, D. Barceló, R. Parra, Trends in Analytical Chemistry Laccase-based biosensors for detection of phenolic compounds, *Trends Anal. Chem.* 74 (2015) 21–45. doi:10.1016/j.trac.2015.05.008.
- [54] I.S. Arvanitoyannis, A.C. Stratakos, Application of modified atmosphere packaging and active / smart technologies to red meat and poultry : a review, *Food Bioprocess Technol.* 5 (2012) 1423–1446. doi:10.1007/s11947-012-0803-z.

- [55] K. Pospiskova, I. Safarik, M. Sebela, G. Kuncova, Magnetic particles – based biosensor for biogenic amines using an optical oxygen sensor as a transducer, *Microchim. Acta.* 180 (2013) 311–318. doi:10.1007/s00604-012-0932-0.
- [56] N. Dolmacı, S. Çete, F. Arslan, A. Yaşar, An amperometric biosensor for fish freshness detection from xanthine oxidase immobilized in polypyrrole polyvinylsulphonate film, *Artif. Cells, Blood Substitutes, Biotechnol.* 40 (2012) 275–279. doi:10.3109/10731199.2011.646410.
- [57] A. Nopwinyuwong, S. Trevanich, P. Suppakul, Development of a novel colorimetric indicator label for monitoring freshness of intermediate-moisture dessert spoilage, *Talanta.* 81 (2010) 1126–1132. doi:10.1016/j.talanta.2010.02.008.
- [58] A. Pacquit, J. Frisby, D. Diamond, K.T. Lau, A. Farrell, B. Quilty, D. Diamond, Development of a smart packaging for the monitoring of fish spoilage, *Food Chem.* 102 (2007) 466–470. doi:10.1016/j.foodchem.2006.05.052.
- [59] M. Peris, L. Escuder-Gilabert, Electronic noses and tongues to assess food authenticity and adulteration, *Trends Food Sci. Technol.* 58 (2016) 40–54. doi:10.1016/j.tifs.2016.10.014.
- [60] C. Medina-Plaza, J.A. de Saja, J.A. Fernández-Escudero, E. Barajas, G. Medrano, M.L. Rodriguez-Mendez, Array of biosensors for discrimination of grapes according to grape variety, vintage and ripeness, *Anal. Chim. Acta.* 947 (2016) 16–22. doi:10.1016/j.aca.2016.10.032.
- [61] H.F. Hawari, N.M. Samsudin, A.Y.M. Shakaff, Y. Wahab, U. Hashim, A. Zakaria, S.A. Ghani, M.N. Ahmad, Highly selective molecular imprinted polymer (MIP)

based sensor array using interdigitated electrode (IDE) platform for detection of mango ripeness, *Sensors Actuators, B Chem.* 187 (2013) 434–444.

doi:10.1016/j.snb.2013.01.045.

- [62] L. Roberts, R. Lines, S. Reddy, J. Hay, Investigation of polyviologens as oxygen indicators in food packaging, *Sensors Actuators B. Chem.* 152 (2011) 63–67.

doi:10.1016/j.snb.2010.09.047.

- [63] A. Farooq, R. Al-jowder, R. Narayanaswamy, M. Azzawi, P.J.R. Roche, D.E. Whitehead, Sensors and Actuators B : Chemical Gas detection using quenching fluorescence of dye-immobilised silica nanoparticles, *Sensors Actuators B. Chem.*

183 (2013) 230–238. doi:10.1016/j.snb.2013.03.058.

- [64] S. Yan, C. Huawei, Z. Limin, Development and characterization of a new amylase type time – temperature indicator, *Food Control.* 19 (2008) 315–319.

doi:10.1016/j.foodcont.2007.04.012.

- [65] T. Ahuja, I. Ahmad, D. Kumar, Biomolecular immobilization on conducting polymers for biosensing applications, 28 (2007) 791–805.

doi:10.1016/j.biomaterials.2006.09.046.

- [66] X. Xiao, Z. Fu, Y. Zhang, Z. Peng, X. Zhang, SMS-CQ: A Quality and Safety Traceability System for Aquatic Products in Cold-Chain Integrated WSN and QR Code, *J. Food Process Eng.* 40 (2017). doi:10.1111/jfpe.12303.

- [67] K. Kyere-Yeboah, J. Denteh, K. Liu, P. Ye, E.-B. Gao, Monitoring Nicotinamide Adenine Dinucleotide and its phosphorylated redox metabolism using genetically encoded fluorescent biosensors, *Sens. Bio-Sensing Res.* 26 (2019) 100307.

doi:10.1016/j.sbsr.2019.100307.

- [68] A. Oseev, M.P. Schmidt, S. Hirsch, A. Brose, B. Schmidt, Two-component dielectric dispersion impedance biosensor for in-line protein monitoring, *Sensors Actuators, B Chem.* 239 (2017) 1213–1220. doi:10.1016/j.snb.2016.09.118.
- [69] M.A. Morris, S.C. Padmanabhan, M.C. Cruz-romero, E. Cummins, J.P. Kerry, Development of active , nanoparticle , antimicrobial technologies for muscle-based packaging applications, *Meat Sci.* 132 (2017) 163–178.
doi:10.1016/j.meatsci.2017.04.234.
- [70] M.Z. Mostafa, H.A. Khater, M.R. Rizk, A.M. Bahasan, A novel GPS/DVL/MEMS-INS smartphone sensors integrated method to enhance autonomous navigation, guidance and control system of AUSVs based on ADSF Combined Filter, *Meas. J. Int. Meas. Confed.* 146 (2019) 590–605.
doi:10.1016/j.measurement.2019.06.048.
- [71] P. Gogoi, R. Boruah, S.K. Dolui, Jatropha curcas oil based alkyd/epoxy/graphene oxide (GO) bionanocomposites: Effect of GO on curing, mechanical and thermal properties, *Prog. Org. Coatings.* 84 (2015) 128–135.
doi:10.1016/j.porgcoat.2014.09.022.
- [72] S.S. Ray, M. Okamoto, Biodegradable polylactide and its nanocomposites : opening a new dimension for plastics and composites, *Macromol. Rapid Commun.* 24 (2003) 815–840. doi:10.1002/marc.200300008.
- [73] H. Schlüter, M. Saboktakin, Biomedical application of carbon nanotubes for proteins Extraction and separation, *J. Pharm. Nutr. Sci.* 6 (2016) 126–143.

doi:10.6000/1927-5951.2016.06.04.2.

- [74] S. Shankar, X. Teng, J.W. Rhim, Properties and characterization of agar/CuNP bionanocomposite films prepared with different copper salts and reducing agents, *Carbohydr. Polym.* 114 (2014) 484–492. doi:10.1016/j.carbpol.2014.08.036.
- [75] M. Mahardika, H. Abral, A. Kasim, S. Arief, F. Hafizulhaq, M. Asrofi, Properties of cellulose nanofiber/bengkoang starch bionanocomposites: Effect of fiber loading, *Lwt.* 116 (2019). doi:10.1016/j.lwt.2019.108554.
- [76] H. Abral, J. Ariksha, M. Mahardika, D. Handayani, I. Aminah, N. Sandrawati, S.M. Sapuan, R.A. Ilyas, Highly transparent and antimicrobial PVA based bionanocomposites reinforced by ginger nanofiber, *Polym. Test.* (2019) 106186. doi:10.1016/j.polymertesting.2019.106186.
- [77] F. Sadegh-Hassani, A. Mohammadi Nafchi, Preparation and characterization of bionanocomposite films based on potato starch/halloysite nanoclay, *Int. J. Biol. Macromol.* 67 (2014) 458–462. doi:10.1016/j.ijbiomac.2014.04.009.
- [78] N. Cioffi, L. Torsi, N. Ditaranto, G. Tantillo, L. Ghibelli, L. Sabbatini, T. Blevetzacheo, M.D. Alessio, P.G. Zambonin, E. Traversa, *D. Chimica, V. Uni, V. Orabona, I. Bari, D. Sanita, C. Km, I. Bari, D. Biologia, V. Uni, R. Tor, R. Scientifica, I. Roma, S. Bari, V.A.B. I, R. V March, V. Re, M. Recei, V. August,* Copper nanoparticle/polymer composites with antifungal and bacteriostatic properties, *Chem. Mater.* 17 (2005) 5255–5262. doi:10.1021/cm0505244.
- [79] M. Friedman, Review of antimicrobial and antioxidative activities of chitosans in food, *J. Food Prot.* 73 (2010) 1737–1761.

- [80] J.W. Rhim, L.F. Wang, S.I. Hong, Preparation and characterization of agar/silver nanoparticles composite films with antimicrobial activity, *Food Hydrocoll.* 33 (2013) 327–335. doi:10.1016/j.foodhyd.2013.04.002.
- [81] N. Sozer, J.L. Kokini, Nanotechnology and its applications in the food sector, *Trends Biotechnol.* 27 (2009) 82–89. doi:10.1016/j.tibtech.2008.10.010.
- [82] M.R. Martelli, T. Barros, Effect of Chitosan Nanoparticles and Pectin Content on Mechanical Properties and Water Vapor Permeability of Banana Puree Films, 78 (2013). doi:10.1111/j.1750-3841.2012.03006.x.
- [83] A.M. Youssef, M.S. Abdel-aziz, S.M. El-sayed, International Journal of Biological Macromolecules Chitosan nanocomposite films based on Ag-NP and Au-NP biosynthesis by *Bacillus Subtilis* as packaging materials, *Int. J. Biol. Macromol.* 69 (2014) 185–191. doi:10.1016/j.ijbiomac.2014.05.047.
- [84] Y. Zhu, G.G. Buonocore, M. Lavorgna, Photocatalytic Activity Of Pla / Tio 2 Nanocomposites And Tio 2 -active Multilayered Hybrid Coatings, (2012) 102–107.
- [85] G. Fuertes, I. Soto, R. Carrasco, M. Vargas, J. Sabattin, C. Lagos, Intelligent packaging systems: sensors and nanosensors to monitor food quality and safety, *J. Sensors.* 2016 (2016) 1–8. doi:10.1155/2016/4046061.
- [86] I.F. Akyildiz, J.M. Jornet, Electromagnetic wireless nanosensor networks, *Nano Commun. Netw.* 1 (2010) 3–19. doi:10.1016/j.nancom.2010.04.001.
- [87] X. Weng, S. Neethirajan, A microfluidic biosensor using graphene oxide and

- aptamer-functionalized quantum dots for peanut allergen detection, *Biosens. Bioelectron.* 85 (2016) 649–656. doi:10.1016/j.bios.2016.05.072.
- [88] P.D. Skottrup, M. Nicolaisen, A.F. Justesen, Towards on-site pathogen detection using antibody-based sensors, *Biosens. Bioelectron.* 24 (2008) 339–348. doi:10.1016/j.bios.2008.06.045.
- [89] K.B. Bijji, C.N. Ravishankar, C.O. Mohan, T.K. Srinivasa Gopal, Smart packaging systems for food applications: a review, *J. Food Sci. Technol.* 52 (2015) 6125–6135. doi:10.1007/s13197-015-1766-7.
- [90] Q. Wang, M.Y. Long, C.Y. Lv, S.P. Xin, X.G. Han, W. Jiang, Lanthanide-labeled fluorescent-nanoparticle immunochromatographic strips enable rapid and quantitative detection of *Escherichia coli* O157:H7 in food samples, *Food Control.* 109 (2020) 106894. doi:10.1016/j.foodcont.2019.106894.
- [91] T. Bu, P. Jia, J. Liu, Y. Liu, X. Sun, M. Zhang, Y. Tian, D. Zhang, J. Wang, L. Wang, Diversely positive-charged gold nanoparticles based biosensor: A label-free and sensitive tool for foodborne pathogen detection, *Food Chem. X.* 3 (2019) 100052. doi:10.1016/j.fochx.2019.100052.
- [92] E. Smits, J. Schram, M. Nagelkerke, R. Kusters, G. Heck, V. Acht, M. Koetse, J. Brand, G. Gelinck, H. Schoo, Development of printed RFID sensor tags for smart food packaging, *IMCS- The14th Int. Meet. Chem. Sensors.* (2012) 20–23. doi:10.5162/IMCS2012/4.5.2.
- [93] M. Vanderroost, P. Ragaert, F. Devlieghere, B. De Meulenaer, Intelligent food packaging : The next generation, *Trends Food Sci. Technol.* 39 (2014) 47–62.

doi:10.1016/j.tifs.2014.06.009.

- [94] N. da Cruz, Ferreira, S. Ferreira, M. Cabral, P. Simões, R.C. Marques, Packaging waste recycling in Europe : Is the industry paying for it ?, *Waste Manag.* 34 (2014) 298–308. doi:10.1016/j.wasman.2013.10.035.
- [95] S. Sanuja, A. Agalya, M.J. Umapathy, Synthesis and characterization of zinc oxide-neem oil-chitosan bionanocomposite for food packaging application, *Int. J. Biol. Macromol.* 74 (2015) 76–84. doi:10.1016/j.ijbiomac.2014.11.036.
- [96] H. Bouwmeester, S. Dekkers, M.Y. Noordam, W.I. Hagens, A.S. Bulder, C. de Heer, S.E.C.G. ten Voorde, S.W.P. Wijnhoven, H.J.P. Marvin, A.J.A.M. Sips, Review of health safety aspects of nanotechnologies in food production, *Regul. Toxicol. Pharmacol.* 53 (2009) 52–62. doi:10.1016/j.yrtph.2008.10.008.
- [97] C. Silvestre, D. Duraccio, S. Cimmino, Food packaging based on polymer nanomaterials, *Prog. Polym. Sci.* 36 (2011) 1766–1782. doi:10.1016/j.progpolymsci.2011.02.003.
- [98] Q. Chaudhry, M. Scotter, J. Blackburn, B. Ross, A. Boxall, L. Castle, R. Aitken, R. Watkins, Applications and implications of nanotechnologies for the food sector, *Food Addit. Contam. - Part A Chem. Anal. Control. Expo. Risk Assess.* 25 (2008) 241–258. doi:10.1080/02652030701744538.
- [99] C. Shan, H. Yang, D. Han, Q. Zhang, A. Ivaska, L. Niu, Graphene/AuNPs/chitosan nanocomposites film for glucose biosensing, *Biosens. Bioelectron.* 25 (2010) 1070–1074. doi:10.1016/j.bios.2009.09.024.

- [100] B. Rukmanikrishnan, F.R.M. Ismail, R.K. Monoharan, S.S. Kim, J. Lee, Blends of gellan gum/xanthan gum/zinc oxide based nanocomposites for packaging application: Rheological and antimicrobial properties, *Int. J. Biol. Macromol.* (2019). doi:10.1016/j.ijbiomac.2019.11.155.
- [101] A. Hayat, A. Rhouati, R.K. Mishra, G.A. Alonso, M. Nasir, G. Istamboulie, J.L. Marty, An electrochemical sensor based on TiO₂/activated carbon nanocomposite modified screen printed electrode and its performance for phenolic compounds detection in water samples, *Int. J. Environ. Anal. Chem.* 96 (2016) 237–246. doi:10.1080/03067319.2015.1137910.
- [102] V. Scognamiglio, Nanotechnology in glucose monitoring: Advances and challenges in the last 10 years, *Biosens. Bioelectron.* 47 (2013) 12–25. doi:10.1016/j.bios.2013.02.043.
- [103] G. Jian, H. Ju, Z. Hu, S. Deng, J. Lei, A glucose biosensor based on direct electrochemistry of glucose oxidase immobilized on nitrogen-doped carbon nanotubes, *Biosens. Bioelectron.* 25 (2009) 373–377. doi:10.1016/j.bios.2009.07.016.
- [104] Q. Sheng, K. Luo, L. Li, J. Zheng, Direct electrochemistry of glucose oxidase immobilized on NdPO₄ nanoparticles/chitosan composite film on glassy carbon electrodes and its biosensing application, *Bioelectrochemistry.* 74 (2009) 246–253. doi:10.1016/j.bioelechem.2008.08.007.
- [105] C.Y. Liu, J.M. Hu, Hydrogen peroxide biosensor based on the direct electrochemistry of myoglobin immobilized on silver nanoparticles doped carbon

- nanotubes film, *Biosens. Bioelectron.* 24 (2009) 2149–2154.
doi:10.1016/j.bios.2008.11.007.
- [106] M. Najafi, M.A. Khalilzadeh, H. Karimi-Maleh, A new strategy for determination of bisphenol A in the presence of Sudan i using a ZnO/CNTs/ionic liquid paste electrode in food samples, *Food Chem.* 158 (2014) 125–131.
doi:10.1016/j.foodchem.2014.02.082.
- [107] M. Sheng, Y. Gao, J. Sun, F. Gao, Carbon nanodots-chitosan composite film: A platform for protein immobilization, direct electrochemistry and bioelectrocatalysis, *Biosens. Bioelectron.* 58 (2014) 351–358.
doi:10.1016/j.bios.2014.03.005.
- [108] V. Mani, B. Devadas, S.M. Chen, Direct electrochemistry of glucose oxidase at electrochemically reduced graphene oxide-multiwalled carbon nanotubes hybrid material modified electrode for glucose biosensor, *Biosens. Bioelectron.* 41 (2013) 309–315. doi:10.1016/j.bios.2012.08.045.
- [109] M. Sevilla, L. Yu, L. Zhao, C.O. Ania, M.M. Titiric, Surface modification of CNTs with N-doped carbon: An effective way of enhancing their performance in supercapacitors, *ACS Sustain. Chem. Eng.* 2 (2014) 1049–1055.
doi:10.1021/sc500069h.
- [110] M. Sevilla, A.B. Fuertes, Direct synthesis of highly porous interconnected carbon nanosheets and their application as high-performance supercapacitors, *ACS Nano.* 8 (2014) 5069–5078. doi:10.1021/nn501124h.
- [111] M. Tasviri, H.A. Rafiee-Pour, H. Ghourchian, M.R. Gholami, Amine

- functionalized TiO₂ coated on carbon nanotube as a nanomaterial for direct electrochemistry of glucose oxidase and glucose biosensing, *J. Mol. Catal. B Enzym.* 68 (2011) 206–210. doi:10.1016/j.molcatb.2010.11.005.
- [112] J.H. Kim, S. Cho, T.S. Bae, Y.S. Lee, Enzyme biosensor based on an N-doped activated carbon fiber electrode prepared by a thermal solid-state reaction, *Sensors Actuators, B Chem.* 197 (2014) 20–27. doi:10.1016/j.snb.2014.02.054.
- [113] P. Veerakumar, R. Madhu, S.M. Chen, C. Te Hung, P.H. Tang, C. Bin Wang, S. Bin Liu, Porous carbon-modified electrodes as highly selective and sensitive sensors for detection of dopamine, *Analyst.* 139 (2014) 4994–5000. doi:10.1039/c4an01083c.
- [114] J.I. Morán, A. Vázquez, V.P. Cyras, Bio-nanocomposites based on derivatized potato starch and cellulose, preparation and characterization, *J. Mater. Sci.* 48 (2013) 7196–7203. doi:10.1007/s10853-013-7536-x.
- [115] N. Vigneshwaran, S.T. Mhaske, N.R. Savadekar, V.S. Karande, A.K. Bharimalla, Preparation of nano cellulose fibers and its application in kappa-carrageenan based film, *Int. J. Biol. Macromol.* 51 (2012) 1008–1013. doi:10.1016/j.ijbiomac.2012.08.014.
- [116] S.M. Gupta, M. Tripathi, A review of TiO₂ nanoparticles, *Chinese Sci. Bull.* 56 (2011) 1639–1657. doi:10.1007/s11434-011-4476-1.
- [117] J. Qiu, S. Zhang, H. Zhao, Recent applications of TiO₂ nanomaterials in chemical sensing in aqueous media, *Sensors Actuators, B Chem.* 160 (2011) 875–890. doi:10.1016/j.snb.2011.08.077.

- [118] M.B.K. Niazi, Z. Jahan, S.S. Berg, Ø.W. Gregersen, Mechanical, thermal and swelling properties of phosphorylated nanocellulose fibrils/PVA nanocomposite membranes, *Carbohydr. Polym.* 177 (2017) 258–268.
doi:10.1016/j.carbpol.2017.08.125.
- [119] T.S. Ortolani, T.S. Pereira, M.H.M.T. Assumpção, F.C. Vicentini, G. Gabriel de Oliveira, B.C. Janegitz, Electrochemical sensing of purines guanine and adenine using single-walled carbon nanohorns and nanocellulose, *Electrochim. Acta.* 298 (2019) 893–900. doi:10.1016/j.electacta.2018.12.114.
- [120] M. Chaichi, M. Hashemi, F. Badii, A. Mohammadi, Preparation and characterization of a novel bionanocomposite edible film based on pectin and crystalline nanocellulose, *Carbohydr. Polym.* 157 (2017) 167–175.
doi:10.1016/j.carbpol.2016.09.062.
- [121] Y. Chen, L. Yu, X. Ge, H. Liu, A. Ali, Y. Wang, C. Ling, Preparation and characterization of edible starch film reinforced by laver, *Int. J. Biol. Macromol.* 126 (2019) 21. doi:10.1037//0033-2909.126.1.78.
- [122] L.N. Remedio, J.W. Silva dos Santos, V.B. Vieira Maciel, C.M.P. Yoshida, R. Aparecida de Carvalho, Characterization of active chitosan films as a vehicle of potassium sorbate or nisin antimicrobial agents, *Food Hydrocoll.* 87 (2019) 830–838. doi:10.1016/j.foodhyd.2018.09.012.
- [123] E. Jamróz, P. Kopel, L. Juszczak, A. Kawecka, Z. Bytesnikova, V. Milosavljević, M. Kucharek, M. Makarewicz, V. Adam, Development and characterisation of furcellaran-gelatin films containing SeNPs and AgNPs that have antimicrobial

- activity, *Food Hydrocoll.* 83 (2018) 9–16. doi:10.1016/j.foodhyd.2018.04.028.
- [124] Z. Cao, H. Pan, Y. Chen, L. Han, J. Bian, H. Zhang, L. Dong, Y. Yang, Ductile and biodegradable poly (lactic acid) matrix film with layered structure, *Int. J. Biol. Macromol.* 137 (2019) 1141–1152. doi:10.1016/j.ijbiomac.2019.07.047.
- [125] A. Jafari, A. Amini, Lactic acid gas sensor based on polypyrrole thin film, *Mater. Lett.* 236 (2019) 175–178. doi:10.1016/j.matlet.2018.10.066.
- [126] D.Y. Liu, G.X. Sui, D. Bhattacharyya, Synthesis and characterisation of nanocellulose-based polyaniline conducting films, *Compos. Sci. Technol.* (2014). doi:10.1016/j.compscitech.2014.05.001.
- [127] Y. Farrag, S. Malmir, B. Montero, M. Rico, S. Rodríguez-llamazares, L. Barral, R. Bouza, *LWT - Food Science and Technology Starch edible films loaded with donut-shaped starch microparticles*, *LWT - Food Sci. Technol.* 98 (2018) 62–68. doi:10.1016/j.lwt.2018.08.020.
- [128] L. Dai, J. Zhang, F. Cheng, Effects of starches from different botanical sources and modification methods on physicochemical properties of starch-based edible films, *Int. J. Biol. Macromol.* 132 (2019) 897–905. doi:10.1016/j.ijbiomac.2019.03.197.
- [129] M. Wu, M. Wang, M. Ge, Investigation into the performance and mechanism of SiO₂ nanoparticles and starch composite films, *J. Text. Inst.* 100 (2009) 254–259. doi:10.1080/00405000701757677.
- [130] V. Gautam, K.P. Singh, V.L. Yadav, Preparation and characterization of green-nano-composite material based on polyaniline, multiwalled carbon nano tubes and

- carboxymethyl cellulose: For electrochemical sensor applications, *Carbohydr. Polym.* 189 (2018) 218–228. doi:10.1016/j.carbpol.2018.02.029.
- [131] X. Sun, M. Jia, L. Guan, J. Ji, Y. Zhang, L. Tang, Z. Li, Multilayer graphene-gold nanocomposite modified stem-loop DNA biosensor for peanut allergen-Ara h1 detection, *Food Chem.* 172 (2015) 335–342. doi:10.1016/j.foodchem.2014.09.042.
- [132] H.C. Voon, R. Bhat, A.M. Easa, M.T. Liong, A.A. Karim, Effect of Addition of Halloysite Nanoclay and SiO₂Nanoparticles on Barrier and Mechanical Properties of Bovine Gelatin Films, *Food Bioprocess Technol.* 5 (2012) 1766–1774. doi:10.1007/s11947-010-0461-y.
- [133] C.M.O. Müller, J.B. Laurindo, F. Yamashita, Effect of nanoclay incorporation method on mechanical and water vapor barrier properties of starch-based films, *Ind. Crops Prod.* 33 (2011) 605–610. doi:10.1016/j.indcrop.2010.12.021.
- [134] S. Tunç, O. Duman, Preparation and characterization of biodegradable methyl cellulose/montmorillonite nanocomposite films, *Appl. Clay Sci.* 48 (2010) 414–424. doi:10.1016/j.clay.2010.01.016.
- [135] D. Dehnad, Z. Emam-Djomeh, H. Mirzaei, S.M. Jafari, S. Dadashi, Optimization of physical and mechanical properties for chitosan- nanocellulose biocomposites, *Carbohydr. Polym.* 105 (2014) 222–228. doi:10.1016/j.carbpol.2014.01.094.
- [136] R. da S. Oliveira, M.A. Bizeto, F.F. Camilo, Production of self-supported conductive films based on cellulose, polyaniline and silver nanoparticles, *Carbohydr. Polym.* 199 (2018) 84–91. doi:10.1016/j.carbpol.2018.06.049.

- [137] J.H. Ryu, N. Koo Han, J.S. Lee, Y.G. Jeong, Microstructure, thermal and mechanical properties of composite films based on carboxymethylated nanocellulose and polyacrylamide, *Carbohydr. Polym.* 211 (2019) 84–90. doi:10.1016/j.carbpol.2019.01.109.
- [138] Y. Niu, R.M. Crooks, Dendrimer-encapsulated metal nanoparticles and their applications to catalysis, *Comptes Rendus Chim.* 6 (2003) 1049–1059. doi:10.1016/j.crci.2003.08.001.
- [139] Z.M. Huang, Y.Z. Zhang, M. Kotaki, S. Ramakrishna, A review on polymer nanofibers by electrospinning and their applications in nanocomposites, *Compos. Sci. Technol.* 63 (2003) 2223–2253. doi:10.1016/S0266-3538(03)00178-7.
- [140] R.A. Ganeev, M. Baba, A.I. Ryasnyansky, M. Suzuki, H. Kuroda, Characterization of optical and nonlinear optical properties of silver nanoparticles prepared by laser ablation in various liquids, *Opt. Commun.* 240 (2004) 437–448. doi:10.1016/j.optcom.2004.06.049.
- [141] L.Y. Ng, A.W. Mohammad, C.P. Leo, N. Hilal, Polymeric membranes incorporated with metal/metal oxide nanoparticles: A comprehensive review, *Desalination.* (2013). doi:10.1016/j.desal.2010.11.033.
- [142] A.L. Incoronato, G.G. Buonocore, A. Conte, M. Lavorgna, M.A. Nobile, Del, Active systems based on silver-montmorillonite nanoparticles embedded into bio-based polymer matrices for packaging applications, *J. Food Prot.* 73 (2010) 2256–2262. doi:10.4315/0362-028x-73.12.2256.
- [143] Y. Wang, Q. Yang, G. Shan, C. Wang, J. Du, S. Wang, Y. Li, X. Chen, X. Jing, Y.

Wei, Preparation of silver nanoparticles dispersed in polyacrylonitrile nanofiber film spun by electrospinning, *Mater. Lett.* 59 (2005) 3046–3049.

doi:10.1016/j.matlet.2005.05.016.

- [144] J.H.K. and B.R.M. Seung Yun Lee, Hee Jin Kim, Rajkumar Patel, Se Joon Im, Silver nanoparticles immobilized on thin film composite polyamide membrane: characterization, nanofiltration, antifouling properties, *Polym. Adv. Technol.* 18 (2007) 562–568. doi:10.1002/pat.
- [145] E. Fortunati, I. Armentano, Q. Zhou, A. Iannoni, E. Saino, L. Visai, L.A. Berglund, J.M. Kenny, Multifunctional bionanocomposite films of poly(lactic acid), cellulose nanocrystals and silver nanoparticles, *Carbohydr. Polym.* 87 (2012) 1596–1605. doi:10.1016/j.carbpol.2011.09.066.
- [146] S.J. Peighambaroust, S.H. Peighambaroust, N. Mohammadzadeh Pournasir, P. Pakdel, Properties of active starch-based films incorporating a combination of Ag, ZnO and CuO nanoparticles for potential use in food packaging applications, *Food Packag. Shelf Life.* 22 (2019) 100420. doi:10.1016/j.fpsl.2019.100420.
- [147] S. Deghani, S.H. Peighambaroust, S.J. Peighambaroust, S.V. Hosseini, J.M. Regenstein, Improved mechanical and antibacterial properties of active LDPE films prepared with combination of Ag, ZnO and CuO nanoparticles, *Food Packag. Shelf Life.* 22 (2019) 100391. doi:10.1016/j.fpsl.2019.100391.
- [148] T. Baygar, N. Sarac, A. Ugur, I.R. Karaca, Antimicrobial characteristics and biocompatibility of the surgical sutures coated with biosynthesized silver nanoparticles, *Bioorg. Chem.* 86 (2019) 254–258.

doi:10.1016/j.bioorg.2018.12.034.

- [149] A. Sobhan, J.-H. Oh, M.-K. Park, S.W. Kim, C. Park, J. Lee, Single walled carbon nanotube based biosensor for detection of peanut allergy-inducing protein ara h1, *Korean J. Chem. Eng.* 34 (2017) 1–7. doi:10.1007/s11814-017-0259-y.
- [150] A. Sobhan, J.H. Oh, M.K. Park, J. Lee, Reusability of a single-walled carbon nanotube-based biosensor for detecting peanut allergens and *Y. enterocolitica*, *Microelectron. Eng.* 225 (2020) 111281. doi:10.1016/j.mee.2020.111281.
- [151] P. Yu, X. Zhao, Y. Li, Q. Zhang, Controllable growth of polyaniline nanowire arrays on hierarchical macro/mesoporous graphene foams for high-performance flexible supercapacitors, *Appl. Surf. Sci.* 393 (2017) 37–45.
doi:10.1016/j.apsusc.2016.09.119.
- [152] Q. Wei, Z. Chen, Y. Cheng, X. Wang, X. Yang, Z. Wang, Preparation and electrochemical performance of orange peel based-activated carbons activated by different activators, *Colloids Surfaces A Physicochem. Eng. Asp.* 574 (2019) 221–227. doi:10.1016/j.colsurfa.2019.04.065.
- [153] Q. Wang, Y. Zhang, S. Jia, Y. Han, J. Xu, F. Li, C. Meng, Amorphous manganese silicate anchored on multiwalled carbon nanotubes with enhanced electrochemical properties for high performance supercapacitors, *Colloids Surfaces A Physicochem. Eng. Asp.* 548 (2018) 158–171. doi:10.1016/j.colsurfa.2018.03.072.
- [154] Y. Kumar, G.P. Pandey, S.A. Hashmi, Gel polymer electrolyte based electrical double layer capacitors: Comparative study with multiwalled carbon nanotubes and activated carbon electrodes, *J. Phys. Chem. C.* 116 (2012) 26118–26127.

doi:10.1021/jp305128z.

- [155] A. Sobhan, K. Muthukumarappan, Z. Cen, L. Wei, Characterization of nanocellulose and activated carbon nanocomposite films' biosensing properties for smart packaging, *Carbohydr. Polym.* 225 (2019) 115189. doi:10.1016/j.carbpol.2019.115189.
- [156] Y. Gao, D. Shan, F. Cao, J. Gong, X. Li, H.Y. Ma, Z.M. Su, L.Y. Qu, Silver/polyaniline composite nanotubes: One-step synthesis and electrocatalytic activity for neurotransmitter dopamine, *J. Phys. Chem. C.* 113 (2009) 15175–15181. doi:10.1021/jp904788d.
- [157] D.Y. Shin, I. Kim, Self-patterning of fine metal electrodes by means of the formation of isolated silver nanoclusters embedded in polyaniline, *Nanotechnology.* 20 (2009). doi:10.1088/0957-4484/20/41/415301.
- [158] G. Zhu, Z. Chen, B. Wu, N. Lin, Dual-enhancement effect of electrostatic adsorption and chemical crosslinking for nanocellulose-based aerogels, *Ind. Crops Prod.* 139 (2019) 111580. doi:10.1016/j.indcrop.2019.111580.
- [159] T.P.M. Ferreira, N.C. Nepomuceno, E.L.G. Medeiros, E.S. Medeiros, F.C. Sampaio, J.E. Oliveira, M.P. Oliveira, L.S. Galvão, E.O. Bulhões, A.S.F. Santos, Antimicrobial coatings based on poly(dimethyl siloxane) and silver nanoparticles by solution blow spraying, *Prog. Org. Coatings.* 133 (2019) 19–26. doi:10.1016/j.porgcoat.2019.04.032.
- [160] M.A. Dahlem, C. Borsoi, B. Hansen, A.L. Catto, Evaluation of different methods for extraction of nanocellulose from yerba mate residues, *Carbohydr. Polym.* 218

- (2019) 78–86. doi:10.1016/j.carbpol.2019.04.064.
- [161] M.R. Nunes, M. de S.M. Castilho, A.P. de L. Veeck, C.G. da Rosa, C.M. Noronha, M.V.O.B. Maciel, P.M. Barreto, Antioxidant and antimicrobial methylcellulose films containing Lippia alba extract and silver nanoparticles, *Carbohydr. Polym.* 192 (2018) 37–43. doi:10.1016/j.carbpol.2018.03.014.
- [162] J.C. Ontong, S. Paosen, S. Shankar, S.P. Voravuthikunchai, Eco-friendly synthesis of silver nanoparticles using Senna alata bark extract and its antimicrobial mechanism through enhancement of bacterial membrane degradation, *J. Microbiol. Methods.* (2019) 105692. doi:10.1016/j.mimet.2019.105692.
- [163] K.B. Narayanan, S.S. Han, Dual-crosslinked poly(vinyl alcohol)/sodium alginate/silver nanocomposite beads – A promising antimicrobial material, *Food Chem.* 234 (2017) 103–110. doi:10.1016/j.foodchem.2017.04.173.
- [164] Y. Ebrahimi, S.J. Peighambaroust, S.H. Peighambaroust, S.Z. Karkaj, Development of Antibacterial Carboxymethyl Cellulose-Based Nanobiocomposite Films Containing Various Metallic Nanoparticles for Food Packaging Applications, *J. Food Sci.* 84 (2019) 2537–2548. doi:10.1111/1750-3841.14744.
- [165] A. Bahrami, R. Rezaei Mokarram, M. Sowti Khiabani, B. Ghanbarzadeh, R. Salehi, Physico-mechanical and antimicrobial properties of tragacanth/hydroxypropyl methylcellulose/beeswax edible films reinforced with silver nanoparticles, *Int. J. Biol. Macromol.* 129 (2019) 1103–1112. doi:10.1016/j.ijbiomac.2018.09.045.
- [166] M.G. Gordienko, V. V. Palchikova, S. V. Kalenov, A.A. Belov, V.N. Lyanikova,

- D.Y. Poberezhniy, A. V. Chibisova, V. V. Sorokin, D.A. Skladnev, Antimicrobial activity of silver salt and silver nanoparticles in different forms against microorganisms of different taxonomic groups, *J. Hazard. Mater.* 378 (2019) 120754. doi:10.1016/j.jhazmat.2019.120754.
- [167] T.N. Rao, P. Babji, N. Ahmad, R.A. Khan, I. Hassan, S.A. Shahzad, F.M. Husain, *Saudi Journal of Biological Sciences* Green synthesis and structural classification of *Acacia nilotica* mediated-silver doped titanium oxide (Ag / TiO₂) spherical nanoparticles : Assessment of its antimicrobial and anticancer activity, *Saudi J. Biol. Sci.* (2019). doi:10.1016/j.sjbs.2019.09.005.
- [168] G.A. Rance, D.H. Marsh, S.J. Bourne, T.J. Reade, A.N. Khlobystov, Van der waals interactions between nanotubes and nanoparticles for controlled assembly of composite nanostructures, *ACS Nano.* 4 (2010) 4920–4928. doi:10.1021/nn101287u.
- [169] H.J. Kwon, J.R. Cha, M.S. Gong, Preparation of silvered polyimide film from silver carbamate complex using CO₂amine, and alcohol, *J. CO₂ Util.* 27 (2018) 547–554. doi:10.1016/j.jcou.2018.09.005.
- [170] Y. Xing, X. Zhang, H. Chen, M. Chen, Q. Li, Enhancing buckypaper conductivity through co-deposition with copper nanowires, *Carbon N. Y.* 61 (2013) 501–506. doi:10.1016/j.carbon.2013.05.030.
- [171] N. Smigic, I. Djekic, I. Tomasevic, J. Miocinovic, R. Gvozdenovic, Implication of food safety measures on microbiological quality of raw and pasteurized milk, *Food Control.* 25 (2012) 728–731. doi:10.1016/j.foodcont.2011.12.022.

- [172] M. V. Kiryukhin, H.H. Lau, S.H. Goh, C. Teh, V. Korzh, A. Sadovoy, A membrane film sensor with encapsulated fluorescent dyes towards express freshness monitoring of packaged food, *Talanta*. 182 (2018) 187–192. doi:10.1016/j.talanta.2018.01.085.
- [173] B. Kuswandi, A. Nurfawaidi, On-package dual sensors label based on pH indicators for real-time monitoring of beef freshness, *Food Control*. 82 (2017) 91–100. doi:10.1016/j.foodcont.2017.06.028.
- [174] H. Zhang, A. Hou, K. Xie, A. Gao, Smart color-changing paper packaging sensors with pH sensitive chromophores based on azo-anthraquinone reactive dyes, *Sensors Actuators, B Chem*. 286 (2019) 362–369. doi:10.1016/j.snb.2019.01.165.
- [175] X. He, Y. Wang, Highly Thermally Conductive Polyimide Composite Films with Excellent Thermal and Electrical Insulating Properties, *Ind. Eng. Chem. Res.* 59 (2020) 1925–1933. doi:10.1021/acs.iecr.9b05939.
- [176] J. Rezek, P. Novák, J. Houška, A.D. Pajdarová, T. Kozák, High-rate reactive high-power impulse magnetron sputtering of transparent conductive Al-doped ZnO thin films prepared at ambient temperature, *Thin Solid Films*. 679 (2019) 35–41. doi:10.1016/j.tsf.2019.04.009.
- [177] C. Sánchez, Fungal potential for the degradation of petroleum-based polymers: An overview of macro- and microplastics biodegradation, *Biotechnol. Adv.* 40 (2020) 107501. doi:10.1016/j.biotechadv.2019.107501.
- [178] Y. Li, C. Jia, X. Zhang, Y. Jiang, M. Zhang, P. Lu, H. Chen, Synthesis and performance of bio-based epoxy coated urea as controlled release fertilizer, *Prog.*

- Org. Coatings. 119 (2018) 50–56. doi:10.1016/j.porgcoat.2018.02.013.
- [179] K. Doudin, S. Al-Malaika, H.H. Sheena, V. Tverezovskiy, P. Fowler, New genre of antioxidants from renewable natural resources: Synthesis and characterisation of rosemary plant-derived antioxidants and their performance in polyolefins, *Polym. Degrad. Stab.* 130 (2016) 126–134. doi:10.1016/j.polymdegradstab.2016.05.030.
- [180] T. Siripongpreda, K. Siraalertmukul, N. Rodthongkum, Colorimetric sensor and LDI-MS detection of biogenic amines in food spoilage based on porous PLA and graphene oxide, *Food Chem.* 329 (2020) 127165.
doi:10.1016/j.foodchem.2020.127165.
- [181] B. Palai, M. Biswal, S. Mohanty, S.K. Nayak, In situ reactive compatibilization of polylactic acid (PLA) and thermoplastic starch (TPS) blends; synthesis and evaluation of extrusion blown films thereof, *Ind. Crops Prod.* 141 (2019) 111748.
doi:10.1016/j.indcrop.2019.111748.
- [182] P. Müller, J. Bere, E. Fekete, J. Móczó, B. Nagy, M. Kállay, B. Gyarmati, B. Pukánszky, Interactions, structure and properties in PLA/plasticized starch blends, *Polymer (Guildf)*. 103 (2016) 9–18. doi:10.1016/j.polymer.2016.09.031.
- [183] C. Martins, F. Vilarinho, A. Sanches Silva, M. Andrade, A. V. Machado, M.C. Castilho, A. Sá, A. Cunha, M.F. Vaz, F. Ramos, Active polylactic acid film incorporated with green tea extract: Development, characterization and effectiveness, *Ind. Crops Prod.* 123 (2018) 100–110.
doi:10.1016/j.indcrop.2018.06.056.
- [184] J.M. Ferri, O. Fenollar, A. Jorda-Vilaplana, D. García-Sanoguera, R. Balart, Effect

- of miscibility on mechanical and thermal properties of poly(lactic acid)/ polycaprolactone blends, *Polym. Int.* 65 (2016) 453–463. doi:10.1002/pi.5079.
- [185] B. Kumar, M. Castro, J.F. Feller, Poly(lactic acid)-multi-wall carbon nanotube conductive biopolymer nanocomposite vapour sensors, *Sensors Actuators, B Chem.* 161 (2012) 621–628. doi:10.1016/j.snb.2011.10.077.
- [186] N. Nisa, B. Mohammad, A. Arsad, H. Jin, N. Ngadi, *Materials Today : Proceedings Influences of pristine carbon nanotube on the rheological properties of compatibilized polylactic acid / natural rubber nanocomposite*, *Mater. Today Proc.* (2020). doi:10.1016/j.matpr.2020.04.211.
- [187] D. She, J. Dong, J. Zhang, L. Liu, Q. Sun, Z. Geng, P. Peng, Development of black and biodegradable biochar/gutta percha composite films with high stretchability and barrier properties, *Compos. Sci. Technol.* 175 (2019) 1–5. doi:10.1016/j.compscitech.2019.03.007.
- [188] X. Dong, L. He, Y. Liu, Y. Piao, Preparation of highly conductive biochar nanoparticles for rapid and sensitive detection of 17 β -estradiol in water, *Electrochim. Acta.* 292 (2018) 55–62. doi:10.1016/j.electacta.2018.09.129.
- [189] X. Tan, Y. Liu, G. Zeng, X. Wang, X. Hu, Y. Gu, Z. Yang, Application of biochar for the removal of pollutants from aqueous solutions, *Chemosphere.* 125 (2015) 70–85. doi:10.1016/j.chemosphere.2014.12.058.
- [190] T. Huggins, H. Wang, J. Kearns, P. Jenkins, Z.J. Ren, Biochar as a sustainable electrode material for electricity production in microbial fuel cells, *Bioresour. Technol.* 157 (2014) 114–119. doi:10.1016/j.biortech.2014.01.058.

- [191] M.M. Titirici, R.J. White, C. Falco, M. Sevilla, Black perspectives for a green future: Hydrothermal carbons for environment protection and energy storage, *Energy Environ. Sci.* 5 (2012) 6796–6822. doi:10.1039/c2ee21166a.
- [192] P.R. de Oliveira, C. Kalinke, J.L. Gogola, A.S. Mangrich, L.H.M. Junior, M.F. Bergamini, The use of activated biochar for development of a sensitive electrochemical sensor for determination of methyl parathion, *J. Electroanal. Chem.* 799 (2017) 602–608. doi:10.1016/j.jelechem.2017.06.020.
- [193] X. Dong, L. He, H. Hu, N. Liu, S. Gao, Y. Piao, Removal of 17 β -estradiol by using highly adsorptive magnetic biochar nanoparticles from aqueous solution, *Chem. Eng. J.* 352 (2018) 371–379. doi:10.1016/j.cej.2018.07.025.
- [194] W. Qu, L. Wei, Z. Ma, J. Julson, Fast pyrolysis of corn stover and sawdust in a novel reactor, *Am. Soc. Agric. Biol. Eng. Annu. Int. Meet. 2012, ASABE 2012.* 3 (2012) 2364–2378. doi:10.13031/2013.41833.
- [195] A. Sobhan, J.-H. Oh, M.-K. Park, J. Lee, Detection of peanut allergen Ara h 6 in commercially processed foods using a single-walled Carbon nanotube-based biosensor, *J. AOAC Int.* 101 (2018) 1558–1565. doi:10.5740/jaoacint.18-0041.
- [196] M. Genovese, J. Jiang, K. Lian, N. Holm, High capacitive performance of exfoliated biochar nanosheets from biomass waste corn cob, *J. Mater. Chem. A.* 3 (2015) 2903–2913. doi:10.1039/c4ta06110a.
- [197] M.W. Smith, I. Dallmeyer, T.J. Johnson, C.S. Brauer, J.S. McEwen, J.F. Espinal, M. Garcia-Perez, Structural analysis of char by Raman spectroscopy: Improving band assignments through computational calculations from first principles, *Carbon*

- N. Y. 100 (2016) 678–692. doi:10.1016/j.carbon.2016.01.031.
- [198] Z.Z. Chowdhury, M. Ziaul Karim, M.A. Ashraf, K. Khalid, Influence of carbonization temperature on physicochemical properties of biochar derived from slow pyrolysis of durian wood (*Durio zibethinus*) sawdust, *BioResources*. 11 (2016) 3356–3372. doi:10.15376/biores.11.2.3356-3372.
- [199] A.Y. Elnour, A.A. Alghyamah, H.M. Shaikh, A.M. Poulouse, S.M. Al-Zahrani, A. Anis, M.I. Al-Wabel, Effect of pyrolysis temperature on biochar microstructural evolution, physicochemical characteristics, and its influence on biochar/polypropylene composites, *Appl. Sci.* 9 (2019) 7–9. doi:10.3390/app9061149.
- [200] Y. Jia, S. Shi, J. Liu, S. Su, Q. Liang, X. Zeng, T. Li, Study of the effect of pyrolysis temperature on the Cd²⁺ adsorption characteristics of biochar, *Appl. Sci.* 8 (2018). doi:10.3390/app8071019.
- [201] C. Yang, H. Tang, Y. Wang, Y. Liu, J. Wang, W. Shi, L. Li, Development of PLA-PBSA based biodegradable active film and its application to salmon slices, *Food Packag. Shelf Life*. 22 (2019). doi:10.1016/j.fpsl.2019.100393.
- [202] A. Sobhan, K. Muthukumarappan, L. Wei, T. Van Den Top, R. Zhou, Development of an activated carbon-based nanocomposite film with antibacterial property for smart food packaging, *Mater. Today Commun.* (2020) 101124. doi:10.1016/j.mtcomm.2020.101124.
- [203] B. Zhang, S. Ye, G. Xiao, D. Dong, Identification of beef spoilage via the analysis of volatiles using long optical-path Fourier transform infrared spectroscopy, *Anal.*

- Methods. 7 (2015) 5891–5897. doi:10.1039/c5ay00033e.
- [204] K.H. Eom, K.H. Hyun, S. Lin, J.W. Kim, The meat freshness monitoring system using the smart RFID tag, *Int. J. Distrib. Sens. Networks*. 2014 (2014). doi:10.1155/2014/591812.
- [205] M.M. Swe, T. Eamsa-Ard, T. Sriksirin, T. Kerdcharoen, Monitoring the Freshness Level of Beef Using Nanocomposite Gas Sensors in Electronic nose, 2019 IEEE Int. Conf. Consum. Electron. - Asia, ICCE-Asia 2019. (2019) 100–103. doi:10.1109/ICCE-Asia46551.2019.8941605.
- [206] N.A. Travlou, M. Seredych, E. Rodríguez-Castellón, T.J. Badosz, Activated carbon-based gas sensors: Effects of surface features on the sensing mechanism, *J. Mater. Chem. A*. 3 (2015) 3821–3831. doi:10.1039/c4ta06161f.
- [207] D. Kang, B. Wang, X. Wang, Y. Li, Z. Chen, C. He, Y. Wu, Stably dispersed metallophthalocyanine noncovalently bonded to multiwalled carbon nanotubes for ammonia sensing at room temperature, *Sensors Actuators, B Chem*. 246 (2017) 262–270. doi:10.1016/j.snb.2017.02.083.
- [208] N. Maftoonazad, H. Ramaswamy, Design and testing of an electrospun nanofiber mat as a pH biosensor and monitor the pH associated quality in fresh date fruit (Rutab), *Polym. Test*. 75 (2019) 76–84. doi:10.1016/j.polymertesting.2019.01.011.
- [209] S. Cui, H. Pu, G. Lu, Z. Wen, E.C. Mattson, C. Hirschmugl, M. Gajdardziska-Josifovska, M. Weinert, J. Chen, Fast and selective room-temperature ammonia sensors using silver nanocrystal-functionalized carbon nanotubes, *ACS Appl. Mater. Interfaces*. 4 (2012) 4898–4904. doi:10.1021/am301229w.

- [210] Y. Zhang, B.W.B. Holman, Y. Mao, X. Chen, X. Luo, D.L. Hopkins, Y. Zhang, Determination of a pH threshold for dark cutting beef based on visual evaluation by Asian consumers, *Meat Sci.* 172 (2021) 108347.
doi:10.1016/j.meatsci.2020.108347.
- [211] L. Huang, P. Jiang, D. Wang, Y. Luo, M. Li, H. Lee, R.A. Gerhardt, A novel paper-based flexible ammonia gas sensor via silver and SWNT-PABS inkjet printing, *Sensors Actuators, B Chem.* 197 (2014) 308–313.
doi:10.1016/j.snb.2014.02.081.
- [212] S. Abdulla, T.L. Mathew, B. Pullithadathil, Highly sensitive, room temperature gas sensor based on polyaniline-multiwalled carbon nanotubes (PANI/MWCNTs) nanocomposite for trace-level ammonia detection, *Sensors Actuators, B Chem.* 221 (2015) 1523–1534. doi:10.1016/j.snb.2015.08.002.
- [213] S.J. Choi, B.H. Jang, S.J. Lee, B.K. Min, A. Rothschild, I.D. Kim, Selective detection of acetone and hydrogen sulfide for the diagnosis of diabetes and halitosis using SnO₂ nanofibers functionalized with reduced graphene oxide nanosheets, *ACS Appl. Mater. Interfaces.* 6 (2014) 2588–2597.
doi:10.1021/am405088q.
- [214] M. Kołtowski, B. Charmas, J. Skubiszewska-Zięba, P. Oleszczuk, Effect of biochar activation by different methods on toxicity of soil contaminated by industrial activity, *Ecotoxicol. Environ. Saf.* 136 (2017) 119–125.
doi:10.1016/j.ecoenv.2016.10.033.
- [215] A.S. Al Hosni, J.K. Pittman, G.D. Robson, Microbial degradation of four

- biodegradable polymers in soil and compost demonstrating polycaprolactone as an ideal compostable plastic, *Waste Manag.* 97 (2019) 105–114.
doi:10.1016/j.wasman.2019.07.042.
- [216] D.C. Borghesi, M.F. Molina, M.A. Guerra, M.G.N. Campos, Biodegradation study of a novel poly-caprolactone-coffee husk composite film, *Mater. Res.* 19 (2016) 752–758. doi:10.1590/1980-5373-MR-2015-0586.
- [217] G. Lo Re, M. Morreale, R. Scaffaro, F.P. La Mantia, Biodegradation paths of Mater-Bi®/kenaf biodegradable composites, *J. Appl. Polym. Sci.* 129 (2013) 3198–3208. doi:10.1002/app.39027.
- [218] M. Brodhagen, M. Peyron, C. Miles, D.A. Inglis, Biodegradable plastic agricultural mulches and key features of microbial degradation, *Appl. Microbiol. Biotechnol.* 99 (2015) 1039–1056. doi:10.1007/s00253-014-6267-5.
- [219] G. Ning, F. Wei, G. Luo, Y. Jin, Online BET analysis of single-wall carbon nanotube growth and its effect on catalyst reactivation, *Carbon N. Y.* 43 (2005) 1439–1444. doi:10.1016/j.carbon.2005.01.013.
- [220] Z. Tang, X. Li, T. Sun, S. Shen, X. Huixin, J. Yang, Porous crumpled graphene with hierarchical pore structure and high surface utilization efficiency for supercapacitor, *Microporous Mesoporous Mater.* 272 (2018) 40–43.
doi:10.1016/j.micromeso.2018.06.020.
- [221] L. Cui, M. Lu, Y. Li, B. Tang, C. yang Zhang, A reusable ratiometric electrochemical biosensor on the basis of the binding of methylene blue to DNA with alternating AT base sequence for sensitive detection of adenosine, *Biosens.*

- Bioelectron. 102 (2018) 87–93. doi:10.1016/j.bios.2017.11.025.
- [222] C. Cannilla, G. Bonura, F. Frusteri, D. Spadaro, S. Trocino, G. Neri, Development of an ammonia sensor based on silver nanoparticles in a poly-methacrylic acid matrix, *J. Mater. Chem. C*. 2 (2014) 5778–5786. doi:10.1039/c4tc00515e.
- [223] O. Pourret, D. Houben, Characterization of metal binding sites onto biochar using rare earth elements as a fingerprint, *Heliyon*. 4 (2018) e00543. doi:10.1016/j.heliyon.2018.e00543.
- [224] L. Qian, B. Chen, Dual role of biochars as adsorbents for aluminum: The effects of oxygen-containing organic components and the scattering of silicate particles, *Environ. Sci. Technol.* 47 (2013) 8759–8768. doi:10.1021/es401756h.
- [225] Y. Zhang, Y. Mao, K. Li, P. Dong, R. Liang, X. Luo, Models of *Pseudomonas* growth kinetics and shelf life in chilled longissimus dorsi muscles of beef, *Asian-Australasian J. Anim. Sci.* 24 (2011) 713–722. doi:10.5713/ajas.2011.10404.
- [226] M. Alizadeh-Sani, M. Tavassoli, E. Mohammadian, A. Ehsani, G.J. Khaniki, R. Priyadarshi, J.W. Rhim, pH-responsive color indicator films based on methylcellulose/chitosan nanofiber and barberry anthocyanins for real-time monitoring of meat freshness, *Int. J. Biol. Macromol.* (2020). doi:10.1016/j.ijbiomac.2020.10.231.
- [227] B. Schumann, M. Schmid, Packaging concepts for fresh and processed meat – recent progresses, *Innov. Food Sci. Emerg. Technol.* 47 (2018) 88–100. doi:10.1016/j.ifset.2018.02.005.

- [228] C. Vasile, Polymeric nanocomposites and nanocoatings for food packaging: A review, *Materials (Basel)*. 11 (2018). doi:10.3390/ma11101834.
- [229] P. Ezati, J.W. Rhim, pH-responsive chitosan-based film incorporated with alizarin for intelligent packaging applications, *Food Hydrocoll.* 102 (2020) 105629. doi:10.1016/j.foodhyd.2019.105629.
- [230] L.J.R. Foster, S. Ho, J. Hook, M. Basuki, H. Marçal, Chitosan as a biomaterial: Influence of degree of deacetylation on its physiochemical, material and biological properties, *PLoS One*. 10 (2015) 1–22. doi:10.1371/journal.pone.0135153.
- [231] M. Hasan, D.A. Gopakumar, N.G. Olaiya, F. Zarlaida, Alfian, C. Aprinasari, T. Alfatah, S. Rizal, H.P.S.A. Khalil, Evaluation of the thermomechanical properties and biodegradation of brown rice starch-based chitosan biodegradable composite films, *Int. J. Biol. Macromol.* 156 (2020) 896–905. doi:10.1016/j.ijbiomac.2020.04.039.
- [232] A. Riaz, C. Lagnika, H. Luo, Z. Dai, M. Nie, M.M. Hashim, C. Liu, J. Song, D. Li, Chitosan-based biodegradable active food packaging film containing Chinese chive (*Allium tuberosum*) root extract for food application, *Int. J. Biol. Macromol.* 150 (2020) 595–604. doi:10.1016/j.ijbiomac.2020.02.078.
- [233] Y. Qian, L. Bian, K. Wang, W.Y. Chia, K.S. Khoo, C. Zhang, K.W. Chew, Preparation and characterization of curdlan/nanocellulose blended film and its application to chilled meat preservation, *Chemosphere*. (2020) 128948. doi:10.1016/j.chemosphere.2020.128948.
- [234] A. Khosravi, A. Fereidoon, M.M. Khorasani, G. Naderi, M.R. Ganjali, P. Zarrintaj,

- M.R. Saeb, T.J. Gutiérrez, Soft and hard sections from cellulose-reinforced poly(lactic acid)-based food packaging films: A critical review, *Food Packag. Shelf Life*. 23 (2020) 100429. doi:10.1016/j.fpsl.2019.100429.
- [235] V. Sessini, I. Navarro-Baena, M.P. Arrieta, F. Dominici, D. López, L. Torre, J.M. Kenny, P. Dubois, J.M. Raquez, L. Peponi, Effect of the addition of polyester-grafted-cellulose nanocrystals on the shape memory properties of biodegradable PLA/PCL nanocomposites, *Polym. Degrad. Stab.* 152 (2018) 126–138. doi:10.1016/j.polymdegradstab.2018.04.012.
- [236] G. Chen, Y. Chen, N. Jin, J. Li, S. Dong, S. Li, Z. Zhang, Y. Chen, Zein films with porous polylactic acid coatings via cold plasma pre-treatment, *Ind. Crops Prod.* 150 (2020) 112382. doi:10.1016/j.indcrop.2020.112382.
- [237] B. Kuswandi, A. Nurfawaidi, On-package dual sensors label based on pH indicators for real-time monitoring of beef freshness, *Food Control*. 82 (2017) 91–100. doi:10.1016/j.foodcont.2017.06.028.
- [238] E. Taherkhani, M. Moradi, H. Tajik, R. Molaei, P. Ezati, Preparation of on-package halochromic freshness/spoilage nanocellulose label for the visual shelf life estimation of meat, *Int. J. Biol. Macromol.* 164 (2020) 2632–2640. doi:10.1016/j.ijbiomac.2020.08.177.
- [239] D. Kim, S. Lee, K. Lee, S. Baek, J. Seo, Development of a pH indicator composed of high moisture-absorbing materials for real-time monitoring of chicken breast freshness, *Food Sci. Biotechnol.* 26 (2017) 37–42. doi:10.1007/s10068-017-0005-6.

- [240] Y.A.R. Gaviria, N.S.N. Palencia, C. Capello, T.C. Trevisol, A.R. Monteiro, G.A. Valencia, Nanostructured pH-Indicator Films Based on Cassava Starch, Laponite, and Jambolan (*Syzygium cumini*) Fruit Manufactured by Thermo-Compression , *Starch - Stärke*. 2000208 (2021) 2000208. doi:10.1002/star.202000208.
- [241] B. Merz, C. Capello, G.C. Leandro, D.E. Moritz, A.R. Monteiro, G.A. Valencia, A novel colorimetric indicator film based on chitosan, polyvinyl alcohol and anthocyanins from jambolan (*Syzygium cumini*) fruit for monitoring shrimp freshness, *Int. J. Biol. Macromol.* 153 (2020) 625–632. doi:10.1016/j.ijbiomac.2020.03.048.
- [242] J. Ye, S. Wang, W. Lan, W. Qin, Y. Liu, Preparation and properties of polylactic acid-tea polyphenol-chitosan composite membranes, *Int. J. Biol. Macromol.* 117 (2018) 632–639. doi:10.1016/j.ijbiomac.2018.05.080.
- [243] M.R. Plutino, E. Guido, C. Colleoni, G. Rosace, Effect of GPTMS functionalization on the improvement of the pH-sensitive methyl red photostability, *Sensors Actuators, B Chem.* 238 (2017) 281–291. doi:10.1016/j.snb.2016.07.050.
- [244] P. Ezati, H. Tajik, M. Moradi, Fabrication and characterization of alizarin colorimetric indicator based on cellulose-chitosan to monitor the freshness of minced beef, *Sensors Actuators, B Chem.* 285 (2019) 519–528. doi:10.1016/j.snb.2019.01.089.
- [245] V.R. Heerthana, R. Preetha, Biosensors: a potential tool for quality assurance and food safety pertaining to biogenic amines/volatile amines formation in aquaculture

systems/products, *Rev. Aquac.* 11 (2019) 220–233. doi:10.1111/raq.12236.

- [246] M. Papageorgiou, D. Lambropoulou, C. Morrison, E. Kłodzińska, J. Namieśnik, J. Płotka-Wasyłka, Literature update of analytical methods for biogenic amines determination in food and beverages, *TrAC - Trends Anal. Chem.* 98 (2018) 128–142. doi:10.1016/j.trac.2017.11.001.
- [247] E. Food, S. Authority, Health risk of ammonium released from water filters, *EFSA J.* 10 (2012) 1–16. doi:10.2903/j.efsa.2012.2918.
- [248] S. Talegaonkar, H. Sharma, S. Pandey, P.K. Mishra, R. Wimmer, *Bionanocomposites: smart biodegradable packaging material for food preservation*, Elsevier Inc., 2017. doi:10.1016/b978-0-12-804302-8.00003-0.

PUBLICATIONS

Peer-reviewed journal papers

1. Sobhan, A., Muthukumarappan, K., Wei, L., Zhou, R., & Tummala, H. (2021). Development of a polylactic acid-coated nanocellulose/chitosan-based film indicator for real-time monitoring beef spoilage. *Analytical Methods*.
2. Sobhan, A., Muthukumarappan, K., Wei, L., Qiao, Q., Rahman, T., & Nabin Ghimire, N. (2021). Development and characterization of a novel activated biochar-based polymer composite for biosensors. *International Journal of Polymer Analysis and Characterization*, 1-17.
3. Sobhan, A., Muthukumarappan, K., Wei, L., Van Den Top, T., & Zhou, R. (2020). Development of an activated carbon-based nanocomposite film with antibacterial property for smart food packaging. *Materials Today Communications*, 23, 101124.
4. Sobhan, A., Muthukumarappan, K., Cen, Z., & Wei, L. (2019). Characterization of nanocellulose and activated carbon nanocomposite films' biosensing properties for smart packaging. *Carbohydrate polymers*, 225, 115189.

Conference papers

1. Sobhan, A., Muthukumarappan, K., & Wei, L. (2020). Development of a novel PLA coated bio-nanocomposite film indicator for monitoring meat freshness. In *2020 ASABE Annual International Virtual Meeting* (p. 1). American Society of Agricultural and Biological Engineers.
2. Sobhan, A., Muthukumarappan, K., & Wei, L. (2020). Development of bio-nanocomposite films by combination of PLA and biochar for smart food packaging. In *2020*

ASABE Annual International Virtual Meeting (p. 1). American Society of Agricultural and Biological Engineers.